



Rolo, Sonia (2025) *Investigating the role of Ajuba LIM domain protein in Pancreatic Ductal Adenocarcinoma*. PhD thesis.

<https://theses.gla.ac.uk/84843/>

Copyright and moral rights for this work are retained by the author

A copy can be downloaded for personal non-commercial research or study, without prior permission or charge

This work cannot be reproduced or quoted extensively from without first obtaining permission from the author

The content must not be changed in any way or sold commercially in any format or medium without the formal permission of the author

When referring to this work, full bibliographic details including the author, title, awarding institution and date of the thesis must be given

Enlighten: Theses

<https://theses.gla.ac.uk/>  
[research-enlighten@glasgow.ac.uk](mailto:research-enlighten@glasgow.ac.uk)

# Investigating the role of Ajuba LIM domain protein in Pancreatic Ductal Adenocarcinoma

Sonia Rolo

Thesis submitted in fulfilment of the requirements for the  
Degree of Doctor of Philosophy

School of Cancer Sciences  
College of Medical, Veterinary & Life Sciences

University of Glasgow  
CRUK Scotland Institute

June 2024



Scotland  
Institute



University  
of Glasgow

## Abstract

The relationship between a cell and its microenvironment is complex, dynamic and bidirectional. In cancer, an altered extracellular matrix (ECM) composition promotes tumour development through the modification of activities such as cellular proliferation, metabolism, mobility and survival. In pancreatic ductal adenocarcinoma (PDAC), the high matrix rigidity results in large tumours and leads to increased invasiveness. The ECM stiffness is sensed by cells through mechanosensing proteins and transduced by mechanotransduction actors into a cellular response. YAP/TAZ, several LIM domain proteins and a plethora of other proteins are involved in mechanotransduction pathways. Using polyacrylamide hydrogels of tuneable stiffnesses, I showed that cell morphology, proliferation, mRNA expression, transcription factors activities and cellular metabolism are modified by stiffness in a pancreatic KPC-derived mouse cell line (KRas<sup>G12D</sup> and p53<sup>R172H</sup>) named PDACA. The combination of polyacrylamide hydrogel stiffness and the use of RNA sequencing technology allowed me to identify Ajuba, a LIM protein, as a mechanosensitive protein. Ajuba was shown to be a versatile scaffold protein involved in many cellular activities such as adhesion, cell migration, invasion, and proliferation in many cancer types. However, in PDAC, the role of Ajuba is mostly unexplored. Our study shows that Ajuba localises at mature focal adhesions in PDACA cells. Interestingly, the downregulation of Ajuba induces a decrease in cell-matrix adhesion and an increase in cell invasion. However, no modification of focal adhesion formation, focal adhesion turnover or cellular migration was found. Finally, using a combination of polyacrylamide hydrogel stiffness and the use of RNA sequencing technology, I also showed that the downregulation of Ajuba modifies both mRNA expression and transcription factor activities. Collectively our results indicate that Ajuba is both a mechanosensitive and a mechanotransducer in PDAC.

# Table of Contents

ABSTRACT .....	I
TABLE OF CONTENTS .....	II
LIST OF TABLES .....	VII
LIST OF FIGURES .....	VIII
ACKNOWLEDGEMENTS .....	XI
AUTHOR'S DECLARATION .....	XIII
ABBREVIATION .....	XIV
CHAPTER 1. INTRODUCTION .....	1
1.1 CELLULAR MICROENVIRONMENT AND SURROUNDING FORCES .....	2
1.2 CANCERS AND UNBALANCED FORCES .....	3
1.2.1 CANCER .....	3
1.2.2 PANCREATIC CANCER AND ITS MICROENVIRONMENT .....	4
1.3 THE JOURNEY OF MECHANICAL CUES: FROM MEMBRANE TO NUCLEUS .....	6
1.3.1 MECHANOSENSING AND MECHANOTRANSDUCTION .....	6
1.3.2 CELLULAR MEMBRANE .....	7
1.3.3 FOCAL ADHESION .....	8
1.3.4 TRANSMISSION OF TENSION THROUGH THE CYTOSKELETON .....	11
1.3.5 TRANSCRIPTIONAL COACTIVATORS: YAP/TAZ .....	12
1.3.6 NUCLEAR MECHANOTRANSDUCTION .....	13
1.3.7 ACTIN IN THE NUCLEUS .....	16
1.4 LIM DOMAIN PROTEINS .....	16
1.4.1 THREE GROUPS OF LIM DOMAIN PROTEINS .....	18
1.5 AJUBA LIM PROTEIN FAMILY .....	20
1.6 THE LIM PROTEIN AJUBA .....	22
1.6.1 AN OVERVIEW .....	22
1.6.2 AJUBA IN CELL ADHESION .....	23
1.6.3 AJUBA, A CELL CYCLE REGULATOR .....	23

1.6.4	AJUBA MODULATES TRANSCRIPTIONAL ACTIVITIES. ....	24
1.6.5	AJUBA, A METABOLIC REGULATOR.....	26
1.6.6	AJUBA IN CELL MOVEMENT.....	27
1.6.7	AJUBA IN PANCREATIC CANCER AND MECHANOSENSING .....	28
1.7	MIMICKING THE MECHANICAL PROPERTIES OF ECM IN VITRO .....	29
1.8	AIMS: .....	30
CHAPTER 2. MATERIALS AND METHODS .....		32
2.1	MATERIAL AND REAGENTS .....	33
2.2	METHODS.....	43
2.2.1	CELL CULTURE.....	43
2.2.1.1	CELL LINES ORIGINS .....	43
2.2.1.2	CELL LINES MAINTENANCE .....	43
2.2.1.3	CELL LINES CRYOPRESERVATION .....	44
2.2.2	TRANSFECTION .....	44
2.2.2.1	LIPOFECTAMINE 2000 .....	44
2.2.2.2	AMAXA REAGENTS.....	44
2.2.2.3	CALCIUM PHOSPHATE.....	45
2.2.2.4	TRANSFECTION OF SMALL INTERFERING RNA (SIRNA) IN CELLS .....	45
2.2.2.5	LENTIVIRAL TRANSFECTION AND SELECTION OF STABLE CELL LINES .....	46
2.2.3	MOLECULAR BIOLOGY AND CLONING.....	47
2.2.3.1	SGRNA DESIGN AND INSERTION INTO PURO PLENTI CRISPR VECTOR .....	47
2.2.3.2	POLYMERASE CHAIN REACTION (PCR).....	47
2.2.3.3	ELECTROPHORESIS AND GEL PURIFICATION.....	48
2.2.3.4	RESTRICTION DIGESTION .....	48
2.2.3.5	DNA LIGATION .....	49
2.2.3.6	TRANSFORMATION INTO DH5A E. COLI AND COLONY SELECTION .....	49
2.2.3.7	MINIPREPS.....	49
2.2.3.8	SEQUENCING .....	49
2.2.3.9	MAXIPREP.....	50

2.2.3.10	AJUBA CONSTRUCTS DESIGN AND CLONING .....	50
2.2.4	BIOENGINEERING POLYACRYLAMIDE HYDROGELS .....	50
2.2.4.1	ACTIVATION.....	50
2.2.4.2	PASSIVATION .....	51
2.2.4.3	PREPARATION OF POLYACRYLAMIDE HYDROGEL (PAAM) .....	51
2.2.4.4	FUNCTIONALIZATION.....	51
2.2.4.5	COATING.....	52
2.2.5	RNA BASE METHODS .....	52
2.2.5.1	RNA EXTRACTION .....	52
2.2.5.2	CDNA SYNTHESIS .....	53
2.2.5.3	QRT-PCR .....	53
2.2.5.4	RNA SEQUENCING FROM PAAM HYDROGELS .....	53
2.2.6	PROTEIN-BASE METHODS.....	54
2.2.6.1	PROTEIN LYSATES .....	54
2.2.6.2	PROTEIN QUANTIFICATION.....	55
2.2.6.3	SDS-PAGE PROTEIN SEPARATION.....	55
2.2.6.4	WESTERN BLOTS .....	55
2.2.7	CELL BIOLOGY WORK.....	56
2.2.7.1	XCELLIGENCE.....	56
2.2.7.2	PROLIFERATION ASSAY .....	56
2.2.7.3	SCRATCH WOUND MIGRATION ASSAY.....	57
2.2.7.4	CIRCULAR INVASION ASSAY: ESSEN PROTOCOL .....	57
2.2.7.5	FOCAL ADHESION TURNOVER.....	57
2.2.7.6	IMMUNOFLUORESCENCE .....	58
2.2.7.6.1.	IMMUNOFLUORESCENCE FOR CIRCULAR INVASION ASSAY .....	58
2.2.7.6.1.1.	BSA PERMEABILISATION .....	58
2.2.7.6.1.2.	PFS PERMEABILISATION.....	59
2.2.7.7	SPREADING ASSAY .....	59
2.2.7.8	CONCANAVALIN A .....	60

2.2.8	STATISTICAL ANALYSIS AND REPRODUCIBILITY .....	60
<b>CHAPTER 3. THE IMPACT OF STIFFNESS ON PDACA CELLS AND THE SELECTION OF MECHANOTRANSDUCTION CANDIDATES .....</b>		
3.1	INTRODUCTION: .....	62
3.2	STIFFNESSES IMPACTS PDACA CELLULAR BEHAVIOUR. ....	63
3.2.1	PREPARATION OF POLYACRYLAMIDE HYDROGEL .....	63
3.2.2	ENVIRONMENTAL STIFFNESS, MIMICKED BY PAAM HYDROGEL, IMPACTS PDACA MORPHOLOGY, PROLIFERATION, AND YAP ACTIVITY. ....	65
3.2.3	ENVIRONMENTAL STIFFNESS, MIMICKED BY PAAM HYDROGEL, CHANGES GENE EXPRESSION AT THE RNA LEVEL IN THE PDACA CELL LINE. ....	69
3.3	CONCLUSION .....	80
3.4	DISCUSSION.....	80
<b>CHAPTER 4. THE ROLE OF AJUBA IN PANCREATIC CANCER .....</b>		
4.1	INTRODUCTION .....	84
4.2	LOCALISATION OF AJUBA IN THE PANCREATIC CELL LINE PDACA.....	85
4.2.1	AJUBA LOCALISES AT FOCAL ADHESIONS IN PDACA CELLS.....	87
4.3	AJUBA EXPRESSION IS INDEPENDENT OF FOCAL ADHESION FORMATION IN PDACA CELLS. ....	89
4.4	DESIGN, OPTIMISATION AND VALIDATION OF TOOLS TO UPREGULATE AND DOWNREGULATE THE EXPRESSION OF AJUBA IN PDACA CELLS.....	91
4.4.1	OVEREXPRESSION OF AJUBA .....	91
4.4.2	DOWNREGULATION OF AJUBA .....	92
4.5	AJUBA DOWNREGULATION COULD IMPACT PDACA CELL-ECM ATTACHMENT.....	96
4.6	THE DOWNREGULATION OF AJUBA DOESN'T IMPACT FOCAL ADHESION DYNAMICS .....	102
4.6.1	THE DOWNREGULATION OF AJUBA SPECIFICALLY INCREASES PDACA CELL INVASION ABILITIES. ....	104
4.7	IMPACT OF AJUBA DOWNREGULATION IN PDACA CELLS EXPOSED TO STIFFNESS. ....	109
4.8	CONCLUSION:.....	110
4.9	DISCUSSION:.....	111
<b>CHAPTER 5. PAAM STIFFNESSES AND AJUBA IMPACTS TRANSCRIPTION FACTORS ACTIVITIES.....</b>		
5.1	INTRODUCTION .....	116

5.2	PDACA GENE EXPRESSION IS DEEPLY IMPACTED BY ECM STIFFNESSES.....	117
5.3	OVERVIEW OF PATHWAYS, FUNCTIONS, AND TRANSCRIPTION FACTORS THROUGH G: PROFILER ANALYSIS, IN PDACA CELL LINE. ....	121
5.3.1	TRANSCRIPTION FACTOR ACTIVITIES ARE MODIFIED ACCORDING TO STIFFNESS IN PDACA CRISPR EV	121
5.3.2	BIOLOGICAL PROCESS VARIES ACCORDING TO STIFFNESSES IN PDACA CELL LINE.....	124
5.4	AJUBA DOWNREGULATION IMPACTS BOTH TRANSCRIPTION FACTOR ACTIVITIES AND GENE EXPRESSION AT RNA LEVELS .....	134
5.4.1	VALIDATION OF AJUBA DOWNREGULATION IN PDACA CRISPR 01 AND 02 AT RNA LEVELS .....	134
5.4.2	AJUBA DOWNREGULATION MODIFIES TRANSCRIPTION FACTOR ACTIVITIES IN A STIFFNESS-DEPENDANT MANNER .....	136
5.4.3	AJUBA DOWNREGULATION MODIFIES GENE EXPRESSION IN A STIFFNESS-DEPENDANT MANNER IN PDACA .....	141
5.4.4	DISTINGUISHING THE EFFECTS OF THE DOWNREGULATION OF AJUBA AND THE EFFECT OF ENVIRONMENTAL STIFFNESS ON GENE EXPRESSION AT RNA LEVELS. ....	144
5.5	VALIDATION OF CANDIDATES.....	148
5.6	CONCLUSION .....	155
5.7	DISCUSSION.....	157
CHAPTER 6.	FUTURE DIRECTIONS.....	166
6.1	THE ENVIRONMENT STIFFNESS DEEPLY MODIFIES PDAC GENE EXPRESSION AND TRANSCRIPTION FACTOR ACTIVITIES .....	167
6.2	AJUBA: A NEW MECHANOTRANSDUCER PROTEIN? .....	168
CHAPTER 7.	ANNEXES .....	170
CHAPTER 8.	REFERENCES:.....	179



## List of Tables

TABLE 2- 1 UNITS OF MEASUREMENT.....	33
TABLE 2- 2 : CELL LINES AND CELL CULTURE CONSUMABLES.....	33
TABLE 2- 3: PLASMIDS.....	35
TABLE 2- 4: CLONING AND CONSTRUCTS.....	35
TABLE 2- 5: WESTERN BLOTS, IMMUNOFLUORESCENCE AND ANTIBODIES.....	36
TABLE 2- 6: RNA REAGENTS AND PRIMERS.....	38
TABLE 2- 7: DNA PRIMERS.....	39
TABLE 2- 8: KITS .....	41
TABLE 2- 9: PAAM HYDROGELS.....	42
TABLE 2- 10: SOFTWARE.....	43
TABLE 5-1: THE TRANSCRIPTION FACTORS ACTIVITIES OF PDACA CRISPR EV AND PDACA CRISPR 01 SHOWS SEVERAL DIFFERENCES. ....	139
TABLE 5-2: LIST OF “CRISPR-BASED” GENES, MODIFIED IN PDACA CRISPR 01 CELLS COMPARED TO PDACA CRISPR EV CELLS. ....	145
TABLE 5-3: LIST “STIFFNESS-BASED” GENES, MODIFIED IN 0.7 KPA IN PDACA CRISPR 01 CELLS COMPARED TO PDACA CRISPR EV CELLS. ....	146
TABLE 5-4: LIST OF “STIFFNESS-BASED” GENES, MODIFIED IN 38 KPA IN PDACA CRISPR 01 CELLS COMPARED TO PDACA CRISPR EV CELLS. ....	147

## List of Figures

FIGURE 1-1: REPRESENTATION OF THE MECHANOSENSING AND MECHANOTRANSDUCTION JOURNEY WITHIN THE CELL.....	7
FIGURE 1-2: REPRESENTATION OF THE FOCAL ADHESION MATURATION STAGES.....	10
FIGURE 1-3: THE LOCALISATION OF LIM DOMAIN PROTEINS IS STIFFNESS-DEPENDENT.....	18
FIGURE 1-4: REPRESENTATION OF AJUBA/ZYXIN SUBFAMILY MEMBERS (HUMAN).....	21
FIGURE 1-5: SCHEMATIC REPRESENTATION OF THE CELL CYCLE AND ITS CHECKPOINTS.....	24
FIGURE 1-6: SUMMARY OF THE MECHANICAL PROPERTIES REPRODUCIBLE IN VITRO AND ASSOCIATED TECHNIQUES.....	30
FIGURE 3-1: ILLUSTRATION OF THE POLYACRYLAMIDE HYDROGEL CREATION PROCESS.....	64
FIGURE 3-2: PDACA CELLS CULTURED ON PAAM HYDROGELS DISPLAY CHANGES IN YAP LOCALISATION AND CELL MORPHOLOGY. ....	67
FIGURE 3-3: PAAM STIFFNESS IMPACTS THE CELLULAR PROLIFERATION OF PDACA CELLS.....	68
FIGURE 3-4: PAAM STIFFNESSES IMPACTS PDACA GENE EXPRESSION AT RNA LEVEL.....	70
FIGURE 3-5: EPSIN 3 RNA LEVELS ARE INCREASED ON 0.7 KPA COMPARED TO 38 KPA IN PDACA CELLS.....	73
FIGURE 3-6: SORBS2 RNA EXPRESSION IS NOT MODIFIED BY PAAM STIFFNESSES.....	75
FIGURE 3-7: TETRASPANIN 8 RNA LEVELS ARE INCREASED ON 0.7 KPA COMPARED TO 38 KPA IN PDACA CELLS. ....	77
FIGURE 3-8: AJUBA RNA AND PROTEIN LEVELS ARE DECREASED ON 0.7 KPA COMPARED TO 38 KPA IN PDACA CELLS.....	79
FIGURE 4-1: AJUBA IS LOCALISED AT THE CELL EDGE, THE CYTOPLASM AND THE NUCLEUS OF PDACA CELLS. ....	86
FIGURE 4-2: AJUBA LOCALISES AT MATURE SITES OF FOCAL ADHESION.....	88
FIGURE 4-3: THE EXPRESSION OF AJUBA IS INDEPENDENT OF FOCAL ADHESION FORMATION IN PDACA CELLS. ....	90
FIGURE 4-4: THE AJUBA SIRNA (3/5/7/8) TREATMENTS EFFICIENTLY DOWNREGULATE THE RNA AND PROTEIN LEVELS OF AJUBA IN PDACA CELLS.....	95
FIGURE 4-5: SUCCESSFUL DOWNREGULATION OF AJUBA AT RNA AND PROTEIN LEVELS IN PDACA CRISPR 01, PDACA CRISPR 02 AND PDACA CRISPR ALL CELL LINE COMPARED TO PDACA CRISPR EV. ....	96
FIGURE 4-6: THE DOWNREGULATION OF AJUBA INDUCES A DECREASE IN CELL-MATRIX ADHESION IN PDACA CRISPR 01, PDACA CRISPR 02, PDACA CRISPR ALL CELL LINES.....	99

FIGURE 4-7: THE DOWNREGULATION OF AJUBA HAS NO IMPACT ON THE PROLIFERATION IN PDACA CRISPR 01, PDACA CRISPR 02 AND PDACA CRISPR ALL, COMPARED TO PDACA CRISPR EV CELLS.....	100
FIGURE 4-8: THE DOWNREGULATION OF AJUBA DOESN'T CHANGE CELL SIZES IN PDACA CRISPR 01, PDACA CRISPR 02 AND PDACA CRISPR ALL COMPARED TO PDACA CRISPR EV.....	101
FIGURE 4-9: AJUBA DEPLETION DOESN'T IMPACT FOCAL ADHESION TURNOVER IN PDACA CRISPR 01 AND PDACA CRISPR 02 CELLS COMPARED TO PDACA CRISPR EV.....	103
FIGURE 4-10: THE DOWNREGULATION OF AJUBA HAS NO IMPACT ON THE MIGRATION OF PDACA CRISPR 01, PDACA CRISPR 02 COMPARED TO PDACA CRISPR EV CELLS.....	106
FIGURE 4-11: THE DOWNREGULATION OF AJUBA INCREASES PDACA CRISPR 01, PDACA CRISPR 02 AND PDACA CRISPR ALL CELLULAR INVASION COMPARED TO PDACA CRISPR EV CELLS.....	107
FIGURE 4-12: PDACA CRISPR EV, PDACA CRISPR 01, AND PDACA CRISPR 02 CELLS INVADING THROUGH MATRIGEL.....	108
FIGURE 4-13: THE DOWNREGULATION OF AJUBA DOESN'T VISUALLY IMPACT CELL SHAPE NOR CELL SIZE IN PDACA CRISPR 01, PDACA CRISPR 02 COMPARED TO PDACA CRISPR EV.....	110
FIGURE 5-1: PAAM STIFFNESSES HAVE A STRONG EFFECT ON PDACA RNA GENE EXPRESSION.....	120
FIGURE 5-2: PAAM STIFFNESSES HAVE A STRONG EFFECT ON THE TRANSCRIPTION FACTORS ACTIVITIES IN PDACA CRISPR EV.....	123
FIGURE 5-3: PAAM STIFFNESSES CAN INFLUENCE BIOLOGICAL PROCESSES IN PDACA CRISPR EV. ....	126
FIGURE 5-4: PAAM STIFFNESS STRONGLY IMPACTS BIOLOGICAL PROCESSES OF DNA TEMPLATED DNA REPLICATION AND FATTY ACID METABOLIC PROCESS IN PDACA CRISPR EV. ....	133
FIGURE 5-5: THE RNA EXPRESSION OF AJUBA IS IMPACTED BY PAAM HYDROGEL STIFFNESSES. ....	135
FIGURE 5-6: PAAM HYDROGEL STIFFNESS IMPACTS THE TRANSCRIPTION ACTIVITIES IN PDACACRISPR 01 CULTURED ON 38 KPA VERSUS PDACA CRISPR 01 CULTURED ON 0.7 KPA. ....	138
FIGURE 5-7: THE DOWNREGULATION OF AJUBA IN PDACA CRISPR 01 CELLS MODIFIES TRANSCRIPTION FACTORS ACTIVITIES.....	140
FIGURE 5-8: THE DOWNREGULATION OF AJUBA MODIFY THE RNA EXPRESSION OF SEVERAL GENES IN PDACA CRISPR 01 CELLS COMPARED TO PDACA CRISPR EV CELLS. ....	142
FIGURE 5-9: THE DOWNREGULATION OF AJUBA MODIFY THE RNA EXPRESSION OF FEW GENES IN PDACA CRISPR 02 CELLS COMPARED TO PDACA CRISPR EV CELLS. ....	143

FIGURE 5-10: REPRESENTATION OF THE RNA EXPRESSION IN PDACA CRISPR 01 OF AQP1, CADH16, FSN1 AND CGAS GENES ON 0.7 KPA AND 38 KPA. ....	152
FIGURE 5-11: CGAS AND FSCN1 RNA GENE EXPRESSION TESTED BY QPCR DOES NOT RECAPITULATE THE RNA SEQUENCING RESULTS. ....	153
FIGURE 5-12: AQP1 AND CDH16 GENE EXPRESSION TESTED BY QPCR RECAPITULATE THE RNA SEQUENCING RESULTS ON THE 0.7 KPA CONDITIONS. ....	154
FIGURE 7-1: AJUBA DEPLETION DOES NOT IMPACT FOCAL ADHESION NUMBER.....	170
FIGURE 7-2: THE STANDARD ERROR OF THE LOG FOLD CHANGE OF THE 2017 RNA SEQUENCING DATASET IS SUPERIOR TO THE 2023 DATASET.....	171
FIGURE 7-3: THE STANDARD ERROR RELATED TO COMMON GENES IS SUPERIOR IN THE 2017 RNA SEQUENCING DATASET COMPARED TO THE 2023 DATASET.....	172
FIGURE 7-4: THE STANDARD ERROR RELATED TO GENES, BOTH COMMON AND SIGNIFICANTLY MODIFIED, IS SUPERIOR IN THE 2017 RNA SEQUENCING DATASET COMPARED TO THE 2023 DATASET. ....	173
FIGURE 7-5: THE FOLD CHANGE DIRECTIONALITY OF THE SIGNIFICANT GENES IS CONSERVED IN BOTH DATASETS.....	174
FIGURE 7-6: THE COMMON BIOLOGICAL PROCESSES HAVE SIMILAR DIRECTIONALITY WITH LOWER P-VALUES OBSERVED IN THE 2017 DATASET.....	175
FIGURE 7-7: FUNCTIONAL ENRICHMENT ANALYSIS RESULTS REPRESENTING THE 2017 DATASET.....	176
FIGURE 7-8: FUNCTIONAL ENRICHMENT ANALYSIS RESULTS REPRESENTING THE 2023 DATASET.....	177
FIGURE 7-9: FUNCTIONAL ENRICHMENT ANALYSIS RESULTS REPRESENTING THE SIGNIFICANT GENES COMMON TO BOTH DATASETS.....	178

## Acknowledgements

I would like to thank my supervisor Laura Machesky for the opportunity to start a PhD in her lab and be part of this incredible team. Her support and guidance over the last four years have been instrumental in my development as a scientist, especially in navigating the challenges of the COVID-19 pandemic. I also want to thank her extensively for the support and time she gave me when I needed it. I would like to thank Cancer Research UK for funding my PhD and the Scotland Institute for the opportunity to work in such good conditions and environment, surrounded by cutting-edge scientists and advanced technologies. I would like to thank the Scotland Institute facilities such as the molecular technology department, the bioinformatic department and the microscopy department for their wonderful jobs and for being such wonderful talented and helpful men and women.

The past four years have been incredibly character-building years, and I wouldn't have been able to go through them without the unwavering support and guidance of all the R02 and R06 past and present members. Special thanks to both Amelie and Heather for their unwavering help, kindness and support, going far beyond the R02 benches. Too many to cite by name individually but each of them made the lab a welcoming environment filled with laughter, pranks and of course amazing science. I would like to thank them all deeply for it. I would like to thank especially Amelie, Heather, Jamie, Vassilis, Simona, Peggy and Nikki for their guidance, problem-solving skills and help both in and out of the lab. Thanks to Anh, I discovered the full discography of Taylor Swift, and over four years I fell under her charm as well and can now call myself a true Swifty. As a PhD student, the synergy going on between lab members creates powerful friendships fuelled by unlimited laughs and amazing cakes. I feel very lucky to have met all these wonderful people in my time in the R02-R06 lab. To Elaine and Hakem, doing this PhD alongside you was an incredible experience, filled with many challenges of course but I am glad we did this together. And of course, Amelie, a fellow compatriot and great friend, I would like to extend my deepest gratitude for your friendship, your bits of advice and your time. You were always here no matter

what was happening. These four years wouldn't have been the same without you so thank you for everything.

I would also thank my family for all the opportunities they gave me, and for their willingness to let me go live so far away even though I might only come back home once or twice a year. I truly appreciate all the sacrifices they made to allow this to happen and for their unwavering support along the way. To my friends who kept me going through this emotional rollercoaster, you are the absolute best and I will soon come back home to celebrate the start of this new era with you.

Finally, to Nathan, my partner, best friend and future husband. We have come a long way since the university benches, where we talked about our future careers and future PhD. We didn't expect to both start our PhD in Scotland, a mere 145 miles away from one another. Despite the distance, I truly wouldn't have been able to manage these four years without your love and support. I am deeply grateful to you for everything you have done, and I look forward to this post-PhD life by your side.

## Author's Declaration

I declare that this thesis is the result of my own work, unless stated otherwise. No part has been submitted for the accomplishment of another degree at the University of Glasgow or any other University.

Sonia Rolo

June 2024

## Abbreviation

°C Degree celsius .....	44
µg Microgram .....	45
µL Microlitre .....	45
µM Micromolar .....	54
2D Two dimension .....	30
3D Three dimension .....	30
AKT Protein kinase B .....	77
AP2 Adaptor complex 2 .....	72
APS Ammonium persulfate .....	52
AQP1 Aquaporin 1 .....	149
ArgBP2 Arg-binding protein 2 .....	74
Arp 2/3 complex Actin Related Protein 2/3 complex .....	28
ATP Adenosine triphosphate .....	27
bHLH Basic helix-loop-helix .....	122
BP Biological process .....	118
BRCA2 Breast cancer gene 2 .....	5
BUB Budding uninhibited by benzimidazoles .....	25
BUBR1 Bub1-related kinase .....	25
C-abl Abelson Tyrosine Kinase .....	75
Cas9 CRISPR associated protein 9 .....	48
CBM Clathrin binding motif .....	72
c-CBL Casitas B lineage lymphoma .....	75
CDH16 Cadherin 16 .....	149
cdk1 Cyclin dependent kinase 1 .....	25
CDKN2A Cyclin-dependent kinase inhibitor 2A .....	5
CGAS Cyclic GMP-AMP Synthase .....	149
CI Cell Index .....	98
cm Centimetre .....	44
CO <sub>2</sub> carbon dioxide .....	44
ConA Concanavalin-a .....	90
CRISPR Clustered regularly interspaced short palindromic repeats .....	48
CRP Cysteine-rich protein .....	20
DMEM Dulbecco modified eagle media .....	44
DMSO Dimethyl sulfoxide .....	45
DNA Deoxyribonucleic acid .....	3
ECM Extracellular Matrix .....	2



ENTH Epsin N terminal homology .....	72
ER Endoplasmic reticulum .....	16
ETS E26 transformation-specific .....	122
FA Focal adhesion.....	9
F-actin Filamentous actin .....	10
FAK Focal adhesion kinase .....	9
FBS Foetal bovine serum .....	44
Fscn1 Fascin 1.....	149
G-actin Globular actin .....	13
Gfi1 Growth factor independent-1 .....	26
GLUT1 Glucose transporter 1 .....	28
GSEA Gene set enrichment analysis.....	55
GTP Guanosine triphosphate .....	5
h Hours .....	46
h <sub>2</sub> O <sub>2</sub> hydrogen peroxide .....	52
HDAC histone deacetylase .....	26
HEPES 4-(2-hydroxyethyl)-1-piperazineethanesulfonic acid .....	53
Hpo Hippo .....	21
kb Kilobases.....	49
Kid3 Zinc Finger Protein 354C .....	123
kPa kilo Pascal .....	30
KRAS Kirsten rat sarcoma viral oncogene homolog .....	5
Krox20 Early Growth Response Protein 2 .....	15
LATS1/2 Large tumour suppressor kinase1/2 .....	14
LB L-Broth .....	50
LIM Lin-11, Isl1,MEC-domain .....	17
Limd1 LIM domains protein 1 .....	17
LIM-hd LIM- homeodomains.....	20
Lmk1 LIM domain kinase 1.....	20
Lmk2 LIM domain kinase 2.....	20
LMO LIM domain Only genes .....	20
LMO1 LIM domain only 1 .....	20
LMO4 LIM domain only 4 .....	20
Lpp lipoma-preferred partner .....	22
LXR $\alpha$ Liver X receptor alpha .....	27
Lyl-1 LYL1 Basic Helix-Loop-Helix Family Member .....	123
M Molar.....	46
MAD Mitotic arrest deficient .....	25

Mats Mob-as-tumor-suppressor .....	21
min minute .....	44
mL milliliter .....	44
MMP Metalloprotease .....	29
MRF4 Myogenic regulatory factor 4 .....	123
mRNA Messenger RNA .....	32
MRTFs myocardin-related transcription factors .....	15
MST1/2 Mammalian STE20-like kinase 1/2 .....	14
MTUS1 Microtubule-associated tumor-suppressor 1 gene .....	75
MyoD Myogenic differentiation 1 .....	123
NES nuclear export signal .....	22
NF-Y Nuclear Factor-Y .....	15
NF- $\kappa$ B Nuclear factor- $\kappa$ B .....	15
NH <sub>3</sub> Ammonium hydroxide .....	52
NLS Nuclear localisation signal .....	22
nM Nanomolar .....	46
NPC Nuclear pore complex .....	16
OD Optical density .....	56
Pa Pascals .....	3
PAAM Polyacrylamide hydrogel .....	52
PanIN Pancreatic intraepithelial neoplasia .....	5
PBS Phosphate buffer saline .....	53
PCR Polymerase chain reaction .....	48
PDAC Pancreatic ductal adenocarcinoma .....	4
PFA Paraformaldehyde .....	59
PFS PBS, fish skin gelatin, saponin buffer .....	60
pH Potential of hydrogen .....	2
PPAR $\gamma$ Peroxisome proliferator-activated receptors $\gamma$ .....	27
Prmt5 Protein arginine methyltransferase-5 .....	26
PTP-PEST protein-tyrosine phosphatase – PEST .....	75
RAR Retinoic acid receptors .....	27
RAR $\alpha$ Retinoic acid receptor alpha .....	27
Rho Ras homolog gene family .....	20
RIN RNA integrity number .....	55
RNA Ribonucleic acid .....	48
RORA Retinoic acid receptor-related orphan receptor .....	75
RT Room temperature .....	45
RXRs Retinoid X receptors .....	27

Sav Salvador .....	21
SCAR Suppressor of cAMP receptor .....	28
sec Seconds .....	49
SF Stress fibers .....	8
sgRNA Single guides RNA .....	48
siRNA small interfering RNA .....	46
SMAD Suppressor of Mothers against Decapentaplegic.....	122
SMAD4 SMAD family member 4 .....	5
SNAG SNAIL/Gfi-1.....	26
SOHO Sorbin homology.....	75
Sorbs Sorbin and SH3 domain-containing protein .....	74
Sorbs1 c-Cbl associated protein .....	75
Sorbs2 Sorbin and SH3 domain-containing protein 2 .....	74
Sorbs3 Sorbin and SH3 domain-containing protein 3 .....	75
Sox2 SRY (sex determining region Y)-box 2 .....	15
Sp1 Specific protein 1 .....	26
SRF serum response factor.....	15
STAT3 Signal transducer and activator of transcription 3 .....	77
Sulfo-SANPAH Sulfosuccinimidyl 6-(4' -azido- 2' -nitrophenylamino) hexanoate .....	52
TAE Tris base, acidic and EDTA.....	49
TEAD Transcriptional enhanced associate domain .....	14
TEMED N,N,N',N' -Tetramethylethylenediamine .....	52
Tp53 Tumor protein 53 .....	5
Trip6 Thyroid hormone receptor-interacting protein 6 .....	22
UIM Ubiquitin interacting motif.....	72
UV Ultraviolet.....	49
V Volt.....	56
WAVE WASP-family vevprolin homology protein .....	28
Wtip Wilms tumour 1 interacting protein.....	21
Wts Warts.....	21
WWTR1/TAZ WW Domain-Containing Transcription Regulator Protein 1 .....	7
YAP Yes-associated protein .....	7
$\alpha$ Alpha .....	9
$\beta$ Beta .....	9

## Chapter 1. Introduction

## 1.1 Cellular microenvironment and surrounding forces

Since 1889 and the publication of the “seed and soil theory”, researchers have aimed to better understand cancers and metastatic events (Paget, 1889). Stephen Paget hypothesised that metastasis isn’t a random event but rather a seeding ability in specifically targeted microenvironments and organs. In his theory, the cancer cell represents the “seed”, while the microenvironment represents the “soil”. Paget’s hypothesis was validated which opened research opportunities aiming to elucidate how cellular microenvironments impact cellular behaviour (Langley & Fidler, 2011). The cellular microenvironment is defined as a niche composed of the cells, fluids and the extracellular matrix (ECM). The ECM, a major component of the cellular microenvironment, is a well-organized three-dimensional network of macromolecules, which includes fibres and growth factors, alongside proteoglycans and a plethora of bioactive molecules. (Mierke, 2024; Yue, 2014). It provides biochemical and biomechanical cues, serves as a scaffold for cells and maintains hydration and potential of hydrogen (pH) in the environment. The relationship between cells and their ECM is dynamic and bidirectional (Miller et al., 2020). ECM composition and structure depend on the synthesis, deposition, and remodelling of the ECM protein by surrounding cells. Whereas changes in the ECM composition and structure can alter tissue homeostasis and development, as well as cells function, adhesion, proliferation, morphology and survival (Karamanos et al., 2021; Mierke, 2024; Miller et al., 2020). Researchers, like Alexandra Naba, have been dedicating their time to study and facilitate ECM research. They have developed new tools through the Matrisome project including, MatrixDB and MatrisomeDB (Apte & Naba, 2023), which are databases where researchers can learn more about the ECM of various healthy and diseased tissues.

Reaction to mechanical stimuli is key for the survival of cellular organisms and is evolutionarily ancient, as it reflects the need for adaptability of cells and organisms to environmental modification. For example, mechanosensitive ion

channels emerged early in evolution, as evidenced by their presence in lower eukaryotes, and prokaryotes, such as bacteria, in response to osmotic pressure (Martinac & Kloda, 2003). Mechanical signals from the ECM include among others, tensile/ compression, elasticity, and stiffness (Northey et al., 2017; Vining & Mooney, 2017).

-Compression/tensile stress: reaction to a linear force, resulting in the decrease or increase in the area of an object.

-Elasticity represents the ability of an object to invert its deformed state back to its original form after the strain has been removed.

-Stiffness: related notion to the elasticity of a material and depends on the load-displacement curve of the tested material.

In the engineering field, the Young's modulus, measured in Pascals (Pa), has been defined as mathematical calculation of the elasticity of an object, representing the ratio of tensile stress to tensile strain. This measurement is used heavily in bioengineering to measure the elasticity of materials, also referred to as stiffness.

Each cell type will experience one or a combination of different mechanical forces (Wang & Li, 2010). The cohesion of tissue and organs requires attachment between cells, the balance of forces and attachment with ECM. Each tissue and organ's composition is specific; therefore, every ECM will be unique to its surrounding environment (Buxboim et al., 2010).

## **1.2 Cancers and unbalanced forces**

### **1.2.1 Cancer**

Cancer represents a disease where a cell escapes the body's surveillance system and checkpoints that are responsible for balanced proliferation (Cell cycle transitions checkpoints), assuring genetic stability (deoxyribonucleic acid (DNA) damage checkpoint), and immune surveillance (Chung et al., 2010; Molinari, 2000; Wu et al., 2022). These mechanisms were grouped and unified around the term hallmark of cancer (Hanahan & Robert, 2011; Hanahan &

Weinberg, 2000; Natalya & Craig, 2016). The hallmarks of cancer consist of the fundamental steps of the malignant transformation. Cancer evolves around the ability to sustain proliferative signalling, evade growth suppressors, activate invasion and metastasis, enable replicative immortality, induce angiogenesis, induce metabolic reprogramming and resist cell death (Hanahan, 2022; Natalya & Craig, 2016). When cancer cells escape physiological regulation, it creates abnormal forces both inside the cells and in the surrounding environment. For example, pancreatic cancer is known for drastic changes in its ECM.

Changes in the ECM composition or structure can promote or result from the apparition of diseases so much that it is now used as prognosis value for some diseases and treatment opportunities (Ahluwalia et al., 2021; Parker et al., 2022; Y. Wu et al., 2021). For example, in cancer, the changes in the ECM are driven by the development and growth of the tumor as well as the modified deposition and remodelling by cancer and cancer-associated cells. The dysregulated ECM, tailored around abnormal tumour secretions, and abnormal proliferation by cancer cells and cancer-associated fibroblasts becomes a source of aberrant environmental cues and is considered a hallmark of solid cancer (Cox, 2021; Kai et al., 2019).

### **1.2.2 Pancreatic cancer and its microenvironment**

Pancreatic cancer is a genetically heterogeneous cancer and currently listed as the 4<sup>th</sup> deadliest cancer worldwide. Pancreatic cancer patients suffer from low chances of survival and tend to be diagnosed at advanced stages. Indeed, 80% of patients are diagnosed with unresectable or metastatic forms of pancreatic cancer. In 2016 Bailey et al. published a classification of pancreatic cancers (Bailey et al., 2016; Mizrahi et al., 2020). Four subtypes of pancreatic ductal adenocarcinoma (PDAC) were defined: squamous, pancreatic progenitor, ADEX and immunogenic subtypes, based on gene expression, histopathology characteristics and survival (Bailey et al., 2016). Appropriate classification can be a great tool for better therapeutic approaches and improve future outcomes for patient survival (Torres & Grippo, 2018).

PDAC is the most common type of pancreatic cancer, accounting for 90% of the cases (Kleeff et al., 2016; Orth et al., 2019). PDAC is an aggressive solid tumour with important invasion and metastasis abilities (Orth et al., 2019). Highly resistant to therapy, PDAC is one of the most lethal solid tumours, highly difficult to diagnose at an early stage and therefore to cure (Hadden et al., 2020). Nowadays, treatments include a combination of traditional treatments (for example surgery, radiotherapy and chemotherapy) with targeted therapies and immunotherapies, tailored around knowledge of tumour stage, tumour specificity and patient-based sensitivity (Zhao & Liu, 2020).

PDAC displays multiple genetic mutations acquired throughout the stages of pancreatic intraepithelial neoplasia (PanIN) lesion, for example, Kirsten rat sarcoma viral oncogene homolog (KRAS) in panIN-1, panIN-2 will acquire mutation on cyclin-dependent kinase inhibitor 2A (CDKN2A), panIN-3 on breast cancer gene 2 (BRCA2),

SMAD family member 4 (SMAD4) and tumor protein 53 (Tp53), which will promote PDAC formation (Feldmann et al., 2007; Iacobuzio-Donahue et al., 2012; Olaoba et al., 2024). KRAS mutations have been discovered in over 90% of PDAC and could be one of the triggering signals of tumour initiation (Orth et al., 2019). KRAS is a small GTPase protein regulating cell migration, survival, differentiation, and proliferation through its guanosine triphosphate(GTP)-ase activity downstream of growth factor receptors (Luo, 2021). The mutation in the KRAS genes triggers a constant active state of oncogenic protein driving tumour development and progression (Zhang et al., 2023).

PDAC's particularity among solid tumours is its extreme desmoplastic reaction (Iacobuzio-Donahue et al., 2012). The desmoplastic reaction combines overproduction, deposition of extracellular matrix proteins and important proliferation of myofibroblast-like cells (Whatcott et al., 2012). It leads to large tumour and high matrix rigidity. The desmoplastic reaction would result in elevated hydrodynamic pressure, hypoxia, nutrient deprivation and increased matrix stiffness (Hadden et al., 2020). It therefore increases invasiveness and poses major restrictions to drug delivery to the tumour. Understanding the

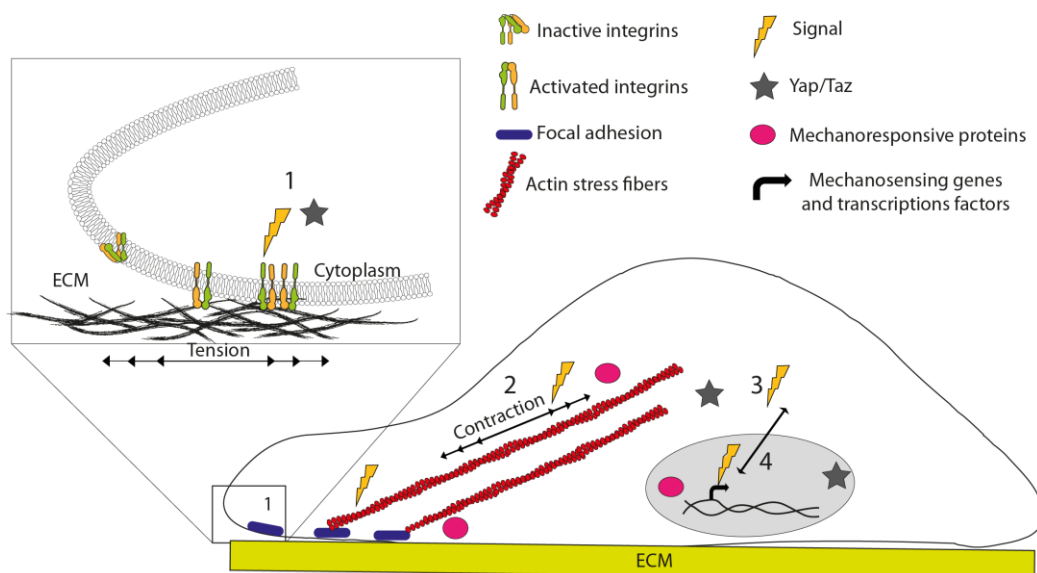


complexity of forces within solid tumours and how they affect cellular behaviour would improve the development of new therapies more suited to target complex solid tumours like PDAC (Hadden et al., 2020).

### **1.3 The journey of mechanical cues: from membrane to nucleus**

#### **1.3.1 Mechanosensing and mechanotransduction**

Mechanical signals will arise from the ECM (topography, composition, forces) triggering changes in cell behaviour and functions. In this section, I will articulate the detailed journey of these mechanical cues, from the cell membrane to the nucleus (Figure 1-1). First of all, the signalling starts with a “mechanosensing” event where the cell senses mechanical stimuli at the cell membrane using mechanosensing molecules (Jansen et al., 2017). Mechanosensing molecules are defined as molecules or proteins undergoing a conformation change in response to a mechanical input, for example: integrin, force-sensitive ion channels and membrane receptors (Jansen et al., 2017). This change of state can be different among mechanosensors. For example, talin, a focal adhesion protein, will undergo a structural change to expose cryptic hydrophobic binding sites, which will bind to vinculin via its head domain (Martino et al., 2018). After the mechanical cues are sensed, the forces are converted into a biological response (Martino et al., 2018). This conversion is called mechanotransduction and uses intracellular biochemical signalling through signalling cascades of cellular and molecular events (Wang & Li, 2010). Proteins and molecules taking part in the production or transmission of mechanical-induced signalling throughout the cell are called mechanotransduction actors or mechanotransducers (Martino et al., 2018).



**Figure 1-1: Representation of the mechanosensing and mechanotransduction journey within the cell.**

1: Binding of membrane receptors to ECM ligand, activation of membrane receptors (mechanosensing), triggering their conformation change and inducing the formation of focal adhesion sites. 2: The signal is converted into an intracellular signalling and into intracellular forces transmitted by actin stress fibers, through cytoskeleton contractions and by secondary messengers. 3: The information is transmitted from the cytoplasmic compartment to the nuclear compartment by Yes-associated protein (YAP)/ WW Domain-Containing Transcription Regulator Protein 1 (WWTR1/TAZ) and other mechanotransduction actors. 4: The transmitted signal will induce changes in transcription factors activities and gene expressions.

### 1.3.2 Cellular membrane

Mechanical inputs directly impact the membrane due to its proximity to the ECM. Cell membranes exhibit mechanical elasticity, enabling them to deform under force. When force is applied, it triggers the deformation of the membrane or the displacement and diffusion of its molecules within the membrane. This also triggers a mechanical restoring force, as required by the principle of mechanical equilibrium, which states that every applied force generates an equal and opposite reaction (Groves, 2019). Changes to the membrane, induced by mechanical forces, can also include changes in membrane shape, fluidity, tension, and molecular organisation (Groves, 2019). These changes will have a ripple effect on membrane dynamics, permeability, vesicle formation, and transport processes (Ferguson et al., 2017). Mechanosensing proteins within the membrane, such as integrins, force-activated ion channels, and receptors, detect mechanical forces and initiate mechanotransduction pathways through conformation changes.

(Martino et al., 2018). One specific structure involved in membrane mechanical sensing is the Caveolae. Caveolae are cup-shaped invaginated membrane domains enriched in cholesterol and sphingolipids, highly abundant in mechanically stressed cells (Sinha et al., 2011). These dynamic structures are associated with several cytoskeletal filaments (actin filaments, microtubules, and intermediate filaments and actin stress fibers (SF) (Echarri & Del Pozo, 2015; Sotodosos-Alonso et al., 2023). While their precise roles remain debated, they contribute to membrane organisation, tension adaptation, and lipid homeostasis (Echarri & Del Pozo, 2015; Sinha et al., 2011). Caveolae also regulate cellular processes such as several mechanotransduction pathways and clathrin-independent endocytosis. Due to their localisation at the plasma membrane, mechanical inputs such as tension will alter caveolae shapes, affecting their invagination and curvature, thereby offering a tension buffering system (Del Pozo et al., 2021; Sinha et al., 2011; Sotodosos-Alonso et al., 2023). At low tension or upon the release of mechanical tension, the caveolae structure will be organised into caveolae clusters or rosettes (Del Pozo et al., 2021; Sotodosos-Alonso et al., 2023). In contrast, an increase in tension induces the rapid disassembly of caveolae, first into single caveolae, which will progress into the flattening of caveolae, and release some of their components, which in turn are involved in intracellular signalling (Del Pozo et al., 2021). In addition to their mechanoprotective role, caveolae function as mechanosensors through the release of several components such as Eps15 homology domain 2 (EHD2) and cavins (Del Pozo et al., 2021).

### 1.3.3 Focal adhesion

A focal adhesion (FA) is an integrin-mediated adhesion structure, serving as the primary hub of interaction between the ECM and the cell, linking them together (Dufort et al., 2011; Elosegui-Artola et al., 2014; Shemesh et al., 2005). In mechanosensing, the role of FA will be to transfer mechanical cues from outside the cell to the cellular cytoskeleton (Martino et al., 2018; Oakes & Gardel, 2014).

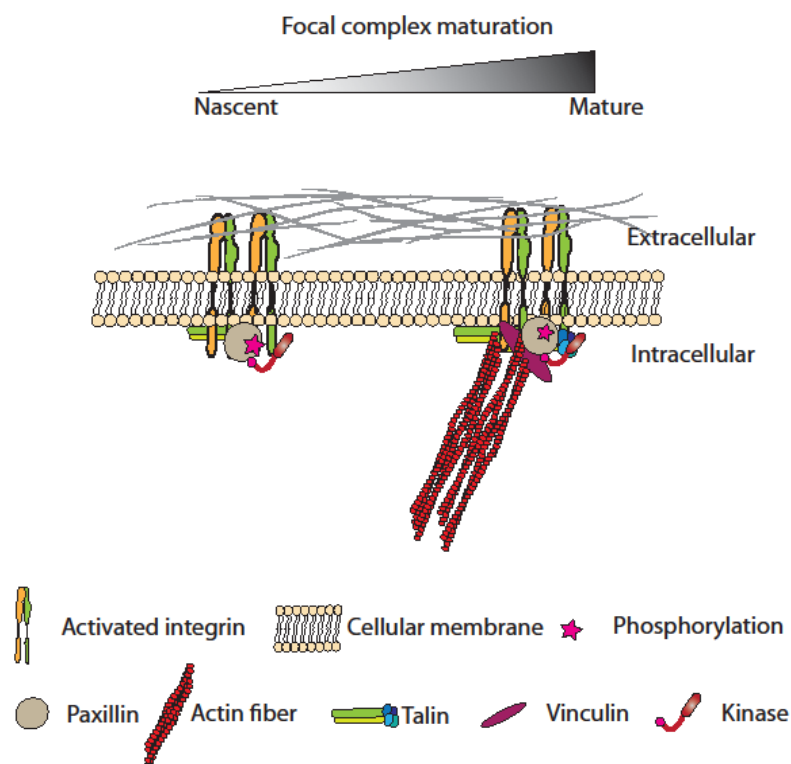
Focal adhesions are highly dynamic complexes, constantly assembling and disassembling to reflect a signal in the ECM or cellular need in adhesion or movement (Figure 1-2). The integrin adhesion complexes proteomes have shown 2,412 proteins in the meta-adhesome, from which 60 proteins were identified as part of the consensus adhesome (Horton et al., 2015; Horton et al., 2016). These complexes are composed of over 150 different components and their compositions is dictated by the integrin-specific ECM ligands (Oakes & Gardel, 2014). Integrins are heterodimeric transmembrane receptors embedded in the cell membrane, containing both transmembrane and intracellular components. Integrins are composed of alpha ( $\alpha$ ) and beta ( $\beta$ ) subunits, which will dictate their affinity with matrix molecules (Sun et al., 2016). Integrins' affinity and regulation are part of the "inside-out" signalling, regulating adhesion and migration capabilities (Springer & Dustin, 2012).

The initial step of focal adhesion formation is the activation of integrin (from a low to a high-affinity state) by binding to a specific ECM ligand, triggering the conformational change of integrin and its clustering (Schumacher et al., 2022). After activation of the integrins, adaptor proteins will be recruited at these sites of nascent focal adhesion. Adaptor proteins are crucial in focal adhesions, as they help the docking of all other proteins and interactors to the complexes as well as create a link between the cytoplasmic side of the integrin and the cytoskeleton (Henning Stumpf et al., 2020).

Nascent focal adhesions are submicron structures, highly unstable, composed of a cluster of activated integrins and several scaffold/adaptor proteins and kinases including, focal adhesion kinase (FAK), talin, and paxillin (Figure 1-2) (Henning Stumpf et al., 2020). Only a portion of the nascent focal adhesions will go through the maturation process. At nascent focal adhesion, FAK will autophosphorylate and recruit downstream cytoskeletal mechanotransducers (Martino et al., 2018; Tilghman & Parsons, 2008). Talin contains a site of adhesion for integrin, several sites for vinculin and two for filamentous actin (F-actin) (Martino et al., 2018). Under mechanical force, talin will open binding sites for vinculin, activating vinculin via conformation changes upon binding (Yao et al., 2014). Altogether, these proteins and kinases will enhance the recruitment of binding partners,

secondary messengers and other mechanosensors to build a stable focal adhesion site and propagate mechanical signals through the cytoskeleton (Martino et al., 2018).

Activated vinculin, linked to talin, will bind to F-actin to create a strong and stable connection between the activated integrin and the actin stress fibers component F-actin (Sun et al., 2016). Actin stress fibers are bundles of actin filaments (between 10 and 30) attached together by crosslinking proteins, creating a bridge between the actin cytoskeleton and the membrane (Pellegrin & Mellor, 2007). Actin stress fibres will be recruited and linked to the FA complex when the complex is both mature and stable enough to transmit forces as the tension/stiffness information will be transduced as contraction/tension through the cytoskeleton (Figure 1-2).



**Figure 1-2: Representation of the focal adhesion maturation stages.**

The formation of focal adhesion is dynamic and based on an assembly/disassembly cycle, involving a wide range of actors.

### 1.3.4 Transmission of tension through the cytoskeleton

The cytoskeleton is a dynamic network coordinating the organisation, shape and overall architecture of the cell (Martino et al., 2018). This network maintains the integrity of the intracellular compartments by physically resisting deformation and will additionally generate and direct forces through the polymerisation and depolymerisation of its networks. The cytoskeleton is composed of three main fibrous networks: microtubules, intermediate filaments and the actin cytoskeleton.

Microtubules are dynamic tubular structures composed of 13 protofilaments, made of polymerised  $\alpha$  and  $\beta$  tubulin dimers into a long hollow polymer, organised around a centrosome, undergoing continual assembling and disassembling cycles to participate in the cytoskeleton organisation and force generation (Horio & Murata, 2014). Microtubules are multitasking elements with roles in capturing membrane-bound organelles and chromosomes, modifying the position of the nucleus, remodelling the membranes as well as generating pulling forces (Gudimchuk & McIntosh, 2021). The two ends of each microtubule are different; indeed, the Minus end has  $\alpha$ -tubulin exposed while the Plus end has  $\beta$ -tubulin exposed. Each protofilament is assembled by the addition of GTP-tubulin at their ends, which turns into GDP-tubulin after incorporation. Their assembly/disassembly cycles happen from both ends and are known as “dynamic instability”.

Intermediate filaments are non-polar and highly flexible filaments, whose composition depends on the cell type analysed (Herrmann & Aebi, 2016). Six groups of intermediate filaments were identified, regrouping more than 70 different proteins, including vimentins, keratins, and laminins (Schwarz & Leube, 2023). Although the composition can be different, they all share a common tripartite structure made of a defined central rod and highly divergent, polypeptide-specific head and tail domains (Schwarz & Leube, 2023). The intermediate filaments connect to several cytoskeleton components like microtubules, the actin cytoskeleton, thus allowing the stabilization of cellular

protrusions, organelle functions and positioning, metabolism, stress responses, structuring of cell shapes, and protection of the nucleus (Schwarz & Leube, 2023). The different functions will be dictated by the unique filament network composition and architecture.

Actin filaments are two stranded helical polymers formed of globular actin (G-actin), F-actin and actin binding proteins assembled in a polar fashion (David Sept, 1999). The actin polymerization process consists of an actin nucleation step followed by the quick elongation of actin filament by polymerisation. The actin nucleation step is the formation of a G actin trimer. The polymerisation of actin filament is an ATP-Mg<sup>2+</sup> dependent process and consists of the addition of monomers to pre-existing filaments (Zigmond, 1998). ATP-Mg<sup>2+</sup> needs to bind cytoplasmic G-actin, which in turn will be incorporated in the filament “barbed-end”. After incorporation, ATP will be hydrolysed into ADP-actin in a gradient manner. Opposite to the “barbed end”, the “pointed end” will be ADP-actin rich, from where ADP-actin can be released for depolymerization purposes or for replenishing the cytoplasmic pool of G-actin, transformed back into ATP-actin, and reincorporated back on the actin filament’s “barbed end” (Bindschadler et al., 2004). The nucleation and polymerisation steps are tightly regulated by activators such as the Arp2/3 and the SCAR/WAVE complexes, and by inhibitors like the ADF/Cofilin family members and myosin II (Sibony-Benyamini & Gil-Henn, 2012). This tight regulation allows the cells to generate contractile forces by polymerisation, modify cellular morphology, cellular locomotion, as well as cellular processes (Sibony-Benyamini & Gil-Henn, 2012; Svitkina, 2018; Zigmond, 1998).

### **1.3.5 Transcriptional coactivators: YAP/TAZ**

The formation of focal adhesions leading to an increase in actin fibers will induce the activation and translocation of YAP/TAZ to the nucleus (Cheng et al., 2023). YAP/TAZ is a key element in mechanotransduction, relaying cytoskeleton tension signal to the nucleus, which in turn regulates cell function and cell homeostasis

through gene and transcription factors regulation (Cai et al., 2021; Dupont et al., 2011). To date, various inputs have been linked to YAP/TAZ activity, including, among others, mechanical force, proliferation, cell adhesion, hypoxia, energy metabolism, and osmotic stress (Cassani et al., 2023; Chang et al., 2023; Dupont et al., 2011). YAP/TAZ can be both tumour promotor and tumour suppressor, by acting either as transcription coactivators or corepressor (Luo et al., 2023). YAP/TAZ is part of the Hippo pathway and can help the cell to sense its shape (geometry, polarity), cell environment and allow the communication of mechanical signals to coordinate cell responses (Mokhtari et al., 2023; Antonio Totaro et al., 2018). The Hippo pathway was first identified in *Drosophila* 20 years ago and was identified as a key regulator in organ development (Staley & Irvine, 2012). The Hippo pathway's core is a kinase cascade formed by Mammalian STE20-like kinase 1/2 (MST1/2) and large tumour suppressor kinase1/2 (LATS1/2). It has been previously demonstrated that YAP/TAZ activity is modulated by ECM stiffness and growth signals through the Hippo pathway (Zhao et al., 2007). Hippo kinases LATS1 and LATS2 can be phosphorylated by MST1 and MST2 kinases (upstream kinases), activating them. LATS1 and LATS2 will then be able to phosphorylate YAP/TAZ (Zhao et al., 2007). The phosphorylation of YAP/TAZ triggers its inactivation, and sequestration in the cytoplasm, leading in certain occasions to proteasomal degradation (Panciera et al., 2017; Zhao et al., 2023).

To deliver the signal to the nucleus, YAP/TAZ needs to be dephosphorylated, allowing YAP/TAZ to shuttle to the nucleus. For example, high ECM stiffness leads to cytoskeleton tension which results in Hippo pathway inactivation and YAP/TAZ translocation in the nucleus (Elosegui-Artola et al., 2017; Emon et al., 2023).

### 1.3.6 Nuclear mechanotransduction

Following the translocation of YAP/TAZ into the nucleus, YAP and TAZ lack the ability to bind to DNA directly. Instead, YAP/TAZ must bind to transcription factors or to the transcriptional enhanced associate domain (TEAD) complex to bind to DNA molecules (Panciera et al., 2017; Zhao et al., 2023). The TEAD-YAP/TAZ complex will be recruited at distant enhancers to induce the transcription of targeted genes (Zhao et al., 2023). Distant enhancers are regulatory DNA



sequences activating over long-distance gene transcription. The recruitment to distance enhancer will allow YAP/TAZ to modify gene expression and trigger a cascade of effects on cell behaviour. Although YAP/TAZ are major actors in mechanotransduction, they are not the only actors involved in the signalling cascade of mechanical signals from the cytoplasm to the nucleus.

Many transcription factors will show a mechanoresponsive activity, including YAP/TAZ (Matsuda & Mofrad, 2022), myocardin-related transcription factors (MRTFs) (Matsuda & Mofrad, 2022), serum response factor (SRF) (Parreno et al., 2017; Sidorenko & Vartiainen, 2019), Nuclear Factor-Y (NF-Y) (Ebrahimighaei et al., 2024), SRY (sex determining region Y)-box 2 (Sox2) (Rosso et al., 2022), Early Growth Response Protein 2 (Krox20) (Rosso et al., 2022), Nuclear factor- $\kappa$ B (NF- $\kappa$ B) (Ishihara et al., 2013). Among these, MRTF is a key mechanosensitive transcriptional co-activator linking the cytoskeleton organisation and gene expression (Speight et al., 2016). MRTF is a central molecule the cytoskeleton uses to regulate the expression of its components. Both YAP and MRTF shuttle between the cytoplasm and the nucleus, accumulating in response to matrix stiffness and cellular tension (Speight et al., 2016). MRTF's N-terminal binds to G-actin, which masks its MRTF NLS, and suppresses its ability to shuttle to the nucleus. During actin polymerisation, the cytoplasmic G-actin pool will be recruited to sustain actin polymerisation. G-actin molecules will be recruited, inducing the dissociation of G-actin from the MRTF N-terminal. Freeing the MRTF, NLS will facilitate its uptake by the nucleus, in which MRTF binds to SRF. MRTF-SRF complex will then drive gene expression, which is mainly targeted towards regulating the expression of cytoskeleton components (Speight et al., 2016). SRF is a conserved transcription factor whose activation can be regulated by the polymerisation of actin in the cytoplasm (Sidorenko & Vartiainen, 2019). Additionally, nuclear actin also plays an important role in the regulation of MRTF-A (homologous MRTF member), via regulation of its localisation and its intranuclear activity (Parreno et al., 2017; Sidorenko & Vartiainen, 2019).

The nucleus possesses also its own ability as a mechanosensitive apparatus (Niethammer, 2021). Indeed, the nuclear membrane, the nuclear pore complex (NPC), chromatin and nuclear lamina are nuclear components articulating nuclear

mechanotransduction (Swift & Discher, 2014). Primarily, the nuclear membrane is composed of an inner and outer membranes, forming invagination called nucleoplasmic reticulum. The nucleoplasmic reticulum, linked to the endoplasmic reticulum (ER), can sense and transduce mechanical signal from nuclear shape changes. The deformation of the nucleus by forces triggers calcium release through mechanosensitive cation channels at the nuclear membrane (Miroshnikova & Wickström, 2022). Secondly, nuclear pore complexes are large multiprotein complexes located within the nuclear envelope. NPCs link the nucleoplasm and cytoplasm compartments facilitating molecular exchanges in eukaryotic cells. Small molecules will travel via passive diffusion while transporters will allow the transport of large molecules such as functional proteins, RNAs and ribosomes both ways between the nucleus to the cytoplasm (Jamali et al., 2011). Additionally, their roles also include the regulation of transcription activities (spatial and temporal), and gene expression, via interaction with the chromatin and its organization (Jamali et al., 2011; Pascual-Garcia & Capelson, 2021; Raices & D'Angelo, 2017). Mechanical forces modify NPCs, triggering the dilatation of NPC pores, reducing the transport barrier, and promoting the entry of transcription factors into the nucleus (Matsuda & Mofrad, 2022).

Thirdly, the chromatin refers to the compacted genome organised in the nucleus around histones. The compaction of the chromatin is dynamic due to the chromatin remodelling complexes and histone modifications (Sahu et al., 2020). Indeed, the chromatin condensation varies and adapts according to histone methylation and nuclear deformation, both factors which can open or close the accessibility for gene transcription (Martire & Banaszynski, 2020; Willcockson et al., 2021). Finally, the nuclear lamina is a layer of intermediate filaments localised between the nuclear membrane and the chromatin, arranged into a thick meshwork of filaments, acting as a protective barrier against mechanical forces (Swift & Discher, 2014). Indeed, without the nuclear lamina, ECM and cytoskeletal tensions could damage the chromatin (Niethammer, 2021).

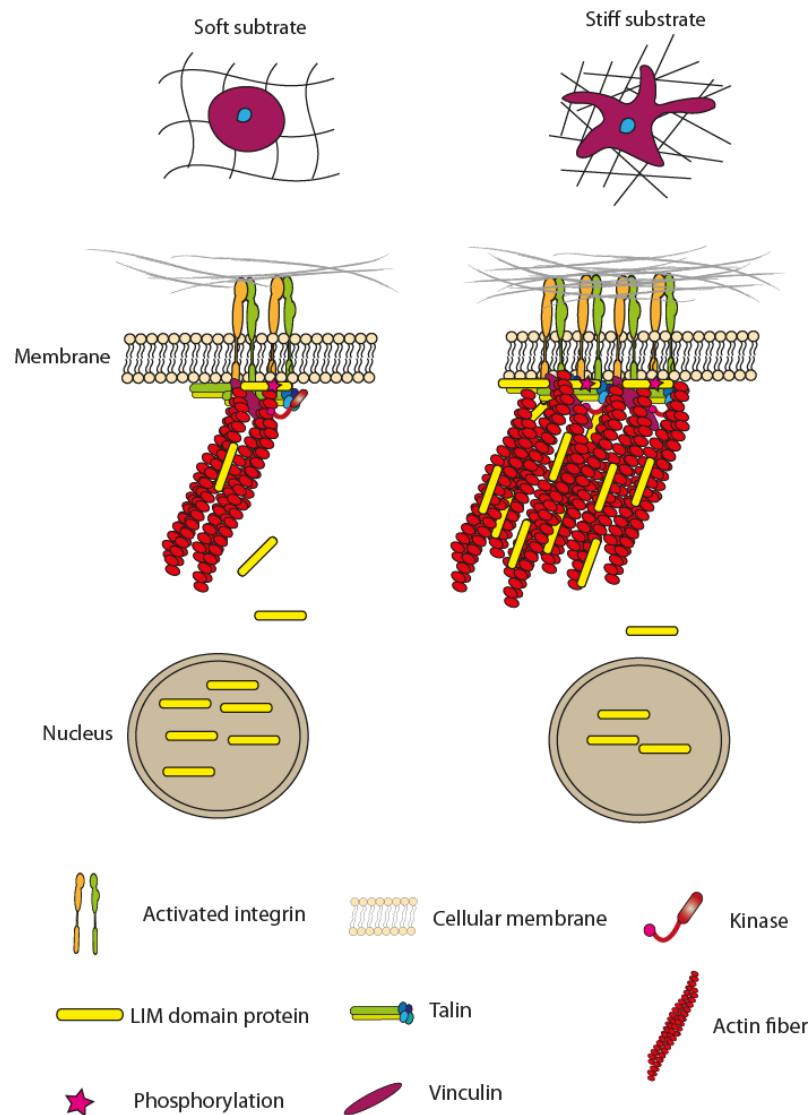
### 1.3.7 Actin in the nucleus

The first report on nuclear actin was in 1963. Since then, the mechanism of actin localisation in the nucleus was investigated and showed that due to the lack of NLS sequence on actin, cofilin and actin form a complex, which binds to an importin, allowing its transport in the nucleus through NPCs (D. J. Kelsch & T. L. Tootle, 2018). However, actin will bind an export complex to be exported out of the nucleus through NPC. Nuclear actin has been discovered in three forms: actin as a monomeric form (G-actin) and two polymerised forms: polymers and rods. Polymers are oligomers of actins but lack a filament structure, whereas rods are large polymers made of actin and cofilin that can be compared to actin bundles. The function of nuclear actin encompasses a wide range of mechanisms such as the regulation of transcription, DNA replication, chromatin remodelling, DNA damage repair, and the modulation of the nuclear structure (Daniel J. Kelsch & Tina L. Tootle, 2018; Maurer & Lammerding, 2019).

### 1.4 LIM domain proteins

As previously mentioned, YAP and TAZ are not the only proteins involved in mechanotransduction pathways. Several studies have linked Lin-11, Isl1, MEC- (LIM) proteins to mechanotransduction pathways. LIM domain proteins have been found in eukaryotic organisms, with some located in the nucleus, others in the cytoplasm, and some shuttling between both compartments (Kadmas & Beckerle, 2004). LIM motifs are a 60 amino acid sequence, made of a tandem of zinc fingers, with cysteine-histidine-rich sequences. In 2021, Anderson et al., showed that 41 LIM domain proteins were enriched at cell adhesion and cytoskeleton, and 26 were identified at focal adhesion. 11 LIM proteins displayed force-sensitive localisation at adjacent junctions. Among the identified listed proteins at cell adhesion and cytoplasm were listed Zyxin (focal adhesion, adjacent junction and actin stress fibers), Paxillin (focal adhesion, actin stress fibers), Ajuba (adjacent junction) and LIM domains protein 1 (LIMD1) (adjacent junction and focal adhesion) proteins (Anderson et al., 2021). Multiple studies have highlighted the LIM domains as

protein-protein interaction domains, allowing interaction with a wide range of proteins (including also other LIM proteins) and multi-protein complexes, impacting structure, protein assembly, and functions (Kadmas & Beckerle, 2004; Khurana et al., 2002; Velyvis A, 2013; Zheng & Zhao, 2007). The wide range of LIM domains protein and the diversity of sequences and functions allow an important repartition of these proteins throughout the cells, from the cell surface, the cytoskeleton and the nucleus (Figure 1-3) (Kadmas & Beckerle, 2004). LIM domains protein are sensing the mechanical strain of the actin cytoskeleton. LIM domains can directly bind to tensed F-actin, through their LCR domain, in the presence of a mechanical load as it has been showed for a number of LIM domain families such as the Zyxin, Tes, Enigma and Paxillin family (Sun et al., 2020). Due to the mechanical load on SF, structural damage can be observed, which triggers the need for repair in order to maintain the mechanical homeostasis of the actin cytoskeleton. Stress fiber strain sites (SFSS) will form within contractile fibroblast cells, where a mechanical failure occurs at an SF site, leading to the retraction of the SF. Zyxin and Paxillin are among 18 LIM domains proteins identified as recruited at SFSS sites (Winkelman et al., 2020). The interaction between LIM domain protein and SFSS can induce specific signalling for SF remodelling and repair, through the recruitment of actin polymerisation and crosslinking factors (Anderson et al., 2021).



**Figure 1-3: The localisation of LIM domain proteins is stiffness-dependent.**

Schematic of the localisation LIM domain proteins in cells exposed to soft or stiff substrates. The LIM domain protein localisation to focal adhesions and stress fibers is modified depending on the ECM forces. Adapted from (Anderson et al., 2021).

### 1.4.1 Three groups of LIM domain proteins

LIM domain proteins have been associated with several biological processes, including adhesions, gene transcription, organization of the actin cytoskeleton, organ development and cell fate specification (Khurana et al., 2002; Zheng & Zhao, 2007). LIM proteins can be separated into three groups based on structure and LIM domain homology (Bach, 2000).

- Group 1 is constituted of 3 subclasses: Lim- Kinases, LIM- homeodomains (LIM-hd) and LIM domain Only genes (LMO) contains two LIM domains(Bach, 2000).
  - o LIM kinases are mostly cytoplasmic serine protein kinases. Two members, LIM domain kinase 1 (Lmk1) and LIM domain kinase 2 (Lmk2), belong to this subclass. They act as regulators of microtubule disassembly through cofilin phosphorylation and act on the cytoskeleton organisation through Ras homolog gene family (Rho) signalling as well as the regulation of the mitotic spindle structure and positioning (Bach, 2000; Khurana et al., 2002; Scott & Olson, 2007).
  - o LIM-hd contains two LIM domains fused with a conserved homeodomain. LIM-hd interact with transcription factors and are important for cell fate decisions and organ development (Bach, 2000).
  - o LMOs contain exclusively two LIM domains. This family are nuclear-only proteins, nuclear transcriptional co-regulators and contains four members (LIM domain only 1 (LMO1)- LIM domain only 4 (LMO4)). LMOs do not bind to DNA, instead, they regulate gene transcription by mediating of protein-protein interaction and forming multiprotein complexes of transcriptional regulators (Sang et al., 2014).
- Group 2: LIM proteins with 2-spaced LIM domains. This group contains 3 cysteine-rich proteins (CRP)1-CRP3, involved in myogenesis and embryonic development. No other domains are associated with the LIM domain in this group (Velyvis A, 2013).
- Group 3: LIM domain proteins that lack high homology with other LIM domain groups. It contains from one to five LIM domains and can be localised in the nucleus and the cytoplasm, for example, zyxin (3 LIM

domains), Paxillin (4 LIM domains), and Ajuba (3 LIM domains) (Velyvis A, 2013).

## 1.5 Ajuba LIM protein family

First studied in *Drosophila melanogaster*, Ajuba LIM proteins are only represented as a single orthologue protein: Jub. Jub is essential for embryonic and organ development regulating organ growth by negatively regulating the hippo pathway (Das Thakur et al., 2010). The hippo pathway is equally important in physiological conditions and in cancer, as a major determinant of growth. It contains multiple members including Hippo (Hpo), Salvador (Sav), Warts (Wts), and Mob-as-tumor-suppressor (Mats) (Staley & Irvine, 2012). Jub acts downstream of Hpo, downstream of Wts (which correspond to LATS in mammals) and Yorkie (orthologue of Yki, YAP/TAZ in mammals), regulating organ size through inhibition of apoptosis, as well as promoting cell proliferation through cyclin E expression (Das Thakur et al., 2010). Jub localisation to adherence junctions is promoted by cytoskeletal tension. At adherence junctions, Jub is recruited by  $\alpha$ -catenin through direct interaction. Jub will recruit Warts to adherence junctions in a force-dependent manner. Jub's recruitment to adherence junctions was linked to an increase of Yorkie activity, leading to organ growth (Alégot et al., 2019).

In mammals, the Ajuba LIM protein family contains Ajuba, the LIM domains protein 1 (LIMD1) and the Wilms tumour 1 interacting protein (Wtip). These three proteins are adaptor/scaffold proteins, transcriptional co-repressors and especially abundant in epithelial tissue (Ayyanathan et al., 2007; Langer et al., 2008; Xu et al., 2019). In many publications, the Ajuba LIM protein family is combined with the Zyxin family, creating the Ajuba/Zyxin subfamily (also called Zyxin/Ajuba LIM proteins), which includes Zyxin, Thyroid hormone receptor-interacting protein 6 (Trip6) and Lipoma-preferred partner (Lpp) to the previously listed members (Feng & Longmore, 2005; Li et al., 2016). These five members have similar protein domains as illustrated in Figure 1-4. Each contains three LIM domains and a Pre-LIM region, although the localisation of their nuclear export signal (NES) and

nuclear localisation signal (NLS) (Figure 1-4) sequences varies. The NES/NLS localisation of Zyxin, Lpp and WTIP were not available.

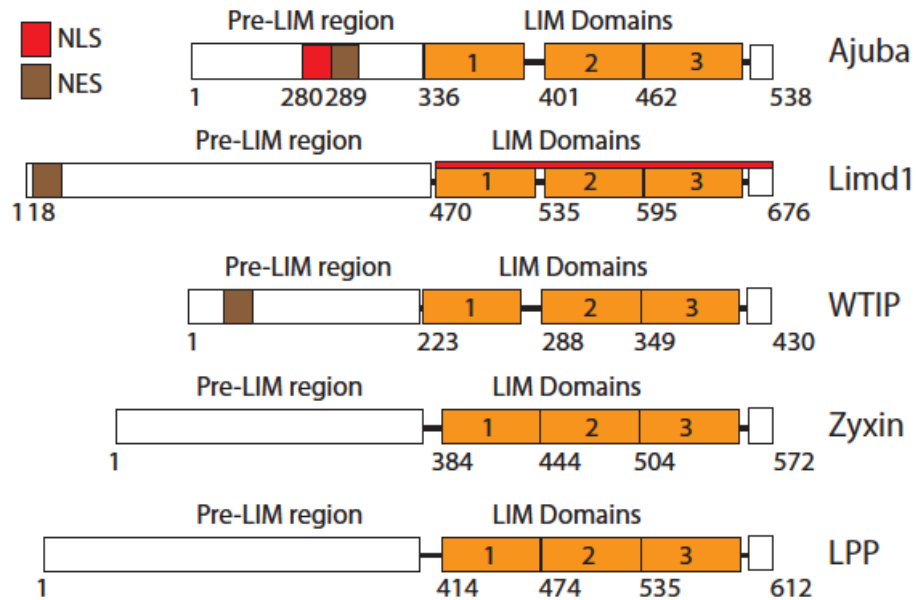


Figure 1-4: Representation of Ajuba/Zyxin subfamily members (Human).

The UniProt database information was used as reference for Ajuba (Q96If1), LIMD1 (Q9UGP4), WTIP (A6NIX2), Zyxin (Q15942) and Lpp (Q93052). The members of the Ajuba/Zyxin have three LIM domains (in orange). The numbers represent the positioning of each domain within each protein. Ajuba, LIMD1 and WTIP contain nuclear export signal (NES) and nuclear localisation signal (NLS) to allow their shuttling in and out of the nucleus.

Belonging to LIM protein group 3, the Ajuba LIM protein family members have three LIM domains and shuttle between the cell surface, the cytoplasm, and the nucleus where they participate in many cellular processes, including cell adhesion, proliferation, cell cycle progression, transcription, migration, invasion and mitosis (Huggins & Andrulis, 2008; Schimizzi & Longmore, 2015; Tang et al., 2019; Wang et al., 2021; Zhou et al., 2019). Additionally, Ajuba LIM domain protein members have been localised at adhesion sites more specifically to adherence junctions and focal adhesions (Marie et al., 2003).

Moreover, Ajuba family proteins have been also studied in the case of cancers including Hepatocellular carcinoma (Zhang et al., 2020), breast cancer (Li et al.,



2022; Xu et al., 2019) oesophageal squamous carcinoma (Ghosh et al., 2010), gastric cancer (H. Li et al., 2019) colorectal cancer (Jia et al., 2017) and pancreatic cancer (Zhang et al., 2019).

## 1.6 The LIM protein Ajuba

### 1.6.1 An overview

The LIM protein Ajuba is, in this thesis, referred to as Ajuba. This protein was discovered in 1999 and means “curiosity” in the Indian dialect Urdu. Ajuba is part of the Ajuba/zyxin family, contains 3 LIM domains, one NLS and one NES. The NES and NLS sequences will allow the protein to enter and leave the nucleus.

Ajuba is a scaffold/adaptor protein and a transcriptional corepressor/activator, whose role in tumorigenesis is highly disputed. Indeed, Ajuba is described as an oncogene, driving cell proliferation, in a wide range of cancer types, while in other paper Ajuba acts as a tumour suppressor. Interestingly, Ajuba is significantly upregulated in several cancers (Jia et al., 2020) including breast (Li et al., 2022), colorectal (Z. Wu et al., 2021), lung (Song et al., 2022) and pancreatic cancer (Zhang et al., 2019). Through different studies, Ajuba has been involved, over time in many cellular processes: cell-cell adhesion (Razzell et al., 2018), gene transcription (Zhang et al., 2019), cell proliferation (Chen et al., 2016), mitosis/cytokinesis (Chen et al., 2016), metabolism (H. Li et al., 2019) and cell migration/invasion (Shi et al., 2016). Interestingly, during *in vivo* studies two phenotypes were reported during the generation of AJUBA KO mice. The generated homozygous Ajuba KO mice were embryonically lethal (Dommann et al., 2022; Loganathan et al., 2020). This was also reported during the generation of several AJUBA KO cell lines *in vitro* (Dommann et al., 2022). However, Ajuba KO mice were generated and studied by Pratt *et al*, in 2005 (Pratt et al., 2005). In this study, only a mild phenotype was observed.

## 1.6.2 Ajuba in cell adhesion

Ajuba localises at the cell edge, mainly at adherent junctions, occasionally at focal adhesion sites, with an interesting strong concentration at intercellular vertices (Ibar et al., 2018; Marie et al., 2003; Nola et al., 2011). First shown in *Drosophila*, Ajuba has been discovered to perfectly localise at cell-cell borders and delimiting cell edges in epithelial tissue. Ajuba will also facilitate the stabilisation of newly formed junctions by coupling the cadherin-based complex to the actin cytoskeleton during convergent extension in *Drosophila* embryo (Razzell et al., 2018). In human primary keratinocytes, Ajuba co-localises with the cadherin adhesive complex at cell-cell contact, through direct interaction with  $\alpha$ -catenin via its LIM domain (Marie et al., 2003).

## 1.6.3 Ajuba, a cell cycle regulator

The cell cycle is composed of the interphase (G1, S and G2 phase), the mitosis and the G0 phase (Figure 1-5) (Wang, 2022). The mitosis is the cell cycle phase where a cell divides into two identical daughter cells. Cell cycle contains different checkpoints (G1, G2, Spindle checkpoint) to ensure the regulation of the cell division (Figure 1-5). The G1 checkpoint, localised at the G1/S transition will monitor both the viability and the integrity of the cell before allowing its entry into the S phase (Wang, 2022). The G2 checkpoint localised at the G2/M will assess several parameters: the cell size, the presence of molecular signal for proliferation, the DNA integrity and the availability of energy necessary for the cell division process. The Spindle checkpoint localises at the metaphase/anaphase transition and verifies the attachment of each chromosome to the spindle microtubules at the metaphase plaque.

Ajuba acts as a cell cycle regulator, allowing the cell to enter and regulate the progression of mitosis. Ajuba was shown to interact with various targets throughout the cell cycle. First, Ajuba binds to Aurora-A through the LIM-2 and LIM-3 domains, which triggers Aurora-A's autoactivation, a necessary step in the late G2 phase for entering mitosis (Hirota et al., 2003) and for the activation of cyclin B/cyclin dependent kinase 1 (cdk1) complex. Then, during early mitosis,

Ajuba is phosphorylated by the cdk1-cyclin B complex and will control the expression of cell cycle regulators (BUB1, Wee1 and cdc25C) (Chen et al., 2016). In addition, during the prometaphase, Ajuba is localised at the centrosomes where it binds to microtubules (through the Pre-LIM region), follows the microtubule dynamics towards the kinetochore and eventually binds to the kinetochore, where it stays throughout metaphase and anaphase stage (Ferrand et al., 2009; Hirota et al., 2003). The spindle checkpoint, at the metaphase-anaphase transition, is insured by mitotic arrest deficient (MAD) and BUB family protein. Finally, Bub1-related kinase (BUBR1), a protein of the budding uninhibited by benzimidazoles (BUB) family, is phosphorylated by Aurora-B, and interacts with Ajuba to form the BUBR1-Ajuba-Aurora-B complex which is important for the metaphase-anaphase transition (Ferrand et al., 2009).

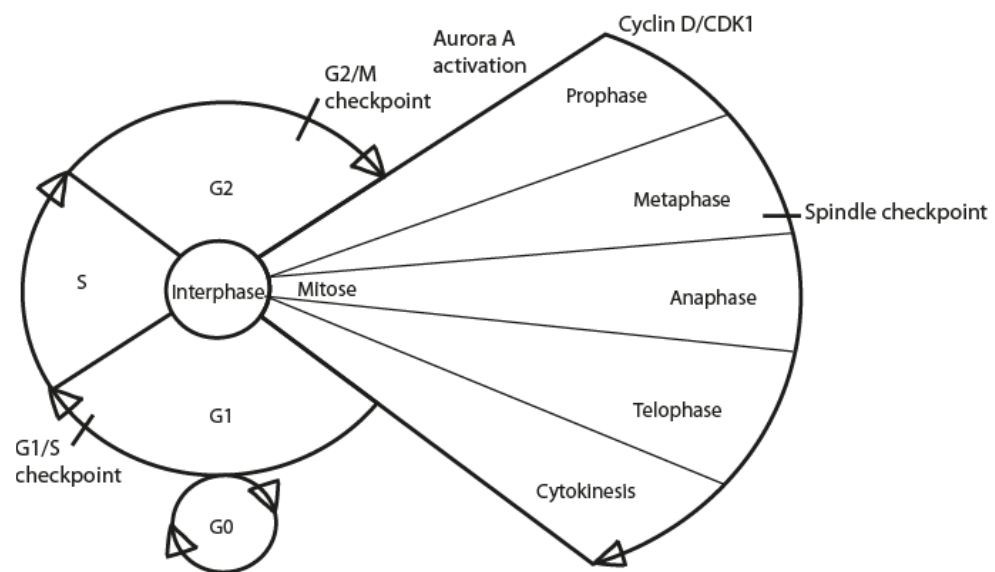


Figure 1-5 : Schematic representation of the cell cycle and its checkpoints.

The indication of Aurora-A activation, cyclin D/CDK1 serve as a point of reference for the role of Ajuba within the cell cycle.

#### 1.6.4 Ajuba modulates transcriptional activities.

In this section, will describe the roles of Ajuba in the nucleus. Ajuba displays a cytoplasmic and nuclear localisation, using respectively its NLS and NES sequences to enter and leave the nucleus. Indeed, in the nucleus, Ajuba acts as a co-

repressor or co-activator but lacks the ability to bind to DNA directly. This means that Ajuba associates with DNA-bound transcription factors to either repress or activate the expression of their specific gene targets. To act on transcription activities, Ajuba has many binding partners such as Snail, protein arginine methyltransferase-5 (Prmt5), growth factor independent-1 (Gfi1) and specific protein 1 (Sp1) (Chiu et al., 2023; Hou et al., 2008; Jia et al., 2020; Langer et al., 2008).

On one hand, Ajuba was described to have a transcriptional co-repressor role of the SNAIL/Gfi-1 (SNAG) family of transcription factors (Ayyanathan et al., 2007). Snail is a transcription factor from the SNAG family of transcription factors. Due to their important role in the regulation of development and stem cell self-renewal, Snail has an important role in tumour progression (Wu & Zhou, 2010).

Ajuba was described to have a transcriptional co-repressor role on Snail's target, E-cadherin, and in turn alters cell-cell adhesion (Ayyanathan et al., 2007). More specifically, Ajuba binds to Snail's SNAG domain with its LIM domain and recruits Prmt5 to the Ajuba-Snail complex. It triggers their translocation in the nucleus where Ajuba-Snail-Prmt5 binds to the E-cadherin promoter (Ayyanathan et al., 2007; Hou et al., 2008; Hou et al., 2010). Prmt5 is an enzyme that regulates gene expression by methylating transcription factors and histones at specific positions (Zhu & Rui, 2019).

Ajuba also associates with Gfi1, a nuclear transcriptional repressor protein, through its SNAG domain to represses transcription in a histone deacetylase (HDAC) dependant manner via the co-repressor complex Gfi1-HDAC-ajuba. Furthermore, Ajuba also inhibit GIF1 autoregulation by binding to its promoter (Diego E. Montoya-Durango et al., 2008).

In addition to its LIM domains, Ajuba contains four conserved nuclear receptor motifs (3 NR boxes and CoRNR boxes) (Fan et al., 2015). Using these motifs, Ajuba will interact with retinoic acid receptors (RARs), especially the retinoic acid receptor alpha (RAR $\alpha$ ), via the NR boxes, and retinoid X receptors (RXRs) to repress the transcription of their targets. The regulation of RAR $\alpha$  seems to be

bidirectional as Ajuba is regulated by retinoic acid and regulates retinoic acid (Hou et al., 2010).

On the other hand, Ajuba acts as a coactivator of gene expression. In pancreatic cancer, Ajuba can bind to Sp1, enhancing ajuba and SP1 transcription as well as the transcription of the SP1 target genes (Zhang et al., 2019). Ajuba also binds to peroxisome proliferator-activated receptors  $\gamma$  (PPAR $\gamma$ ) in adipocytes or liver X receptor alpha (LXR $\alpha$ ) in liver cells. PPAR $\gamma$  is a member of the nuclear receptor superfamily of ligand-dependent transcription factors, while LXR $\alpha$  is an oxysterol-activated transcription factor. The binding to Ajuba to PPAR $\gamma$  and LXR $\alpha$  increases the transcriptional activities of PPAR $\gamma$  and LXR $\alpha$  targets (Fan et al., 2015; Hou et al., 2010; Li et al., 2016; Xu et al., 2019; Yan et al., 2022). PPAR are important for the energy homeostasis of adipocytes while LXR are important in the regulation of lipid, glucose and cholesterol homeostasis in liver cells by controlling the transcription of the genes involved in metabolism (Fan et al., 2015; Li et al., 2016).

### 1.6.5 Ajuba, a metabolic regulator

In the previous section, I mentioned the interaction between Ajuba and the transcription activities of metabolism-related transcription factors and genes. These interactions are not solely reserved for the liver and adipocyte cells. In cancer, we often observe metabolic reprogramming, which is listed as one of the hallmarks of cancer (Natalya & Craig, 2016). Due to the Warburg effect, cancer cells have an increased glucose uptake leading to the production of lactate (Liberti & Locasale, 2016). Although in normal cells, this would be a problem, in cancer cells this allows rapid adenosine triphosphate (ATP) synthesis, supports enhanced cell proliferation, increases invasiveness via a decrease in environmental pH and acts as a signal for the cells to activate several processes (Liberti & Locasale, 2016). Tumours depend on ATP production to support their proliferation. To supply this energy demand, cells need to use glucose transporters, to carry it across the cell (Seo et al., 2014). In gastric cancer, the overexpression of Ajuba regulates glucose intake and mitochondrial potential. Gastric cancer cells upregulate the uptake of glucose, through an upregulation of glucose transporter 1 (GLUT1) and

consumption of glucose, as well as the production of ATP and lactate when Ajuba is overexpressed (H. Li et al., 2019).

### 1.6.6 Ajuba in cell movement

While energy is important for cancer survival, the ability of cells to migrate and invade is key for physiological processes (such as wound healing, embryonic development) and pathological processes (metastasis) (Lin & Wellstein, 2022). Cell migration is a multistep process requiring the coordination of the actin cytoskeleton, the polymerisation of actin, cell polarization, protrusion formation (lamellipodia, filipodia), directionality and the activation of the actin related protein 2/3 complex (Arp 2/3 complex). Lamellipodia are highly dynamic protrusions, rich in actin filaments and focal adhesions (Innocenti, 2018). They are responsible for pulling the cell forward by generating forces via the actin cytoskeleton. The lamellipodia contain branched actin networks, while filopodia have long and parallel bundles of actin (Xue et al., 2010). The filopodia are thin finger-like protrusions, actin-rich structures that emerge from the lamellipodia to function as antennas, sensing the environment. As for lamellipodia, the dynamism of filopodia relies on the polymerisation and depolymerisation of actin filaments. The Arp 2/3 complex is an actin nucleator responsible for generating the polymerisation of an actin filament when activated by nucleation-promoting factors like Suppressor of cAMP receptor (SCAR)/ WASP-family veprolin homology protein (WAVE) (Swaney & Li, 2016). This complex is extremely important in the formation of lamellipodia protrusion. The actin filaments are polarized and oriented from the fast-growing end to push the leading edge of cell creating a driving force for the protrusion (Ridley et al., 2003). The driving force generated at the protrusion necessitates the cell to be polarised with a front and rear end. While the front end creates forces to move forward, the rear end will go through adhesion disassembly, recycling and tail retraction.

Cellular invasion requires the disruption or degradation of the matrix microenvironment to invade. To do so, cells can use invadopodia or linear invadosomes. These structures are highly dynamic actin-rich protrusions

combining adhesion and lytic activity, via metalloproteases (MMP), to degrade the ECM matrix (Linder et al., 2023).

Many cancer studies have demonstrated that the expression of Ajuba was found proportional to the ability of cells to migrate and invade *in vitro* and *in vivo* (Li et al., 2022; Shi et al., 2016; Zhang et al., 2020). Interestingly, another study showed the opposite result where Ajuba depletion enhances invasion (Liu et al., 2018). Thus, we will consider the impact of Ajuba expression on cell invasion could potentially be context-dependent. Additionally, in oesophageal squamous cell carcinoma, Ajuba promotes invasion through MMP overexpression (MMP10 and MMP 13) (Shi et al., 2016).

### **1.6.7 Ajuba in pancreatic cancer and mechanosensing**

Pancreatic cancer is known for its desmoplastic reaction leading to a drastic increase in environmental and tumor stiffnesses. In pancreatic cancer cell lines, Ajuba promotes SP1-mediated cell proliferation (Zhang et al., 2019). SP1 is a transcription factor from the SP/Kruppel-like factor which controls a wide range of gene expressions involved in regulating cellular processes. Unfortunately, a single publication was published on the role of Ajuba in pancreatic cancer (Zhang et al., 2019).

Based on the published literature about Ajuba and Jub, Ajuba could be involved in the four steps of the mechanosensing and mechanotransduction as illustrated in Figure 1-1. Briefly, (1) Ajuba is localised at adherent junctions, with some focal adhesion localisations. (2) Ajuba can modify its localisation due to cytoskeletal tension (Rauskolb et al., 2014). (3) NES and NLS sequences allow the shift of Ajuba to and from the nucleus. (4) Ajuba has transcriptional coregulator functions. Together, the literature points towards a possible role of Ajuba as a mechanosensing protein.

## 1.7 Mimicking the mechanical properties of ECM in vitro

Within the body, ECM is a dynamic structure, with a complex composition, designed specifically by each organ and tissue. Since Paget's seminal 'seed' and 'soil' theory from 1889, in which he hypothesised that the microenvironment plays a critical role in dictating metastatic seeding, a necessity to mimic the microenvironment *in vitro* arose. It triggered the development of natural (alginate, hyaluronic acid, agarose), synthetic (polyacrylamide, polyethylene glycol) and composite biomaterials through collaborations between engineers and biologists (Xie et al., 2023). ECM-mimicking biomaterials were tailored around our knowledge of body-specific ECM parameters, which can be classified into architectural (geometry, topography, porosity), chemical and mechanical parameters, some of these parameters are dynamics (Mierke, 2024; Woodbury et al., 2023).

Focusing on the static properties of biomaterials, several parameters can be controlled: Architectural (dimension, geometry, topology and porosity) and mechanical (stiffness and elasticity) (Naqvi & McNamara, 2020) (Figure 1-6). To mimic the stiffness of ECM environment, the stiffnesses of organs, tissue or specific environments were measured. The Young's modulus of various tissues and organs, representing their stress-to-strain ratio was measured (Narasimhan et al., 2020). This unit of measurement (unit: kilo Pascal (kPa)) serves as a reference to tailor biomaterials development, dictating how each biomaterial can be used, and the range of stiffness that can be created with it. In addition to Young's modulus, another parameter is essential to any mechanobiology study: two-dimensional (2D) versus three dimension (3D) systems. This choice between 2D and 3D systems lies in the parameter to investigate within the study. When studying the complexity of the ECM dynamic *in vitro*, it will require the use of a complex 3D system in which cell can remodel their environment (Yang et al., 2021). In contrast, the study of a singular parameter, for example in this thesis, the impact of stiffness on cellular behaviour, can be studied in both a coated 2D system and a 3D system.



As a 3D system, synthetic 3D hydrogels incorporating full-length ECM proteins are currently in development (Trujillo et al., 2020). This system will allow increased interactions between cells-hydrogel, cells-ECM proteins, and a cell-ECM mediated degradability. This system includes tuneable environmental stiffness, reproducible and controllable environment complexity and defined ECM protein compositions(Trujillo et al., 2020).

Natural : alginate, hyaluronic acid, agarose  
 Synthetic : polyacrylamide, polyethylene glycol  
 Composite : contains two or more material

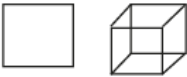
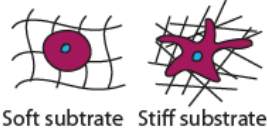

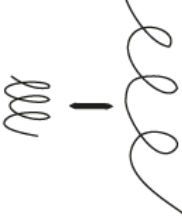
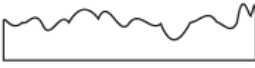
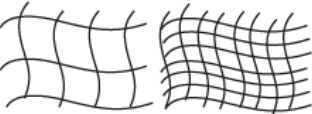
Architectural			Mechanical		
Name	Techniques	Example	Name	Techniques	Example
Dimension	Hydrogels	 2D      3D	Stiffness	Hydrogels and pillars	 Soft substrate      Stiff substrate
Geometry	Lithography pattern		Elasticity	Active biomaterials	
Topography	Lithography pattern				
Porosity	3D porous scaffold	 High porosity      Low porosity			

Figure 1-6: Summary of the mechanical properties reproducible *in vitro* and associated techniques.

Inspired by Mierke, 2014 and Xie et al., 2023 (Mierke, 2024; Xie et al., 2023).

## 1.8 Aims:

Since the publication of the “seed and soil theory”, researchers have aimed to better understand the relationship between a cell and its environment. The

mechanobiology research field aims to uncover the dynamic interaction between the environmental mechanical forces and the mechanisms each cell possesses to sense, react and interact with it. In pancreatic cancer, understanding the impact an increase of ECM stiffness, induced by the desmoplastic reaction, has on pancreatic cancer cell might bring therapeutic opportunities in the treatment of PDAC. Cells use mechanosensing proteins and mechanotransduction pathways to sense ECM mechanical forces and transform them into cellular biological responses. To do so, the cell will use a plethora of signalling pathways and proteins. I hypothesised that environmental stiffness has an important effect on PDAC gene expression (Chapter 3 and Chapter 5). The use of the messenger RNA (mRNA) expression levels of PDACA genes allowed the selection of multiple mechanotransduction candidates (Chapter 3). From this selection, a LIM domain protein called Ajuba was selected. The LIM domain proteins are a family increasingly known for their force-sensitive localisation and for their involvement in the transfer of mechanical forces. Ajuba, part of the Ajuba LIM family, has been studied in many cancer types and associated with roles in cell adhesion, cell cycle, metabolism, movement and transcription activities. In pancreatic cancer, very little is known about the role of Ajuba. We hypothesised that Ajuba could act as a mechanotransduction actor in pancreatic cancer (Chapter 3, Chapter 4, Chapter 5). Specifically, we investigated the roles of Ajuba in cell morphology, adhesion, proliferation and movement in pancreatic cancer cells. Finally, we explored the role of Ajuba on transcription factor activities and gene transcription (Chapter 5).

## **Chapter 2. Materials and methods**

## 2.1 Material and reagents

Table 2- 1 Units of measurement

Units	
Symbol	Name
°C	Degree celsius
cm	Centimetre
h	Hours
min	Minutes
sec	Seconds
M	Molar
mL	Milliliter
kPa	Kilopascal
rpm	Revolution per minutes
g	Gravitational force
V	Volt
µg	Microgram
µL	Microlitre
µM	Micromolar
nM	Nanomolar

Table 2- 2 : Cell lines and cell culture consumables

Cell lines and bacterial strains		
Name	Description	Supplier
PDACA	Mouse KPC cell line	Dr. J. P. Morton lab
PDACA CRISPR EV	Mouse KPC cell line containing CRISPR Empty vector	Generated
PDACA CRISPR 01	Mouse KPC cell line containing a CRISPR vector bearing sgRNA 1	Generated
PDACA CRISPR 02	Mouse KPC cell line containing a CRISPR vector bearing sgRNA 2	Generated
PDACA CRISPR All	Mouse KPC cell line containing a CRISPR vector bearing sgRNA 1, 2 and 3	Generated
PDACB	Mouse KPC cell line	Dr. J. P. Morton lab
HEK293T	Human embryonic cell line	Prof. L. M. Machesky
DH5alpha	Chemically competent cells	Generated
Cell culture		
Name	Description	Supplier
DMEM		Gibco #21969035

L-glutamine		Gibco #A1451801
PBS	3.3 mM KCl, 137 mM NaCl, 8 mM Na <sub>2</sub> PO <sub>4</sub> , 1.5 mM KH <sub>2</sub> PO <sub>4</sub> , pH = 7.3	Beatson central services
FBS		Gibco #10270-106
2.5 % trypsin		Gibco #15090046
PE buffer	0.037 % (w/v) EDTA in PBS	Beatson central services
Matrigel		Corning #734-1100
Lipofectamine 2000	Transfection method	Thermo fisher scientific #11668019
Amaxa kit V	Transfection method	Lonza #VCA-1003
Calcium phosphate kit	Transfection method	Thermo fisher scientific #K2780-01
Fibronectin		Sigma #F1141
Doxyxycline		Sigma #D9891
DMSO		Fisher chemical #D/4121/PB08
Puromycin		Gibco #A11138-03
Tet System approved FBS		Takara Clontech #631106
Concanavalin A (ConA)		Sigma-Aldrich #L7647
10 cm plastic dish		Falcon #430147
6-well plastic plates		Falcon #353046
Glass beads	PAAM Hydrogels cell lysis	Milipore #1.04016.0500
19 mm glass coverslips		VWR #631-0156
32 mm glass coverslips		VWR #631-0162
Cryovials, 1 mL		Greiner bio-one #03961-1-003
Culture insert 2-well sterile		Ibidi # IB-80209
96-Well ImageLock Plates	Wound healing incucyte	Essen Bioscience, Sartorius #4379
E-plate 16	xCELLigence	Cambridge Biosciences #5469830001

Table 2-3: Plasmids

Plasmids		
Name	Description	Supplier
pLentiCRISPR	CRISPR	Prof. L. M. Machesky
pLKO	Lentiviral infection	Prof. L. M. Machesky
pSPAX2	Lentiviral infection	Prof. L. M. Machesky
pVSVG	Lentiviral infection	Prof. L. M. Machesky
pcdna 3.1 +		Prof. L. M. Machesky
pEGFP-c1		Addgene #6084-1
pEGFP-n1		Addgene #6085-1
pLHCX	Retroviral infection	Prof. L. M. Machesky
pJet	Intermediate vector	Thermo Fisher Scientific #K1231
Ptripz-egfp:AJUBA	Dox-inducible Ajuba vector	Addgene #108229

Table 2-4: Cloning and constructs

Cloning		
Name	Description	Supplier
Prime Star mix 2X		Clontech Takara #R045B
TAE 50X		The Scotland Institute central services
Agarose high grade		Melford #MB1200
Midori green		Nippon genetics #MG04
Thermo Scientific gene ruler 1kb DNA ladder		Thermo Fisher Scientific #SM1163
DNA gel recovery kit		Zymo Research #D4008
Rapid DNA ligation kit		Thermo Fisher Scientific #K2800
L-broth		The Scotland Institute central services
L-broth agar plate		The Scotland Institute central services
Xba1		NEB #R0145S
BAMH1 HF		NEB #R3136S
ECOR1 HF		NEB #R3101S
Cut smart buffer		NEB #B6004S
Ampicillin		Sigma
Kanamycin		Sigma
DNA Constructs		

Name	Backbone	Source
pEGFPC1 empty vector		Prof. L. M. Machesky
pEGFPN1 empty vector		Prof. L. M. Machesky
pEGFPC1-Ajuba	pEGFPC1	Generated
pEGFPN1-Ajuba	pEGFPN1	Generated
Ajuba-Myc-pJet	pJet	Generated
Myc-Ajuba-pJet	pJet	Generated
Ajuba-Flag-pJet	pJet	Generated
Flag-Ajuba-pJet	pJet	Generated
Ajuba-Myc-plhcx	plhcx	Generated
Ajuba-Myc-pcdna 3.1	pcdna 3.1	Generated
Flag-Ajuba pcdna 3.1	pcdna 3.1	Generated
pTRIPZ-EGFP:Ajuba		Addgene #108229
pLenti CRISPR sgRNA1	pLenti CRISPR vector	Generated
pLenti CRISPR sgRNA2	pLenti CRISPR vector	Generated
pLenti CRISPR sgRNA3	pLenti CRISPR vector	Generated

**Table 2-5: Western blots, immunofluorescence and antibodies**

<b>Western blot</b>		
Name	Description	Supplier
RIPA buffer	150 mM NaCl, 10 mM Tris-HCl pH = 7.5, 1 mM EDTA, 1 % Triton X-100, 0.1 % SDS	The Scotland Institute central service
1X Halt phosphatase inhibitor cocktail		Thermo Fisher Scientific #78427
1X Halt protease inhibitor cocktail		Thermo Fisher Scientific #78438
Precision red		Cytoskeleton, Inc. #ADV02
Cuvettes		VWR #634-0676
NuPage LDS sample BUFFER (4X)	Sample preparation	Invitrogen #2165462
NuPage sample reducing agent (10X)	Sample preparation	Invitrogen #NP0004

NuPage MOPS SDS Running Buffer (20X)		Novex #NP0001
NuPage 4-12 % Bis-Tris Gel		Invitrogen #NP0321BOX
PageRuler pre stained protein ladder		Thermo Fisher Scientific #26619
Nitrocellulose blotting membrane	0.45 $\mu$ m	GE Healthcare #10600002
Transfer buffer	1 % SDS, 250 mM Tris, 1.92 M Glycine	The Scotland Institute central service
TBS-T	150 mM NaCl, 10 mM Tris-HCl pH = 7.4, 2.7 mM KCl, 0.1 % Tween 20	The Scotland Institute central service
Cell lysis glass beads		Millipore #1.04016.0500
<b>Immunofluorescence</b>		
Name		Supplier
16 % PFA		Electron Microscopy Sciences #15710
PFS	3.5 g fish skin gelatin (Sigma) and 1.25 mL of 10 % saponin/PBS	Homemade by Emma Sandilands
ProLong Diamond Antifade Mountant		Invitrogen #P36965
Permeabilisation buffer	20 mM glycine, 0.05 % Triton X-100	Homemade
Bovine serum albumin fraction V		Sigma #10735108001
Triton X-100		Sigma #T9284-100ML
<b>Antibodies</b>		
Name	dilution	Supplier
P-YAP	WB: 1/1,000	Cell Signalling technology #13008S
YAP (D8H1X) XP Rabbit mAb	WB: 1/1,000	Cell signalling technology #14074
Ajuba (E-3): sc-374610	IF: 1/200	Santa Cruz Biotechnology #sc-374610
Ajuba #4897S		Cell signalling technology ##4897S
Anti-Ajuba antibody (Atlas)	WB: 0.2 $\mu$ g	Atlas antibody #HPA006171
Anti-Ajuba antibody (ab244285)		Abcam #ab244285



GAPDH (D4C6R)	WB: 1/1,000	Cell signalling technology #97166S
Vinculin	IF: 1/200	Invitrogen #700062
P-paxilin (Tyr31)	IF: 1/200	Invitrogen #44-720G
Alexa Fluor™ 647 Phalloidin	IF: 1/1,000	Invitrogen #A22287

Table 2-6: RNA reagents and primers

<b>RNA extraction, cDNA and qPCR</b>		
Name		Supplier
MicroAmp Fast 96-well reaction plate (0.1 mL)		Applied Biosystems #4346907
Optical Adhesive Covers		Applied Biosystems #4360954
Dynamo HS SYBR green qPCR Kit		Thermo Fisher scientific #F410L
Nuclease free water		Ambion #AM9937
<b>siRNA and sgRNA</b>		
Name	Sequence	Supplier
FlexiTube siRNA Mm_Jub_8	TCCGTGGGCATGGAACGGTTA	Qiagen #SI04449921
FlexiTube siRNA Mm_Jub_7	TGCATTGGATCTGACCTGTTA	Qiagen #SI04449914
FlexiTube siRNA Mm_Jub_5	TTCCTGAACGCCAGATTATAA	Qiagen #SI04420241
FlexiTube siRNA Mm_Jub_3	CACCTTAAGCAGGATGTCTTA	Qiagen #SI01079841
sgRNA 1 (Exon 1 Ajuba)	5'- CACCCGGACACTCGGTTACAGGCTAC -3'	Designed using horizondiscovery.com
sgRNA 2 (Exon 1 Ajuba)	5'- CACCGAAATCAGGAGGCGACGACAG -3'	Designed using horizondiscovery.com
sgRNA 3 (Exon 2 Ajuba)	5'- CACCGAGTGCAACAAAGGTATCTAT -3'	Designed using horizondiscovery.com
sgRNA 1 (Exon 1 Ajuba) reverse	3'- CCTGTGAGCCAATGTCCGATGCAAA -5'	Designed using horizondiscovery.com

sgRNA 2 (Exon 1 Ajuba) reverse	3'- CTTTAGTCCTCCGCTGCTGTCCAAA -5'	Designed using horizondiscovery.com
sgRNA 3 (Exon 2 Ajuba) reverse	3'- CTCACGTTGTTTCCATAGATACAAA -5'	Designed using horizondiscovery.com

Table 2-7: DNA Primers

<b>Primers (qPCR and sequencing)</b>				
Name	Species	Sequence or References	Supplier	Method
Gapdh – Forward	<i>Mus musculus</i>	5' - CATGGCCTACATGG CCTCCA - 3'	Thermo Fisher Scientific	qPCR
Gapdh - Reverse	<i>Mus musculus</i>	5' - TGGGATAGGGCCTC TCTTGC - 3'	Thermo Fisher Scientific	qPCR
Cdk2 - Forward	<i>Mus musculus</i>	5' - TGAAATGCACCTAG TGTGTACC - 3'	Thermo Fisher Scientific	qPCR
Cdk2 - Reverse	<i>Mus musculus</i>	5' - TCCTTGTGATGCAG CCACTT - 3'	Thermo Fisher Scientific	qPCR
Ajuba	<i>Mus musculus</i>	#QT00127414	Qiagen QuantiTect primers	qPCR
LIMD1	<i>Mus musculus</i>	#QT00115472	Qiagen QuantiTect primers	qPCR
YAP	<i>Mus musculus</i>	#QT01061130	Qiagen QuantiTect primers	qPCR
TAZ	<i>Mus musculus</i>	#QT00146440	Qiagen QuantiTect primers	qPCR
Epsin 3	<i>Mus musculus</i>	#QT00145929	Qiagen QuantiTect primers	qPCR
Sorbs2	<i>Mus musculus</i>	#QT02523780	Qiagen QuantiTect primers	qPCR
Tetraspanin 8	<i>Mus musculus</i>	#QT02379727	Qiagen QuantiTect primers	qPCR

Cadherin 16	<i>Mus musculus</i>	#QT00101766	Qiagen QuantiTect primers	qPCR
Fascin1	<i>Mus musculus</i>	#QT00165907	Qiagen QuantiTect primers	qPCR
Aquaporin 1	<i>Mus musculus</i>	#QT00109242	Qiagen QuantiTect primers	qPCR
Mb21d1	<i>Mus musculus</i>	#QT00131929	Qiagen QuantiTect primers	qPCR
pEGFPn1 EcoR1 Ajuba - Forward	<i>Mus musculus</i>	5' – GTTACGGAATTCAT GGAGCGGTTAGGA GAGAA - 3'	Thermo Fisher Scientific	Sequencing
pEGFPn1 BAMH1 Ajuba - Reverse	<i>Mus musculus</i>	5' - CAATGCGGATCCCG GATATAGTTGGCAG GGGGTT - 3'	Thermo Fisher Scientific	Sequencing
pEGFP c1 EcoR1 Ajuba - Forward	<i>Mus musculus</i>	5' - GTTACGGAATTCAA TGGAGCGGTTAGG AGAGAA - 3'	Thermo Fisher Scientific	Sequencing
pEGFP c1 BAMH1 Ajuba - Reverse	<i>Mus musculus</i>	5' – CGTAACGGATCCTC AGATATAGTTGGCA GGGG - 3'	Thermo Fisher Scientific	Sequencing
Myc start 5 prime - Forward	<i>Mus musculus</i>	5' - ATGGAACAAAAACT CATCTCAGAAGAGG - 3'	Thermo Fisher Scientific	Sequencing
Myc 3 prime end - Reverse	<i>Mus musculus</i>	3' – TCACAGATCCTCTTC TGAGATGAG - 5'	Thermo Fisher Scientific	Sequencing
Ajuba 3 prime end stop - Reverse	<i>Mus musculus</i>	3' - TCAGATATAGTTGG CAGGGGGTTGTCTG - 5'	Thermo Fisher Scientific	Sequencing
Ajuba 5 prime start - Forward	<i>Mus musculus</i>	5' - ATGGAGCGGTTAG GAGAG - 3'	Thermo Fisher Scientific	Sequencing
Ajuba mid 1 - Forward	<i>Mus musculus</i>	5' – TACGACCAGCGCCA CG - 3'	Thermo Fisher Scientific	Sequencing
Ajuba mid 2 - Forward	<i>Mus musculus</i>	5' – CGGCACCTGTATCA AGTG - 3'	Thermo Fisher Scientific	Sequencing
Flag 5 prime start - Forward	<i>Mus musculus</i>	5' – ATGGACTACAAAGA	Thermo Fisher Scientific	Sequencing

		CGATGACGACAAG – 3'		
Flag 3 prime - Reverse	<i>Mus musculus</i>	3' – TCACTTGTCGTCATC GTCTTTG – 5'	Thermo Fisher Scientific	Sequencing
Egfp end - Reverse	<i>Mus musculus</i>	3' - TCACTTGACAGCT CGTCC - 5'	Thermo Fisher Scientific	Sequencing
Flag end - Reverse	<i>Mus musculus</i>	3' – TCACTTGTCGTCATC GTCTTTG - 5'	Thermo Fisher Scientific	Sequencing
pJet1 - Forward	<i>Mus musculus</i>	5' - CGACTCACTATAGG GAGAGCGGC - 3'	Thermo Fisher Scientific	Sequencing
pJet1 - Reverse	<i>Mus musculus</i>	3' – AAGAACATCGATTT TCCATGGCAG - 5'	Thermo Fisher Scientific	Sequencing

Table 2-8: Kits

Kits		
Name	Description	Source
Lipofectamine 2000		Thermo Fisher Scientific #11668019
Lullaby		OzBiosciences #FLL73000
Calcium phosphate kit		Thermo fisher Scientific #K2780-01
Amaya nucleofector kit V		Lonza #VCA-1003
Zymoclean DNA gel recovery		ZymoResearch #D4008
Rapid DNA ligation kit		Thermo Fisher Scientific #K2800
RNeasy mini kit		Qiagen #74104
RNase-Free DNase set		Qiagen #79254
SuperScript III Reverse Transcriptase kit		Thermo Fisher Scientific #18080-093
Dynamo HS SYBR green qPCR kit		Thermo Fisher Scientific #F410L

Table 2-9: PAAM hydrogels

<b>PAAM hydrogel preparation</b>		
Name	Description	Supplier
3-(Acryloyloxy)propyltrimethoxysilane (acrylsilane)	Coverslip treatment	Alfa Aesar #I16400
Rain-x	Coverslip treatment	Amazon UK
Acrylamide 40 % solution	PAAM Hydrogel component	Sigma-Aldrich #A4058
N,N' -methylene-bis-acrylamide 2 % solution	PAAM Hydrogel component	Sigma-Aldrich #M1533
N,N,N',N' - Tetramethylethylenediamine (TEMED)	PAAM Hydrogel component	Sigma-Aldrich #T9281
Ammonium persulfate (APS)	PAAM Hydrogel component	Sigma-Aldrich #A3678
HEPES	PAAM Hydrogel coating	Formedium #HEPES01
Sulfosuccinimidyl 6-(4' -azido- 2' - nitrophenylamino) hexanoate (sulfo-SANPAH)	PAAM Hydrogel coating	Thermo Fisher Scientific #22589
Fibronectin, bovine plasma	PAAM Hydrogel coating	Sigma-Aldrich #F1141
Ammonium hydroxide	RCA cleaning	Sigma-Aldrich #221228
Hydrogen peroxide	RCA cleaning	Sigma-Aldrich #31642
<b>PAAM hydrogels composition</b>		
Stiffness	Acrylamide (%)	Bis-Acrylamide (%)
0.7 kPa	3	0.06
7 kPa	5	0.3
38 kPa	10	0.3

Table 2-10: Software

Software		
Name	Supplier	Version
Image studio Lite	LICOR Biosciences Ltd	5.2
ApE	M. Wayne Davis	3.1.5
Prism	GraphPad	10.2.3
R studio	R Studio, Inc.	4.4.1
Adobe Illustrator CS5.1	Adobe Systems	15.1.0
Incucyte Zoom	Incucyte	2023
Image J- win 64	NHI, USA	2.1.7

## 2.2 Methods

### 2.2.1 Cell culture

#### 2.2.1.1 Cell lines origins

The PDACA cell line is a KPC cell line derived from mice bearing the mutations KRas<sup>G12D</sup> and p53<sup>R172H</sup> in the pancreas (Morton et al., 2010).

#### 2.2.1.2 Cell lines maintenance

PDACA, PDACB, and Hek293T cells were cultured on 10 cm) petri dishes using Dulbecco modified eagle media (DMEM) growth media supplemented with 10 % Foetal bovine serum (FBS) and 1 % L-glutamine. Serum-free media contains DMEM and 1 % L-glutamine. PDACA CRISPR cell lines (PDACA CRISPR EV, PDACA CRISPR 01, PDACA CRISPR 02, PDACA CRISPR All) were cultured using the same media with the addition of 0.2 % Puromycin. The cell lines were grown at 37 degrees celsius (°C) in a humidified incubator containing 5 % carbon dioxide (CO<sub>2</sub>).

When cell lines reached 80 % confluency, the cells were washed with PDB and trypsinised using 1 milliliter (mL) of PE buffer containing 0.25 % trypsin. After 4 minutes (min) incubation at 37 °C, cells were detached and resuspended in 10 mL of fresh media. From this 10 mL suspension of cells, 1mL was added into a new 10 centimetres (cm) petri dish with 10 mL of fresh media and placed into a 37 °C

humidified incubator containing 5 % CO<sub>2</sub>. Hek293T cell line maintenance followed a similar protocol with the exception of the trypsin phase, which was replaced by simply flushing the cells with fresh media.

### **2.2.1.3 Cell lines cryopreservation**

Cells were cultured on 15 cm petri dishes, at 80 % confluency cells were collected using PE -0.25 % trypsin and collected into a 15 mL falcon tube. Cells were pelleted by centrifugation and the cell pellet was resuspended in 20 % FBS-10 % Dimethyl sulfoxide (DMSO) solution and placed into cryotubes. The cryotubes were wrapped into cotton wool and immediately placed into a -80 °C freezer.

From the -80 °C freezer, cells were recovered by thawing the cryotube content in a 37 °C water bath. Cells were resuspended in fresh media and centrifuged to remove DMSO from the media. The cell pellet was resuspended in fresh media, placed into a 10 cm petri dish and incubated in a 37 °C humidified incubator containing 5 % CO<sub>2</sub>. The media was changed the next day to remove dead cells and debris.

## **2.2.2 Transfection**

### **2.2.2.1 Lipofectamine 2000**

In an Eppendorf 1 microgram (µg) of DNA was diluted in 500 microlitres (µL) of serum-free media. In a second Eppendorf were diluted 5 µL of Lipofectamine 2000 in 495 µL of serum free media. The contents of both Eppendorf were reunited, mixed together, and incubated for 10 minutes at room temperature (RT). The DNA-lipofectamine solution was added into 6-well plate wells on top of cells and incubated overnight in 37 °C humidified incubator containing 5 % CO<sub>2</sub>. The next day, the media as replaced with fresh media.

### **2.2.2.2 Amaxa reagents**

Cells were sequentially trypsinized and counted before  $1 \times 10^6$  cells per condition were centrifuged for 4 minutes at 1200 rpm. Cells were transfected using 5 µg of DNA construct using Amaxa Cell Line Nucleofactor kit, kit V. Each transfection

contains, 85 of Solution V and 15  $\mu\text{L}$  of supplement 1, mixed in an eppendorf before were added 5  $\mu\text{g}$  of DNA construct. The eppendorf content was then homogenised before being added to the pelleted cells. The resuspended cells were added in cuvettes and the electroporation was performed using programme P-031 from the AMAXA electroporator (Lonza Bioscience). The transfected cells were transferred into a 6-well plate well containing 2 mL of culture media. The culture media was changed 6 hours (h) after transfection to allow optimal cell survival and transfection efficiency. Cells were used 24 h after transfection.

Regarding the transfection of Ptripz-egfp:AJUBA, the transfected cells were transferred into a 6-well plate containing 2 mL of DMEM supplemented with Tet system-approved FBS and L-glutamine. The next day, 0.02 ng to 1  $\mu\text{g}\cdot\text{mL}^{-1}$  of doxycycline was added to the media and incubated between 12 to 48 hours.

### **2.2.2.3 Calcium phosphate**

In plastic bijou were mixed thoroughly together 5  $\mu\text{g}$  selected DNA construct in a final volume of 440  $\mu\text{L}$  of water. 500  $\mu\text{L}$  2 x HBS were mixed in the plastic bijou before adding 60  $\mu\text{L}$  2 molar (M) CaCl. Using a pipetman, the plastic bijou content was swooshed up and down multiple times before being placed to incubate at 37 °C for 30 minutes. The content was added gently to the plated cells and incubated overnight at 37°C in a humidified incubator containing 5 % CO<sub>2</sub>.

### **2.2.2.4 Transfection of small interfering RNA (siRNA) in cells**

In an Eppendorf were diluted 7.5  $\mu\text{L}$  of lullaby in 500  $\mu\text{L}$  serum-free. In parallel, in another Eppendorf were diluted 10 nanomolar (nM) siRNA or control siRNA in 100  $\mu\text{L}$  of serum-free media. The contents of both Eppendorf were combined and incubated at RT for 10 min before being added to the cells with a final volume of 2.5 mL. The cells were incubated for 48 hours before this protocol was applied once more. After the second siRNA transfection, the cells were left to incubate for 24 hours and analysed.



### 2.2.2.5 Lentiviral transfection and selection of stable cell lines

The generation of stable cell lines used throughout this thesis was created using CRISPR-Cas9 technology.  $1 \times 10^6$  cells of HEK293T cells were plated on 10 cm dish and incubated overnight at 37 °C in a humidified incubator containing 5 % CO<sub>2</sub>. The next day, HEK293T cells were transfected using the calcium phosphate method. To do so, in plastic bijou were mixed thoroughly together 10 µg selected lentiviral construct, 4 µg pVSVG and 7.5 µg of pSPAX2 in a final volume of 440 µL of water. 500 µL 2xHBS were added and mixed in the plastic bijou. 60 µL of 2 M CaCl were added slowly, and the plastic bijou content was mixed up and down several times using a P1000 pipette before being incubated at 37 °C for 30 minutes. The content was added gently to the plated HEK293T cells and incubated overnight at 37 °C. The next day, HEK293T cultured media was removed and replaced with 6 mL of DMEM complemented with 20 % Foetal bovine serum, which will help with virus production.  $5 \times 10^5$  PDACA cells were plated in culture media. At day four, the media from HEK293T cells was removed using a syringe, filtered through a 0.45 µm filter. 2.5 µL of polybrene was added to the filtered media. In the meantime, the media was removed from the PDACA cells and replaced by filtered HEK293T media containing polybrene. Fresh DMEM-20 % FBS was added to HEK293T cells and cells were incubated overnight at 37 °C. At day five, the steps from day 4 were repeated with the only exception being HEK293T cells being discarded. At day six, PDACA cells were washed and DMEM/10 % FBS/ 0.02 % puromycin media (selection media) was added to the cells. In parallel, as a puromycin selection control, untransfected PDACA cells were cultured with DMEM/10 % FBS/ 0.02 %. PDACA CRISPR cells were selected and cultured for two weeks in selection media before testing the CRISPR efficacy by western blot.

## 2.2.3 Molecular biology and cloning

### 2.2.3.1 sgRNA design and insertion into PURO pLenti CRISPR vector

To realise a clustered regularly interspaced short palindromic repeats (CRISPR)-CRISPR associated protein 9 (Cas9)-mediated knockout, single-guide ribonucleic acid (RNA) oligos were designed by horizon discovery (<https://horizondiscovery.com/en/gene-editing>). Single guides RNA (sgRNA) sequences were modified by including at the sgRNA forward 5' "CACCG-", at the sgRNA reverse 3' "C-" and at the sgRNA 5' "CAAA" (Table 2-6). Each sgRNA was annealed using 1  $\mu$ L of forward (stock 100  $\mu$ M) and 1  $\mu$ L of reverse (stock 100  $\mu$ M). Oligos were mixed together with 1  $\mu$ L of T4 DNA Ligase buffer and 7  $\mu$ L of nuclease-free H<sub>2</sub>O to a final volume of 10  $\mu$ L and PCR reaction included:

1. 30 min at 37 °C
2. 5 min at 95 °C
3. 1 min per step at gradually decreasing temperatures from 90 °C to 30 °C with each step decreasing by 5 °C.
4. 1 min at 25 °C
5. Holding step at 4 °C

Meanwhile, 5  $\mu$ g of pLenti CRISPR vector were mixed with 3  $\mu$ L of esp31 enzyme HF, 6  $\mu$ L HF buffer and nuclease-free H<sub>2</sub>O to a final volume of 60  $\mu$ L and were incubated overnight at 37 °C in a water bath. An electrophoresis was performed the next day to isolate the cut vector. The annealed oligonucleotides were ligated into Puro pLenti CRISPR vector using Roche ligation kit and transformed into *E. coli* dh5 alpha competent bacteria.

### 2.2.3.2 Polymerase chain reaction (PCR)

Each PCR reaction contained 10 ng of the DNA template mixed with 100 ng of the forward and reverse primers, 25  $\mu$ L of PrimeStar Max Premix and nuclease-free

water for a final volume of 50  $\mu\text{L}$ . The PCR reaction was performed using a T100 Thermal Cycler (BioRad) using the following program:

1. 5 min at 98 °C
2. 10 seconds (sec) at 98 °C
3. 15 sec at  $T_m$  (specific to each primer set)
4. 1 min/kilobase (kb) at 72 °C
5. repeat the steps 2 to 4, for 30 cycles
6. 15 min at 72 °C
7. Holding at 4 °C

### **2.2.3.3 Electrophoresis and gel purification**

The PCR products or restriction digests were loaded on an 1 % high grade agarose gel diluted in Tris base, acidic and EDTA (TAE) buffer, left to set with 5  $\mu\text{L}$  of Midori green per 100 mL of agarose gel. In the sample were added a loading dye to visualise the migration front. The samples were then added into the agarose gel wells. 6  $\mu\text{L}$  of 1 kb DNA ladder (Invitrogen) were added to the gel. The size chosen will depend on PCR product size of interest. The gel was then placed into an electrophoresis tank and 1xTAE buffer was poured over it to fully cover the agarose gel. The electrophoresis was performed at 100 V for 30 minutes. The DNA fragments of interest were visualised using a ultraviolet (UV) transilluminator, cut out of the gel using scalpels, placed into separate eppendorfs and recovered using a Zymoclean DNA gel recovery kit. The gel fragments were dissolved in 3 volumes of ADB reagent heated at 50 °C. Within the Zymoclean DNA gel recovery kit, filter columns were used to isolate DNA fragments from diluted gel. The columns were loaded with the samples, centrifuged at 10,000 x g for 30 minutes, and washed twice with washing buffer before the DNA was eluted in nuclease-free water.

### **2.2.3.4 Restriction digestion**

Two to five  $\mu\text{g}$  of DNA was digested using 1 $\mu\text{L}$  of restriction enzymes and 2  $\mu\text{L}$  of the corresponding NEB buffer, in a final volume of 20  $\mu\text{L}$  of nuclease-free water,

incubated overnight in a 37 °C water bath. Reaction products were loaded in agarose gel to verify DNA fragment sizes before purification.

### **2.2.3.5 DNA ligation**

DNA ligations were performed following rapid DNA ligation kit manufacturer instructions. 1 µg of DNA insert was added to 5 µg of DNA vector, alongside 1µL T4 DNA ligase, into a final volume of 20µL nuclease-free water, incubated for 5 minutes at RT. 5µL were used for transformation into competent cells.

### **2.2.3.6 Transformation into DH5α *E. coli* and colony selection**

Chemically competent DH5α *E. coli* were removed from the -80 °C freezer and thawed on ice for 15 minutes. The DH5α *E. coli* were transferred into a tube, the selected plasmid was added and mixed gently. The tube was then kept on ice for 15 min. Plasmid was inserted into the cells by a heat shock achieved by incubation of the tube at 42 °C for 50 seconds and swiftly placed back on ice. 1 mL of L-broth media was added, and the cells were incubated for 1 hour at 37 °C. On L-Broth (LB-agar plates of selected antibiotics were spread 200 µL of the transformed DH5α *E. coli* and the plates were incubated overnight in a 37 °C incubator.

### **2.2.3.7 Minipreps**

Individual colonies were selected from LB-agar plates after incubation overnight. The selected colonies were individually placed into tubes using a sterile tip and incubated overnight in 3 mL LB media supplemented with the selected antibiotic, shaking at 200 rpm in a 37 °C incubator. The resulting bacterial culture was centrifuged, the bacterial pellet was harvested, and the plasmid purifications were performed by the Scotland Institute Molecular Technology Services using the QIAprep Spin Miniprep kit.

### **2.2.3.8 Sequencing**

Sequencing was performed by the Scotland Institute Molecular Technology Services, from plasmid purified samples. The resulting sequences were aligned

against the plasmid reference sequence using ApE (v3.1.4). After sequence validation, the specific colonies were transformed into competent cells to generate maxipreps cultures.

### **2.2.3.9 Maxiprep**

As described for minipreps, colonies were selected from LB-agar plates and transferred into an Erlenmeyer containing 150 mL of LB-selected antibiotic. The Maxipreps were then incubated overnight at 37 °C, shaking at 200 rpm. The cultures were then centrifuged, the pellet was harvested. The plasmid purifications were performed by The Scotland Institute Molecular Technology Services.

### **2.2.3.10 Ajuba constructs design and cloning**

Human Ajuba protein sequence was extracted for CCDS (Consensus CDS). Ajuba sequence was modified by adding specific tags (Myc, Flag) at either side (either N or C terminal) of the sequence and XbaI restriction site at both 5' and 3' ends. These constructs were produced by GENEWIZ. Upon delivery, each construct was first inserted into pJet, an intermediary vector and then inserted into plhcx or pcdna 3.1 vectors using restriction digestion (XbaI), ligation and transformation into competent bacteria. After transformation into a vector, the newly created vector was validated by sequencing.

The Human Ajuba protein sequence was extracted from the myc-Ajuba construct by PCR and subsequently cloned into pEGFP N1 and pEGFP C1 vectors using restriction digestion (BamH1, EcoR1), ligation and transformation into competent bacteria. Minipreps were created and sequenced to validate each clone. The validated clones were transferred into maxipreps and tested in PDACA cells.

## **2.2.4 Bioengineering polyacrylamide hydrogels**

### **2.2.4.1 Activation**

Coverslips were cleaned by ultrasonic baths of 30 min with respectively miliQ water and 100 % ethanol. Coverslips were RCA cleaned, through submersion in a

5:1:1 ratio of respectively water, 30 % w/w hydrogen peroxide (H<sub>2</sub>O<sub>2</sub>) and Ammonium hydroxide (NH<sub>3</sub>), heated at 70 °C, for 10 minutes. Coverslips were rinsed in miliQ water before submersion in a solution of acrylsilane (made of 50 mL of ethanol, 2.5 mL of miliQ water and 231 µL of 3-(Acryloyloxy)propyltrimethoxysilane). Coverslips were incubated for 2 hours before they were rinsed with 100 % ethanol and dried in an oven at 120 °C.

#### **2.2.4.2 Passivation**

Coverslips were cleaned by ultrasonic baths of 30 min with respectively miliQ water and 100 % ethanol. Coverslips were then passivated in Rain-X solution for 3 minutes. Coverslips were washed with 100 % ethanol and air-dried.

#### **2.2.4.3 Preparation of polyacrylamide hydrogel (PAAM)**

Polyacrylamide hydrogels were created by mixing, while on ice, 40 % w/w acrylamide, 2 % w/w bis-acrylamide, 1.5 % w/w N,N,N',N' - Tetramethylethylenediamine (TEMED) and 5 % Ammonium persulfate (APS). Different polyacrylamide hydrogels stiffnesses were created by modulating the proportion of acrylamide and bis-acrylamide, while the remaining components remained unchanged. The resulting solutions were placed between a passivated and an activated coverslip. After 30 minutes, the PAAM were separated from the passive coverslips and rinsed with miliQ water. PAAM hydrogels were stored at 4 °C.

#### **2.2.4.4 Functionalization**

Polyacrylamide hydrogels were functionalized using a protein crosslinker, Sulfo-succinimidyl 6-(4'-azido-2'-nitrophenylamino) hexanoate (Sulfo-SANPAH). Sulfo-SANPAH were diluted to 0.2 mg.mL<sup>-1</sup> in miliQ water, added on top of hydrogels and incubated for 5 min at RT. Hydrogels were UV-treated at 365 nm for 15 minutes. The Sulfo-SANPAH allow binding of the ECM molecule amine

residues, at PAAM hydrogels surface, through its binding to Sulfo-SANPAH's nitrophenyl azide residue, activable by UV treatment. The hydrogels were washed with 4-(2-hydroxyethyl)-1-piperazineethanesulfonic acid (HEPES) buffer.

#### **2.2.4.5 Coating**

Polyacrylamide hydrogels were functionalized using Sulfo-SANPAH, acting as a link between PAAM hydrogel surface and ECM molecule. In pancreatic cancer, fibronectin is the most represented ECM protein in the stroma surrounding the tumor. Functionalized hydrogels were coated with  $10 \mu\text{g}\cdot\text{mL}^{-1}$  of fibronectin, diluted in HEPES buffer. Hydrogels were incubated overnight at  $37^\circ\text{C}$ . Hydrogels were rinsed three times with PBS before being used.

### **2.2.5 RNA base methods**

#### **2.2.5.1 RNA extraction**

Cells, cultured on either 6-well plates or 10 cm dishes, were placed on ice, and washed with ice-cold Phosphate buffer saline (PBS). For cells cultured on top of 32 mm fibronectin-coated PAAM hydrogels and glass coverslips placed in a 6-well plate, the coverslips/PAAM hydrogels were first transferred into a new 6-well plate containing ice-cold PBS. The RNA was extracted on ice using RNeasy Mini Kit (Qiagen), following the manufacturer's instructions. 350  $\mu\text{L}$  RLT buffer was added to the cells, and the resulting lysate was added in an Eppendorf containing 350  $\mu\text{L}$  of 70 % EtOH and mixed together. The lysates were then transferred into RNeasy spin columns placed in 2 mL collection tubes. The columns were centrifuged for 30 sec at  $8,000 \times g$ . The collected flow-through was then discarded and 700  $\mu\text{L}$  of the RW1 buffer was added to the columns. The columns were centrifuged for 30 sec at  $8,000 \times g$ . The collected flow-through was then discarded. The columns were washed by adding 500  $\mu\text{L}$  of RPE buffer and centrifuging the column for 30 sec at  $8,000 \times g$ . This step was repeated twice. The collected flow-through was discarded. The RNA was eluted with 30  $\mu\text{L}$  nuclease-free water by centrifugation of the column during a 1 min at  $8,000 \times g$ . For RNA to be used in an RNA sequencing experiment, the following steps were performed after centrifugation of the column containing the RW1 buffer. 10  $\mu\text{L}$  of DNase I stock solution were added to

70µL of RDD buffer and mixed gently. The Dnase1-RDD buffer was added onto the column and incubated for 15 minutes at RT. The membranes were washed with 350 µL of RW1 buffer, followed by a 15-second centrifugation at 8,000 x g. From this point forward, the protocol resumed with the addition of 500 µL of RPE buffer.

### **2.2.5.2 CDNA synthesis**

1 µg of total RNA was used to synthesised cDNA using Invitrogen SuperScript III Reverse Transcriptase protocol according to the manufacturer's instructions. PCR reaction was performed using the following steps: 5 min at 25 °C, 30 min at 50 °C, 15 min at 70 °C, hold at 4 °C.

### **2.2.5.3 qRT-PCR**

qRT-PCR was performed using DyNAmo HS SYBR Green qPCR kit according to the manufacturer's instructions. 300 ng of cDNA diluted in 1µL was used in each well of MicroAmp Fast 96-well reaction plate (Applied biosystems) and combined with 9 µL of SYBR Green master mix. The SYBR Green master mix contains 10 micromolars (µM) Primer mix, 5 µL of DyNAmo HS SYBR Green qPCR mix, in nuclease free water, in a final volume of 10 µL. Each condition was performed and analysed in technical triplicate. PCR reaction was performed on a C1000 Thermal Cycler (CFX96 Real time system, BioRad). Quantification have been performed using the 2<sup>-ddCT</sup> method for all gene analysed.

### **2.2.5.4 RNA Sequencing from PAAM hydrogels**

The RNA extraction was realised as described in the 2.2.5.1 section and the RNA quality check was performed by Jillian Murray (Scotland Institute, Molecular technology services) using Agilent Technologies TapeStation according to the manufacturer's instructions. 5 µL of RNA sample buffer was mixed with 1 µL of RNA ladder and added to the tube of an RNase-free mini-tube strip. 5 µL of RNA sample buffer was mixed with 1 µL of RNA sample and loaded onto the strip. The samples were vortexed and centrifuged at 2,000 rpm for 1 minute. Samples were heated to 72°C for 3 minutes and directly placed for 2 min on ice. Samples were centrifuged for 1 minute at 2,000 rpm and subsequently loaded into the Agilent



2200 TapeStation instrument. Qubit and RNA integrity number (RIN) scores were calculated and samples with an RIN score above 9 were considered for RNA sequencing experiments.

cDNA libraries were prepared using the Illumina TruSeq RNA Sample prep kit v2 according to previously established protocols (Fisher et al., 2011). The libraries were sequenced by Dr Graeme Clark (Scotland Institute, Molecular technology services) using the Illumina NextSeq500 platform and the High Output v2 75cycles sequencing kit (2 x 36 cycles Paired-End, single index). The quality of the raw RNASeq data files were checked using fastqc (<http://www.bioinformatics.bbsrc.ac.uk/projects/fastqc>) and fastq screen ([http://www.bioinformatics.babraham.ac.uk/projects/fastq\\_screen/](http://www.bioinformatics.babraham.ac.uk/projects/fastq_screen/)).

The RNA-seq reads were aligned to the mouse genome and the expression levels were determined and statistically analysed by Ryan Kwan (Scotland Institute, Bioinformatic department) from the Scotland Institute bioinformatic department. The differential gene expression analysis was performed using DESeq2. Significantly changed genes ( $\text{padj} < 0.05$ ) were analysed for gene ontology (GO) analysis and Gene set enrichment analysis (GSEA).

The comparison of 2017 versus 2023 RNA sequencing was performed by Robin shaw, from the Scotland Institute bioinformatic department, through the analysis in both dataset of significant genes, standard errors of log 2 fold change and functional enrichment analysis (g:Profiler)

## 2.2.6 Protein-base methods

### 2.2.6.1 Protein lysates

The cultured cell media was removed, replaced with ice-cold PBS and washed three times. Plates were placed on ice for the duration of the cell lysis. Cells lysis was performed using RIPA buffer complemented with 1X Halt phosphatase inhibitor cocktail and 1X Halt protease inhibitor cocktail. Cells were scraped and then collected into Eppendorf tubes, swiftly placed on ice. Tubes were

centrifuged at 4 °C, 10 minutes. The supernatant was transferred into a new Eppendorf tube.

For cells cultured on PAAM hydrogels, cells were lysed using the same protocol except cells were not scraped but were lysed using glass beads.

### **2.2.6.2 Protein quantification**

The precise protein content of each sample was assessed using the Precision red advanced protein assay 5 µL of lysate was added to 995 µL of Precision red solution into cuvettes. The resulting solution was incubated for 1 minute at RT and mixed thoroughly. The cuvettes were placed in a spectrophotometer and the absorbance was measured at optical density (OD)<sub>600nm</sub>. The protein concentration was measured.

### **2.2.6.3 SDS-PAGE protein separation**

Samples containing 15 µg of protein (25 µg for PAAM hydrogels samples) were prepared by mixing 15 µg worth of protein lysate, 1X NuPAGE LDS sample buffer and 1X NuPAGE reducing agent. Samples were boiled for 3 minutes at 100 °C and loaded on NuPage 4-12 % Bis Tris Gel (Invitrogen) pre-cast gels. 7 µL of PageRuler pre-stained protein ladder (molecular ladder) was loaded on the first well of the gels. Within the tank was placed NuPAGE MOPS SDS running buffer to conduct the electric current and allow the protein to migrate within the gel. The gels were run at 170 Volts (V) for 1 h or until the samples reached the bottom of the gels.

### **2.2.6.4 Western blots**

The SDS-PAGE-gel containing protein was placed in a western blotting apparatus tank (BioRad), along a 0.45 µm nitrocellulose membrane (Bio-rad), compressed between Whatman paper and two sponges. 1X transfer buffer was used to fill the BioRad tank. The transfer was performed at 120 V for 1 h with an ice-cold pack inside the tank. Membranes were blocked with 5 % BSA in TBS-T (10 mM Tris pH = 8.0, 150 mM NaCl, 0.5 % Tween-20). Membranes were incubated with the primary

antibody diluted in blocking buffer, overnight at 4 °C. Membranes were washed 3 times with using 1X TBS-T. Membranes were incubated one hour at RT with the secondary Alexa Fluor conjugated antibodies diluted at 1/10,000 in blocking buffer. Membranes were washed 3 times using 1X TBS-T. The membranes were imaged by the Li-Cor Odyssey CLX system using the automated signal intensity mode and analysed by Image Studio Lite software.

## 2.2.7 Cell Biology Work

### 2.2.7.1 xCELLigence

E-plate 16-well (xCELLigence) were coated with fibronectin overnight at 4 °C. 100 µL of pre-warmed culture media was added to each well and the plate was equilibrated in the Acea RTCA DP xCELLigence machine, 45 minutes before imaging.  $5 \times 10^3$  cells homogenised in 50 µL of media were added on top of the well and swiftly inserted in the Acea RTCA DP xCELLigence machine within a 30 °C, 5 % CO<sub>2</sub> incubator. Cell impedances were measured for 8 hours, with measurements taken at 5minute intervals. The impedances were measured over time and changes were tracked using Cell index. Quadruplicates readings were taken for each condition. Cell index was measured by the following equation:

$$Cell\ index\ (t) = \frac{R_{ce}(t) - R_b}{15}$$

Where:  $R_{ce}(t)$  represents the impedance at a time point  $t$ ,  $R_b$  represents the impedance background, and 15 represents the nominal impedance value for the device.

### 2.2.7.2 Proliferation assay

96-well Image Lock plate (Essen) wells were coated with  $10\ \mu\text{g}\cdot\text{mL}^{-1}$  fibronectin overnight and plated with  $2 \times 10^3$  cells in each well. Cells were left to seed for 3 hours at 37 °C in a humidified incubator containing 5 % CO<sub>2</sub>. 96-well Image Lock plate was loaded onto the Incucyte Zoom system and images were acquired every hour for 4 days. The proliferation was assessed with the automated Incucyte Zoom software by tracking the cellular confluency over time.

### **2.2.7.3 Scratch wound migration assay**

Confluent cell monolayers were prepared by seeding  $3 \times 10^5$  cells per mL on 96-well Incucyte Imagelock plates. Cells were incubated overnight at 37 °C in a humidified incubator containing 5 % CO<sub>2</sub>. The wound was performed using the 96-pin WoundMaker (Essen Bioscience). The plates were loaded into the Incucyte Zoom system (Essen Bioscience) and images were acquired at 60 min intervals for 24 hours. The Wound healing was analysed with the automated Incucyte Zoom software providing a relative wound density over time.

### **2.2.7.4 Circular invasion assay: Essen protocol**

96-well Image Lock plate (Essen)wells were coated with 25 µL of 1 % Matrigel (corning) diluted in culture media overnight at 37 °C. The next day, the media was removed from the plate. Cells were trypsinized, counted, and  $8 \times 10^5$  cells were resuspended in 100 µL and seeded in each well. Every condition was seeded as sextuplicate and incubated overnight at 37 °C. The following day, a wound was made using 96 pin WoundMaker (ESSEN BioScience). Wells were washed twice with media and dried before 50 µL of Matrigel was added. The plate was then incubated for 15 minutes at 37 °C. 100 µL of culture media was added on top of each well and placed on the Incucyte Zoom system (Essen Bioscience). The wound healing videos were extracted and analysed using ImageJ studio.

### **2.2.7.5 Focal adhesion turnover**

35mm glass bottom MatTek were coated with fibronectin for one hour at room temperature. Cells were trypsinized and counted.  $1 \times 10^6$  cells per conditions were centrifuged for 4 minutes at 1,200 x g. The culture media was removed, and cells were transfected using 5 µg of DNA construct using Amaxa Cell Line Nucleofactor kit, kit V, programme P-031 (Lonza Bioscience). 1 mL of fresh culture media was added to the cells after nucleofection, and 200 µL were plated on 35 mm glass bottom MatTek coated with fibronectin. The culture media was changed 3 h after transfection to ensure optimal cell survival and transfection rate, and cells were incubated overnight at 37 °C. The media was changed 4 hours before imaging on

the Ayriscan 880 microscope. Images were acquired every 20 seconds for 30 cycles. Images were consecutively airyscan processed and stabilized. Images were turned to greyscale and processed using a 15-pixel rolling ball to remove the background and expose the focal adhesion before submitting to FAAS (<http://faas.bme.unc.edu/>) with the following parameters: the adhesions were not split, a media filter was applied and the detection threshold was set to 4.5. The adhesion size minimum was set to 15 pixels. The minimum FA phase length was set to 5 images with a minimum FAAI ratio of 3. The detection threshold has been determined in advance by submitting Tiff format, grey scaled, 8-bit, single images, using the FAAS adhesion threshold setting, and maintained across all images.

### **2.2.7.6 Immunofluorescence**

Cells previously seeded on sterile coverslips, were rinsed once in PBS before being fixed with 4 % paraformaldehyde (PFA) for 10 minutes at RT. Cells were washed thoroughly 3 times with PBS. The permeabilisation was carried out using 20 mM glycine, 0.05 % Triton X-100 diluted in PBS, for 5 minutes at RT. Cells were then incubated with the blocking buffer (0.2 % Triton X-100, 2 % BSA, diluted in PBS) for 10 minutes at RT. The primary and secondary antibodies were respectively diluted in blocking buffer and incubated for one hour. Cells were washed using 0.2 % Triton X-100 diluted in PBS. Cells were then mounted on glass slides using ProLong Diamond Antifade Mountant (Invitrogen).

#### **2.2.7.6.1. Immunofluorescence for circular invasion assay**

Cells were prepared following the Circular invasion assay protocol and left to invade overnight in the incubator at 37 °C. The next day, the media was removed, and the wells were washed with PBS.

##### **2.2.7.6.1.1. BSA permeabilisation**

The PBS was removed from the wells and cells were fixed with 4 % PFA for 30 minutes at RT. After thorough washes with PBS, the cells were permeabilised using

0.1 % Triton X-100 for 30 minutes. Cells were washed three times with PBS and were then blocked, using 1 % BSA for 30 minutes. Primary antibodies were diluted in blocking buffer and incubated overnight at 4 °C. Cells were washed and the secondary antibodies were diluted in blocking buffer and incubated overnight at 4 °C. Cells were washed 3 times with PBS and imaged in PBS using the Zeiss 880 Laser Scanning Microscope with Airyscan.

#### **2.2.7.6.1.2. PFS permeabilisation**

Following the Bryant protocol, PBS was removed and 100 µL of 4 % PFA was added and incubated for 15 minutes at RT. PFA was removed and wells were washed twice in PBS. Cells were blocked using 100 µL with PBS, fish skin gelatin, saponin buffer (PFS) for 1 hour at RT, with gentle agitation. PFS was made of 3.5 g of fish skin gelatin (Sigma), 1.25 mL of 10 % saponin/PBS, diluted into a final volume of 500 mL. PFS was sterilised by filtration and stored at 4 °C. Primary antibody (1/100) was diluted in PFS and incubated overnight at 4 °C with gentle agitation. The primary antibody was removed, and the cells were washed several times, for 5 minutes, with PFS. The secondary antibody was diluted in PFS (50 µL), and incubated for one hour at RT, away from light. The secondary antibody was removed, and cells were washed with PFS and several times with PBS, with gentle agitation. PBS was added to each well and the plate was imaged using the Zeiss 880 Laser Scanning Microscope with Airyscan.

#### **2.2.7.7 Spreading assay**

19 mm Coverslips were coated with fibronectin overnight at 4 °C.  $1 \times 10^4$  cells were then seeded on top of the coverslips and incubated overnight at 37 °C in a humidified incubator containing 5 % CO<sub>2</sub>. Cells were fixed with 4 % PFA at different intervals. Images were acquired using the Nikon AIR Inverted Confocal Microscope. Cell and nucleus areas were selected by applying a threshold (min: 100pixels) and measured using an analyse particle tool (parameters: size: 5-infinity, avoid borders) on Fiji software.

### **2.2.7.8 Concanavalin A**

6-well plates and 19 mm coverslips were coated with  $10 \mu\text{g}\cdot\text{mL}^{-1}$  and incubated overnight at  $4^\circ\text{C}$ . Plates and coverslips were washed with PBS and cells were plated in either serum-free media or culture media, incubated overnight in a humidified incubator containing 5 %  $\text{CO}_2$  before use.

### **2.2.8 Statistical analysis and reproducibility**

All datasets and statistics were analysed using Prism software v10.2.3. For comparisons of two conditions, unpaired/paired t-test was performed. For the comparisons of more than two conditions, an ANOVA test was performed. Statistical annotations represent the following: ns = not significant, \* < 0.05, \*\*  $\leq$  0.01, \*\*\*  $\leq$  0.001, \*\*\*\*  $\leq$  0.0001.

**Chapter 3. The impact of stiffness on PDACA cells  
and the selection of mechanotransduction  
candidates**



### 3.1 Introduction:

The field of mechanobiology and tissue engineering is aimed at deciphering the impact of environmental factors on cells. At a broader level, it aims at the regeneration of damaged tissues by controlling their environment (D'Angelo et al., 2019; Yi et al., 2022). Cell fate is tightly linked to ECM cues (composition, forces, topography), and grasping the impact between these factors would bring a better understanding of cancer cells and metastasis behaviours (Guilak et al., 2009; Wolfram et al., 2024). ECM mechanical cues are sensed by the cell, which is referred to as mechanosensing, and converted into a biological response by processes referred to as mechanotransduction.

A key protein in mechanotransduction is YAP. YAP is a transcriptional co-activator, which relays the mechanical cues from the ECM, which is linked via cytoskeleton tension to the nucleus, to regulate gene expression accordingly. Due to the role of YAP in the transmission of the mechanical cues from the cytoskeleton to the nucleus, YAP will be activated and translocated in the nucleus in stiff ECM conditions whereas YAP, in soft conditions will be sequestered in the cytoplasm (Nasrollahi S, 2017). In PDAC, the desmoplastic reaction triggers an increase in tissue stiffness which be an indicator of cancer stage and patient prognostic (Maccurtain et al., 2021; Rice et al., 2017). In healthy individuals, pancreatic cells are surrounded with <1kPa stiffness while PDAC tumours could reach between 4 to 10kPa (Rice et al., 2017). This difference frequently contributes to chemotherapy resistance and increases both cancer invasion and metastasis (Rice et al., 2017). It is to be highlighted that a similar stiffness can have different effects on different cell lines and different cancer types (Butcher et al., 2009). This notion is true for both *in vivo* and *in vitro* studies. *In vitro* studies are commonly performed by culturing adherent cell lines on plastic or glass bottom plates. *In vitro* studies are highly impacted by this type of culture, masking effects only observable in their respective physiological or pathological environmental stiffnesses (Birgersdotter et al., 2005). Through collaboration between mechanobiology and engineering studies, different options to mimic cells' natural environment were created such as hydrogels, patterns, pillars, and scaffolds, using natural, synthetic or composite biomaterials (Eyckmans et al.,

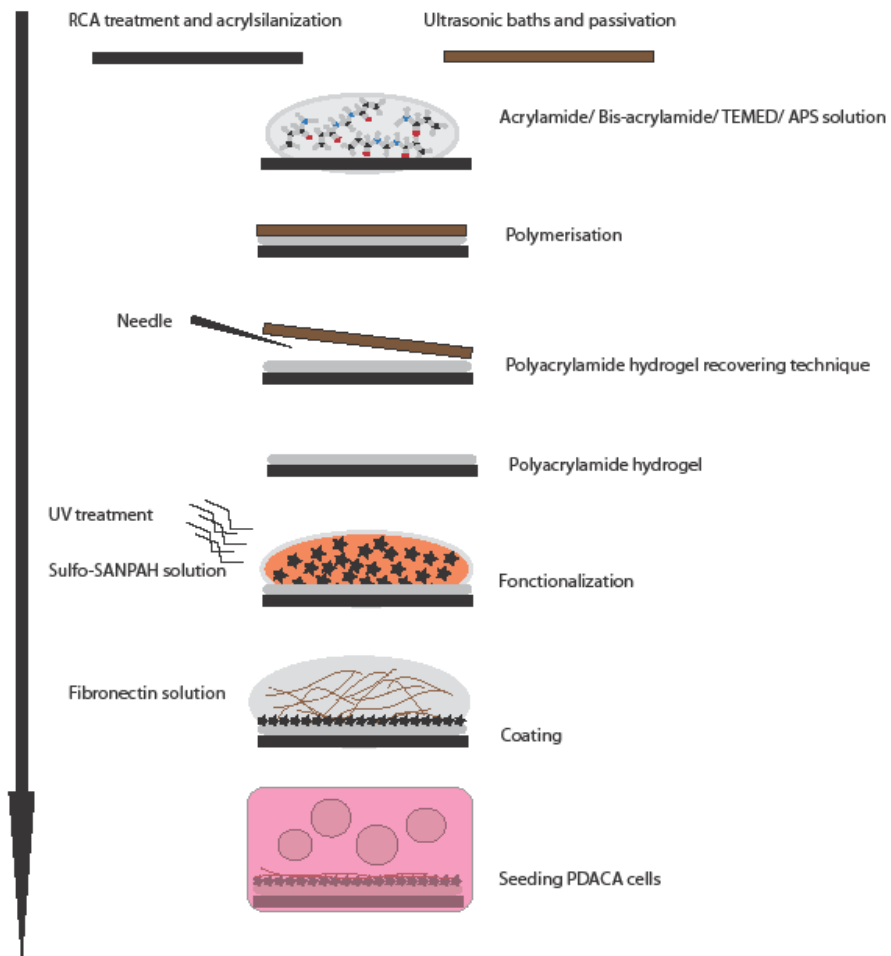
2011; Han et al., 2016). Although not all the parameters (composition, forces, topography) can be reproduced at once, many options are available to study parameters separately. In this chapter, I will investigate how the mechanical aspect of the environment affects pancreatic cancer cell lines' morphology, proliferation and gene expression. I will also select and validate four possible candidates involved in mechanotransduction in PDACA cells at RNA levels.

## **3.2 Stiffnesses impacts PDACA cellular behaviour.**

### **3.2.1 Preparation of polyacrylamide hydrogel**

Common tissue culture practices for *in vitro* studies are the culture of adherent cell lines on plastic or glass-bottom plates. Plastic and glass are extremely stiff materials, corresponding to around 2 to 4 GPA. To mimic a stiffness closer to a physiological or pathological stiffness, polyacrylamide hydrogels were created from crosslinking of two types of monomers, acrylamide and bis-acrylamide, between two specially treated coverslips (Figure 3-1). Polyacrylamide hydrogels were created following Tse and Engler protocol published in 2010 (Tse & Engler, 2010). This protocol allows the creation of a wide range of tunable stiffnesses and facilitates the study of biophysical environmental effects on cellular behaviour *in vitro*. Following polyacrylamide hydrogels polymerisation between the acrylsillanised coverslip and the passive coverslip, hydrogels were functionalized using a protein crosslinker, Sulfo-SANPAH. The acrylsillanised coverslips were treated to increase the adherence of the hydrogel to the glass coverslips. The passive coverslips were treated to become water repellent which allows the detachment of the hydrogel after polymerisation with a plane surface for the cell to adhere to. Sulfo-SANPAH would act as a physical link between the PAAM hydrogel surface and ECM molecules, allowing the attachment of ECM molecules to the gel, which is otherwise unlikely. In pancreatic cancer, fibronectin is one of the ECM proteins in the PDAC environment alongside elastin, laminin, and collagens (Ferrara et al., 2021). Fibronectin is a major ECM mechanoregulator due to its structural flexibility and its strong cellular adhesion properties, making fibronectin a highly used ECM component in mechanobiology (Wang et al., 2016; Zollinger & Smith, 2017). Sulfo-SANPAH allows binding of the fibronectin amine

residues at PAAM hydrogels surface by binding to Sulfo-SANPAH's nitrophenyl azide residue, activable by UV treatment (Mustapha et al., 2022). PDACA cells were seeded and cultured on these fibronectin-coated polyacrylamide hydrogels of different stiffnesses overnight. Three stiffnesses were chosen to embody tissue and tumour stiffnesses. 0.7 kPa PAAM hydrogel will recapitulate the physiological stiffnesses of a healthy pancreas, while 7kPa mimics PDACA tissue and 38 kPa recapitulates stiff tissue. The different types of PAAM hydrogels differ in monomer concentration resulting in different stiffnesses after polymerisation.



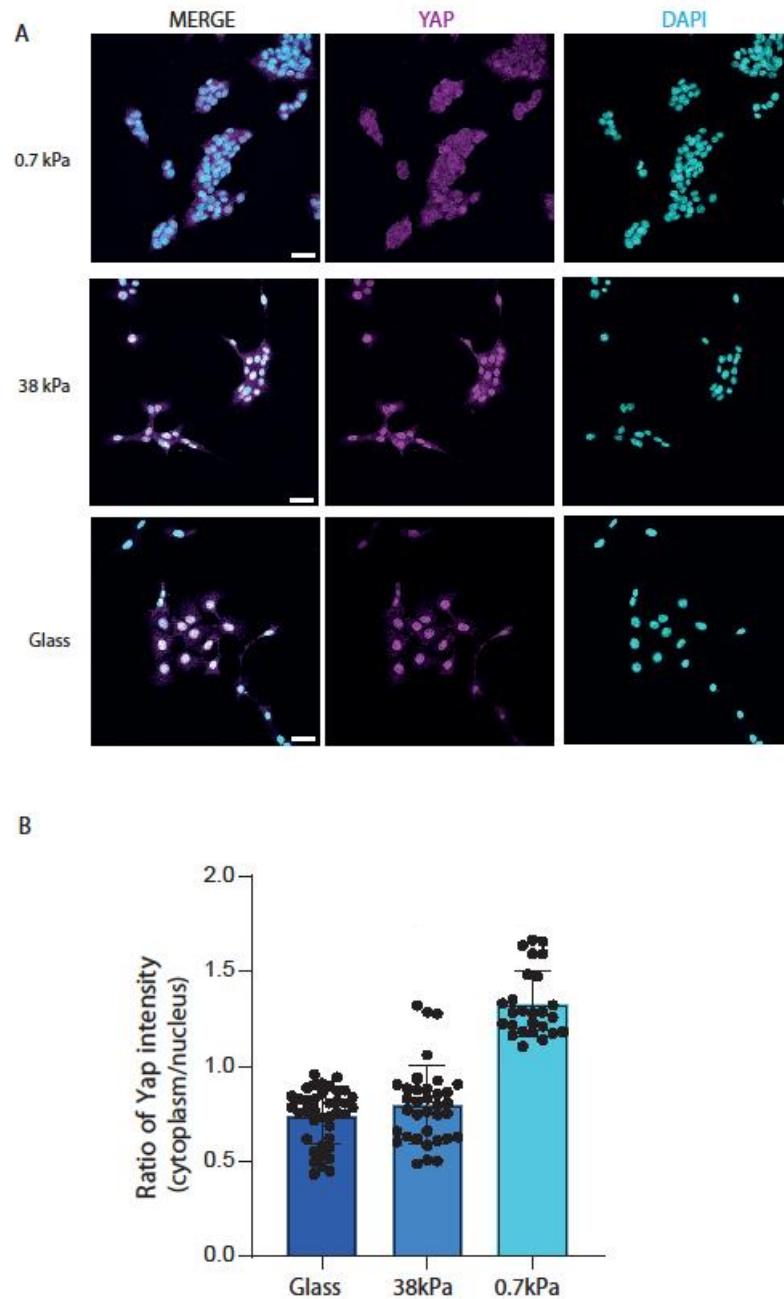
**Figure 3-1: Illustration of the polyacrylamide hydrogel creation process.**

The detailed steps are available in the 2.2.4 section.

### 3.2.2 Environmental stiffness, mimicked by PAAM hydrogel, impacts PDACA morphology, proliferation, and YAP activity.

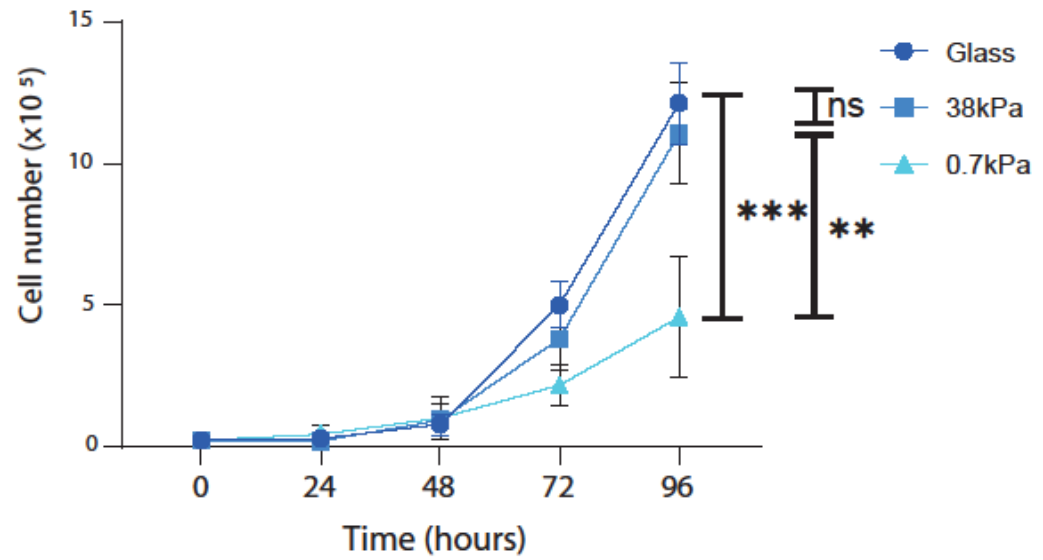
Environmental cues like stiffness will be sensed by cells, triggering mechanosensing and mechanotransduction pathways and cascade events, leading to modified morphologies, behaviours, and cell fates. Since the ECM triggers modification of cellular morphology and behaviour in cells, we asked whether PDACA cells have modified their morphologies and behaviours when cultured on 0.7 kPa, 38 kPa PAAM or glass coverslips. We also investigated if the modification of substrate stiffness modifies YAP localisation in PDACA cells. PDACA cells were exposed overnight to fibronectin-coated 0.7 kPa, 38 kPa PAAM hydrogels and glass coverslips to study morphological modification on each condition. In Figure 3-2-A, we can observe a modification of the PDACA cell shape and the modification of YAP localisation between 0.7 kPa, 38 kPa and glass coverslips. On 0.7 kPa, cells are round, small, aggregated into clumps of cells and display a cytoplasmic YAP. In contrast on 38 kPa and glass conditions, cells are more elongated and spread, with a clear nuclear localisation of YAP. Additionally, YAP fluorescence intensity was measured in both the cytoplasm and the nucleus to assess YAP localisation shift according to stiffness (Figure 3-2-B). A cytoplasmic/nucleus intensity ratio superior to 1 indicates that YAP localises mostly in the cytoplasm while ratio inferior to 1 indicates a nuclear localisation of YAP. On glass and 38 kPa conditions, YAP ratio is inferior to 1 highlighting a nuclear localisation of YAP (Figure 3-2-B). On 0.7 kPa, YAP ratio is superior to 1, which indicates the cytoplasmic localisation of YAP. A important shift in the YAP ratio was observed between 0.7 kPa and both 38 kPa and glass conditions. No difference was observed between Glass and 38 kPa when looking at the YAP intensity ratio (Figure 3-2-B). In addition to the morphological modification and the localisation of YAP, many cellular activities (adhesion, proliferation, metabolism, transcription activities) are modified on different stiffnesses (D'Angelo et al., 2019; Ge et al., 2021). We then investigated whether the proliferation of PDACA cells was modified by ECM stiffness (Figure 3-3). The proliferation of the PDACA cell line was assessed on 0.7 kPa, 38 kPa polyacrylamide hydrogels and glass bottom plates and compared to the

proliferation of PDACA cells on glass bottom plates. PDACA cell proliferation was quantified over four days when exposed to 0.7 kPa, 38 kPa and glass stiffnesses. In Figure 3-3, we observe a strong decrease in proliferation between 0.7 kPa and both 38 kPa and Glass, which shows a highly statistically significant difference in cell proliferation. In conclusion, the modification of ECM stiffness, mimicked by glass and PAAM hydrogels of 0.7 kPa and 38 kPa, triggers changes of cell morphology and proliferation as well as YAP localisation.



**Figure 3-2: PDACA cells cultured on PAAM hydrogels display changes in YAP localisation and cell morphology.**

A: Representatives immunofluorescence images of PDACA cell cultured overnight on fibronectin-coated PAAM hydrogels of 0.7 kPa and 38 kPa stiffnesses, as well as fibronectin-coated glass coverslips. Images were acquired through Z-stack imaging and recomposed using Z projection. The merge images represent the overlapped image of YAP (magenta) and DAPI (cyan). The scale bar represents 30  $\mu\text{m}$ . B: Quantification of YAP activity represented by YAP localisation within the cells, using a ratio between cytoplasm (inactive) versus nucleus (active) intensity. A ratio below 1 represents a higher intensity in the nucleus while a ratio above 1 represents a higher cytoplasmic localisation. N=2, Statistical differences were measured by one-way ANOVA.



**Figure 3-3: PAAM stiffness impacts the cellular proliferation of PDACA cells.**

The proliferation of PDACA cells was quantified by culturing PDACA cells on different fibronectin-coated PAAM hydrogel stiffnesses (0.7 kPa and 38 kPa) and fibronectin-coated glass coverslips, for 96 hours. Each condition was performed with two technical replicates and three biological replicates. Significant differences were measured on the 96-hour time points using One-way ANOVA.

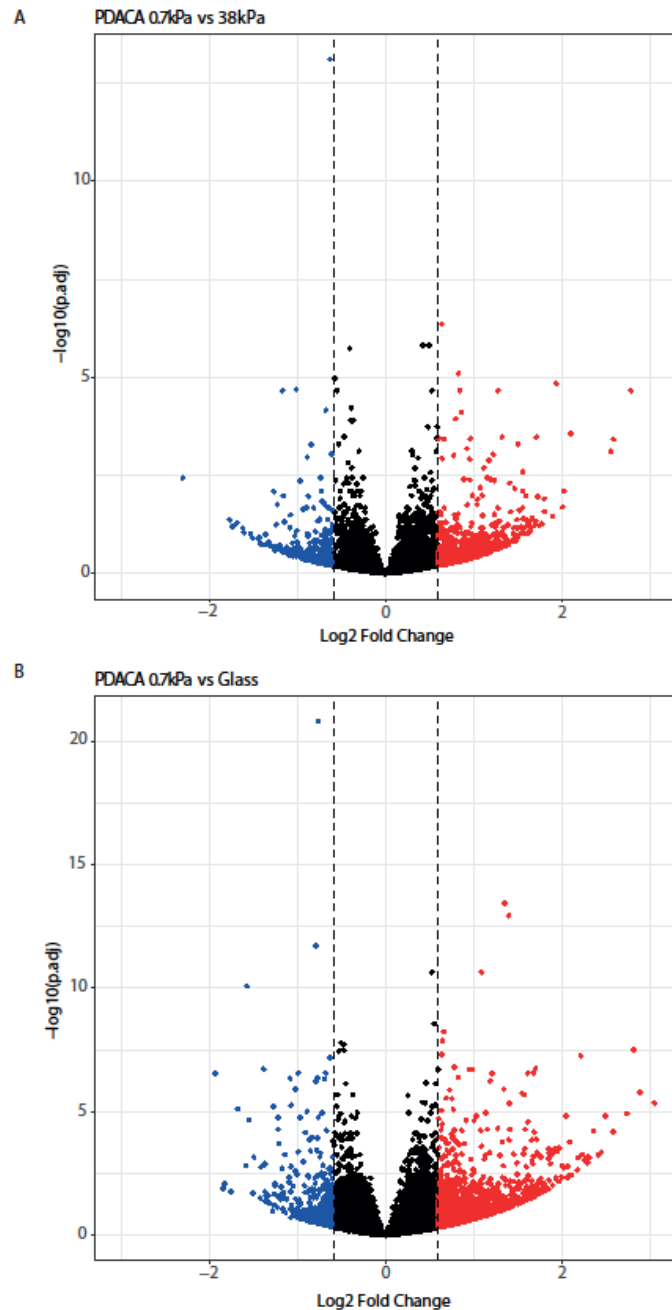
### 3.2.3 Environmental stiffness, mimicked by PAAM hydrogel, changes gene expression at the RNA level in the PDACA cell line.

The cellular modifications triggered by environmental stiffness go deeper than a change of cell morphology or cell proliferation. Mechanical cues from the ECM will be transmitted via mechanosensing and mechanotransduction, leading to the modification of gene expression which in turn will modify cellular behaviour and processes such as proliferation, metabolism, cell mobility, and cell adhesion.

A former PhD student (Vassilis Papalazarou) in the lab previously studied the metabolic behaviour of PDAC cells to ECM rigidity and explored the role of the creatine phosphagen system as a potential mechanoresponsive pathway. To do so, among all his experiments, he measured the RNA expression of PDACA genes cultures on different PAAM hydrogels, using RNA sequencing experiment (referred as the 2017 dataset). Using the RNA sequencing data gathered by Vassilis Papalazarou, who measured the gene expression of PDACA and PDACB cells on 0.7 kPa, 38 kPa PAAM hydrogel and glass bottom plates, I decided to investigate if some genes whose RNA expressions were modified by stiffness could be mechanotransduction actors. To do so, I started by comparing the gene expression of PDACA on 0.7 kPa versus glass and 38 kPa versus glass using Vassilis' RNA sequencing data. To visualise how PDACA gene expression was impacted, gene expression was plotted in Figure 3-4 according to Log 2-fold change and  $-\log_{10}(p.adj)$ , using R studio. The volcano plots were created by overlapping overall gene expression with upregulated (Red) and downregulated (blue) genes (Figure 3-4). We observed the downregulation and upregulation of genes in both 0.7 kPa versus glass and 38 kPa versus glass comparisons with an increase in genes modified in 0.7 kPa versus glass than 38 kPa versus glass comparisons. Next, I investigated which genes, whose expression is modified by stiffness, could be part of a mechanotransduction process. To do so, I first filtered the dataset to only select genes whose expressions were modified similarly in PDACA and PDACB cells, and whose expressions were higher than 200 (normalized expression from `deseq2`) to ensure their detection in cells. Then, each gene was thoroughly investigated



according to multiple parameters: roles in physiological conditions, cancer conditions, localisation within the cell, overall mechanosensitive abilities and their expression (increase or decrease) depending on environmental stiffness.



**Figure 3-4: PAAM stiffnesses impacts PDACA gene expression at RNA level.**

Representation of PDACA RNA expression when exposed to either PAAM hydrogel stiffnesses or glass bottom plates. The volcano plots were realised on R studio and are based on the available RNA sequencing experiment data performed by Vassilis Papalazarou on PDACA cells. RNA expression was plotted according to genes Log2-fold change and  $-\log_{10}(p.adj)$  for either A: PDACA cells were cultured on 0.7 kPa versus 38 kPa, and B: PDACA cells were cultured on 0.7 kPa versus glass coverslips (2-4 GPa).

The mechanotransduction candidates selected within the RNA sequencing dataset are Epsin 3, Sorbs2, Tetraspanin 8 and Ajuba (Figure 3-5-top panel). An additional validation of each mechanotransduction candidate was performed by qPCR at 0.7 kPa, 38 kPa to which was added a 7 kPa PAAM hydrogel stiffness representing the stiffness of PDAC tissue. In the following sections, each mechanotransduction candidate will be introduced and their expression will be compared between qPCR results (Figure 3-5-Bottom panel, Figure 3-6, Figure 3-7) and RNA sequencing data results (Figure 3-5-Top panel). After comparison, each candidate will be individually validated or invalidated for further testing. Figure 3-5 (top panel) gathered the RNA expression of each mechanotransduction candidate from the RNA sequencing dataset according to surrounding stiffness. The modification of RNA expression was measured by their Log 2-fold change. In Figure 3-5 (top panel), a negative Log 2-fold represents a higher RNA expression on 38 kPa compared to 0.7 kPa. On the other hand, positive Log 2-fold change represents a higher RNA expression on 0.7 kPa compared to 38 kPa.

### 3.2.3.1 Epsin 3

The Epsin family, composed of Epsin 1, Epsin 2 and Epsin 3, involved in the endocytic pathway, more specifically in the clathrin-mediated endocytosis, acting as endocytic adaptors at endocytic sites and as accessory protein to consolidate the endocytic network (Aguilar, 2018). Highly conserved through evolution, Epsin 1 and 2 are expressed in multiple tissues while Epsin 3's expression is very low in physiological conditions. Epsin 3, as well as Epsin 1 and 2, is overexpressed in lung, breast and skin cancer where it correlates with an increase in aggressiveness, migration abilities and metastasis (Coon et al., 2011; Madhivanan et al., 2020). The Epsin proteins contain an Epsin N terminal homology (ENTH) domain which binds to PI(4,5)P<sub>2</sub>, triggering membrane curvature (Ford et al., 2002). They also contain an ubiquitin interacting motif (UIM) to interact with ubiquitinated cargos (targeted for recycling). Lastly, they contain clathrin binding motifs (CBM) and DP[W/E] repeats to respectively bind to clathrin heavy chains and Adaptor complex 2 (AP2) complex (Madhivanan et al., 2020).

In the case of clathrin-related endocytosis, the clathrin coat will assemble on the cytosolic part of the membrane, by interaction with clathrin adaptor proteins (such as AP2 complex, CALM, Epsin). It will facilitate the binding to membrane phosphoinositides, like PI(3,4)P2. AP2 complex will directly interact with PI(4,5)P2, which triggers membrane curvature and the assembly of the endocytic coat (Kaksonen & Roux, 2018). Cargo proteins will be trapped in these coated vesicles, which will later detach by scission. Vesicles will be sorted, their content collected and transferred to their final destinations, unique for each molecule and per the cell's needs. The ECM rigidity, membrane tension, and surrounding mechanical forces, will have a significant impact on endocytosis (Ferguson et al., 2017; Joseph & Liu, 2020). This is due to the need to produce membrane curvature and membrane remodelling.

Epsin 3 RNA expression was measured, in PDACA and PDACB, exposed to PAAM hydrogel stiffnesses, by qPCR and compared to Epsin 3 RNA level obtained by RNA sequencing. The RNA sequencing analysis indicates that Epsin 3 RNA expression presents a higher RNA expression on 0.7 kPa compared to 38 kPa conditions, in both PDACA and PDACB cell lines (Figure 3-5-Top panel). Epsin 3 RNA expression, measured by qPCR, indicates a higher RNA expression on PDACA 0.7 kPa compared to PDACA 38 kPa conditions recapitulates RNA sequencing data on PDACA (Figure 3-5-Bottom panel). Unfortunately, in PDACB cells, among similar stiffnesses, no significant changes were observed (Figure 3-5-Bottom panel), which contradicts RNA sequencing results. In PDACB cells, no significant difference in Epsin 3 expression were found across the tested stiffnesses by qPCR. However, in PDACA cells, significant differences were found when comparing 0.7 kPa to 7 kPa and 0.7 kPa to 38 kPa PAAM hydrogels stiffnesses with an increase in RNA expression at 0.7 kPa.

Due to the differences in RNA expression of Epsin 3 observed in PDACA cells between 0.7 kPa and both 7 kPa and 38 kPa, we can articulate the hypothesis that Epsin 3 could drive a possible increase of endocytosis, migration abilities and metastasis in 0.7 kPa compared to a stiffer environment in PDACA cells.

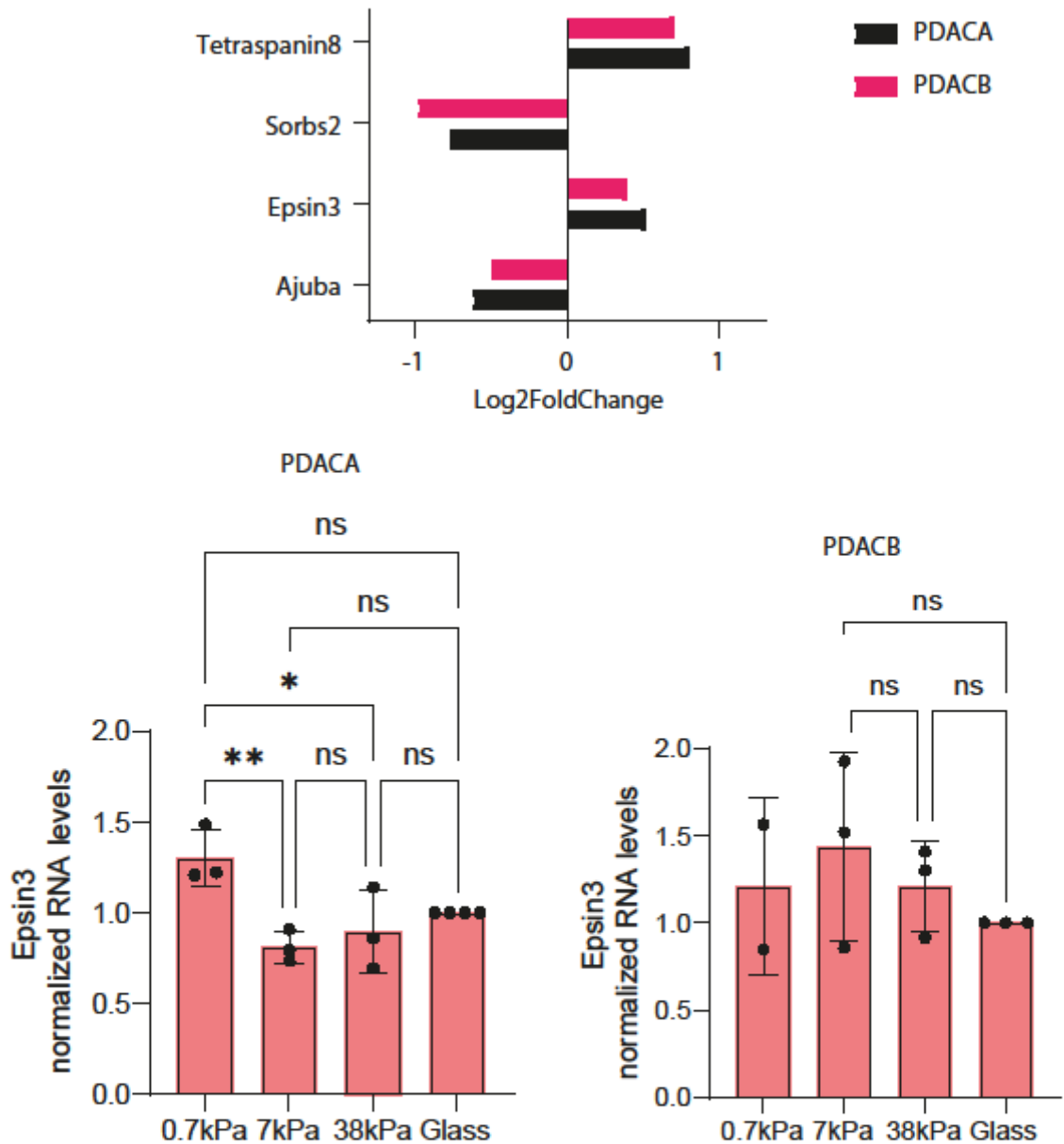


Figure 3-5: Epsin 3 RNA levels are increased on 0.7 kPa compared to 38 kPa in PDACA cells.

Top panel: Overview of the selected mechanotransduction candidates RNA expression extracted from RNA sequencing data, in PDACA and PDACB cells cultured on 0.7 kPa versus 38 kPa PAAM hydrogels. Negative Log2 fold change represents a higher expression in 38 kPa compared to 0.7 kPa. While a positive Log2 fold change represents a higher expression on 0.7 kPa compared to 38 kPa.

Bottom panel: Quantification by qPCR of Epsin 3 RNA expression on PDACA cells (left) and PDACB cells (right), cultured on PAAM hydrogel of 0.7 kPa, 7 kPa, 38 kPa and glass coverslips. N=3 independent experiments, Statistical differences were assessed by one- way ANOVA.

### 3.2.3.2 Sorbs2

Sorbin and SH3 domain-containing protein 2 (Sorbs2), also called Arg-binding protein 2 (ArgBP2) are part of the adaptor family protein called vinexin family (Sorbin and SH3 domain-containing protein (Sorbs)). It contains 3 members: c-Cbl

associated protein (Sorbs1), Sorbs2 and Vinexin (Sorbs3)(Ichikawa et al., 2017). Sorbs2 is a multi-adaptor protein, with binding partners like protein-tyrosine phosphatase - PEST (PTP-PEST), Casitas B lineage lymphoma (c-CBL) , dynamin, Arg and Abelson Tyrosine Kinase (c-abl)(David Taieb, 2008; Kioka et al., 2002).

Sorbs2 is composed of three SH3 domains at its C-terminal. On its N-terminal, Sorbs2 has a Sorbin homology (SOHO) domain, known to interact with a lipid raft-associated protein flotillin (Fredriksson-Lidman et al., 2017). Sorbs2 has been suggested to be involved in the organisation of the actin cytoskeleton as well as the regulation of cell adhesion(Fredriksson-Lidman et al., 2017; Kioka et al., 2002). Sorbs2 also acts as an RNA binding protein, studies show its ability to bind to retinoic acid receptor-related orphan receptor (RORA) 3'UTR mRNA (stabilisation effect) (Han et al., 2019) and microtubule-associated tumor-suppressor 1 gene (MTUS1) mRNA 3'UTR (stabilisation effect) (Lv et al., 2020). RNA binding protein can have a great impact on cellular behaviour since their interaction with RNA could impact post-transcription modification and impact RNA stability (Lv et al., 2020). In pancreatic cancer, SORBS2 is localised at stress fibres and focal adhesion, co-localising with actin filaments and lamellipodia. Sorbs2 expression was enriched in multiple organs such as the pancreas, heart and brain. However, in metastatic pancreatic cancer, a loss of Sorbs2 expression has been observed, revealing a potential anti tumoral role for Sorbs2 (David Taieb, 2008). In pancreatic cancer Sorbs2 interaction with regulators of actin dynamic impacts cell migration and spreading (David Taieb, 2008).

The RNA expression of Sorbs2 measured by qPCR doesn't indicate a decrease in 0.7 kPa conditions compared 38 kPa (Figure 3-6), which doesn't recapitulate the RNA sequencing data results from Figure 3-5-Top panel, in PDACA cells and PDACB cells. Sorbs2 RNA expression, measured by qPCR, indicates a sharp decrease in 0.7 kPa conditions compared to glass conditions, which is only significant in PDACA cells (Figure 3-6). These results do not support the hypothesis that Sorbs2 expression is modified by stiffness (physiological), so I did not perform further experiments with Sorbs2.

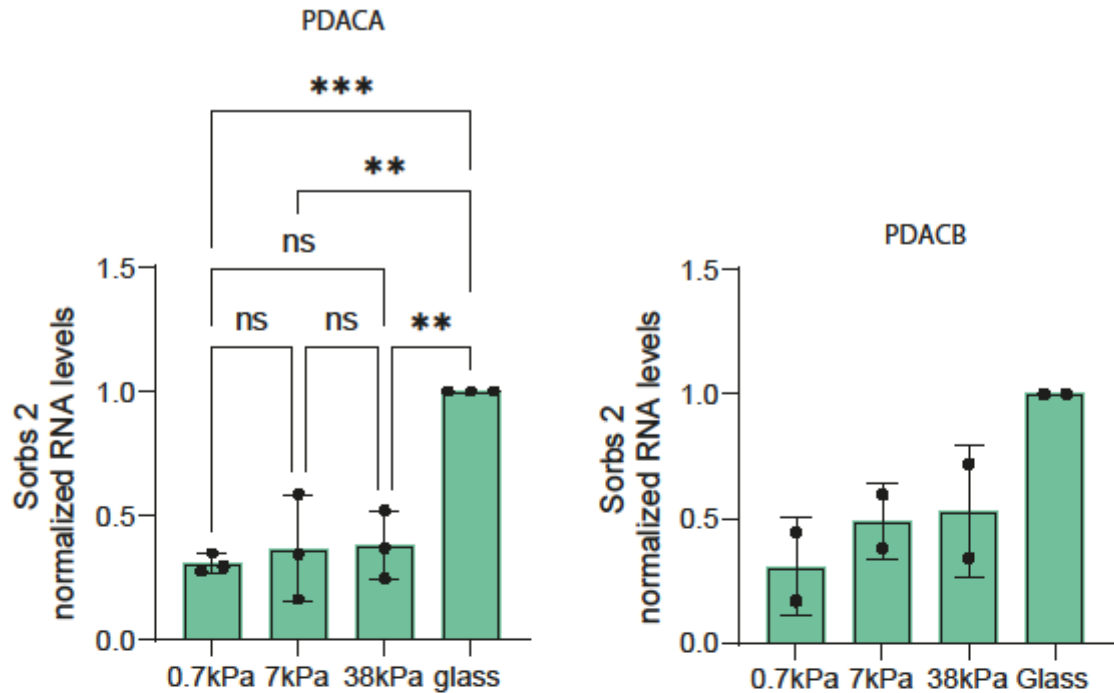


Figure 3-6: Sorbs2 RNA expression is not modified by PAAM stiffnesses.

Quantification by qPCR of the RNA expression of Sorbs2 after culture on polyacrylamide hydrogels of 0.7 kPa, 7 kPa and 38 kPa stiffnesses as well as glass bottom plates. RNA expression of Sorbs2 in PDACA cells (left) and PDACB cells (right). N=3 independent experiment with technical triplicates. Statistical differences were assessed by one-way ANOVA.

### 3.2.3.3 Tetraspanin 8

Tetraspanins are a large family of transmembrane protein, which acts as molecular scaffolds, organising proteins into lipid raft-like microdomains at the membrane (Huang et al., 2021) (Zöller, 2009). They are composed of four transmembrane domains (highly conserved) linked to two extracellular loops (variable regions) (Termini & Gillette, 2017). Transmembrane domains mediate tetraspanin-tetraspanin interaction, allowing the formation of homodimers. Tetraspanins can be impacted by post-transcription modifications, which will modify both their roles and their effects. One of which is the ubiquitination, it can regulate their stability and activities (Termini & Gillette, 2017).

Tetraspanin 8 was found in both the cytoplasm and the nucleus. In the cytoplasm, it associates with integrins and adhesion molecules. Tetraspanin 8 was linked with cancer aggressiveness in different cancer types (such as breast cancer (Sandoval & Weiss, 2022), gastric tumor (Wei et al., 2015), pancreatic cancer (Yue et al.,

2013), liver cancer (Kanetaka et al., 2001)), tumour exosomes, and the regulation of transmembrane metalloproteases (Müller et al., 2022) Its translocation to the nucleus was induced after phosphorylation by protein kinase B (AKT), where it promotes the transcription of signal transducer and activator of transcription 3 (STAT3) target genes (Sandoval & Weiss, 2022). Tetraspanin 8 expression is correlated in breast cancer with cancer progression, treatment resistance and survival (Sandoval & Weiss, 2022). Due to both Tetraspanin 8 known localisations within the cell and its impacts on gene expression, tetraspanin 8 might be part of a mechanotransduction pathway. By comparing the RNA expression of Tetraspanin 8, between 0.7 kPa and 38 kPa from qPCR results (Figure 3-7) and RNA sequencing data (Figure 3-5), we observe that RNA expression of Tetraspanin 8 increases on 0.7 kPa in PDACA, which recapitulate the results for PDACA cells only. Unfortunately, changes observed in RNA sequencing results were not recapitulated in qPCR results in PDACB. In PDACA cells, the expression of Tetraspanin 8 at RNA measured by qPCR, is increased in 0.7 kPa conditions compared to all other tested stiffnesses. These results indicate the possible role of Tetraspanin 8 as a mechanosensitive protein, which may be upregulated in response to a soft environment. I speculate that it could indicate an important role on soft substrate of Tetraspanin 8 in the transmission of ECM cues or the cell's ability to adapt to soft conditions.

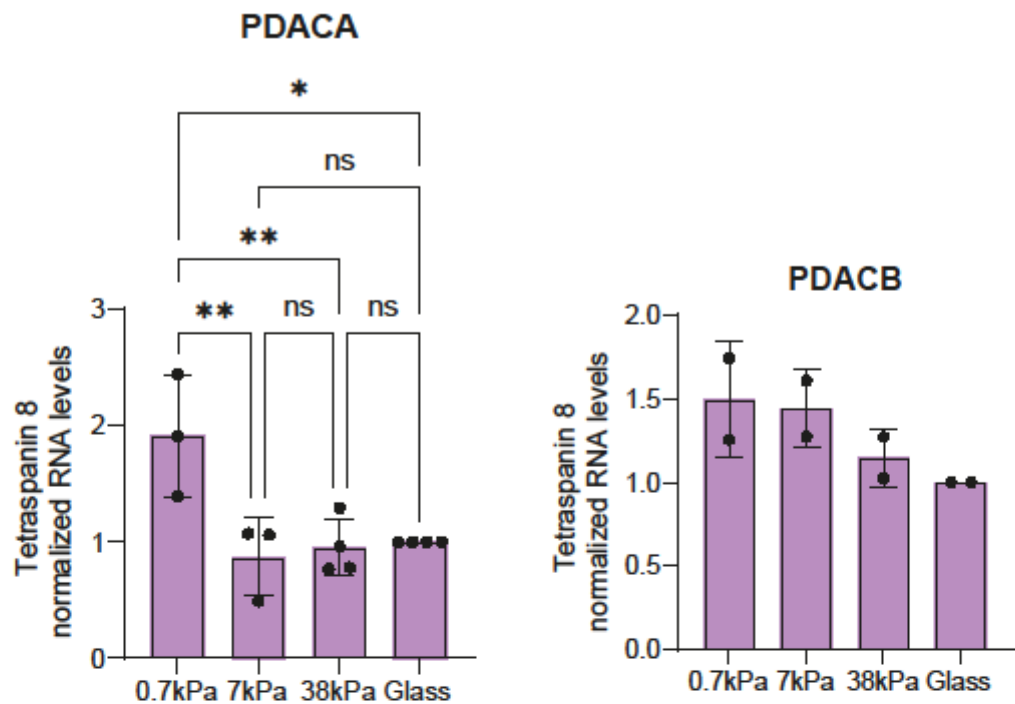


Figure 3-7: Tetraspanin 8 RNA levels are increased on 0.7 kPa compared to 38 kPa in PDACA cells.

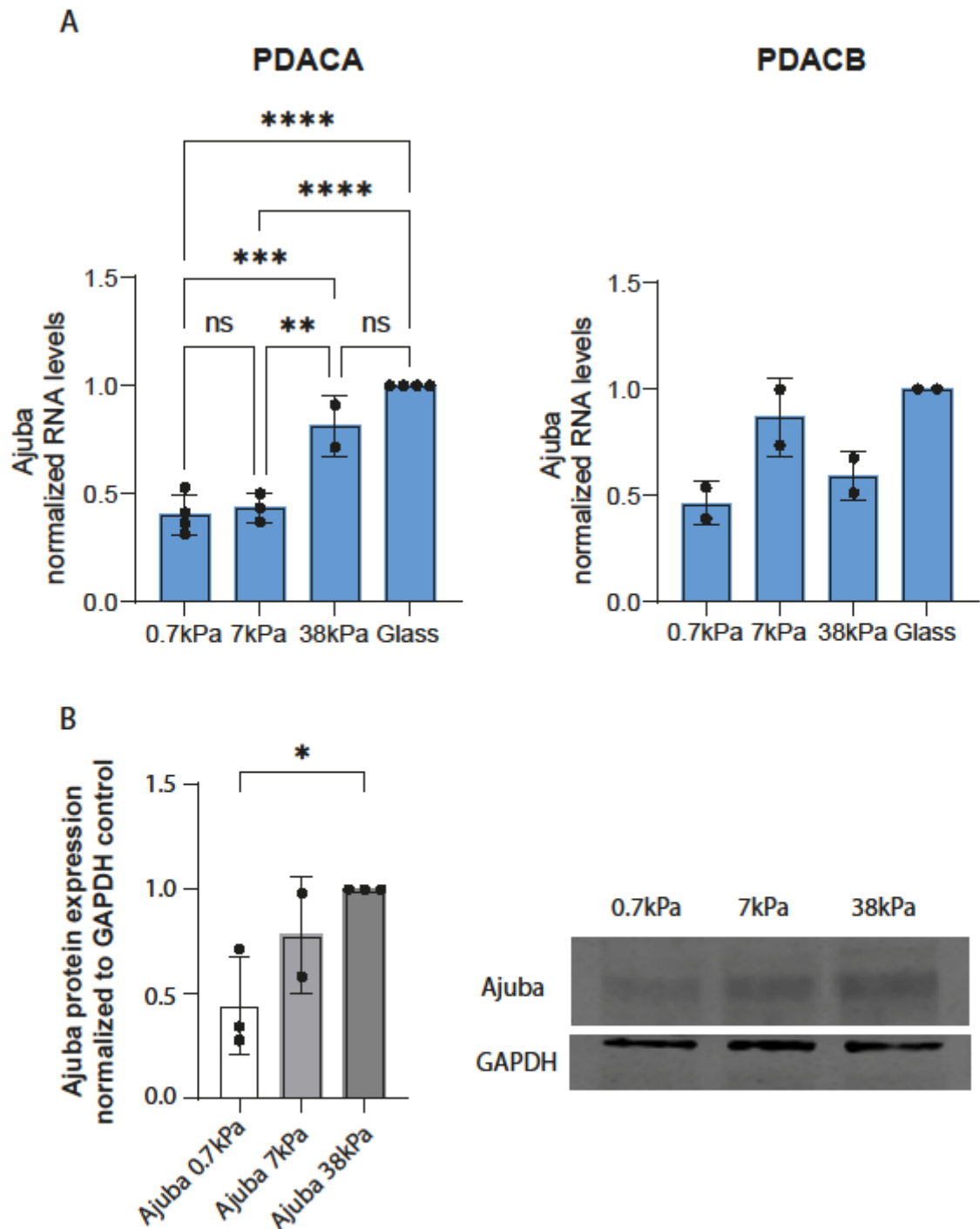
Quantification by qPCR of the RNA expression of Tetraspanin 8 cultured on different polyacrylamide hydrogels (0.7 kPa, 7 kPa and 38 kPa) and on glass bottom plates. Tetraspanin 8 RNA expression on PDACA cells (left) and PDACB cells (right). N=4 independent experiments (PDACA), N=2 independent experiments (PDACB), each performed with technical triplicates. Statistical differences were assessed by one-way ANOVA.

### 3.2.3.4 Ajuba

Ajuba protein belongs to both the Ajuba family and the LIM domain family. Ajuba protein is localised at cell adhesion and can shuttle to the nucleus to modify gene expression and transcription activities. Ajuba protein is involved in cell adhesion, cell proliferation, cell cycle, cell transcription and will be the main subject of both 83 and 3. The RNA expression of Ajuba measured by qPCR, indicates a sharp decrease at 0.7 kPa compared to 38 kPa and glass stiffnesses in PDACA cells (with the exception of 7kPa), which recapitulates RNA sequencing results (Figure 3-8-A, Figure 3-5-Top panel). Unfortunately, the changes between 0.7 kPa and 38 kPa were not recapitulated in PDACB cells. I then investigated if these changes were similar at protein levels in PDACA cells. To do so, I extracted lysates from PDACA cells cultured overnight on PAAM hydrogel of 0.7 kPa, 7kPa and 38 kPa. The lysates were loaded and analysed by western blot. In Figure 3-8-B we can observe a



significant decrease between 0.7 kPa and 38 kPa of Ajuba at protein level. No significant difference in protein level was measured between 0.7 kPa and 7kPa or 7kPa and 38 kPa. Taken together, these results indicate that the expression of Ajuba at RNA and protein levels were modified by stiffness. Ajuba might play a role in mechanosensing and mechanotransduction activities by converting ECM cues at adhesion sites into the modification of genes and transcription activities within the nucleus in a stiffness-dependent manner.



**Figure 3-8: Ajuba RNA and protein levels are decreased on 0.7 kPa compared to 38 kPa in PDACA cells**

A: Quantification by qPCR of the RNA expression of Ajuba on PDACA (left) and PDACB (right) cells cultured overnight on PAAM hydrogels of 0.7 kPa, 7 kPa, 38 kPa and glass coverslips. N=4 independent experiment (PDACA cells), N=2 independent experiment (PDACB cells), each performed with technical triplicates. Statistical differences were assessed by one- way ANOVA.

B: The protein level of Ajuba was measured by western blot in PDACA cells exposed to 0.7 kPa, 7 kPa and 38 kPa PAAM hydrogels overnight. Proteins were normalized to sample loading control GAPDH. Ajuba (55-60kDa), GAPDH (36kDa) N=3. Statistical difference was measured by one way ANOVA.

### 3.3 Conclusion

The study of mechanosensing, especially the study of the effect of stiffness, requires the use of specially designed material able to recapitulate precise stiffnesses for *in vitro* experiments. Throughout this thesis, polyacrylamide hydrogels were used to recapitulate stiffnesses ranging from 0.7 kPa to 38 kPa. Glass coverslips were used as control, representing both generalised cell culture practices and extreme stiffness. PDACA cells were able to sense PAAM hydrogel stiffness and react to it, involving changes in cell morphology, YAP localisation, proliferation as well as modification of cells' RNA expression (Figure 3-2, Figure 3-3, Figure 3-4). The use of previously available RNA sequencing data (2017 dataset), from Vassilis Papalazarou, allowed the selection of mechanotransduction candidates whose RNA expression was modulated in the RNA sequencing data, by stiffness in PDACA and PDACB cell lines. Each candidate was selected for their roles in mechanotransduction-compatible pathways gathered from the literature. Each candidate's RNA expression was tested, in both PDACA and PDACB cells, by qPCR to validate them against previously available RNA sequencing data (Figure 3-5, Figure 3-6, Figure 3-7, Figure 3-8). Tetraspanin8 and Ajuba were the two strongest candidates in the PDACA cell line. While both were interesting, Ajuba was chosen as the main point of interest in this thesis going forward, due to both its protein and RNA levels being modified by stiffness.

### 3.4 Discussion

This chapter was designed around the use of PAAM hydrogels to mimic *in vitro* physiological and pathological stiffnesses. This technique enables us to model a wide range of ECM stiffness by modulating the concentration of acrylamide and bis-acrylamide (Tse & Engler, 2010). Polyacrylamide hydrogel is one of the easiest systems to mimic stiffness *in vitro*. Although exposing cells to specific stiffnesses allows us to study many parameters such as adhesion, proliferation, metabolism, protein and gene expression, this technique is in 2D. To better fit *in vivo* environment, adding a 3D component to mechanosensing studies, would require an encapsulation of cells. In a 3D, we would be able to add complexity to the system with the addition of fibres representing PDAC's ECM such as elastin,

laminin and collagens (Caliari & Burdick, 2016). The encapsulation will add another dimension as cells will be subject of additional stress and environmental cues. Some 3D techniques exist, combining additional tuneable parameters as pores size, degradability of materials, viscosity, elasticity, and stiffness. Different types of materials can also be used in these 3D gels, including polyacrylamide, alginate, gelatin, collagen and hyaluronic acid (Caliari & Burdick, 2016; Łabowska et al., 2021). The use of RNA sequencing experiment from Vassilis Papalazarou allowed the analysis of PDACA and PDACB gene expression, at RNA levels and their modification due to stiffness. He previously used this data to analyse how cellular metabolism and energetic usage is modified in cells exposed to different stiffnesses (Papalazarou et al., 2020). In this chapter, I used his RNA sequencing data to investigate RNA gene expression and identify which genes could potentially have mechanosensing or mechanotransduction abilities. Figure 3-4 represents an overview of PDACA RNA expression, plotted according to their Log<sub>2</sub> fold change and  $-\log_{10}(p.adj)$ . Trends observed between the two volcano plots illustrate that, at RNA levels, when compared to 0.7 kPa, both 38 kPa and glass conditions have similar effects regarding the upregulation and downregulation of genes expression. An in-depth characterisation of PDACA RNA expression between 0.7 kPa and 38 kPa will be the main focus of Chapter 5. An emphasis on how much of an impact Ajuba downregulation has on RNA expression will also be studied. From the list of potential mechanotransduction candidates, genes with overall low RNA expression and genes whose RNA expression was opposingly modified in PDACA and PDACB cells were removed. Five candidates were selected based on a) their RNA expression in PDACA and PDACB cells and b) their previously attributed roles which will be validated in both cell lines by qPCR. Although the RNA sequencing data gathered RNA expression on 0.7 kPa, 38 kPa and Glass (2-4GPa), I included one additional stiffness in the qPCR validation, at 7kPa. 7kPa would represent the stiffness surrounding PDAC due to the desmoplastic reaction, which can range from 4 to 10kPa (Rice et al., 2017). It is to be highlighted that, in PDACB cells, none of the five candidates' RNA expression recapitulates the fold change observed in the RNA sequencing data. This may be due to PDACB cells changing in culture, as pancreatic cancer cells are well known to be genomically unstable, and drift can occur in any tissue culture cell line over time and with passage

number. Focusing on PDACA qPCR validations, Sorbs2 is the only candidate that doesn't successfully recapitulate RNA sequencing data.

All of the three other candidates did recapitulate the RNA sequencing trend (Figure 3-5), from which Ajuba had the strongest statistical significance, between 0.7 kPa and 38 kPa (Figure 3-8). Although a strong significant difference can be observed between the RNA levels of Ajuba on 0.7 kPa versus 38 kPa, and on 0.7 kPa versus glass conditions, the expression of Ajuba at RNA level, on 7kPa is similar to 0.7 kPa. Based on previous paper about Ajuba protein expression in PDAC, high levels of Ajuba are strongly associated with both PDAC and poor patient outcomes (Zhang et al., 2019). Although in 7kPa (PDAC-related stiffness), the RNA and protein expression of Ajuba was not significantly different than levels on 0.7 kPa, strong and significant differences were observed between 0.7 and 38 kPa. Ajuba will be investigated further, in Chapter 4 and Chapter 5 to better understand its role in PDAC and investigate its role as a potential mechanotransduction protein.

## **Chapter 4. The role of Ajuba in pancreatic cancer**

## 4.1 Introduction

In this thesis, I am focused on studying both the role of Ajuba and the impact of ECM stiffness in pancreatic cancer. The pancreatic cancer is known for its desmoplastic reaction leading to a drastic increase in environmental and tumour stiffnesses (Whatcott et al., 2012). In 3.2.3, I demonstrated that environmental stiffness, mimicked using polyacrylamide hydrogels, induces changes in gene expression in PDACA cells. Cells can sense mechanical cues from the ECM and YAP/TAZ (transcriptional coactivators), as well as other mechanotransduction actors, will coordinate the cell response according to these mechanical cues (A. Totaro et al., 2018). In 3.2.3, variation of ECM stiffness led to the modifications of the expression of many genes in PDACA and PDACB cell lines. Genes with differential expression were extracted as mechanotransduction candidates. Ajuba had both its RNA and protein expression modified by stiffness and was selected as the main protein of interest. Ajuba belongs to the Ajuba/Zyxin family and to the LIM domain family, whose members are increasingly identified as proteins involved in mechanotransduction pathways (Anderson et al., 2021). Several cues would indicate that Ajuba corresponds to such proteins:

- Ajuba has been localised at adherence junctions and focal adhesions, where adhesion signals may arise (Ibar et al., 2018; Marie et al., 2003), and stabilizes the newly formed junctions by coupling the cadherin-based complex to the actin cytoskeleton (Razzell et al., 2018).
- Ajuba could modify its localisation depending on the cytoskeletal tension (Ibar et al., 2018; Rauskolb et al., 2022).
- The presence of both NES and NLS sequences implies that Ajuba can shift to and from the nucleus where it acts as a transcriptional co-repressor and/or co-activator (Ayyanathan et al., 2007; Fan et al., 2015; Langer et al., 2008; D. E. Montoya-Durango et al., 2008).

Taken together, these different roles suggest that Ajuba is a potential mechanotransduction candidate. Additionally, Ajuba is involved in a wide range of cellular processes. For example, Ajuba is involved in cell-cell adhesions, cell proliferation, mitosis/cytokinesis, cell migration and invasion (Chen et al., 2016;

H. Li et al., 2019; Razzell et al., 2018; Shi et al., 2016; Zhang et al., 2019). In addition to a potential mechanotransduction role, a substantial number of studies are linking Ajuba with cancer progression and unfavourable prognosis (Razzell et al., 2018; Shi et al., 2016; Song et al., 2022; Zhang et al., 2019). The role of Ajuba in cancer is split between an oncogene and tumour suppressor role, depending on the cancer analysed. Indeed, Ajuba is described as an oncogene by driving cell proliferation in different cancer types (breast cancer, esophageal squamous cell carcinoma, pancreatic cancer, colorectal carcinoma and gastric cancer) (Jia et al., 2017; H. Li et al., 2019; Li et al., 2022; Shi et al., 2016; Zhang et al., 2019). While it acts as a tumour suppressor in hepatocellular carcinoma (Liu et al., 2018) and malignant mesothelioma (Jia et al., 2020; Tanaka et al., 2015).

In pancreatic cancer, a single study is available on the role of Ajuba where Ajuba promotes SP1-mediated cell proliferation but this study doesn't investigate the localisation of Ajuba in cells nor its roles in adhesion, migration or invasion (Zhang et al., 2019). Therefore, due to the lack of studies in pancreatic cancer, it raises the question of whether the roles and localisation of Ajuba are similar to other cancers or if it differs. I started by investigating the localisation of Ajuba in PDACA, more precisely we asked whether Ajuba is present at focal adhesion sites in PDACA cells. I later generated multiple CRISPR cell lines, aiming to downregulate Ajuba in PDACA to study its effect on cellular morphology, proliferation, adhesion, migration and invasion. Furthermore, I investigated whether the downregulation of Ajuba would modify the cell's ability to react to environmental stiffness.

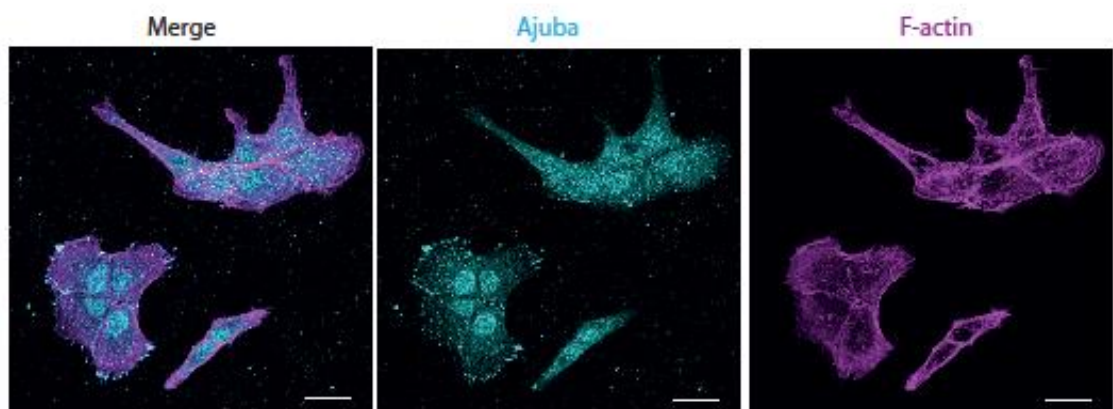
## **4.2 Localisation of Ajuba in the pancreatic cell line PDACA**

Many studies localised Ajuba at adherence junctions, cell edges and in the nucleus (Ayyanathan et al., 2007; Ibar et al., 2018; Marie et al., 2003; Nola et al., 2011). Studies have been conducted on several cell lines for example, MCF10A, MDCKIIIG (Ibar et al., 2018) or HaCAT (Marie et al., 2003) and different cancer types, but in pancreatic cancer cell lines, the localisation of Ajuba is yet unpublished. Therefore, in this section I investigated the localisation of Ajuba in our mouse cell



line PDACA, to begin to decipher the roles of Ajuba in PDAC. To localise Ajuba in PDAC cells, PDACA cells were cultured overnight on fibronectin-coated coverslips and were stained by immunofluorescence with an Ajuba antibody and an F-actin dye (fluorescently labelled Phalloidin). Four Ajuba antibodies (sc-374610: Santa Cruz Biotechnology, Ajuba #4897S: Cell signalling technology, anti-Ajuba HPA006171: Atlas antibody, and anti-Ajuba ab244285: Abcam) were tested. Each antibody was tested at a wide range of concentrations (from 1/1000 to 1/50) for immunofluorescence, but only the antibody targeting Ajuba from Santa Cruz Biotechnology, sc-374610, gave reproducible and detectable staining in PDACA cells.

Immunofluorescence experiments were performed to localise Ajuba in PDACA cells using the antibody sc-374610. An F-actin marker was used to outline the actin cytoskeleton of PDACA cells. In Figure 4-1 the Merge image represents the superposition of Ajuba and F-actin staining. In PDACA cells, Ajuba localises in the cytoplasm and the nucleus with some staining hotspots at the cell edge, as represented in Figure 4-1. Interestingly, PDACA cells are mesenchymal cells and lack conventional E-cadherin-mediated junctions. It may be due to the lack of adherent junctions in PDACA that Ajuba localises differently than previously published. The staining pattern of Ajuba observed in Figure 4-1 at the cell edge was an indication of possible focal adhesion sites.

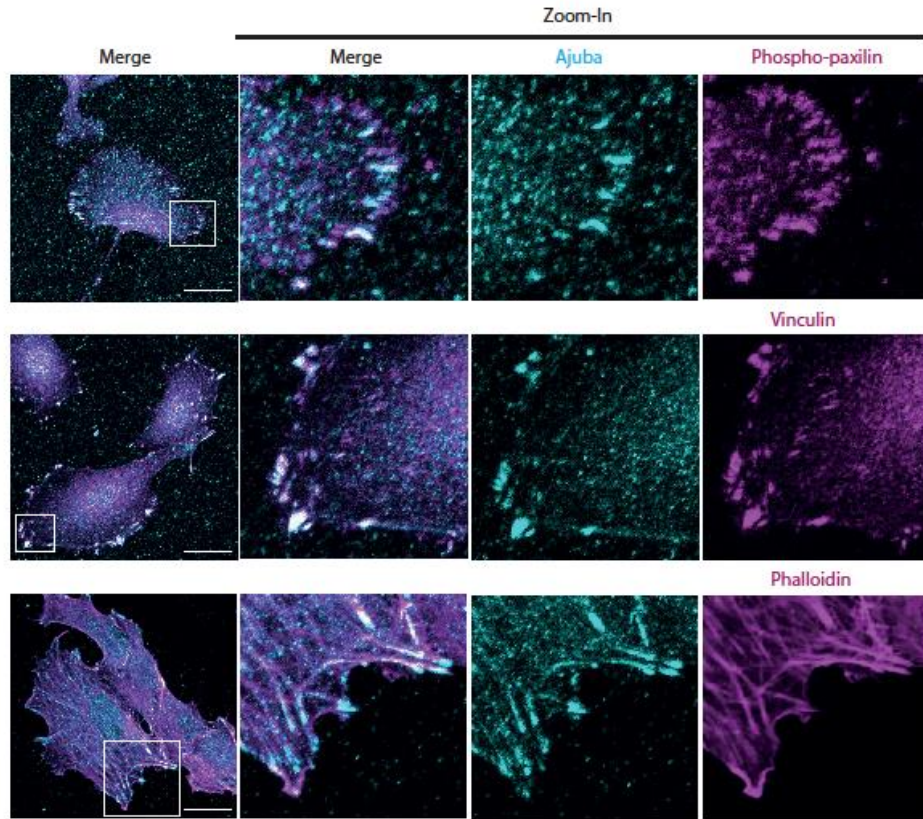


**Figure 4-1:** Ajuba is localised at the cell edge, the cytoplasm and the nucleus of PDACA cells.

Representative immunofluorescence images of PDACA cells, Ajuba is shown Cyan, and F-actin in magenta (F-actin dye: Phalloidin 647). Scale bar represents 20µm.

### 4.2.1 Ajuba localises at focal adhesions in PDACA cells

Having shown that Ajuba localised at the cell edges with a hotspot pattern in PDACA cells, we next asked if Ajuba was present at focal adhesion sites. To investigate this question, different focal adhesion markers were added alongside Ajuba. Additionally, I also aimed to monitor the timing of Ajuba recruitment at focal adhesion sites by tracking the different maturation stages of focal adhesions. To represent a range of focal adhesion maturation stages, phospho-Paxillin, a protein recruited at the earliest stage of focal adhesion formation and remains until focal adhesion disassembly was chosen to mark both immature and mature focal adhesions. In contrast, Vinculin, another focal adhesion protein, crucial for both the maturation of focal adhesions and the physical linkage of the focal adhesion complex to actin stress fibers was added. Therefore, Vinculin will be a marker of mature focal adhesion (Humphries et al., 2007). Additionally, fluorescent phalloidin, was used to stain the actin within the actin stress fibres. The co-localisation of F-actin with focal adhesion markers will allow the visualisation of the contact between FA and actin stress fibres. It is to be noted that PDACA cells is a heterogeneous cell line containing multiple sub-populations, which have different shapes and sizes. Adhesion sites and stress fibre staining might vary depending on the cell shape. In Figure 4-2, we observe that Ajuba co-localises at a small number of sites with Phospho-paxillin, coinciding with long and wide focal adhesions (more mature and stable) rather than small and thin ones (immature and unstable). Ajuba also co-localises perfectly with Vinculin at long and wide focal adhesions. Additionally, Ajuba co-localises at the tip of actin stress fibers which also indicates its presence at mature forms of focal adhesions (Figure 4-2). Taken together and focussing on the focal adhesion shape, size, and staining intensity, we can conclude that Ajuba localises with mature forms of focal adhesions.



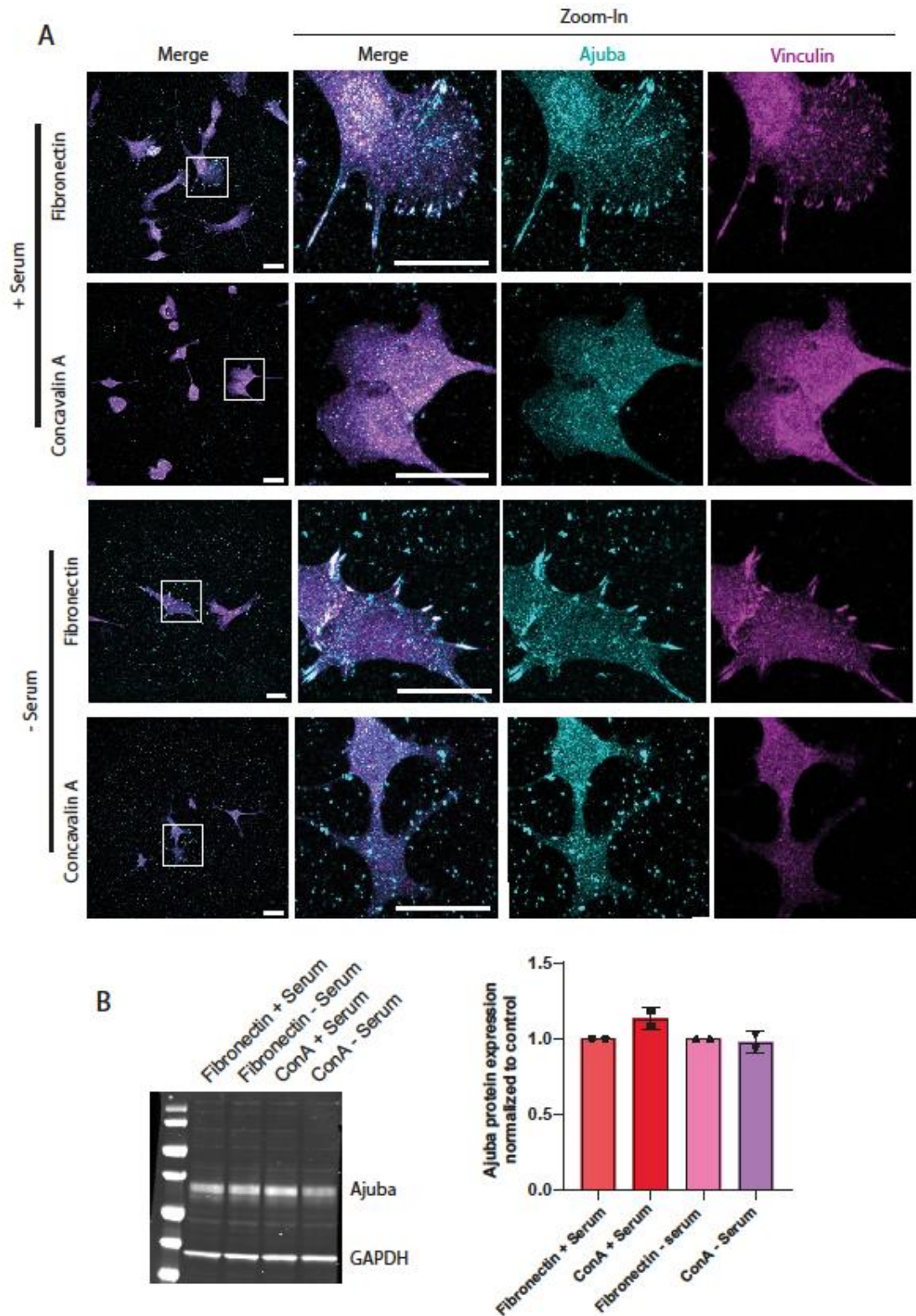
**Figure 4-2: Ajuba localises at mature sites of focal adhesion.**

Representative images from immunofluorescence of the localisation of Ajuba at focal adhesion sites in PDCA cells. White boxes represent the area magnified and displayed in the zoom-in section. Ajuba is displayed in cyan while Vinculin, P-paxillin and F-actin are displayed in magenta. Scale bar:10µm.

### 4.3 Ajuba expression is independent of focal adhesion formation in PDACA cells.

Having shown that Ajuba localises at mature focal adhesion in PDACA cells (Figure 4-2), we next asked whether Ajuba expression is dependent on focal adhesion formation. To assess the requirement of integrins' engagement for the expression of Ajuba, we disrupted integrin receptor attachment using a concanavalin-a (ConA) coating. ConA is a lectin which triggers cytoskeleton remodelling and blocks integrin-mediated cellular attachment. Lectins are carbohydrate-binding proteins, which will be recognised by the cell's carbohydrate-binding receptors on the cell surface and mediates adhesion via binding interactions with them. Cells were either cultured on fibronectin-coated or ConA-coated coverslips and cultured overnight in either serum-free media or media containing 10 % serum. Indeed, cells can use the serum protein content from the media to remodel their environment and create sites of adhesions. Culturing cells in serum-free media will prevent the creation of additional adhesion opportunities for the cells. The presence of focal adhesion was assessed by immunofluorescence using Vinculin, as a focal adhesion marker (Figure 4-3-A). On fibronectin-coated surfaces, we observed the presence of long and wide FA at the cell edge, showing that PDACA cells are forming focal adhesions in both serum and serum-free medium. In contrast, on concanavalin-A-coated surfaces in both serum and serum-free medium, we observe an absence of Vinculin staining at the cell edge, indicating that PDACA cells were not able to form focal adhesion (Figure 4-3-A).

In parallel, the protein expression of Ajuba was measured by western blot in PDACA cells, which were cultured overnight on concanavalin-coated plates or fibronectin-coated plates, reproducing similar conditions as during the immunofluorescence (Figure 4-3-B). Ajuba expression wasn't altered by the disruption of integrin receptor attachment, in either serum or serum-free media compared to the fibronectin controls (Figure 4-3-B). This result might suggest that Ajuba expression at the protein level is not controlled by YAP/TAZ, as YAP fails to enter the nucleus on ConA lectin plates (Papalazarou et al., 2020). An additional control including a YAP staining is required to validate this hypothesis.



**Figure 4-3: The expression of Ajuba is independent of focal adhesion formation in PDACA cells.**

Focal adhesion formation is prevented when cells are cultured on concanavalin-coated surfaces.

A: PDACA cells were cultured overnight on fibronectin and concanavalin-coated plates, in the presence or absence of serum in the culture media. Cells were stained with Ajuba (cyan), and Vinculin (magenta). Cells were imaged using the A1R microscopes with a 60X objective.



B: Representative western blot image of PDACA cells cultured on fibronectin-coated plates and ConA-coated plates, in serum or serum free media, stained for Ajuba (55-60kDa) and GAPDH (36kD). The protein expression of Ajuba was normalized against GAPDH sample loading control. Protein expressions were quantified using Image Studio Lite. N=2

## **4.4 Design, optimisation and validation of tools to upregulate and downregulate the expression of Ajuba in PDACA cells**

### **4.4.1 Overexpression of Ajuba**

We previously demonstrated in Chapter 3 that the expression of Ajuba changes according to stiffness (Figure 3-4). Our working hypothesis is that the expression level of Ajuba could influence cellular behaviour (proliferation, cell cycle, cell movements), cellular attachment and cell ability to react to environmental cues. To investigate this hypothesis, we designed tools to overexpress Ajuba in the PDACA cell line.

We first attempted to overexpress Ajuba using Ptripz-egfp:AJUBA, a Dox-inducible vector. Ptripz-egfp:AJUBA was transfected in PDACA cell line using Amaxa technology. As an inducible vector, multiple concentrations of Doxycycline were tested (0,02 ng.mL<sup>-1</sup>/0,05ng.mL<sup>-1</sup>/0,1 ug.mL<sup>-1</sup>, 0.5 ug.mL<sup>-1</sup>, 1 ug.mL<sup>-1</sup>) as well as different incubation periods (12h, 24h, 48h). Unfortunately, no fluorescence was observed by Immunofluorescence in any of the tested conditions in PDACA cells.

Additional attempts for the overexpression of Ajuba followed, each tested using different transfection methods (Electroporation using Amaxa reagents, cationic lipid-based transfection using Lipofectamine protocols, and calcium phosphate technique) and incubation periods (from 2 to 24 hours). First, the human Ajuba protein sequence was copied from the CCDS, a database clustering verified human protein-coding regions of genes. Myc or Flag tags were then added to either the N- or -C terminal of the Ajuba sequence. These sequences were ordered from GENEWIZ. Sequences were then cloned into an intermediary vector before being cloned into a pcdna3.1 + vector. Each clone was selected and sequenced to match the desired sequences. After the production and extraction, each plasmid was

transfected separately into PDACA cells using different concentrations of plasmids. Unfortunately, myc and flag tags were not detectable.

The Human Ajuba protein sequence was extracted by PCR from myc-Ajuba construct received from Genewiz, and subsequently cloned into pEGFP-N1 plasmid and pEGFP-C1 plasmid, creating Ajuba-pEGFP-N1 and Ajuba-pEGFP-C1 plasmids. Using Electroporation (Amaxa) or cationic lipid-based (Lipofectamine) transfections, Ajuba-pEGFP-N1 and Ajuba-pEGFP-C1 were transfected in PDACA cells, unfortunately no fluorescence was observed by immunofluorescence for Ajuba-pEGFP-N1. On the other hand, very low efficiency was observed after transfection of Ajuba-pEGFP-C1 in PDACA cells. As efficiency control, in PDACA cells were transfected pEGFP-N1 plasmid and pEGFP-C1 plasmid, both transfections were successful with a high transfection efficiency in PDACA cells.

In conclusion, all our efforts to overexpress Ajuba in PDACA cells are to this date, unsuccessful. This might be due to the instability of the tagged version of Ajuba in the cells or the inability of the cells to tolerate it. The use of a bi-cistronic vector might help with these issues. Additionally, due to the low efficiency of transfection of Ajuba-pEGFP-C1 in PDACA cells, an option in the future might be to FACS sort the cells and develop a stable cell line from it.

#### **4.4.2 Downregulation of Ajuba**

Having unsuccessfully attempted to overexpress Ajuba in PDACA cells, we next attempted to downregulate Ajuba in PDACA cells to test whether Ajuba expression could drive cellular behaviour (proliferation, cell cycle, cell movements), cell attachment and reaction to environmental cues. In Chapter 1, I showed that the expression of Ajuba is modified by stiffness, with lower protein and RNA level on 0.7 kPa compared to 38 kPa. It raised the question of whether the downregulation of Ajuba in PDACA cells can induce changes in YAP/TAZ expression or activity. Additionally, it has been shown that Ajuba family members can have close-related roles with functional redundancies and expressions (Langer et al., 2008; Schimizzi & Longmore, 2015). It also raised the question of whether changes in Ajuba expression will modify the expression of other members of Ajuba family. This will

address the possible compensation from LIMD1, an Ajuba family member, in PDACA knockdown/ knockout cells.

To investigate these questions, the downregulation of Ajuba was realised using two different methods: siRNA and CRISPR. The downregulation of Ajuba was first attempted using siRNA, 10nM of each siRNA were pooled together (Ajuba siRNA 3/5/7/8) and were transfected in PDACA cells for two consecutive rounds. siRNA scramble was used as siRNA control throughout the experiment. To assess siRNA efficiencies, both RNA and protein levels were measured (Figure 4-4). The transfection of Ajuba siRNA 3/5/7/8 in PDACA induced the downregulation of the RNA level of Ajuba to 25 % compared to siRNA scramble control (100%) (Figure 4-4-B). Additionally, the RNA expression levels of YAP, TAZ and LIMD1 (Ajuba protein family member) were measured. The RNA levels of YAP, TAZ and LIMD1 were not modified by the downregulation of Ajuba by the pool of Ajuba siRNA 3/5/7/8 compared to their levels on cells transfected by siRNA SCRAMBLE (Figure 4-4-A). The RNA expression of WTIP (the 3<sup>rd</sup> member of the Ajuba family) was not measured.

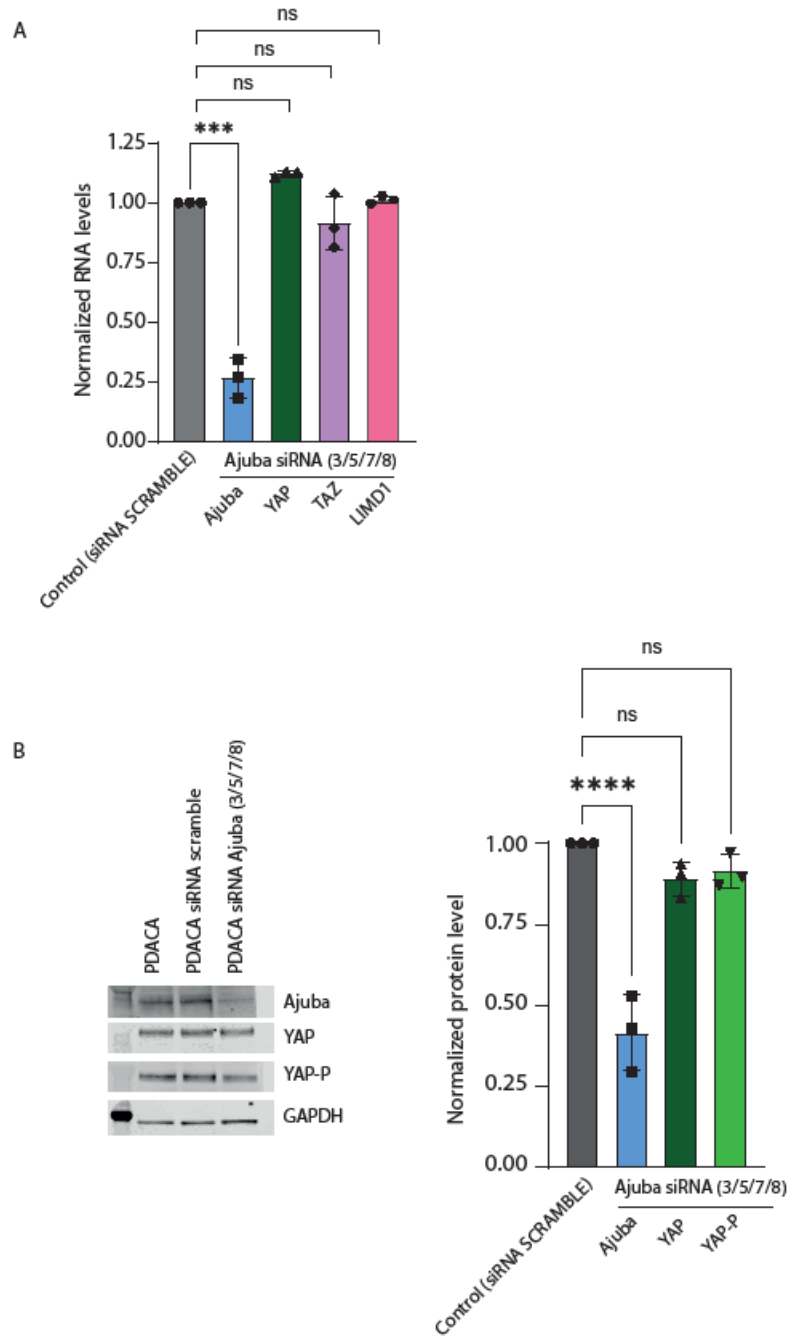
Similarly, after transfection of PDACA cells with either siRNA SCRAMBLE or the pool of Ajuba siRNA (3/5/7/8), the protein levels of Ajuba as well as YAP and YAP-P were measured by western blot (Figure 4-4-B). The protein level of Ajuba decreased significantly in siRNA-treated cells (45%) compared to siRNA SCRAMBLE levels (100%), whereas the levels of YAP and YAP-P were left statistically unchanged in siRNA-treated cells compared to siRNA SCRAMBLE (Figure 4-4-B). Taken together, the downregulation of Ajuba doesn't modify the RNA expression of YAP/TAZ, nor modify the expression of YAP and YAP-P at protein levels. We have not detected a compensation at RNA level by Ajuba family member LIMD1. The expression of WTIP was not tested at protein levels.

The downregulation of Ajuba with the pool of siRNA gave good efficiency in PDACA cells, unfortunately, the use of siRNA is not an ideal method for the needs of experiments lasting multiple days. Indeed, siRNA required multiple rounds of siRNA with batch-dependent efficiency and short-term use of resultant cells.



Instead, engineering the downregulation of Ajuba via CRISPR technique, using lentiviral infection was used to produce the stable cell lines PDACA CRISPR 01, PDACA CRISPR 02 and PDACA CRISPR All. These cell lines were produced using guides RNA targeting different regions of Ajuba, cloned into puro pLenti CRISPR vector and transformed into dh5 $\alpha$  competent bacteria. PDACA CRISPR EV cells were produced by introducing the puro pLenti CRISPR vector only, as a control cell line. All generated cell lines were tested by qPCR and Western Blot (WB) (Figure 4-5). At the RNA levels, the levels of Ajuba decrease to 30-40 % in PDACA CRISPR 01, PDACA CRISPR 02 and PDACA CRISPR All cells, compared to PDACA CRISPR EV cells (Figure 4-5-A). Whereas the protein level of Ajuba decreased significantly to 15-20 % in PDACA CRISPR 01, PDACA CRISPR 02 and PDACA CRISPR All cells, compared to the level of Ajuba in PDACA CRISPR EV cells (Figure 4-5-B).

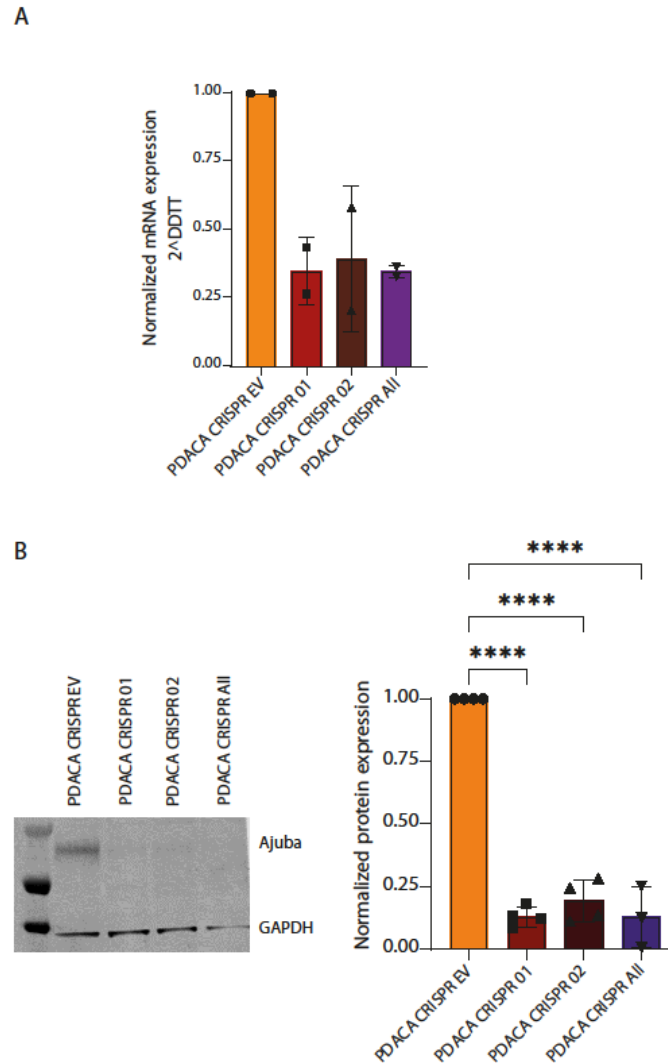
PDACA CRISPR 01, PDACA CRISPR 02 and PDACA CRISPR All cells showed a downregulation of Ajuba at the RNA levels (Figure 4-5A) and protein level (Figure 4-5-B) compared to their levels on PDACA CRISPR EV cells. These cell lines will be used throughout this study.



**Figure 4-4: The Ajuba siRNA(3/5/7/8) treatments efficiently downregulate the RNA and protein levels of Ajuba in PDACA cells.**

**A:** Quantification of the RNA expression of Ajuba, YAP, TAZ and LIMD1 measured in each sample, normalized to GAPDH as a housekeeping gene. Cells were transfected with a pool of 4 siRNAs (3/5/7/8) targeting Ajuba, and control cells were transfected with siRNA scramble (control). The statistical differences were measured by one-way ANOVA. N=3 Each sample was tested with three technical triplicates and three biological replicates.

**B:** (Left) Representative western blot images of Ajuba (55-60kDa), GAPDH (36kDa), YAP (65-78) and YAP-P (65-78) protein levels. (Right) Quantification by western blot of Ajuba, YAP, YAP-p protein levels in PDACA cells treated with either a pool of 4 siRNAs (3/5/7/8) targeting Ajuba or with siRNA scramble (control), normalized to GAPDH protein levels (sample loading control). Statistical differences were measured by one-way ANOVA. N=3.



**Figure 4-5: Successful downregulation of Ajuba at RNA and protein levels in PDACA CRISPR 01, PDACA CRISPR 02 and PDACA CRISPR All cell line compared to PDACA CRISPR EV.**

A: Quantification of the RNA expression of Ajuba by qPCR in each sample, normalised using *cdk2* as a housekeeping gene. Each sample was tested with technical triplicate. N=2.

B: (Left) Representative western blot image of GAPDH and Ajuba protein levels in PDACA CRISPR 01, PDACA CRISPR 02, PDACA CRISPR All and PDACA CRISPR EV cells. (Right) Protein levels of Ajuba in PDACA CRISPR 01, PDACA CRISPR 02, and PDACA CRISPR All cells, normalized to GAPDH protein levels (sample loading control) and subsequently to the levels of Ajuba in PDACA CRISPR EV cells. N=4. Statistical differences were measured by one-way ANOVA.

## 4.5 Ajuba downregulation could impact PDACA cell-ECM attachment.

Having shown that Ajuba localises at focal adhesion sites, we now ask the question whether Ajuba could have a potential function in cell-ECM adhesion events. To assess if ajuba downregulation impacts cell adhesion, I used xCELLigence, a

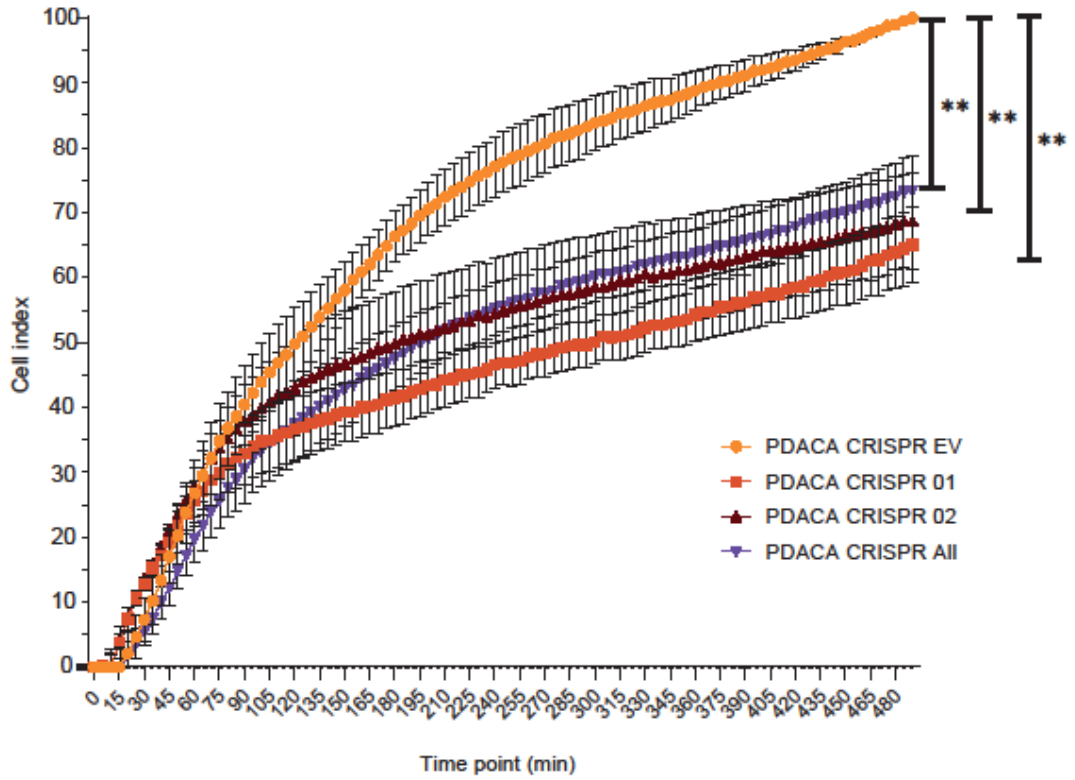
quantitative method to record cell-ECM adhesion over time. This quantification is tailored around the measurement of impedance. The impedance represents the resistance to an alternating electrical current based on the flow of electrons. This electrical current will travel through gold electrodes, placed at the bottom of the plate. The impedance is transformed into a dimensionless parameter called the Cell Index (CI). Cell Index was plotted as the impedance acquired at specific time points, minus the blank's impedance at t0 (before cell addition) and normalized to the nominal impedance of the machine. The CI was recorded over time, starting as soon as cells were added to the media and every five minutes for a total of eight hours (Figure 4-6). As shown in Figure 4-6, it is important to note that for the first hour, CI profiles are identical among PDACA CRISPR EV cells and PDACA CRISPR 01, PDACA CRISPR 02, PDACA CRISPR all cells. CI profiles diverge after one hour and until the end of the experiment. Indeed, the cell indexes of the three Ajuba downregulated PDACA CRISPR cell lines (PDACA CRISPR 01, PDACA CRISPR 02, PDACA CRISPR all) are trending significantly lower than the CI of the PDACA CRISPR EV cell line (Figure 4-6). After 8 hours, PDACA CRISPR 01 cells have the lowest cell index (65) throughout the experiment, among all tested cell lines (PDACA CRISPR 02 (68), PDACA CRISPR all (73), PDACA CRISPR EV (100)) (Figure 4-6). As previously mentioned, the changes in cell index translate to changes in impedance over time. These results could indicate that the downregulation of Ajuba decreases cellular matrix adhesion. However, it is also to be noted that the impedance is dependent on multiple parameters: cell number, cell morphology, cell size, cell-to-cell adhesion and adhesion strength to ECM. To assess if the impedance changes are due to other parameters than cell adhesion to the ECM, cell proliferation and cell areas were then tested.

The cell proliferation of each cell line was monitored over four days using the Incucyte technology. The proliferation rates were emulated by tracking the confluency of each cell line throughout the experiment (Figure 4-7-A). We can observe that the confluency of PDACA CRISPR EV cell line compared to PDACA CRISPR 01, PDACA CRISPR 02, PDACA CRISPR all cells, evolves similarly over time with no statistical differences after four days (Figure 4-7-A). Since the impedance measurements of xCELLigence were realised over eight hours, the first eight hours

of the proliferation assay were isolated and plotted in Figure 4-7-B. Cellular confluency over the first eight hours between PDACA CRISPR 01, PDACA CRISPR 02, PDACA CRISPR All and PDACA CRISPR EV cells were not significantly different from one another. Taken together, the changes observed in Figure 4-6 were not due to changes in cellular proliferation.

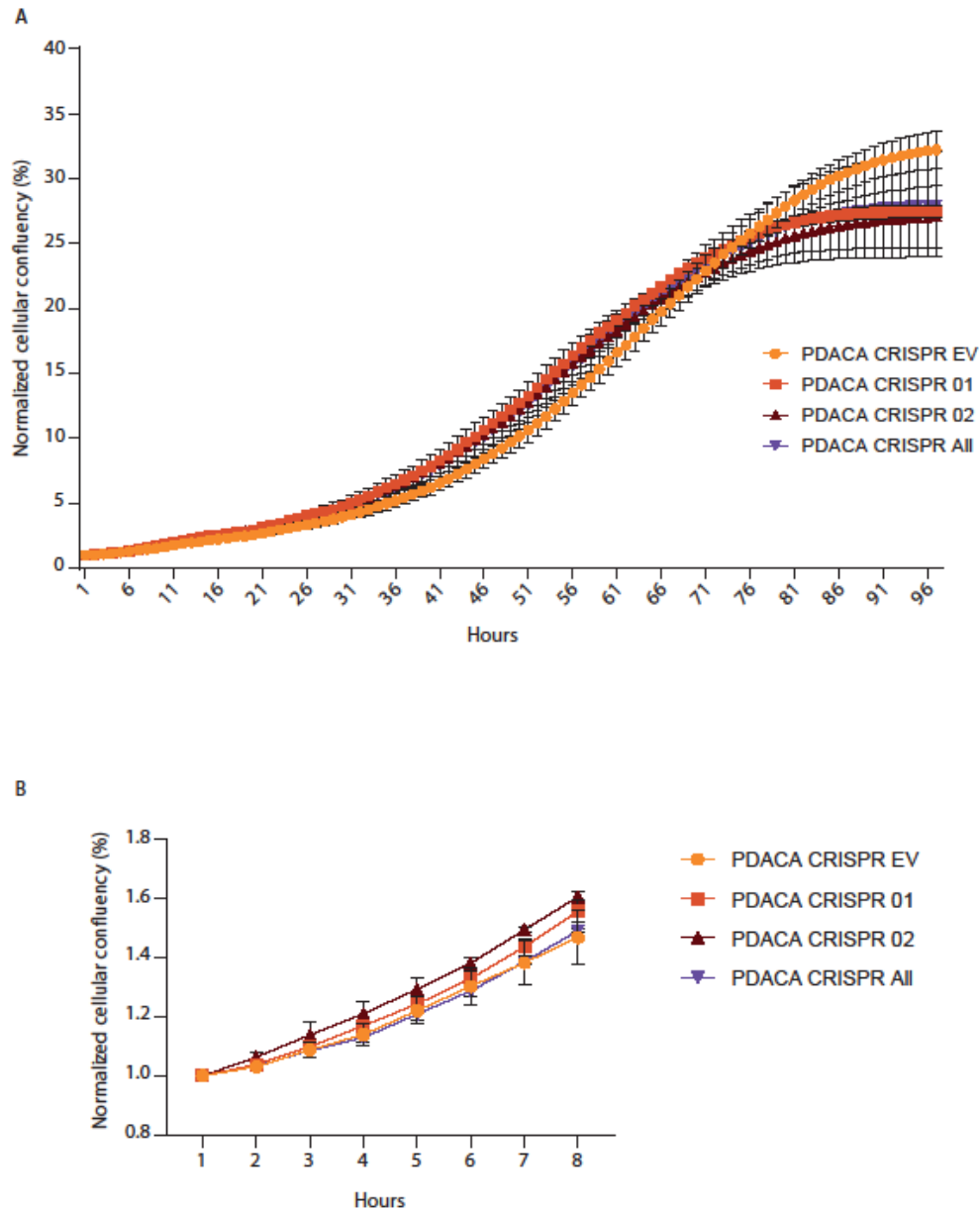
To assess if the differences of CI were due to changes in cellular morphology, PDACA CRISPR EV PDACA CRISPR 01, PDACA CRISPR 02 and PDACA CRISPR All cells were seeded on fibronectin-coated coverslips for 1h (60 min) and 5h (300 min) stained for F-actin by immunofluorescence (Figure 4-8-A). Using the F-actin staining, cell areas were measured for both time points using ImageJ software (Figure 4-8). No differences in cell area were observed after one hour (Figure 4-8-B) or five hours (Figure 4-8-C) of seeding, between PDACA CRISPR EV cells and respectively PDACA CRISPR 01, PDACA CRISPR 02 and PDACA CRISPR All cells. Therefore, we could hypothesise that the differences in CI, between PDACA CRISPR EV and PDACA CRISPR 01, PDACA CRISPR 02, PDACA CRISPR All cells, were not due to modification of cell number or cell size.

I previously mentioned cell-cell adhesion as a possible factor governing the cell index. PDACA cells are not epithelial and not tightly linked to one another as cells would be in epithelial tissue, which can explain why Ajuba doesn't localise at cell-cell adhesion in PDACA cells (Figure 4-1). Taken together, this invalidates the cell-cell adhesion as a factor for the CI changes. We can conclude that the downregulation of Ajuba could trigger changes in cell-ECM adhesion.



**Figure 4-6: The downregulation of Ajuba induces a decrease in cell-matrix adhesion in PDACA CRISPR 01, PDACA CRISPR 02, PDACA CRISPR All cell lines.**

Representation of the evolution of cell index in PDACA CRISPR EV, PDACA CRISPR 01, PDACA CRISPR 02 and PDACA CRISPR All cell lines. The cell index (CI) was measured using the real-time analyser (RTCA) system for 8 hours. For each biological replicates, four technical replicates were measured. N=4. Statistical significance was measured for the last time point of each cell line using One-way ANOVA.

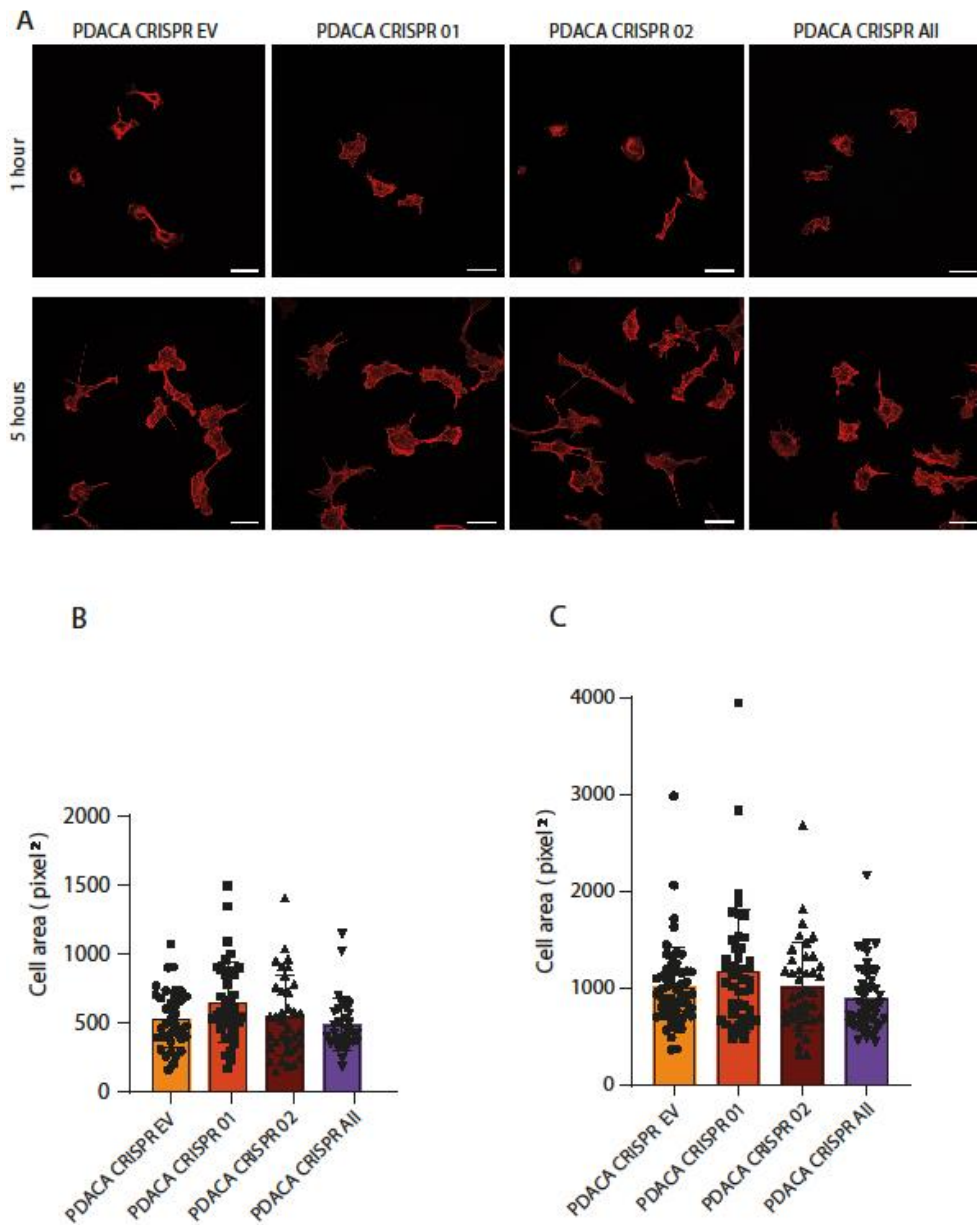


**Figure 4-7: The downregulation of Ajuba has no impact on the proliferation in PDACA CRISPR 01, PDACA CRISPR 02 and PDACA CRISPR All, compared to PDACA CRISPR EV cells.**

An image of each well was taken every hour with a 10X objective, the confluency of PDACA CRISPR EV, PDACA CRISPR 01, PDACA CRISPR 02 and PDACA CRISPR All cells were measured over time. For each of the three biological replicates, cells were seeded as technical triplicates on fibronectin-coated plates and cultured for 4 days.

A: The cellular confluency of PDACA CRISPR EV, PDACA CRISPR 01, PDACA CRISPR 02 and PDACA CRISPR All cells were plotted over time, normalized to PDACA CRISPR EV cells confluency. N=3. No statistical difference was found using one-way ANOVA on the area under the curve calculation.

B: The cellular confluency of PDACA CRISPR EV, PDACA CRISPR 01, PDACA CRISPR 02 and PDACA CRISPR All cells were extracted from the first eight hours, corresponding to the xCELLigence timeframe. N=3. No statistical difference was found between PDACA CRISPR 01, PDACA CRISPR 02, PDACA CRISPR All cells and PDACA CRISPR EV cells using one-way ANOVA.



**Figure 4-8: The downregulation of Ajuba doesn't change cell sizes in PDACA CRISPR 01, PDACA CRISPR 02 and PDACA CRISPR All compared to PDACA CRISPR EV.**

Cells were cultured for either 1 hour or 5 hours after seeding on fibronectin-coated coverslips before fixation, permeabilisation and staining.

A: Representative immunofluorescence images of PDACA CRISPR EV, PDACA CRISPR 01, PDACA CRISPR 02 and PDACA CRISPR All cell lines cultured for 1 hour or 5 hours on fibronectin-coated coverslips and stained for F-actin. Cells were imaged at objective 40X using A1R microscopes. N=2

B: The cell area of PDACA CRISPR EV, PDACA CRISPR 01, PDACA CRISPR 02 and PDACA CRISPR All cell were measured on ImageJ. N=2.

C: PDACA CRISPR EV, PDACA CRISPR 01, PDACA CRISPR 02 and PDACA CRISPR All cell areas were measured using the ImageJ software. N=2.

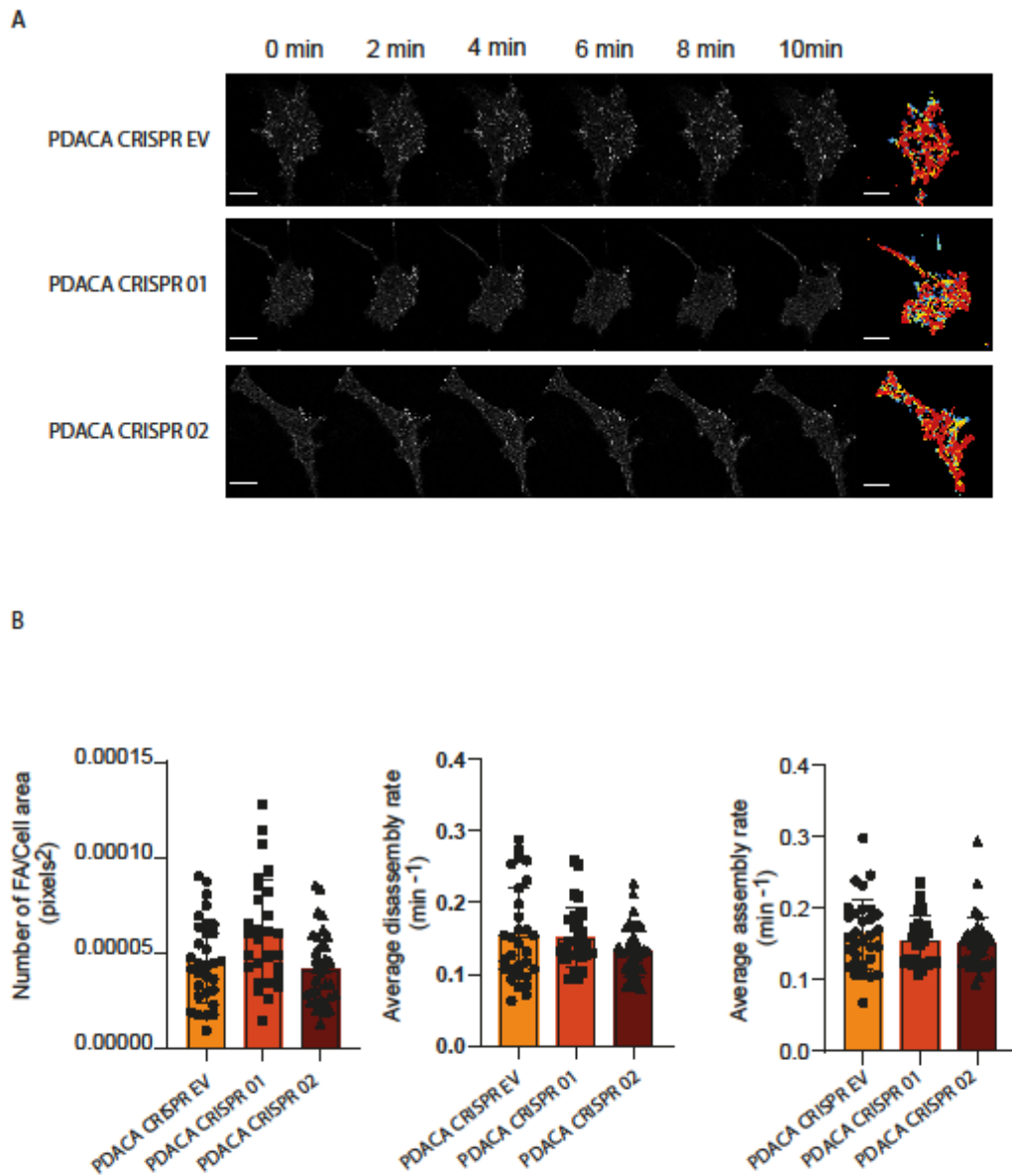


## 4.6 The downregulation of Ajuba doesn't impact focal adhesion dynamics

Having shown that the downregulation of Ajuba could change the cell-ECM adhesion, we asked whether the number of focal adhesions in cells or their dynamism (assembly/disassembly) were changed by the downregulation of Ajuba. To answer this question, we realised a focal adhesion turnover experiment using PDACA CRISPR EV, PDACA CRISPR 01 and 02 cells transfected with 5 µg of gfp-paxillin, 24 hours before imaging on the Airyscan 880 microscope. Videos were acquired and analysed to highlight the focal adhesions and their assembly/disassembly events using the focal adhesion analyser server (FAAS), a publicly available tool at <https://faas.bme.unc.edu/>. First of all, the focal adhesions were tracked over time to highlight their dynamic nature by the FAAS (Figure 4-9-A). Blue colour indicates focal adhesion sites that were stable during the timelapse while orange and red colour indicates highly dynamic sites. We observed in each cell line highly dynamic focal adhesions (Figure 4-9-A). In each analysed cell, the number of focal adhesions was measured by FAAS, and normalized to the cell size (Figure 4-9-B left panel). No significant changes in the number of FA were observed between PDACA EV and PDACA CRISPR 02 cells. However, we observed a slight increase in the focal adhesion number of PDACA CRISPR 01 cells compared to PDACA CRISPR EV cell lines (Figure 4-9-B left panel).

Focal adhesion numbers are as important for cell behaviour as focal adhesion dynamics in a cell. To determine if FA dynamics differed between PDACA CRISPR 01, PDACA CRISPR 02 and PDACA CRISPR EV cell lines, focal adhesion assembly (Figure 4-9-B right panel) and disassembly rates were measured (Figure 4-9-B middle panel). We observed, no changes in FA assembly (Figure 4-9-B, middle panel) or disassembly rates (Figure 4-9-B right panel) of PDACA CRISPR 01 and PDACA CRISPR 02 compared to PDACA CRISPR EV. A manual quantification of the focal adhesion number, using a single timepoint for every cell analysed, also confirmed no difference in focal adhesion number in PDACA CRISPR 01 and PDACA CRISPR 02 cell lines compared to PDACA CRISPR EV (Figure 7-1).

The changes observed in cell-ECM adhesion during the xCELLigence experiment, in PDACA CRISPR cell line 01, and PDACA CRISPR cell line 02 compared to PDACA CRISPR EV were not linked to focal adhesion dynamics nor changes in focal adhesion number.



**Figure 4-9: Ajuba depletion doesn't impact focal adhesion turnover in PDACA CRISPR 01 and PDACA CRISPR 02 cells compared to PDACA CRISPR EV.**

A: Representative montages of PDACA CRISPR EV, PDACA CRISPR 01 and PDACA CRISPR 02 cells transfected with p-paxillin and imaged every 20 seconds, for a total of 10 minutes with Airyscan. Colour-coded images were created to highlight the dynamic properties of focal adhesion and their evolution over time by FAAS. Scale bar: 10µm. N=2.

B: The quantification of focal adhesion numbers (Left panel), FA assembly (middle panel) and FA disassembly (right panel) rates were measured for each cell by FAAS and plotted according to each cell line (PDACA CRISPR EV, PDACA CRISPR 01 or PDACA CRISPR 02). N=2.

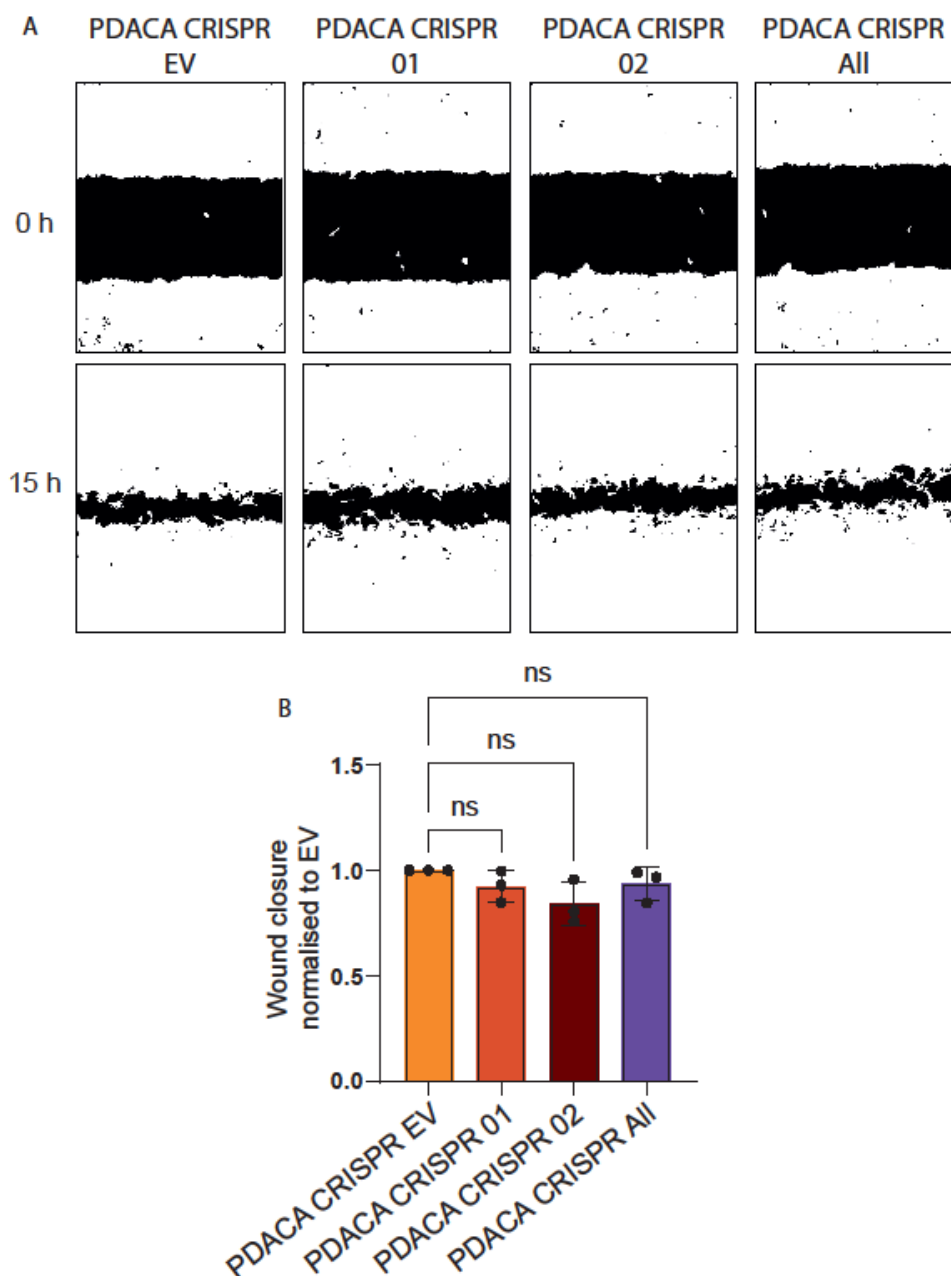
#### **4.6.1 The downregulation of Ajuba specifically increases PDACA cell invasion abilities.**

Having shown that Ajuba is localised at focal adhesion sites, and its expression isn't correlated to focal adhesion formation, dynamics or number, we next asked whether Ajuba has a role in cell movement. To investigate this question, I tested whether the abilities of cells to migrate and invade were impacted by the downregulation of Ajuba. Interestingly, Ajuba expression was correlated with cell migration and invasion in many cancers but no information was available regarding pancreatic cancer cells (Liang et al., 2014; Schleicher & Schramek, 2021; Shi et al., 2016; Zhang et al., 2020). Migration and invasion were measured in PDACA CRISPR EV, PDACA CRISPR 01 and PDACA CRISPR 02 using respectively wound healing assay and invasion assay. To determine if ajuba downregulation would impact cellular movement in 2D in PDACA CRISPR cell lines, a wound-healing assay was performed. To migrate in a 2D environment, cells need to modulate their shape, and their adhesions to the matrix and generate forces by contracting their actomyosin network. The wound closure was measured at the beginning (t=0h) and 15 hours later (t=15h). In Figure 4-10, we observed no significant changes in wound closure after 15 hours of migration, between PDACA CRISPR EV and neither PDACA CRISPR 01 nor PDACA CRISPR 02 cell lines. Interestingly in a 3D environment, cellular invasion combines different mechanisms: Modulation of adhesion, contractibility, force generation and enzymatic activities. Cellular invasion was measured by encapsulating cells in between a layer of 1% Matrigel and covering them with a layer of pure matrigel to mimic a 3D environment. After 50 hours, the distance covered by PDACA CRISPR 01, PDACA CRISPR 02, PDACA CRISPR All cells were compared to the distance covered by PDACA CRISPR EV cells. A significant increase in invasion was observed in PDACA CRISPR 01, 02 and All compared to PDACA CRISPR EV (Figure 4-11). Since an increase of invasion was observed in all Ajuba downregulated cell lines, I asked whether the adhesions, or invadopodia hotspots (Yu et al., 2012) were modified in the Ajuba-depleted PDACA cells.

In 3D, adhesions should look like dot structures, previously described as actin hotspots and invadopodia-like structure (Yu et al., 2012). To stain these hotspots, multiple attempts were made using different antibodies (vinculin and p-paxillin), a range of dilutions (1/50-1/500), incubation temperatures and incubation time. Unfortunately, vinculin and p-paxillin staining were unsuccessful. This technical difficulty was assessed by testing the primary antibodies and secondary antibodies in a standard 2d immunofluorescence. In a standard 2D environment, the focal markers used were consistently staining focal adhesions. As the staining issue might be due to technical difficulties, a second protocol was tested, using different permeabilisation and blocking methods from the one previously used. PFS was used to permeabilise, block cells and dilute antibodies. A gentle agitation was used throughout the protocol, and the primary antibodies diluted in PFS were added and incubated overnight at 4°C. Secondary antibodies and dyes were diluted in PFS for 1 hour at room temperature. Cells were washed once with PFS and three times with PBS for 5 minutes before imaging in PBS solution.

The primary antibodies, p-paxillin and vinculin were tested at concentrations ranging from 1/100, and secondary antibodies were diluted at 1/200. Unfortunately, no focal adhesion marker staining was successful in any of the tested cell lines. As previously, DAPI and F-actin staining were realised and consistently achieved (Figure 4-12).

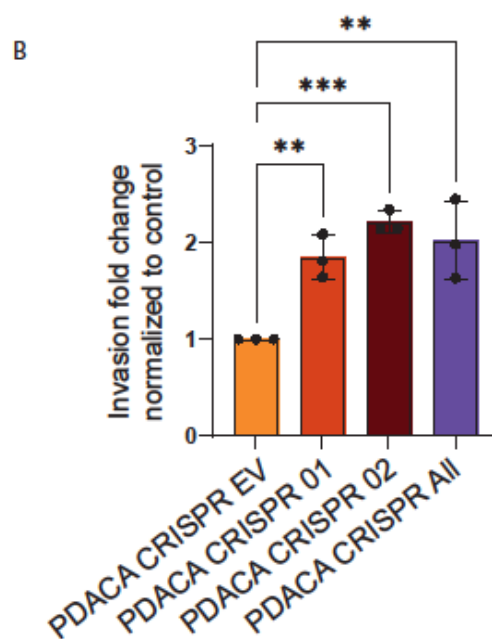
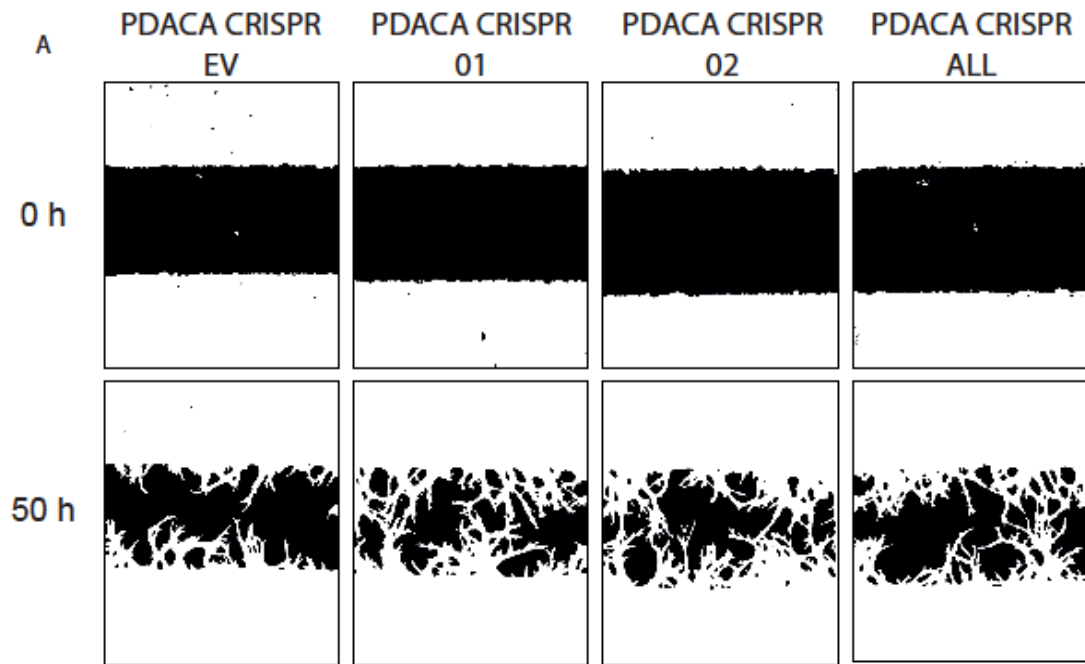
In this section was demonstrated that the downregulation of Ajuba promoted PDACA invasion. This might be due to an increase in MMP activities, an enhanced cytoskeletal turnover or enhanced adhesion dynamics during cellular invasion. The pro-tumoral role of Ajuba was linked to an increase in cellular proliferation but an additional hypothesis could be articulated on the role of Ajuba in tumor invasion in PDAC.



**Figure 4-10: The downregulation of Ajuba has no impact on the migration of PDACA CRISPR 01, PDACA CRISPR 02 compared to PDACA CRISPR EV cells.**

**A:** The wound closure of PDACA CRISPR EV was compared to the wound closure of PDACA CRISPR 01, PDACA CRISPR 02 and PDACA CRISPR All after 15 hours. N=3

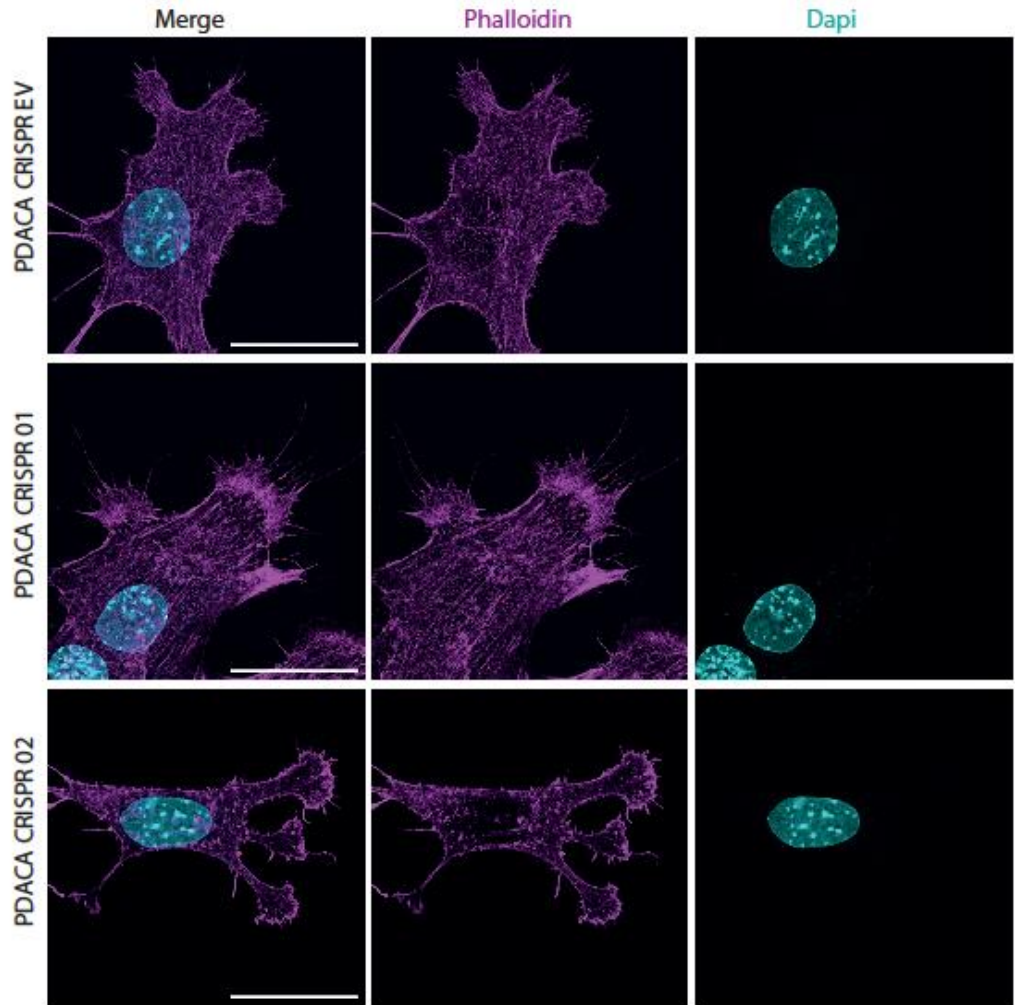
**B:** Quantification of the distance covered by PDACA CRISPR 01, PDACA CRISPR 02 and PDACA CRISPR All cells during 15 hours, normalized to the distance covered by PDACA CRISPR EV cells. N=3, each containing technical triplicates. No significant differences were found, between PDACA CRISPR EV and any of the other tested cell lines using one-way ANOVA.



**Figure 4-11: The downregulation of Ajuba increases PDACA CRISPR 01, PDACA CRISPR 02 and PDACA CRISPR All cellular invasion compared to PDACA CRISPR EV cells.**

A: Representative images from the invasion assay. Images were taken of PDACA CRISPR EV, PDACA CRISPR 01, PDACA CRISPR 02 and PDACA CRISPR All cells, at T=0h and T=50h. The cells were imaged every hour. N=3, each containing technical triplicates

B: Quantification of the invasive area covered by PDACA CRISPR 01, PDACA CRISPR 02, PDACA CRISPR All cells after 50 hours of invasion, normalized to the distance covered by PDACA CRISPR EV cells. N=3, each containing technical triplicates. Significant differences were assessed using one-way ANOVA.

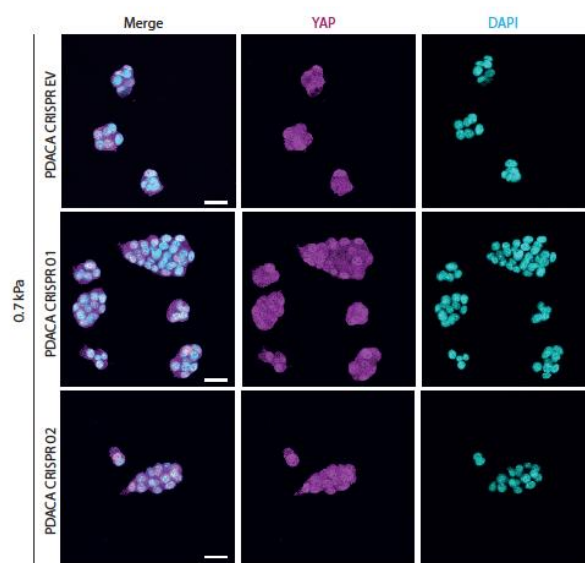


**Figure 4-12: PDACA CRISPR EV, PDACA CRISPR 01, and PDACA CRISPR 02 cells invading through Matrigel**

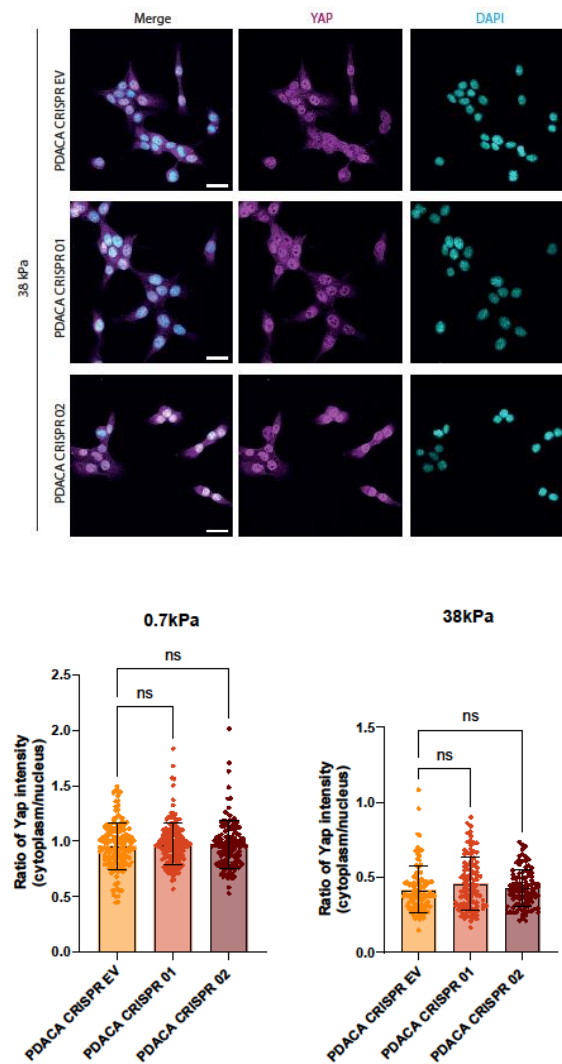
Representative images of PDACA CRISPR EV, PDACA CRISPR 01, and PDACA CRISPR 02 cells invading through Matrigel. PDACA CRISPR cells were left to invade overnight through Matrigel and stained with phalloidin (Magenta) and DAPI (Cyan). Scale bar: 30 $\mu$ m.

## 4.7 Impact of Ajuba downregulation in PDACA cells exposed to stiffness.

In Chapter 1, I demonstrated that the expression of Ajuba at RNA level was changed according to environmental stiffness. Ajuba is a LIM domain protein, which is a family increasingly recognised as members playing a role in the generation and response to mechanical forces (Anderson et al., 2021). Additionally, Ajuba protein was shown to change localisation according to cytoskeleton tension, to be recruited at cell junction and shift to and from the nucleus to act on transcriptional activities (Ayyanathan et al., 2007; Rauskolb et al., 2014; Razzell et al., 2018). Due to the possible role of Ajuba in mechanotransduction, we questioned whether the downregulation of Ajuba would impact the mechanosensing/mechanotransduction abilities of PDACA cells. PDACA CRISPR EV, 01 and 02 were cultured overnight on 0.7 kPa and 38 kPa hydrogels, coated with fibronectin and stained with YAP antibody and DAPI by immunofluorescence. YAP localisation was used to monitor the response of each cell line to stiffness. Cell sizes and shapes don't appear to differ in PDACA CRISPR 01 and 02 compared to PDACA CRISPR EV. Using a cytoplasmic-to-nucleus ratio no significant changes were observed regarding YAP localisation between PDACA CRISPR 01, PDACA CRISPR 02 and PDACA CRISPR EV (Figure 4-13).







**Figure 4-13:** The downregulation of Ajuba doesn't impact cell shape nor cell size in PDACA CRISPR 01, PDACA CRISPR 02 compared to PDACA CRISPR EV.

Representative images were selected as an overview of PDACA CRISPR 01, PDACA CRISPR 02 and PDACA CRISPR EV cell line cultured overnight on polyacrylamide hydrogels of customizable stiffnesses. Immunofluorescence using YAP (Magenta), DAPI (Cyan). N=3, Scale bar: 20 $\mu$ m. Significant differences were assessed using one-way ANOVA.

## 4.8 Conclusion:

In this chapter, I first demonstrated that Ajuba localises at mature focal adhesion, cytoplasm and nucleus in PDACA cells. Interestingly, the expression of Ajuba at the protein level is not linked to focal adhesion formation in PDACA and the downregulation of Ajuba doesn't modify FA numbers, assembly nor disassembly rates in PDACA CRISPR 01, PDACA CRISPR 02 compared to PDACA CRISPR EV. Additionally, the downregulation of Ajuba could impact cell-ECM adhesion while

it doesn't modify cell proliferation, cell shape or cell size in PDACA CRISPR 01, PDACA CRISPR 02, PDACA CRISPR All compared to PDACA CRISPR EV. Finally, the downregulation of Ajuba increases the invasion but not the migration abilities of PDACA CRISPR 01 and PDACA CRISPR 02 compared to PDACA CRISPR EV.

## 4.9 Discussion:

In this chapter, my attention was directed towards understanding the role and localisation of Ajuba in pancreatic cancer. Previously published localisation of Ajuba in drosophila and mammalian cell lines, was predominant at the adherence junction, cell vertices, and co-localising with cadherin complexes. Ibar et al., showed Ajuba at focal adhesions through the co-localisation with vinculin in MDCKIIIG (Madin-Darby canine kidney, canine kidney epithelial cell line) and MCF10A (non-tumorigenic mammary gland cell line) cell lines. Although the presence of Ajuba at FA was minor compared with its presence at adherent junction sites. They hypothesised that the localisation of Ajuba might differ on the cell line analysed (Ibar et al., 2018). In this chapter, I demonstrated that Ajuba has strong localisation at focal adhesion, where it co-localises mostly with mature forms of focal adhesion as well as actin stress fibres in PDACA cell line. The specificity of the Ajuba antibody was created by the specific targeting of an Ajuba peptide, which was confirmed by a 100% specificity to the targeted Ajuba sequence by Blast search, highlighting the specificity for Ajuba. For additional validation, a more thorough set of tests on cells (WT vs KO) should take place. For a more accurate visualisation of the recruitment of Ajuba at focal adhesion sites, a time course of focal adhesion maturation could be realised. Unfortunately, this requires a tagged version of the protein Ajuba which I was unable to successfully transfect in PDACA. It is to be noted that the transfection of pEGFP-C1 in PDACA as a control vector was successful in PDACA cells. The transfection of Ajuba-pEGFP-C1 in HEK293T was successful with a low to medium efficiency. The use of a bicistronic vector might enable us to obtain a stable tagged Ajuba protein, which is currently either not stable or not tolerated in PDACA cells.

Cells use different adhesion types depending on the adhesion substrate, integrin-based adhesions are used for cell-ECM adhesions while cell-cell adhesions are

cadherin-based (Mui et al., 2016). In cancers, there are often modifications of intercellular adhesion, with a loss of adhesion due to the downregulation of cadherins, facilitating invasion and metastatic phenotypes (Joshi et al., 2023). The loss of cell-cell adhesion in PDACA cells might have favoured the localisation of Ajuba toward focal adhesion. The localisation of Ajuba at FA might also be linked with the epithelial-mesenchymal transition status of these cells. To further the understanding of the role of Ajuba in PDACA cells, the downregulation of Ajuba was achieved through CRISPR and validated thoroughly.

Due to a favoured focal adhesion localisation of Ajuba in PDACA, and the requirement of focal adhesion on cell-matrix adhesion, I tested whether the expression of Ajuba was dependent on focal adhesion formation. Due to the absence of correlation between Ajuba and the formation of focal adhesion (Figure 4-3), I tested how cell-matrix adhesion was impacted by Ajuba downregulation. The cell-matrix adhesion was decreased in PDACA CRISPR 01, PDACA CRISPR 02, PDACA CRISPR All cells compared to PDACA CRISPR EV cells, which wasn't due to the cell size (Figure 4-8), focal adhesion numbers nor dynamics which were unchanged (Figure 4-9).

I have previously demonstrated that the downregulation of Ajuba does not influence proliferation in PDACA cells (Figure 4-7). The PDACA cell line was isolated from KPC mice with  $KRAS^{G12D}$  and  $p53^{R172H}$  mutations, which would greatly influence cell proliferation regulation in this cell line (Luo, 2021). Additionally, the effect of Ajuba in proliferation seems to be organism, organ, cancer-type and cell-lines-dependent (Chen et al., 2016; Tanaka et al., 2015; Zhang et al., 2019).

The decrease in cell-matrix adhesion made us ask whether the abilities of cells to migrate and invade were modified by the downregulation of Ajuba. Previously published studies established that Ajuba expression enhances migratory abilities in cells (Pratt et al., 2005; Shi et al., 2016) and showed abnormal lamellipodia formation in primary fibroblasts isolated from Ajuba null mice (Pratt et al., 2005). Migration requires a combination of factors, cell polarization, actomyosin network contractility, focal adhesion maturation and dynamism. In this chapter, I demonstrated that in PDACA, no modification in migration abilities was observed

(Figure 4-10). Interestingly, for cells to invade, in addition to mechanisms already cited for migration, the cell requires metalloprotease activities, the formation and dynamism of invadopodia as well as mechanosensing/mechanotransduction activities (Linder et al., 2023). My results demonstrated a sharp increase in invasion abilities in PDACA CRISPR 01 cells, PDACA CRISPR 02 cells compared to PDACA CRISPR EV cells (Figure 4-11). Additional testing is now required to understand how the downregulation of Ajuba can increase cell invasion and modify cell index in PDACA. Some of the parameters required for additional testing are the metalloprotease activities, strength of adhesion, and invadopodia dynamics. To study if the downregulation of Ajuba modifies metalloprotease (MMP) activities, zymograms and quenched fluorescence (DQ-collagen) can be used to answer the question of whether the increase in invasion is due to MMPs activities. To test the strength of cell-matrix adhesion, we could use micropillars or a nanopillar arrays to measure the force through pillar displacement or fluorescence intensity. For a 3D environment, 3D traction microscopy could bring great insight into 3D traction forces involved in cell invasion. Since all attempts at focal adhesion staining in 3D were unsuccessful (Figure 4-12), transfection of GFP-paxillin in PDACA, as previously realised during the focal adhesion turnover experiment could be another way to observe invadopodia dynamics.

Changing environmental parameters like stiffness using tuneable hydrogels allows us to test the mechanosensitive and mechanotransduction abilities of cells and visualise how they impact cellular functions. Polyacrylamide hydrogels were designed to recapitulate specific stiffnesses, 0.7 kPa and 38 kPa. YAP/TAZ are well-known mechanotransducers and transcriptional coactivators, which relay environmental cues and coordinate cell responses through various mechanisms including the regulation of gene expression (Antonio Totaro et al., 2018). As previously published, YAP will enter the nucleus in response to many cues such as a stiff substrate or growth-promoting signals. During immunofluorescence, YAP staining was realised to monitor the mechanosensing and mechanotransduction signalling of the cells. YAP localisation is changing from nuclear localisation (on stiff) to cytoplasmic localisation (on soft) in reaction to stiffness. I hypothesised that Ajuba, as our mechanotransduction candidate, could have a similar ability as

YAP/TAZ to relay environmental cues from the cell's leading edge to the nucleus impacting cell behaviour and transcription activities. The localisation of Ajuba in PDACA cells cultured on hydrogels was not monitored due to detection issues linked to the antibody's limitations. However, the localisation of YAP was used to monitor changes in the mechanosensing and mechanotransduction signalling of PDACA CRISPR 01 and PDACA CRISPR 02 cells. In Figure 4-13 we can observe no morphological changes among similar stiffnesses between PDACA CRISPR EV cells and PDACA CRISPR 01 and 02 cells. YAP localisation was quantified using a cytoplasmic to nucleus and no significant difference was observed between PDACA CRISPR EV cells and PDACA CRISPR 01 and 02 cells on the tested stiffnesses : 0.7 kPa and 38kPa. Additionally, the role of Ajuba as a potential mechanotransducer will be further analysed through its role as a transcriptional co-repressor in Chapter 5.

**Chapter 5. PAAM stiffnesses and Ajuba impacts  
transcription factors activities**

## 5.1 Introduction

In the Chapter 3, we highlighted the intricate relationship between stiffness and various cellular behaviour in PDACA. Focussing on protein expression and monitoring cell behaviours, a wide range of changes can be tested. Although this approach masks changes that could impact gene expressions at the RNA level. Cellular functions are defined at both protein and RNA levels, which are intertwined, making cells a complex entity. Indeed, protein levels are dictated by everything from transcription factor activities, RNA expression, post-transcriptional modification, translation efficiency, and protein stability.

Ajuba is an adaptor/scaffold protein part of the Zyxin/AJUBA family and a component of the LIM domain protein family. LIM domain proteins are known for their roles in protein-protein interactions (Sang et al., 2014; Zheng & Zhao, 2007). Recently, LIM domain proteins are increasingly recognised as proteins involved in mechanotransduction pathways, with their LIM domain serving as a mechanical response domain (Anderson et al., 2021). Ajuba was part of a group of mechanotransduction candidates selected and tested in Chapter 3, which showed the expression of Ajuba at RNA and protein levels changing according to the stiffness in PDACA cells, cultured on 0.7 kPa and 38 kPa hydrogels. These results suggest that Ajuba is a mechanoresponsive protein, but is Ajuba a mechanotransduction actor in PDACA? Multiple publications show Ajuba as a transcriptional co-regulator (Ayyanathan et al., 2007; Fan et al., 2015; Hou et al., 2008; Zhang et al., 2019), which leads us to investigate how Ajuba downregulation will modify transcription factor activities and gene transcription. The use of deep sequencing technologies like RNA sequencing allows quantification and exploration of the transcriptome, without bias of a specific gene set analysis, broadening our view of transcriptomics (Hong et al., 2020). RNA sequencing is pulling together every aspect of transcriptomics, from general RNA to messenger RNA, non-coding and small RNA.

In this chapter was combined two aims, first we studied the effects of the downregulation of Ajuba and second, we studied the effect of stiffness at the PDACA RNA level. To achieve this, polyacrylamide hydrogels, created using

acrylamide and bis-acrylamide, were generated with tunable stiffnesses of 0.7 and 38 kPa. Studying changes brought by modifying environmental stiffness will allow us to gain insight into mechanotransduction pathways and how they affect PDACA cells. These polyacrylamide hydrogels were functionalised using a protein crosslinker, linking PAAM hydrogel surface and fibronectin fibres, a biocompatible ECM protein usually found, among others, in the ECM of PDAC. Cells seeded on different stiffnesses will modify their behaviour to best fit these environments (Chapter 1). Through RNA gene expression, we will highlight pathway and transcription factors affected by both stiffness and Ajuba downregulation.

In this chapter, our study was built around an RNA sequencing analysis following two leads. The first would be to study the effect of stiffness on the PDACA CRISPR EV cell line through analysis of transcription factor activity and modified biological processes (BP). The second will be to study how the downregulation of Ajuba triggers the modifications of transcription factor activities and gene expressions according to the environmental stiffness. Finally, we will investigate genes whose RNA levels were modified by Ajuba downregulation in the PDACA CRISPR 01 cell line compared to PDACA CRISPR EV, our control cell line.

## **5.2 PDACA gene expression is deeply impacted by ECM stiffnesses.**

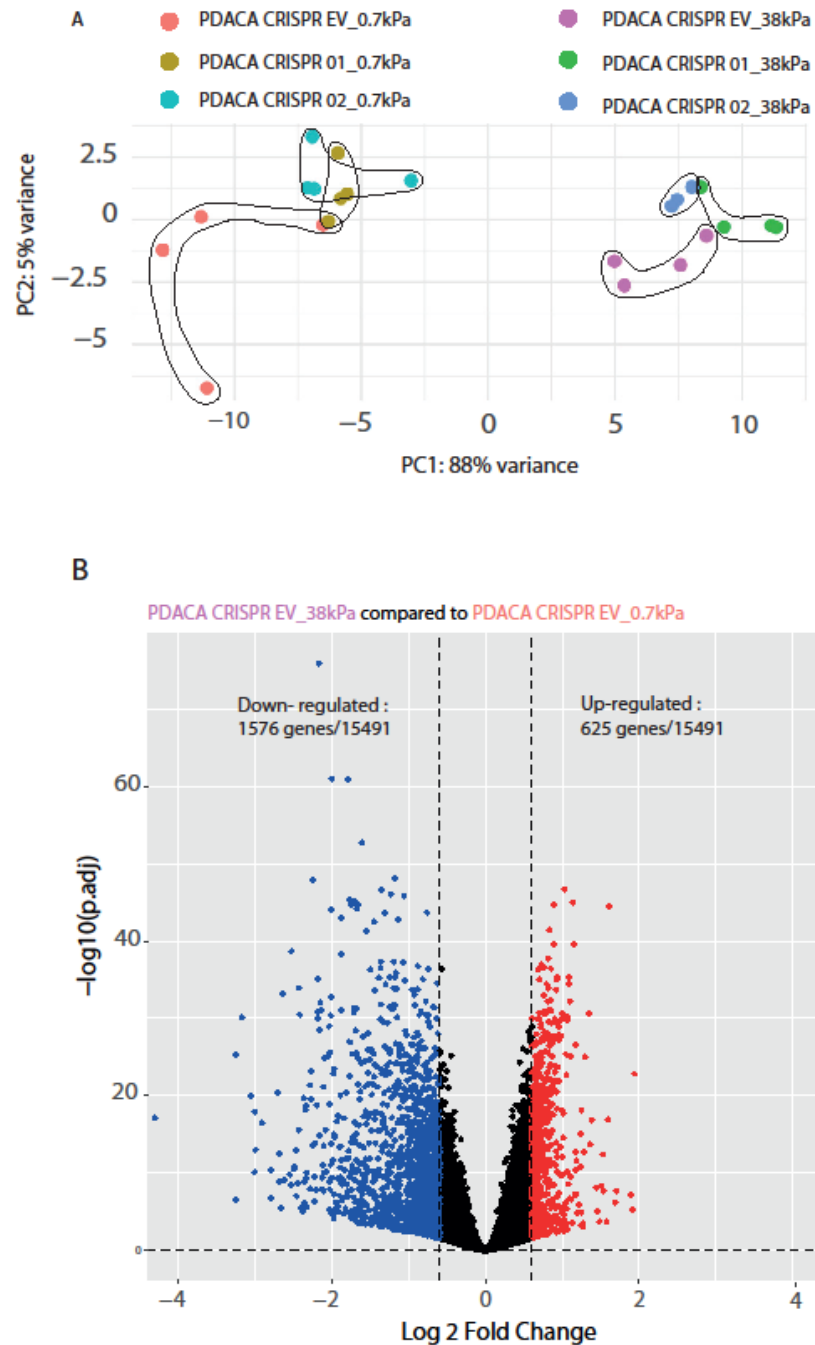
In this final chapter, we will first investigate the effect of stiffness on gene expression. Then, we will investigate the role of Ajuba as a co-activator and co-repressor of transcription factor activities and its impact on gene expression at the RNA level. To do so PDACA CRISPR EV, PDACA CRISPR 01 and PDACA CRISPR 02 cells were cultured overnight on fibronectin-coated polyacrylamide hydrogels of 0.7 kPa and 38 kPa. Four biological replicates of each conditions were prepared, RNA extractions were performed to isolate the RNA in each replicate, to be analysed by RNA sequencing. The cDNA libraries were prepared by the Scotland Institute Molecular technology services, while the Scotland Institute Bioinformatic department analysed RNA seq read alignments, produced PCA plot and performed the Deseq2 and GSEA analysis.



We first asked how each sample would be related to one another, if similar stiffness conditions were clustered. Then we asked whether the biological replicates would cluster representing intra-sample reproducibility. To answer these questions, the principal component analysis (PCA) was used to monitor sample variance and clustering in Figure 5-1-A, among biological replicates. The Beaton bioinformatics department performed the PCA gene selection and the PCA measurements which resulted in the creation of the PCA plot. The PCA plot represents the effect of stiffness (PC1) versus the effect of the downregulation of Ajuba (PC2). Through the analysis of this plot, we can observe two different clusterings: a clustering among stiffness and a clustering among biological replicates.

The effect of the environmental stiffness accounts for the majority of the difference between the samples, with PC1 being responsible for 88% of sample variations. It translates into a shift between 0.7 kPa samples, clustered on the left-hand side of the PCA plot, while 38 kPa samples are clustered on the right-hand side (Figure 5-1-A). However, PC2, reflecting the effect of the downregulation of Ajuba, shows only a 5% variance, which illustrates a weak effect of Ajuba downregulation and doesn't allow a separate clustering between PDACA CRISPR samples and Ajuba downregulated cell lines (PDACA CRISPR 01 and PDACA CRISPR 02). A clustering among sample replicates is a necessity to prove good intra-sample reproducibility. We observed a slight scattering in one replicate of PDACA CRISPR EV 0.7 kPa while the other three replicates of PDACA CRISPR EV 0.7 kPa were clustered (Figure 5-1-A). Both PDACA CRISPR 01 and 02 cell lines are clustering among their respective stiffnesses, with relative proximity to their PDACA CRISPR EV counterparts (0.7 kPa on the left while 38 kPa were on the right side of the PCA plot) (Figure 5-1-A). To assess how much the environmental stiffness impacts the gene expression at RNA level, the RNA expression of PDACA CRISPR EV cells was compared after culture on 0.7 kPa versus 38 kPa polyacrylamide hydrogels (Figure 5-1-B). The differential gene expressions were refined by p-value ( $<0.05$ ), isolating significant genes, as an RNA sequencing differential gene pool. The refined pool of differential genes was subsequently divided into two subsets, genes downregulated ( $\log_2\text{FoldChange} \leq -0.6$ ) and

genes upregulated ( $\log_2\text{FoldChange} \geq 0.6$ ) in R studio. By overlapping the RNA sequencing differential gene pool (black) with upregulated (Red) and downregulated (blue) genes, it brings to light how much gene expressions were impacted by stiffness (Figure 5-1-B). Out of 15491 genes, 2201 gene expression levels were significantly changed, 1576 of whom were downregulated and 625 were upregulated (Figure 5-1-B).



**Figure 5-1: PAAM stiffnesses have a strong effect on PDACA RNA gene expression.**

A: PCA plot, created by Ryan Kwan, representing the PC variation, post batch removal, of RNA sequencing samples coloured by condition. PC1 reflects stiffness effect, PC2 reflects the effect of the downregulation of Ajuba

B: Representation via volcano plot of PDACA RNA gene expression of PDACA CRISPR EV 38 kPa (treatment) vs PDACA CRISPR EV 0.7 kPa (control). The Log<sub>2</sub> fold change indicates the mean RNA expression level of each gene, represented by a dot. Blues dots represent downregulated genes, red dots represent upregulated genes, and black dots represent non-significant genes.

### **5.3 Overview of pathways, functions, and transcription factors through G: Profiler analysis, in PDACA cell line.**

#### **5.3.1 Transcription factor activities are modified according to stiffness in PDACA CRISPR EV**

Transcription factors (TF) are proteins controlling the transcription of genes, from DNA to mRNA, by their ability to bind to gene promoters, using specific binding motifs. I investigated which transcription factor activities were modified when culturing cells on either 0.7 kPa or 38 kPa. G: Profiler offers a pipeline which recognises regulatory motifs of transcription factors (using the TRANSFAC database) and identifies transcription factor activities through the analysis of a user-provided gene list. Through G: Profiler, an important number of transcription factors were found either upregulated (16) or downregulated (37) on 38 kPa compared to their levels on 0.7 kPa (Figure 5-2). I regrouped these transcription factors into their respective families to determine if some of them were particularly represented. The activities of the following transcriptions factors' families: E26 transformation-specific (ETS), Basic helix-loop-helix (bHLH) and (Suppressor of Mothers against Decapentaplegic (SMAD), were found significantly modified in the PDACA CRISPR EV 38 kPa condition, compared to 0.7 kPa (Figure 5-2).

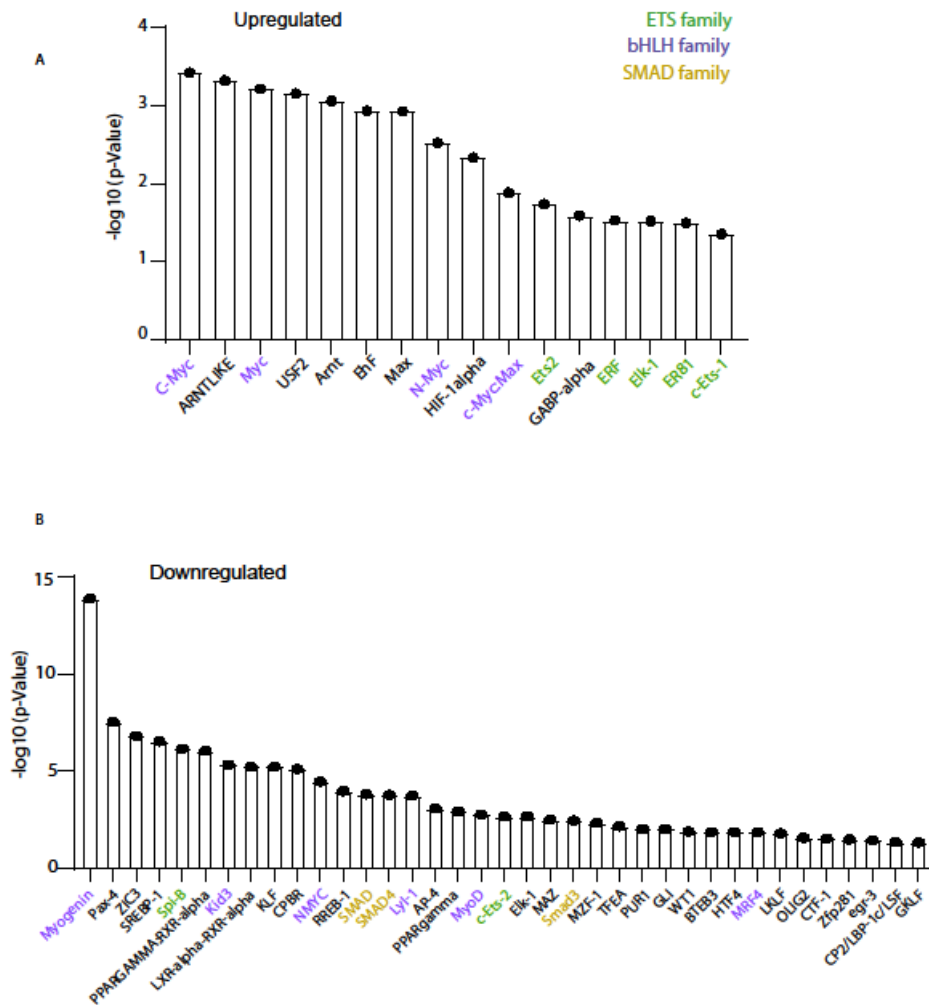
-ETS family: ETS is a superfamily of transcription factors involved in differentiation, proliferation, metastasis, invasion as well as tissue remodelling (Kar & Gutierrez-Hartmann, 2013). Coloured in green, the members C-ets-1, Ets2, ERF, ER81, and Elk-1 were found upregulated (Figure 5-2-A) while C-ets-2, and Spi-B were found downregulated (Figure 5-2-B) on PDACA CRISPR EV 38 kPa condition, compared to PDACA CRISPR EV 0.7 kPa.

-bHLH family: This superfamily is essential for organisms to respond to environmental cues such as nutriment availability or hypoxia (Skinner et al., 2010). Within this superfamily, the expression of the MYC family is controlled by growth-promoting signalling pathways, linked to stimulus from the cell and its

surroundings, and acts to maintain cell fate, growth and gene expression to align with both environmental and cellular cues (Carroll et al., 2018; Farrell & Sears, 2014). MYC is highly involved in cancer progression, for promoting growth and proliferation (Chi, 2012). Coloured in purple, Myogenin, myogenic differentiation 1 (MyoD), myogenic regulatory factor 4 (MRF4), LYL1 Basic Helix-Loop-Helix Family Member (Lyl-1), Zinc Finger Protein 354C (Kid3) and N-MYC, members of this large superfamily of transcriptional factors, were found significantly downregulated on PDACA CRISPR EV under 38 kPa condition, compared to 0.7 kPa. In contrast, C-MYC, N-MYC, and c-Myc: Max, are also members of this family, were found upregulated under the same conditions (Figure 5-2-B).

-SMAD family: SMAD lies in the TGF  $\beta$  pathway, where TGF  $\beta$  membrane receptors directly activate SMAD proteins, which in turn will target and control the activation of specific genes. SMAD2/3 proteins are also ligands of YAP/TAZ, to drive TGF  $\beta$  sensitive genes (Leask & Abraham, 2004). SMAD3 is a direct TGF  $\beta$  pathway substrate, alongside four other SMADs, forming a group called RSmads. SMAD4 serves as a partner of all RSmads. Coloured in orange, Two SMADs, SMAD 3 and SMAD 4, were found downregulated in the PDACA CRISPR EV 38 kPa condition compared to PDACA CRISPR EV 0.7 kPa.

In conclusion, multiple families of transcription factor activities were modified in response to stiffness by PDAC cells. Transcription factors activities play a crucial role in many biological processes such as cell proliferation, metabolism and apoptosis (Cheng et al., 2007).



**Figure 5-2: PAAM stiffnesses have a strong effect on the transcription factors activities in PDACA CRISPR EV.**

Representation of transcription factors (TF) activity induced by PDACA CRISPR EV cultured on 38 kPa versus cultured on 0.7 kPa, analysed through G: Profiler and plotted along their  $-\log_{10}$  (p-value).

A: Upregulated TF on 38 kPa compared to 0.7 kPa, in response to stiffness.

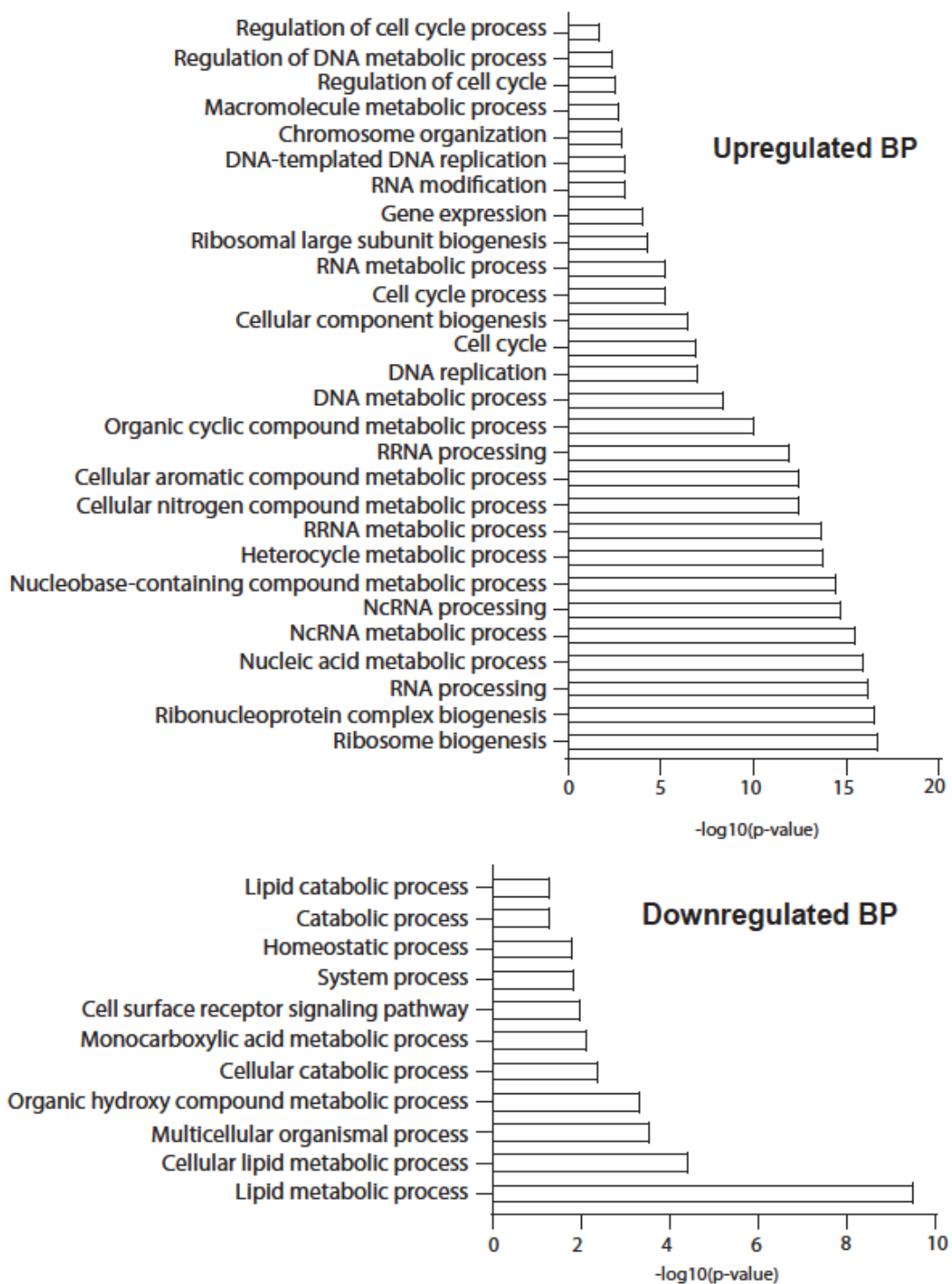
B: Downregulated TF on 38 kPa compared to 0.7 kPa in response to stiffness.

### 5.3.2 Biological process varies according to stiffnesses in PDACA cell line.

In the previous section highlighted different transcription families whose activities are stiffness-dependent. We next asked whether biological processes were impacted by stiffness from the RNA expression of PDACA CRISPR EV in 0.7 kPa versus 38 kPa conditions. The term biological process refers to the gene ontology (GO) classification of biological programs. To answer this question, G:Profiler analysis combined with Gene set enrichment analysis (GSEA), was realised by Ryan Kwan, a member of the Scotland Institute bioinformatic team, to highlight which biological processes were modified according to stiffness. G:Profiler is a free-to-use bioinformatic tool designed to handle and characterise gene lists, available at <https://biit.cs.ut.ee/gprofiler/gost>. Within G:Profiler, g:GOST performs statistical enrichment analysis to provide through functional evidence, diverse functional interpretations for the RNA signatures observed within the gene list provided. These interpretations will detail a wide range of gene ontology such as molecular function, biological process, cellular component and regulatory motifs of transcription factors. In this section, the biological process interpretations generated by G:Profiler will be the main point of interest to understand which BP were modified according to stiffness in PDACA CRISPR EV cells. The G:Profiler analysis identified 28 upregulated BP (Figure 5-3 Top) and 11 downregulated ones (Figure 5-3-Bottom) in PDACA CRISPR EV cells cultured on 38 kPa versus 0.7 kPa conditions (Figure 5-3). Due to redundancies in pathway's names, we regrouped the upregulated biological processes into categories: (1) Cell cycle and its regulation. (2): Chromosome organisation, DNA replication and RNA processing including Ribosome biogenesis and nucleic acid metabolic processes. (3) Metabolic processes including Cellular nitrogen and aromatic compound metabolic process. Whereas 11 BP were downregulated on 38 kPa compared to 0.7 kPa (Figure 5-3 - Bottom), which we regrouped into the following three categories: (4): Lipid metabolism processes. (5): Homeostatic process. (6): Cell surface receptor signalling pathway.

Additionally, a different analysis using the Gene Set Enrichment Analysis (GSEA) (<https://www.gsea-msigdb.org/gsea/index.jsp>) was performed by Ryan Kwan to validate and compare the pathways obtained from the G:Profiler analysis. GSEA analysis uses the differential gene expressions in a threshold-free manner. The three upregulated BP (1, 2, 3), identified previously by G:Profiler, were confirmed by the GSEA results. While only the lipid metabolism processes (4) were consistently highlighted as downregulated biological processes in both GSEA and G:Profiler results. To illustrate the drastic differences in gene signatures linked to these biological processes, two processes commonly identified in both G:Profiler and GSEA analysis, using gene signatures from PDACA CRISPR EV cells cultured on 38 kPa, compared to their 0.7 kPa counterpart were selected and illustrated in Figure 5-4: DNA templated DNA replication (upregulated on 38 kPa) (Figure 5-4-A) and Fatty acid metabolic process (downregulated on 38 kPa) Figure 5-4-B). For both heatmaps on the left side are PDACA CRISPR EV 0.7 kPa replicates while on the right are their 38 kPa counterparts. Using these heatmaps we can observe strong and clear gene signatures, colour-coded as blue (downregulated) and red (upregulated). Interestingly, the GSEA analysis identified additional BP within the lipid metabolism category, including fatty acid metabolism, HEME metabolism, sphingolipid metabolism, and steroid metabolism, all of which were downregulated in 38 kPa. In this subsection, we have put forward how a change in stiffness can modify biological processes which include a wide range of cellular functions like metabolism, cell cycle and proliferation activities.

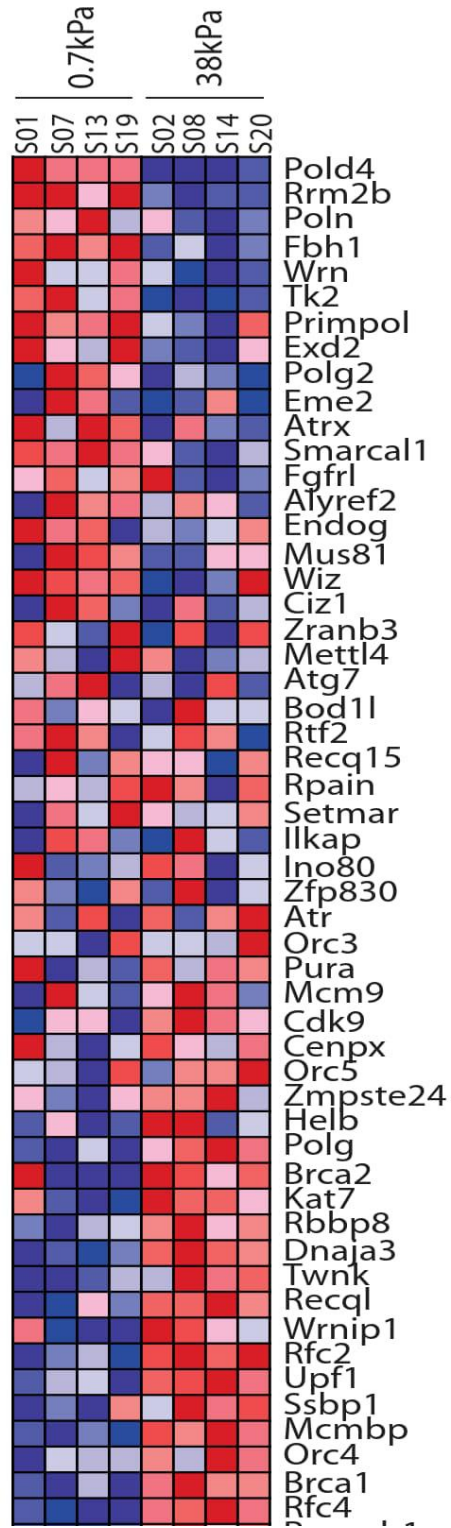


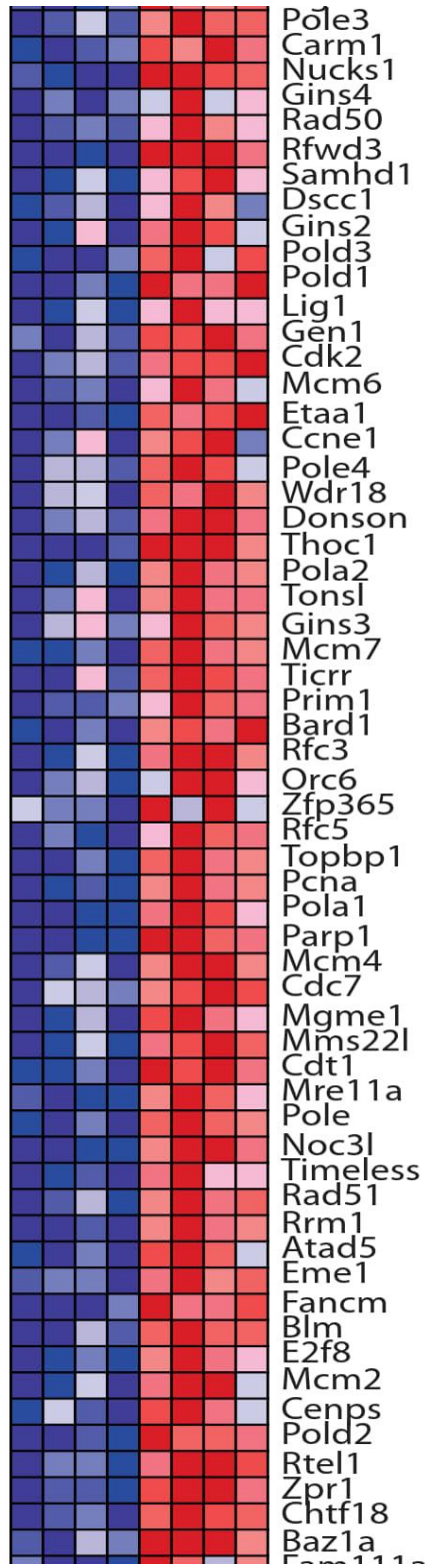


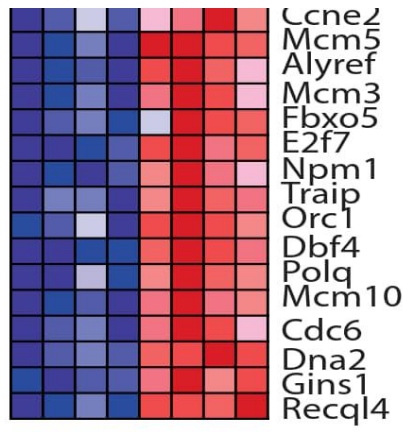
**Figure 5-3: PAAM stiffnesses can influence biological processes in PDACA CRISPR EV.**

Representation of PDACA CRISPR EV biological process (GO annotation) on 38 kPa versus cultured on 0.7 kPa PAAM hydrogels, analysed through G: Profiler and plotted along their  $-\log_{10}(\text{p-value})$ .

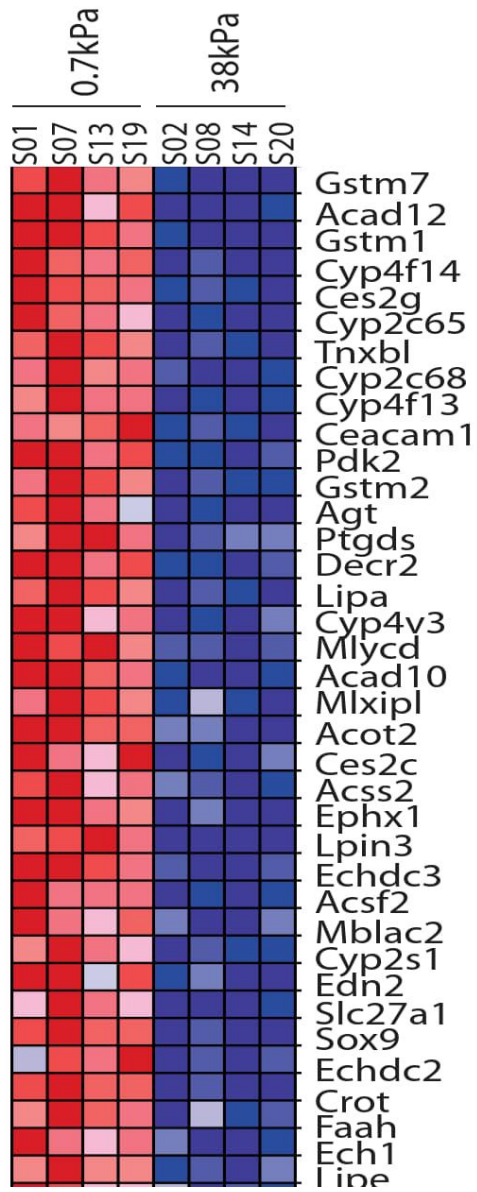
A







B

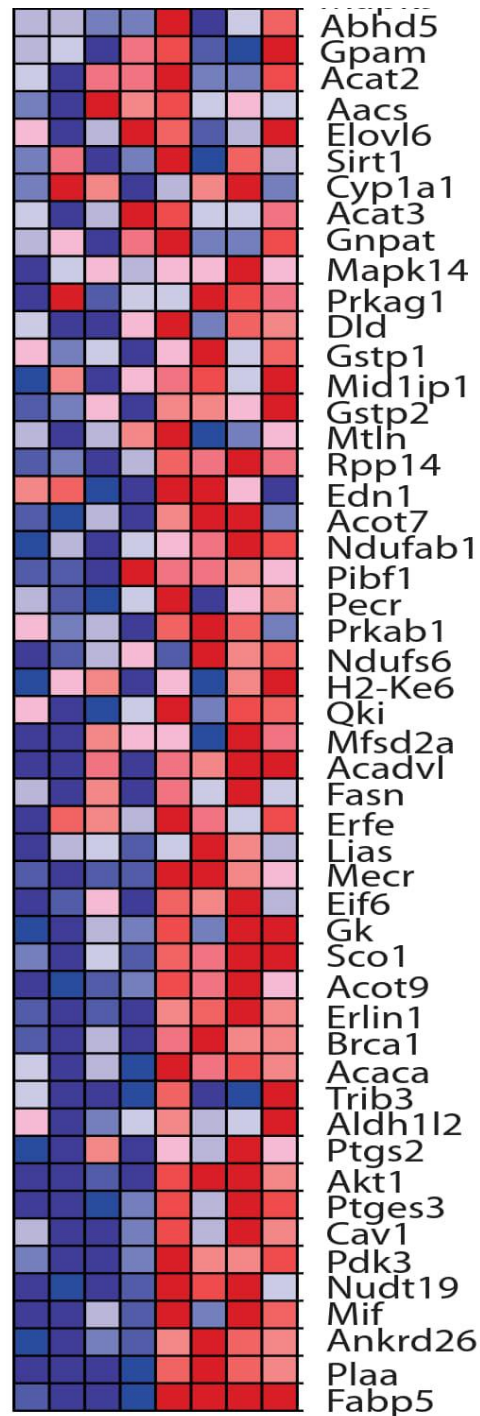












**Figure 5-4: PAAM stiffness strongly impacts biological processes of DNA templated DNA replication and fatty acid metabolic process in PDACA CRISPR EV.**

GSEA results represented via heatmaps of the following two biological processes: DNA templated DNA replication and fatty acid metabolic process. Example of heatmaps comparing PDACA CRISPR EV 38 kPa gene expression versus 0.7 kPa. These heatmaps, created by the GSEA analysis, are colour-coded, red will represent upregulation while blue represents downregulation.

A: Heatmap representing the GSEA results for DNA templated DNA replication

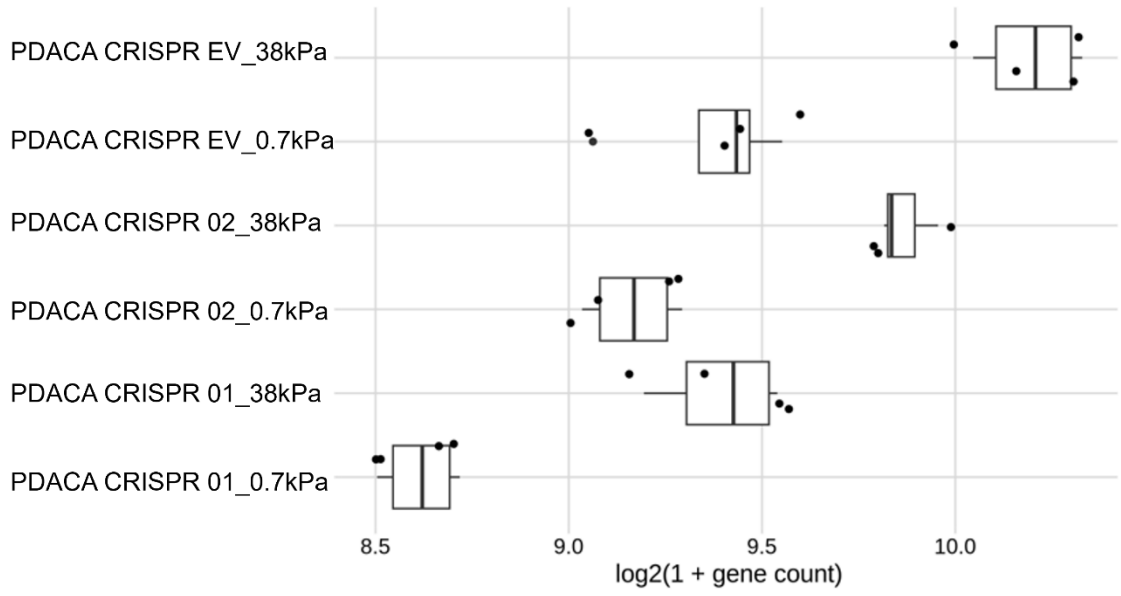
B: Heatmap representing the GSEA results for fatty acid metabolic process.



## **5.4 Ajuba downregulation impacts both transcription factor activities and gene expression at RNA levels**

### **5.4.1 Validation of Ajuba downregulation in PDACA CRISPR 01 and 02 at RNA levels**

In the RNA sequencing experiment, three PDACA CRISPR cell lines were tested: PDACA CRISPR 01, and PDACA CRISPR 02, alongside PDACA CRISPR EV as a control cell line. To validate the downregulation of Ajuba at RNA level ahead of the RNA sequencing analysis, its expression was measured in PDACA CRISPR EV, PDACA CRISPR 01 and PDACA CRISPR 02 cells (Figure 5-5). Through comparison between PDACA CRISPR EV Ajuba RNA levels ( $\log_2 1 + \text{gene counts}$ ) against PDACA CRISPR 01 and PDACA CRISPR 02 cell lines, we observe a decrease in Ajuba gene counts, on similar stiffness. However, we observed that PDACA CRISPR 01 and PDACA CRISPR 02 cell lines still showed some RNA expression of Ajuba on 0.7 kPa and 38 kPa conditions (Figure 5-5). This might be due to the cells being a mixed population, with some cells expressing Ajuba and some being true knockouts or, to a low level of expression in all cells. A low level of expression of Ajuba mRNA in our CRISPR cells might result from there being a gene duplication in our PDACA cell line, so some or all cells could have more than one Ajuba locus resulting in incomplete CRISPR. One noticeable trait of PDACA CRISPR 01 cell line, is a significantly lower Ajuba RNA expression compared to PDACA CRISPR 02 cell line (Figure 5-5). This lower expression stays consistent throughout all stiffnesses tested. Due to this observation, our attention will be only directed toward the differential RNA expression between PDACA CRISPR EV and PDACA CRISPR 01. I next analysed how the expression of Ajuba correlated with the environment stiffness. We observed a drastic decrease in the RNA expression of Ajuba when stiffness shifted from 38 kPa to 0.7 kPa, in all three tested cell lines (Figure 5-5). This decrease is consistent and validates the effect of stiffness on the expression of Ajuba at RNA levels. In this subsection, we have shown that PDACA CRISPR 01 and PDACA CRISPR 02 cell lines have a decrease in Ajuba expression and due to a lower Ajuba expression in PDACA CRISPR 01, this cell line will be used throughout this chapter to explore the effect of Ajuba downregulation at RNA levels.



**Figure 5-5: The RNA expression of Ajuba is impacted by PAAM hydrogel stiffnesses.**

Quantification of Ajuba’s RNA gene expression level on PDACA CRISPR EV, PDACA CRISPR 01, PDACA CRISPR 02 cell lines and tested stiffness, in RNA sequencing samples, created by Ryan Kwan. The expression of Ajuba was tracked according to its  $\log_2(1 + \text{gene count})$ . Each point represents a biological replicate. N=4.

## 5.4.2 Ajuba downregulation modifies transcription factor activities in a stiffness-dependant manner

In 5.3 , we showed multiple transcription factor families whose activities seem to particularly be impacted by stiffness. The literature on Ajuba places a clear emphasis on its role as a transcriptional co-regulator (Ayyanathan et al., 2007; Fan et al., 2015; Hou et al., 2008; Zhang et al., 2019). In this subsection, we will be investigating changes triggered by the downregulation of Ajuba in the PDACA CRISPR 01 cell line. Using G:Profiler results which contains the analysis of the regulatory motifs of transcription factors, similarly as in 5.3 , I investigated which transcription factor activity was modified between PDACA CRISPR 01 cell lines cultured on 38 kPa versus PDACA CRISPR 01 cell lines cultured on 0.7 kPa PAAM hydrogels. We observed 26 downregulated and 7 upregulated transcription factors (Figure 5-6). Through comparison between results from PDACA CRISPR EV (Figure 5-2) and PDACA CRISPR 01 (Figure 5-6), we can detect multiple differences (Table 5-1). Some transcription factors were modified similarly between the two cell lines while others had their activities modified. Both similarities and differences were regrouped in Table 5-1.

- Members of the ETS family of transfection factors highlighted in 5.3 , C-ets-1, Ets2, ERF, ER81, Elk-1 and C-ets-2 were absent from PDACA CRISPR 01. Only one member of The ETS family remains listed, Spi-B, present in both PDACA CRISPR EV and PDACA CRISPR 01. Interestingly, two transcription factors of the ETS family were only listed in PDACA CRISPR 01 results, PU.1 and Elf-1.

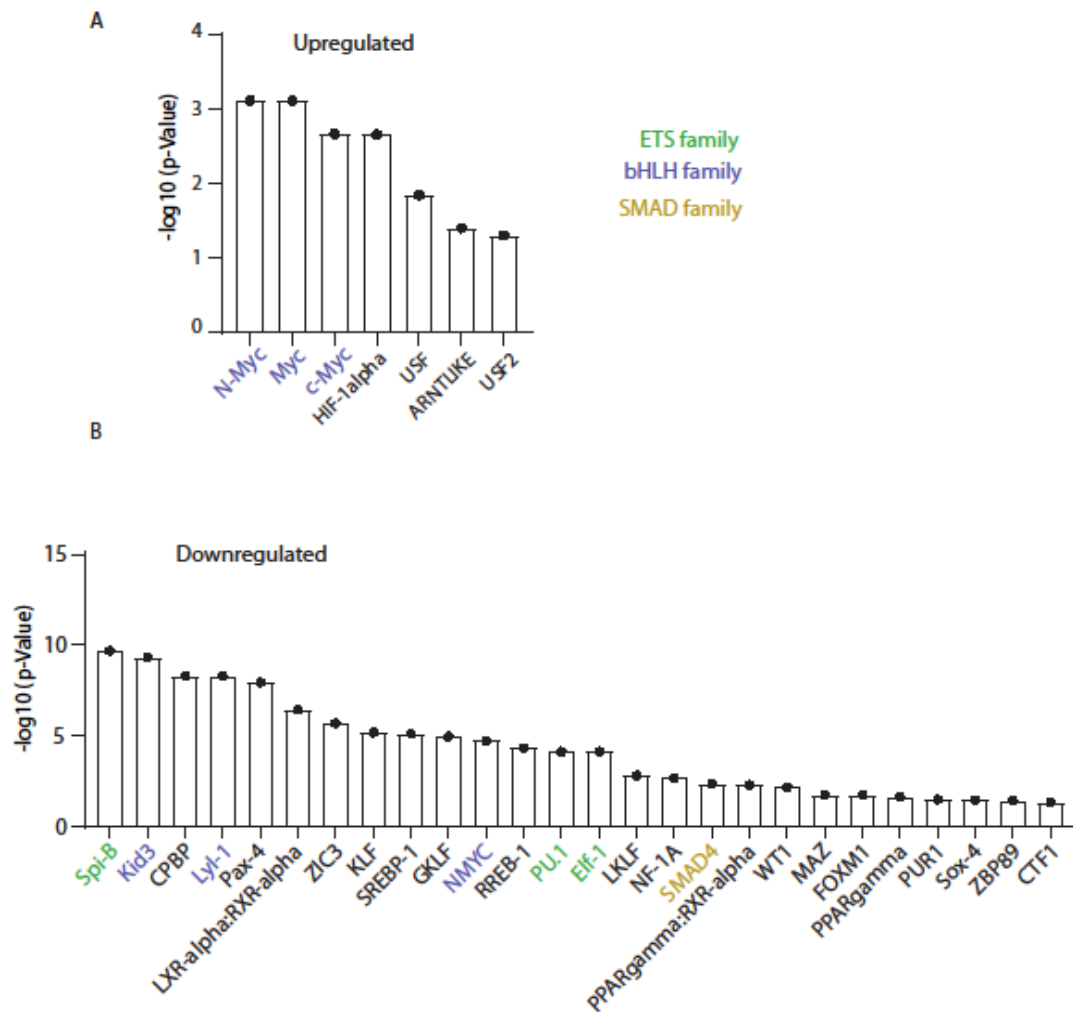
- Three out of nine previously cited members of the bHLH family, Myogenin, MyoD and MRF4, were absent from PDACA CRISPR 01 results, compared to PDACA CRISPR EV.

- Additionally, one member of the SMAD family was also absent, SMAD3.

In this sub-section, we have compared the modification of transcription factor activities between 38 kPa and 0.7 kPa in PDACA CRISPR EV versus PDACA CRISPR 01. The results attest of an effect of the downregulation of Ajuba on transcription factor activities.

Following the differences in the transcription factors activities observed in Figure 5-6 and Table 5-1, between PDACA CRISPR EV cells and PDACA CRISPR 01 cells, I asked whether the transcription factor activities were mainly modified at a specific stiffness or were these modifications of TF activities solely due to the downregulation of Ajuba in PDACA CRISPR 01 cell line? Additionally, can we observe a trend (upregulated/downregulated) related to transcription factor activities? To answer these questions, comparisons of transcription factor activities were made between PDACA CRISPR EV and PDACA CRISPR 01 cell lines at similar stiffness (Figure 5-7). First of all, regarding the comparisons between PDACA CRISPR EV and PDACA CRISPR 01 at 0.7 kPa and 38 kPa, no transcription factor activities were found upregulated compared to PDACA CRISPR EV. However, 15 transcription factor activities were downregulated on 38 kPa, compared to only 4 in 0.7 kPa (Figure 5-7). Within the ETS family, one member was downregulated in 0.7 kPa while in 38 kPa condition, many members of this family were downregulated (Figure 5-7). In the bHLH transcription factor family the downregulation of myogenin, kid3, and Lyl-1 was observed in 38 kPa. Whereas, within the SMAD family the downregulation of both SMAD2 and SMAD3 was observed in 38 kPa (Figure 5-7).

Briefly, in this section, we highlighted how the downregulation of Ajuba triggers changes in transcription factor activities which are greater on the 38 kPa conditions than on 0.7 kPa (Figure 5-7). Following the significant changes observed in transcription factor activities in both PDACA CRISPR EV and PDACA CRISPR 01, the next sub-section will focus on differential gene expression across all tested cell lines and stiffness conditions.



**Figure 5-6: PAAM hydrogel stiffness impacts the transcription activities in PDACACRISPR 01 cultured on 38 kPa versus PDACA CRISPR 01 cultured on 0.7 kPa.**

Representation of transcription factors (TF) activity induced by PDACA CRISPR 01 cultured on 38 kPa versus PDACA CRISPR 01 cultured on 0.7 kPa, analysed through g: Profiler analysis.

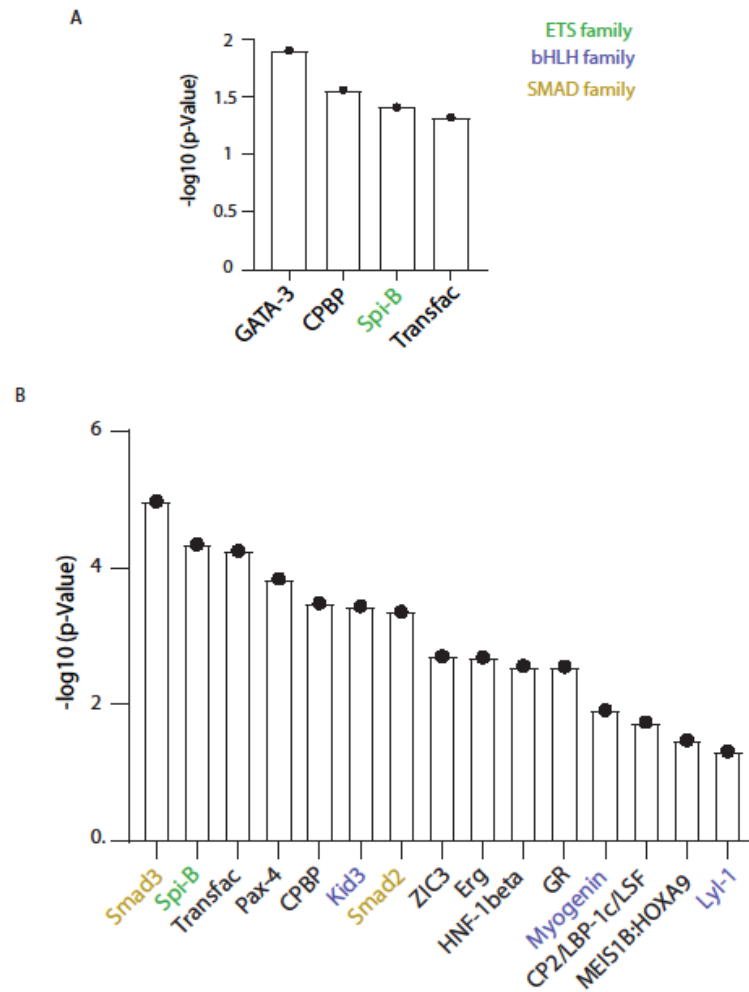
A: Upregulated transcription factors on 38 kPa compared to 0.7 kPa, in response to stiffness

B: Downregulated transcription factors on 38 kPa compared to 0.7 kPa in response to stiffness.

**Table 5-1: The transcription factors activities of PDACA CRISPR EV and PDACA CRISPR 01 shows several differences.**

Representation of the differential transcription factor activities obtained by comparison of transcription factor activities of PDACA CRISPR 01 38 kPa versus PDACA CRISPR 01 0.7 kPa, and PDACA CRISPR EV 38 kPa versus PDACA CRISPR EV 0.7 kPa. Highlighted in bold are the transcription factors that belong to the three most impacted transcription factor families previously described.

	Common between PDACA CRISPR EV and PDACA CRISPR 01	Unique of PDACA CRISPR EV	Unique of PDACA CRISPR 01
Downregulated	<b>Spi-B</b>	<b>Myogenin</b>	<b>PU.1</b>
	<b>Kid3</b>	<b>MyoD</b>	<b>Elf-1</b>
	CPBP	<b>c-Ets-2</b>	NF-1A
	<b>Lyl-1</b>	<b>Elk-1</b>	FOXM1
	Pax-4	<b>Smad3</b>	ZBP89
	LXR-alpha:RXR-alpha	MZF-1	Sox-4
	ZIC3	TFEA	
	KLF	GLI	
	SREBP-1	BTEB3	
	GKLF	HTF4	
	<b>NMYC</b>	<b>MRF4</b>	
	RREB-1	Zfp281	
	<b>SMAD4</b>	egr-3	
	PPARgamma:RXR-alpha	CP2/LBP-1c/LS	
	WT1		
	MAZ		
	PPARgamma		
	PUR1		
CTF1			
	Common between PDACA CRISPR EV and PDACA CRISPR 01	Unique of PDACA CRISPR EV	Unique of PDACA CRISPR 01
Upregulated	<b>N-Myc</b>	Arnt	
	<b>Myc</b>	Ehf	
	<b>c-Myc</b>	Max	
	HIF-1alpha	<b>Elk-1</b>	
	USF	<b>c-MycMax</b>	
	ARNTLIKE	<b>Ets2</b>	
	USF2	GABP-alpha	
		<b>ERF</b>	
		<b>ER81</b>	
	<b>c-Ets-1</b>		



**Figure 5-7: The downregulation of Ajuba in PDACA CRISPR 01 cells modifies transcription factors activities.**

Representation of the transcription factor activities between PDACA CRISPR EV and PDACA CRISPR 01 on similar stiffnesses. No transcription factors were found upregulated in 0.7 kPa nor 38 kPa conditions.

A: Downregulated transcription factors on 0.7 kPa PAAM hydrogels.

B: Downregulated transcription factors on 38 kPa PAAM hydrogels.

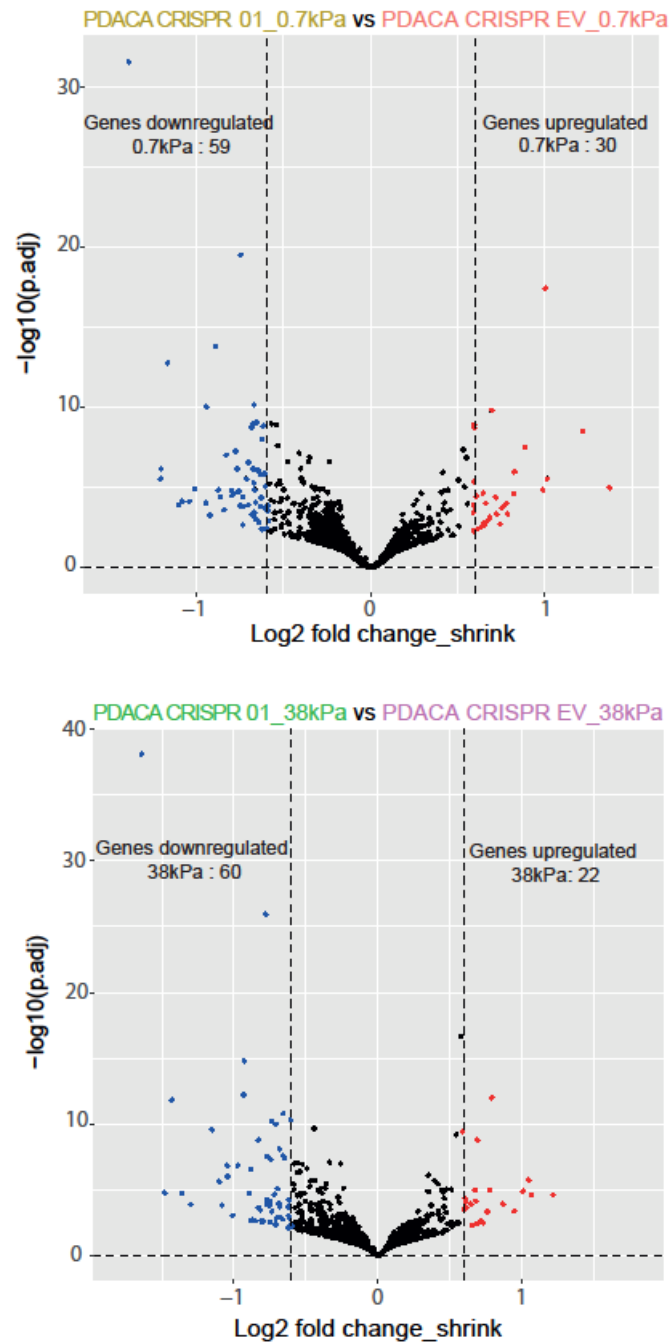
### 5.4.3 Ajuba downregulation modifies gene expression in a stiffness-dependant manner in PDACA

In the previous sections were discussed the effect of stiffness on RNA expression in PDACA CRISPR EV, the modification of transcription factors activities and the upregulation or downregulation of biological processes. We then discussed the effect of the downregulation of Ajuba in transcription factors activities.

In this section we will explore the impact of the downregulation of Ajuba in PDACA CRISPR 01 and PDACA CRISPR 02 cell lines on RNA expression. To isolate the effect of the downregulation of Ajuba, I will first compare the gene expression on similar stiffnesses. Differential genes were divided into two groups: downregulated ( $\log_2\text{FoldChange\_shrink} \leq 0.6$ ) in blue and upregulated ( $\log_2\text{FoldChange\_shrink} \geq 0.6$ ) in red, both with p-adjusted value  $< 0.05$ . Volcano plots in Figure 5-8 represent each stiffness-based comparison between PDACA CRISPR EV and PDACA CRISPR 01 cell lines. Whereas in Figure 5-9, we compared gene expression of PDACA CRISPR 02 versus PDACA CRISPR EV cell lines.

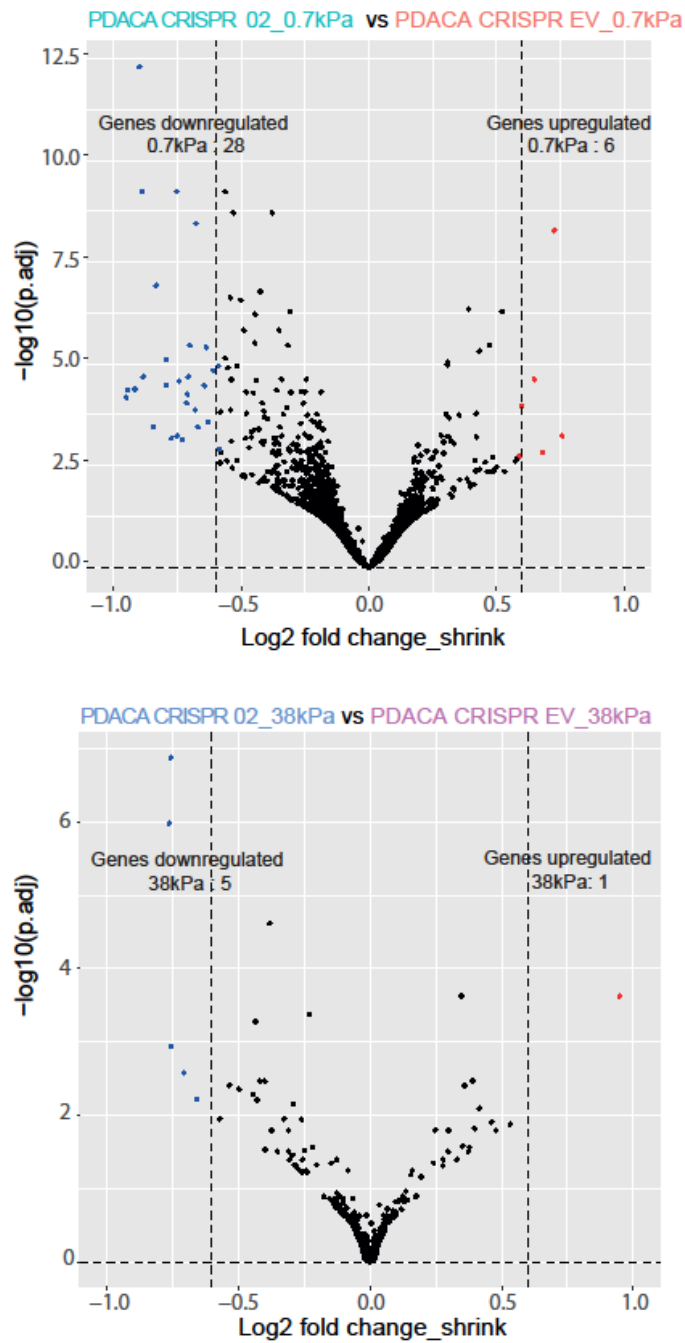
Focussing primarily on PDACA CRISPR 01 vs PDACA CRISPR EV, it is interesting to notice that on 0.7 kPa conditions (Figure 5-8-top panel), the downregulation of Ajuba triggered the downregulation of 59 genes and the upregulation of 30 genes. Interestingly, the same comparison on 38 kPa (Figure 5-8-bottom panel), shows a vast majority of genes downregulated (60), rather than upregulated (22). As previously described, PDACA CRISPR 02 shows more expression of Ajuba mRNA after CRISPR deletion than PDACA CRISPR 01. This is recapitulated by a smaller number of genes impacted on each stiffnesses tested (Figure 5-9).





**Figure 5-8:** The downregulation of Ajuba modifies the RNA expression of several genes in PDACA CRISPR 01 cells compared to PDACA CRISPR EV cells.

Volcano plot representation of PDACA CRISPR 01 versus PDACA CRISPR EV RNA gene expression on 0.7 kPa stiffness (Top panel) and 38 kPa stiffness (bottom panel), plotted with their Log<sub>2</sub>-fold change\_shrink versus -log<sub>10</sub>(p.adj). Differential gene expressions were threshold using the -log<sub>10</sub>(p.adj) >0.05 & Log<sub>2</sub> fold change\_shrink <0.6>. The Log<sub>2</sub> fold change indicates the mean RNA expression level of each gene. Blues dots represent downregulated genes, red dots represent upregulated genes, and black dots represent non - significant genes.



**Figure 5-9:** The downregulation of Ajuba modify the RNA expression of few genes in PDACA CRISPR 02 cells compared to PDACA CRISPR EV cells.

Representation of the gene expression of PDACA CRISPR 02 versus PDACA CRISPR EV on 0.7 kPa stiffness (Top panel) and 38 kPa stiffness (bottom panel) using a volcano plot. These volcano plots represent gene's  $\text{Log}_2$ -fold change\_shrink versus their  $-\log_{10}(\text{p.adj})$ . Differential gene expression were threshold using  $-\log_{10}(\text{p.adj}) > 0.05$  and  $\text{Log}_2 \text{ fold change\_shrink} < 0.6 >$ . The  $\text{Log}_2 \text{ fold change\_shrink}$  represents the mean RNA expression level of each gene with blues dots for downregulated genes, red dots for upregulated genes, and black dots represent non -significant genes.

#### **5.4.4 Distinguishing the effects of the downregulation of Ajuba and the effect of environmental stiffness on gene expression at RNA Levels.**

We showed in the previous section that Ajuba downregulation induces the downregulation and upregulation of several genes. In this subsection, we aim to investigate whether the genes affected by Ajuba downregulation are consistent across different environmental stiffnesses or if they vary depending on stiffness. We will define a “CRISPR-based effect” as representing the modification of RNA expression either upregulated or downregulated consistent across stiffness and therefore these changes were not triggered by stiffness but are directly linked with Ajuba’s expression. In contrast, a “stiffness-based effect” would reflect the modification of the RNA expression of specific genes whose expressions are specific to an environmental stiffness. Through a comparison between PDACA CRISPR EV and PDACA CRISPR 01, 32 genes are similarly impacted in both 0.7 and 38 kPa stiffness, suggesting an effect of Ajuba downregulation on these genes (Table 5-2). We will classify these changes as CRISPR-based. On the other hand, we observed a total of 87 genes which are classified as stiffness-based. The names of each gene were regrouped in Table 5-3 and Table 5-4, alongside their Log 2-fold change.

Interestingly, it would bring a great deal of information to understand the relationship between CRISPR-based effect-genes listed in Table 5-2, and Ajuba. On the other hand, stiffness-based effect genes would need to be investigated to understand the link between their expression and stiffnesses.

**Table 5-2: List of “CRISPR-based” genes, modified in PDACA CRISPR 01 cells compared to PDACA CRISPR EV cells.**

Overview of genes modified due to a CRISPR-based effect. These genes were significantly and consistently impacted on both 0.7 kPa and 38 kPa and were separated into downregulated genes and upregulated genes.

		Downregulated		Upregulated	
		Genes names	Log 2-Fold Change	Genes names	Log 2-Fold Change
Both	<b>Cdh16</b>		-1.390171627	Ak4	1.372927258
	Stc1		-1.207130878	Dpt	1.21879446
	Spats2l		-1.167102676	Slc43a3	1.003654962
	Serpina1b		-1.103590583	Mtus2	0.826072608
	Rasgrf2		-1.041811553	Bcat1	0.823091699
	Sema6a		-1.010637458	<b>Fscn1</b>	0.755410066
	Chst8		-0.946240758	Aldh5a1	0.684674111
	Chst11		-0.944221213	Slc14a1	0.668616292
	Cd34		-0.891955405	Fgf7	0.65994892
	Igfbp5		-0.875413712	Sall1	0.608460972
	St8sia1		-0.829507682	Jag2	0.591318385
	Itga1		-0.79794873	Rps6ka6	0.591155246
	Klhdc7a		-0.796796591		
	Zic3		-0.787590077		
	Flt1		-0.765267195		
	Nebl		-0.758648044		
	Ajuba		-0.747502518		
	Fgfr2		-0.732406502		
	Tppp3		-0.702887296		
	Celsr1		-0.68583233		
	Tnfsf15		-0.681611549		
	Gstm2		-0.678329932		
	<b>Aqp1</b>		-0.674765512		
	Hsd3b2		-0.660709165		
	Sgpp2		-0.634007174		
	Akr1c19		-0.623679545		
	Inpp5j		-0.613976641		
	Slc44a3		-0.608377962		
	Ugt2b34		-0.6045347		
	Crp		-0.596892369		

**Table 5-3: List “stiffness-based” genes, modified in 0.7 kPa in PDACA CRISPR 01 cells compared to PDACA CRISPR EV cells.**

Overview of genes whose RNA expressions were modified due to a stiffness-based effect. These genes were significantly impacted on 0.7 kPa specifically and separated into downregulated genes and up-regulated genes.

		Downregulated		Upregulated	
		Genes names	Log 2-Fold Change	Genes names	Log 2-Fold Change
0.7 kPa	Fxyd3		-1.204955896	<b>Cgas</b>	1.014541243
	Sult1d1		-1.082072566	Col3a1	0.988678252
	Habp2		-0.924788021	Klhl23	0.888429845
	Bche		-0.86410014	Sh3tc2	0.786365904
	Slc1a2		-0.843050875	Cntln	0.779566257
	Kalrn		-0.777454167	Cracr2a	0.745234607
	Tcaf2		-0.747194455	Tigit	0.72508577
	Rtn4rl1		-0.735852601	Soga3	0.717717818
	Cyp2c65		-0.732993529	Fam111a	0.695660164
	Fjx1		-0.712972832	Fbxl16	0.65548471
	Anxa10		-0.701499692	Obsl1	0.650628755
	Adam23		-0.673836633	Sh3rf2	0.64604699
	Cyp2s1		-0.670591241	Epb41l3	0.63174729
	Gpd1		-0.669615948	Rcn1	0.613827813
	Btbd11		-0.66754771	Nt5dc2	0.597973636
	Mmp15		-0.667128733	Hs6st2	0.593959431
	Pla1a		-0.661779254	Pou2af3	0.590983958
	Pdxk		-0.654576195	Cth	0.590938348
	Paqr5		-0.645860606		
	Fras1		-0.642168371		
	Cdhr2		-0.631212492		
	Sdcbp2		-0.628724537		
	Tff3		-0.626722305		
	Gm14608		-0.621885736		
	Cdh6		-0.617166034		
	Spns2		-0.606333589		
	Hexa		-0.593563745		
	Faah		-0.590763682		
	Sprr2a3		-0.586160901		

**Table 5-4: List of “stiffness-based” genes, modified in 38 kPa in PDACA CRISPR 01 cells compared to PDACA CRISPR EV cells.**

These genes were significantly impacted specifically on 38 kPa and categorized into downregulated genes and up-regulated genes.

Downregulated		Upregulated	
Genes names	Log 2-Fold Change	Genes names	Log 2-Fold Change
Muc5b	-1.481139851	Tenm3	1.070632611
Dio1	-1.299864814	Dclk2	0.870957117
Ace2	-1.009464441	Zfp580	0.730585117
Anks4b	-0.930491173	Serpine2	0.715247553
Kif12	-0.892680809	Tbx3	0.690530074
Cutal	-0.880818536	Hoxd8	0.658475686
Ddc	-0.852353448	Il5ra	0.649382188
Ranbp3l	-0.829359528	Lclat1	0.610922006
Cyp4f14	-0.81494751	Ism1	0.600121709
Scara5	-0.807663374	Clstn1	0.58834757
Ambp	-0.802301004		
Evpl	-0.767640343		
Pilra	-0.754402026		
Ppp1r1b	-0.751968709		
Gprc5c	-0.717832047		
Aldob	-0.708717859		
Il18r1	-0.704370258		
Gm49980	-0.683865509		
Spon2	-0.683038902		
Arhgap28	-0.678836597		
Tff1	-0.662811044		
Pklr	-0.657504158		
Rgl1	-0.646923659		
Gjb1	-0.6206515		
Cbr1	-0.620007625		
Cemip	-0.61773793		
Pcdh10	-0.613655817		
Prkd1	-0.605535318		
Megf9	-0.604339394		
Afap1l1	-0.599958744		

## 5.5 Validation of candidates

A shortlist of genes was selected from the pool of CRISPR-based genes extracted from Figure 5-8, Table 5-2 and Table 5-3. To explain the selection process of these genes, we researched the roles of each protein and looked for common themes with the functions and roles of Ajuba within cells. Aquaporin 1(AQP1), and Cadherin 16(CDH16) were downregulated on PDACA CRISPR 01 compared to PDACA CRISPR EV whereas Fascin 1(Fscn1), and Cyclic GMP-AMP Synthase (CGAS) were upregulated.

- Cadherin 16: The cadherin family are well-known transmembrane glycoproteins mediating cell-cell adhesion, tissue cohesion and tissue architecture. Each cadherin has specific ligands and specific tissue distribution (Yu et al., 2019). Cadherin 16, a calcium-dependent cadherin, is a well-known kidney and thyroid cadherin involved in cellular differentiation, cell proliferation and invasion (Yang et al., 2022). Cadherin 16 is detected in many cancer tissues (Siraj et al., 2023), including renal cell carcinoma, follicular carcinoma, and pancreatic cancer. Due to the common adhesion theme between Ajuba and cadherin16, the strong downregulation of CDH16 drew our attention as an interesting partner to Ajuba.
- Aquaporin 1: The aquaporin family plays an important role in regulating osmotic pressure at the plasma membrane by facilitating the passive diffusion of water across the membrane. Aquaporins are integral transmembrane proteins located at the cellular membrane, forming water channels to diffuse ions, water, and soluble factors (Arsenijevic et al., 2019). It is essential for numerous physiological processes such as membrane trafficking activities. Aquaporin 1, is a small water channel, already characterised as a prognostic factor in multiple types of cancer such as colon cancer, breast cancer and melanoma. (Tomita et al., 2017). Over-expressed in many human cancers, AQP1 plays an important role in

tumour cell migration, invasion, and proliferation (Azad et al., 2021; Bruun-Sorensen et al., 2021; Conner et al., 2010; Tomita et al., 2017). The roles of aquaporin 1 in membrane rigidity, migration and invasion made aquaporin 1 an interesting candidate which could be linked to the expression of Ajuba (Tomita et al., 2017).

- Fascin-1: Fascin 1 is an actin-bundling protein, linking F-actin into actin bundles, localised in cell protrusions for cell migration purposes (Li et al., 2014). *In vitro*, Fascin increases invasiveness (Schoumacher et al., 2014). Fascin, usually not expressed in epithelial cells, gets upregulated in multiple cancers such as colorectal cancer and pancreatic cancer (Li et al., 2014; Schoumacher et al., 2014; Smith, 2014). In pancreatic cancer, fascin expression rises during early PDAC transition. Slug, a transcription factor, involved in EMT, is driving the expression of fascin in PDAC (Li et al., 2014). The important link between Fascin, invasion and PDAC development made Fascin an interesting candidate which might be linked to the role of Ajuba in pancreatic cancer and cellular mobility.
  
- Cyclic GMP-AMP Synthase (CGAS): Cytosolic DNA sensing protein, can recognise pathogen DNA and self-DNA. Well-known for its role in autoimmune disease and cancer, CGAS can be a sign of DNA damage response, cell senescence, damaged mitochondria or chromatin instability (Li & Chen, 2018). The selection of CGAS was drawn by its role in DNA damage response, which if validated by the Q-PCR experiment, would need to be investigated further to understand its link with Ajuba expression.

An overview of the RNA expression of each selected gene and their specific RNA Log 2-fold change were regrouped in Figure 5-10. A negative log 2-fold changes indicate a decrease in RNA levels, whereas positive log 2-fold changes indicate an increase in RNA levels compared to controls (Figure 5-10).

After the extraction of new sets of RNA samples from PDACA CRISPR EV and PDACA CRISPR 01 cell lines cultured on 0.7, 38 kPa and glass coverslips, the RNA



expression levels of the selected genes were tested using specific primers by Q-PCR (Figure 5-11, Figure 5-12).

We observed in Figure 5-11-A that Fascin-1 RNA expression isn't modified by stiffness nor by the downregulation of Ajuba in PDACA CRISPR EV and PDACA CRISPR 01 cell lines. These results do not recapitulate the RNA seq results, no further experimentation will be conducted regarding Fascin-1.

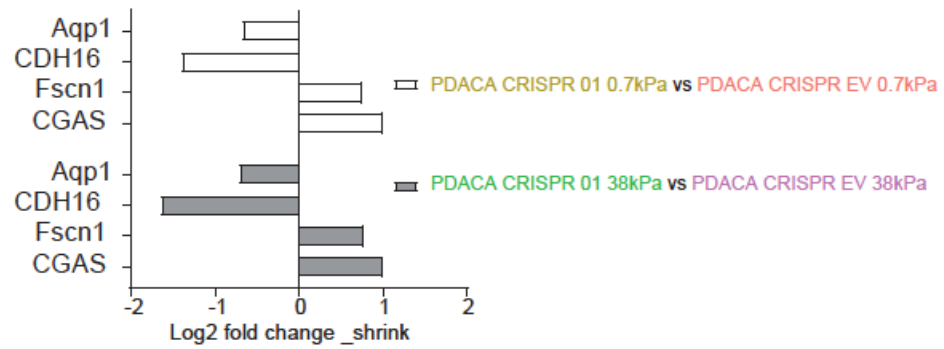
In Figure 5-11-B we observe that CGAS RNA levels on PDACA CRISPR 01 0.7 kPa decreases compared to PDACA CRISPR EV 0.7 kPa, while no modification of CGAS RNA expression was measured between PDACA CRISPR 01 38 kPa compared to PDACA CRISPR EV 38 kPa. These observations contradict the RNA expression of CGAS's from RNA sequencing results, showing an increase of expression in these conditions (Figure 5-10, Figure 5-11-B). Additionally, the RNA expression of CGAS was solely decreased in PDACA CRISPR 01 0.7 kPa compared to both 38 kPa and glass while no changes were observed among PDACA CRISPR EV conditions. No further experimentation will be conducted regarding CGAS.

The RNA expressions of AQP1 measured by qPCR are displayed in Figure 5-12-A. We observed that AQP1 RNA expression levels were decreased in PDACA CRISPR 01 0.7 kPa compared to PDACA CRISPR EV 0.7 kPa. However, the RNA expression levels of AQP1 were not significantly decreased in PDACA CRISPR 01 38 kPa compared to PDACA CRISPR EV 38 kPa. These results recapitulate the RNA seq results on 0.7 kPa conditions but doesn't on 38 kPa conditions. The downregulation of Ajuba seems to modify AQP1 RNA expression on 0.7 kPa stiffness. Additional experimentation regarding the link between the expression of Ajuba and AQP1 are necessary to uncover if Ajuba is a direct or indirect regulator of AQP1 expression. Interestingly, qPCR results highlight an important impact of stiffness over aquaporin 1 RNA level in PDACA CRISPR EV, where 0.7 kPa levels are higher than both 38 kPa and glass levels (Figure 5-12-A). On the other hand, in PDACA CRISPR 01, AQP1 RNA levels, increase significantly on 0.7 kPa compared to glass conditions. The downregulation of Ajuba seems to lessen the impact of stiffness on AQP1 RNA expression Due to the important stiffness-based expression of AQP1,

further experimentations are necessary to investigate the relationship in PDAC between AQP1 and environmental stiffness.

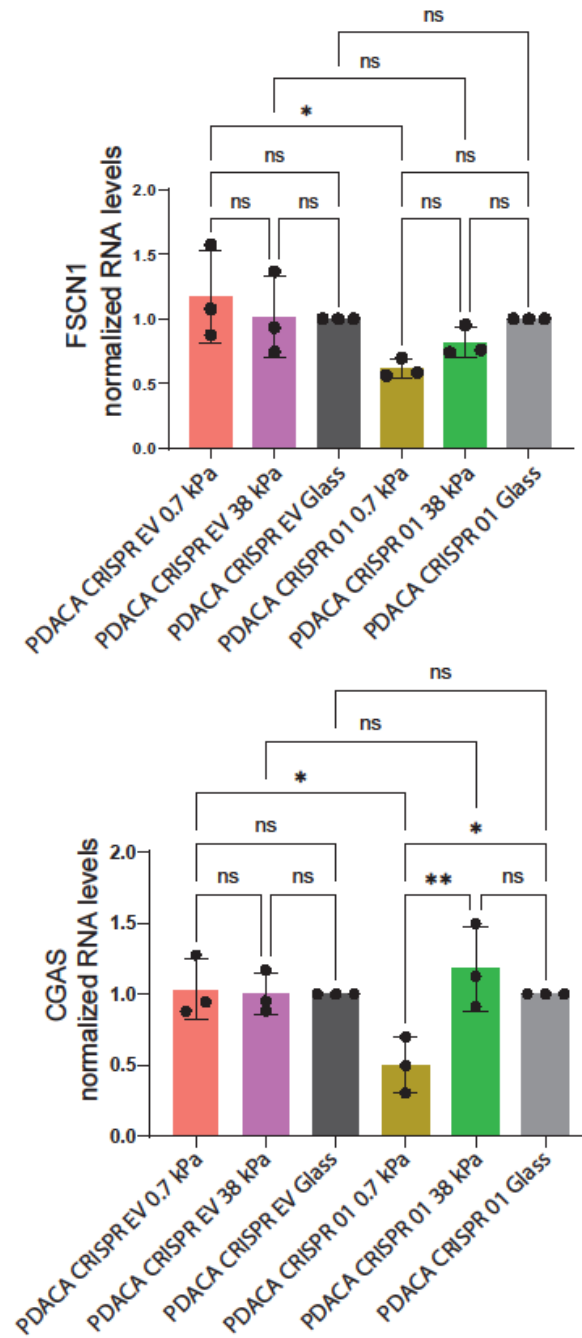
The RNA expression of Cadherin 16 was measured by qPCR and its RNA expression levels were significantly decreased in PDACA CRISPR 01 0.7 kPa compared to PDACA CRISPR EV 0.7 kPa. However, this wasn't the case in PDACA CRISPR 01 38 kPa compared to PDACA CRISPR EV 38 kPa. These results solely recapitulate the RNA seq results on 0.7 kPa conditions. As for AQP1, the downregulation of Ajuba seems to modify cadherin 16 RNA expression on 0.7 kPa stiffness. Additionally, Cadherin 16's qPCR RNA levels show an important effect of stiffness, where PDACA CRISPR EV CDH16's level decreases drastically in 38 kPa and glass conditions compared to 0.7 kPa condition. This impact is lessened by the downregulation of Ajuba in PDACA CRISPR 01. Additional experiments are necessary to investigate and validate the relationship between cadherin 16 expression and environmental stiffness in PDAC.

In this subsection, four candidates were selected (Aquaporin 1(AQP1), Cadherin 16(CDH16), Fascin 1(Fscn1), and Cyclic GMP-AMP Synthase (CGAS)) from the differential gene list obtained from the RNA sequencing experiment by comparing gene expression of PDACA CRISPR 01 to PDACA CRISPR EV. Aquaporin 1 and cadherin 16 RNA levels, tested by Q-PCR, recapitulate the decrease in RNA expression observed in the RNA sequencing data for the 0.7 kPa conditions only (Figure 5-10, Figure 5-12). Further experimentations aiming to monitor their protein levels are required to fully validate a link between the downregulation of Ajuba and their respective expression.



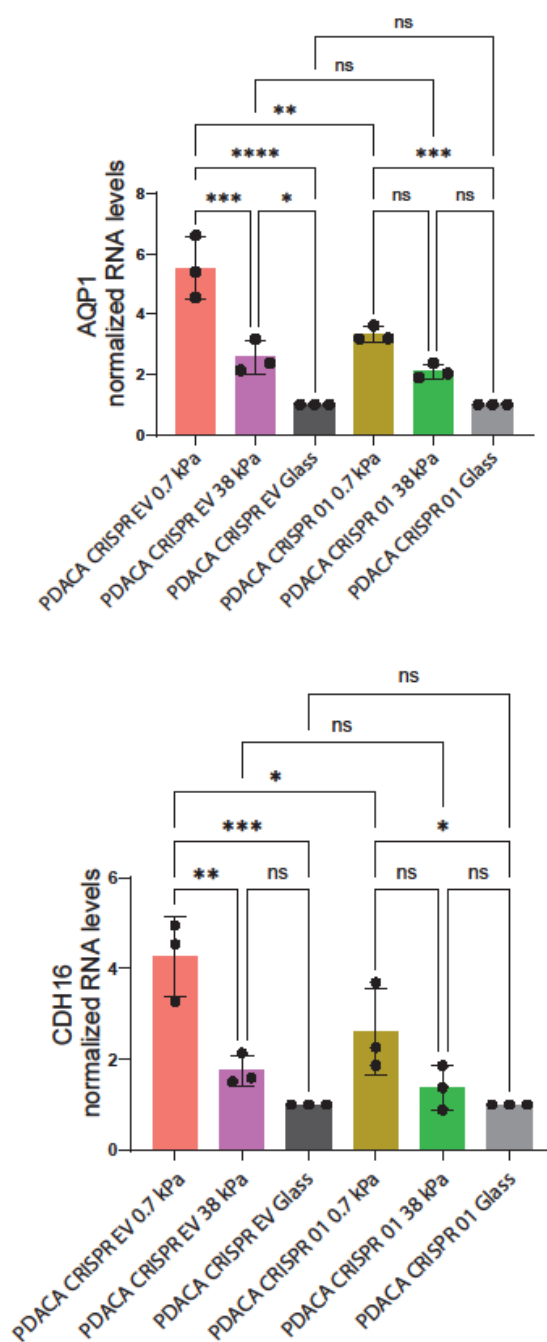
**Figure 5-10: Representation of the RNA expression in PDACA CRISPR 01 of AQP1, CADH16, Fsn1 and CGAS genes on 0.7 kPa and 38 kPa.**

Overview of the different candidate RNA expression levels on 0.7 kPa and 38 kPa in PDACA CRISPR 01 compared to PDACA CRISPR EV RNA levels. The RNA expression levels of each mechanotransduction candidates were plotted against their Log2-fold change\_shrink according to their respective stiffness normalized to PDACA CRISPR EV levels.



**Figure 5-11: CGAS and FSCN1 RNA gene expression tested by qPCR does not recapitulate the RNA sequencing results.**

qPCR quantification of the RNA gene expression of CGAS and FSCN1 in PDACA CRISPR EV and PDACA CRISPR 01 cell lines, cultured on 0.7 kPa, 38 kPa or glass coverslips. N=3, each consisting of three technical replicates. Their levels were normalized against GAPDH expression. One-way ANOVA was performed to assess the statistical significance of each tested condition.



**Figure 5-12: AQP1 and CDH16 gene expression tested by qPCR recapitulate the RNA sequencing results on the 0.7 kPa conditions.**

qPCR quantification of the RNA gene expression of AQP1 and CDH16 in PDACA CRISPR EV and PDACA CRISPR 01 cell lines, cultures on 0.7, 38 kPa hydrogels or glass coverslips. N=3, each consisting of three technical replicates. Their levels were normalized against GAPDH expression levels in each sample. One-way ANOVA was performed to assess the statistical significance of each tested conditions.

## 5.6 Conclusion

In this chapter, I have shown multiple effects in which stiffness affects PDACA gene expression. First of all, the effect of stiffness on PDACA gene expression can be first observed at the RNA level (Figure 5-1-A), where the effect of stiffness is grouped under the variable PC2 which displays a variance of 88%. This signifies that the separation between gene expression at 0.7 kPa and 38 kPa are greatly impacted by environmental stiffness. In Figure 5-1-B, the differential gene expressions (upregulated gene in red, downregulated genes in blue) were represented via a volcano plot, comparing PDACA CRISPR EV gene expression, cultured on 38 kPa versus PDACA CRISPR EV gene expression cultured on 0.7 kPa. The important shift in gene expression can be explained by the conversion of mechanical cues into biological responses by the cell's mechanotransduction signalling, modifying transcriptional programmes and biological processes (such as DNA replication, chromosome organization and metabolism) (Figure 5-1, Figure 5-2, Figure 5-3, Figure 5-4).

To pinpoint the reason behind this drastic modification of gene expression, I analysed the transcription factor activities, and biological processes through G:Profiler and GSEA analysis. Transcription factors bind to specific DNA sequencing of target genes, regulating their transcriptions from DNA to mRNA. 38 transcription factors were downregulated while 16 were upregulated in PDACA CRISPR EV when comparing 37 kPa conditions to 0.7 kPa. Three transcription families were specifically over-represented: ETS, bHLH and SMAD. Additionally, some biological processes were also impacted by environmental stiffnesses (Figure 5-3). In 38 kPa, the upregulation of DNA replication and cell cycle indicates a higher proliferation rate, which also relates to the upregulation of the Myc family of transcription factors.

G:Profiler analysis and GSEA analysis highlight an increase in lipid metabolic processes on 0.7 kPa. Interestingly, the lipid metabolism theme is recapitulated by multiple actors: Peroxisome proliferator-activated receptor gamma (PPAR $\gamma$ ), Sterol regulatory element-binding protein-1 (SREBP-1), PPAR $\gamma$ - Retinoid X receptor alpha (RXR-alpha) and Liver-X receptor alpha (LXR-alpha)- RXR-alpha

were listed as downregulated transcription factors in 38 kPa compared to 0.7 kPa in PDACA CRISPR EV (Figure 5-2).

In this chapter, I aimed to combine the study of the impact of the downregulation of Ajuba and the effect of stiffness on gene expression at the RNA level. I started by analysing the RNA expression level of Ajuba in PDACA CRISPR 01 and PDACA CRISPR 02 cell lines compared to PDACA CRISPR EV cell line. The RNA seq data revealed that PDACA CRISPR 01 and PDACA CRISPR 02 showed some expression of Ajuba at RNA levels (Figure 5-5). The remaining expression can be caused by a mixed population or gene duplication, resulting in incomplete CRISPR. Additional testing would need to be done to determine the origin, such as DNA sequencing of the genomic DNA from our CRISPR cells. Nonetheless, through RNA sequencing analysis, we observe a difference in Ajuba expression when exposed to stiffness. This difference is represented by a shift in  $\text{Log}_2(1+\text{gene count})$  displayed in Figure 5-5. This shift is conserved and similar in depth in each cell line. PDACA CRISPR 02 cell lines, due to a higher Ajuba expression compared to PDACA CRISPR 01, will not be used to assess the effect of the downregulation of Ajuba on gene expression at RNA level.

As previously mentioned, Ajuba is a transcriptional co-regulator, forming multiprotein complexes with specific transcription factors and will activate or repress their effect on the transcription of targeted genes (Ayyanathan et al., 2007; Hou et al., 2008; Hou et al., 2010; Yan et al., 2022). The transcriptional co-regulator role of Ajuba led us to investigate transcription factor activities in PDACA CRISPR 01 cell line. We have highlighted multiple differences between the transcription activities of PDACA CRISPR EV and PDACA CRISPR 01 cells (Figure 5-6, Figure 5-7 and Table 5-1). These differences indicate that the downregulation of Ajuba impacts gene expression and transcription factor activities in PDACA cells. I then compared the transcription factor activities, between PDACA CRISPR EV and PDACA CRISPR 01 cell lines, cultured on either 0.7 kPa or 38 kPa (Figure 5-7). We showed that no transcription factors were found upregulated, at either stiffness, in PDACA CRISPR 01 compared to PDACA CRISPR EV, while 15 were downregulated on 38 kPa, and 4 in 0.7 kPa (Figure 5-7). The downregulation of Ajuba seems to impact the transcription factor activity in PDACA cells. This opens

the possibility that Ajuba acts as a coregulator of these transcription factors. Since transcription factor activities and gene expression go hand in hand, we proceeded to analyse gene expression activities in PDACA CRISPR EV as well as PDACA CRISPR 01 and 02. The difference in the expression of Ajuba at the RNA level between PDACA CRISPR 01 and PDACA CRISPR 02, has an important impact on how much genes were impacted by Ajuba's downregulation, as illustrated in Figure 5-8 and Figure 5-9. Using the PDACA CRISPR 01 and PDACA CRISPR EV cell lines, I defined two effects: a CRISPR-based and a stiffness-based effect. It is to be noted that 32 genes were similarly modified in both 0.7 and 38 kPa, which we classified as a CRISPR-based effect (Table 5-2). In contrast, 87 genes were only impacted at specific stiffnesses which we classified as stiffness-based effects (Table 5-3, Table 5-4).

I selected from Table 5-2 and Table 5-3 four genes whose RNA expression was significantly impacted by the downregulation of Ajuba at RNA level. Aquaporin 1(AQP1), Cadherin 16(CDH16), Fascin 1(Fscn1) and Cyclic GMP-AMP Synthase (CGAS) were selected for their biological functions, gathered in the 5.5 . Each of these genes was tested by qPCR, using specific primers, to validate their RNA expression levels in 0.7 kPa, 38 kPa PAAM hydrogel stiffness as well as glass culture conditions. Aquaporin 1 and cadherin 16'RNA levels were validated on 0.7 kPa conditions by qPCR (Figure 5-10, Figure 5-12). On the other hand, Fascin 1 and CGAS qPCR results do not recapitulate RNA sequencing results in 0.7 nor 38 kPa conditions (Figure 5-10, Figure 5-11). This may be due to a relatively small log<sub>2</sub>-fold change causing a detection issue.

## 5.7 Discussion

In this chapter (using the dataset created in 2023) as well as chapter 3 (using the dataset created in 2017), I have shown multiple effects in which stiffness affects PDACA gene expression. Although both RNA sequencing uses similar stiffnesses, both datasets are indeed quite different. Robin Shaw from the Scotland Institute bioinformatic department performed the comparison between the 2017 and 2023 RNA sequencing datasets, to understand in which aspect they differ. This comparison is articulated from multiple angles. First, the study of the standard



error will help determine the significance of the observed changes in gene expression between conditions. Second, the similarity between dataset will be tested through the log 2-fold change directionality of significant genes and p-value directionality of common biological processes. Lastly, the modified biological processes will be compared through functional enrichment analysis. The standard error was calculated from the DESeq2 to estimate the variability of gene expression levels across different conditions. The higher standard error in the 2017 dataset indicates a higher data variation (Figure 7-2). This variation can suggest that significant genes are less likely to be detected. This lack of precision would adversely affect the calculated fold changes and p-values in the 2017 data compared to the 2023 dataset. However, the presence of high standard error in the 2023 dataset can be due to the improvement of tool accuracies, detecting a greater variability across samples. The standard errors attributed to common genes (Figure 7-3) and significant genes (Figure 7-4) show a similar effect, which was measured significantly different between datasets by a Wilcoxon rank sum test with continuity correction at a p-value of  $1.24 \times 10^{-5}$ . This suggests a greater noise within the 2017 dataset. Lesser amount of noise in the most recent dataset could be due to the improvement of both the analytical tools and sequencing depth and power. Although the standard error differs between datasets, by comparing the directionality of the fold change of significant genes (Figure 7-5), we can see a conserved directionality attesting to similarities between datasets. This is further confirmed by the 33 biological processes (GO term) found conserved in both datasets. Additionally, Gene Set Enrichment Analysis can be used to determine the biological function of the intersecting genes, using Manhattan plots. The resulting plots (Figure 7-7 and Figure 7-8) attest to the strong effect of the number of significant genes in functional enrichment analysis. Indeed, we can observe a larger enrichment in the 2023 dataset due to the larger number of significant genes. By solely analysing the significant genes common to the 2017-2023 datasets, the functional enrichment analysis shows an overlap in biological processes (Figure 7-9). In conclusion, both datasets showed an overlap in both biological processes from the functional analysis and significant genes from the DEGA. The directionality of biological effects was similar. However, the 2023

dataset had a higher number of significant genes and therefore showed more changes in Gene Ontology terms.

We previously discussed in the 5.6 section the reasons behind the difference in the expression of Ajuba at RNA level between PDACA CRISPR 01 and PDACA CRISPR 02. It is important to note that none of PDACA CRISPR 02 RNA sequencing data was analysed further than the differential gene expression (Figure 5-9). The reason for it isn't restricted to the presence of a higher Ajuba expression remaining in this cell line, but also the absence of Ajuba listed as downregulated after filtering the differential gene expression. Due to this fact, gene expressions as well as other results from RNA sequencing from PDACA CRISPR 02 was not analysed further.

We demonstrated in Chapter 3 and Chapter 5 that environmental stiffness has an important impact on cellular behaviour as well as gene expression in PDACA cells. In this chapter, we investigated the gene expression, transcription factor activities and biological processes, gathered from an RNA sequencing experiment, which were modified on cells exposed to 38 kPa versus 0.7 kPa conditions (Figure 5-1-B, Figure 5-2, Figure 5-3, Figure 5-4). The fact that ECM cues can modify transcription factor activities is well established. ECM forces will trigger signalling cascades which will be relayed, and transduced in the nucleus, impacting transcription factor activities and gene expression. Additionally, ECM forces will also induce chromatin remodelling and changes in histone acetylation and methylation, directly impacting gene expression and changing gene accessibility (Downing et al., 2013; Wagh et al., 2021). TF activities will impact multiple layers of cellular activities with a combined effect on gene expression levels, cellular metabolism, cellular behaviour, physiology, homeostasis, and fate (Carthew, 2021; Spitz & Furlong, 2012). In this chapter, using G:profiler analysis which can recognise regulatory motifs of transcription factors based on the TRANSFAC database, we have shown three transcription factor families particularly modified depending on surrounding stiffness: SMAD, ETS and bHLH families. Most of the family members highlighted in this chapter have not had their expression correlated with ECM stiffness in available literature.

We found 10 members of the bHLH family of transcription factors, six of which were downregulated in PDACA CRISPR EV at 38 kPa compared to 0.7 kPa (Figure 5-2). Additionally, to the effect of stiffness on this family, Ajuba downregulation appears to impact specifically the MyoD family (also members of the bHLH family), as the downregulation of these three MyoD members Myogenin, MyoD, MRF4 were not observed in PDACA CRISPR 01 cell lines, in 38 kPa versus 0.7 kPa conditions (Figure 5-5). To my knowledge, no link between Ajuba and the MyoD transcription factor family was found in the literature. MyoD is a transcription factor that activates the transcription of muscle-specific genes while repressing non-muscle genes. MyoD family members are expressed in skeletal muscle lineage cells, myeloid cells of the thymus and myofibroblasts (Zammit, 2017). Interestingly, muscle cells are known to respond to mechanical signals and adapt to external loading, which involves mechanosensors which control the regeneration of the muscle, its metabolism, and its molecular activities (Vanmunster et al., 2022). MRF4, myogenin, myoD are all members of the myogenic regulatory factors which control the myogenic differentiation during the development (Zammit, 2017). It has been demonstrated that substrate stiffness does affect myogenic differentiation, with softer substrates promoting differentiation in skeletal muscle stem cells (Romanazzo et al., 2012). The activities of MRF4, myogenin, myoD could be regulated by stiffness.

C-myc, part of the bHLH family, was upregulated in 38 kPa compared to 0.7 kPa in both tested cell lines. These data suggest a stiffness-related expression of C-myc. C-myc controls the generation and maintenance of pancreatic tissue, by controlling progenitor cell differentiation and cell replacement rates (Bonal et al., 2009). In pancreatic cancer, c-myc activation can trigger the progression of PanIN lesions to PDAC in mice, and C-myc overexpression inhibits cell differentiation in favour of cell proliferation and apoptosis in pancreatic tissue (Bonal et al., 2009). Surprisingly, N-myc is cited in both upregulated and downregulated TF lists (Figure 5-2), this is due to the presence of different recognised motifs: NMYC motif: CAYCTG, N-MYC: NNCCACGTGNNN. The presence of N-myc can therefore not be considered as either upregulated or downregulated.

The SMAD family members, SMAD 3 and SMAD4 were downregulated in PDACA CRISPR EV 38 kPa condition compared to PDACA CRISPR EV 0.7 kPa condition (Figure 5-2). This change suggests an effect of the stiffness over the expression of both SMAD3 and SMAD4 at RNA level in PDACA CRISPR EV. The literature identified SMAD3 and SMAD4 as important transcription factors for TGF- $\beta$  signalling, where TGF  $\beta$ RI phosphorylates SMAD3, in the SMAD2/3 complex, which binds to SMAD4 leading to their translocation into the nucleus (Leask & Abraham, 2004). SMAD4 loss or inactivation can be found in a vast majority of PDAC patients in the early stages of pancreatic cancer leading to poor prognosis in PDAC patients (Ahmed et al., 2017). To my knowledge, no published studies correlate SMAD4 expression with ECM stiffness, in any context, including in PDAC. However, the LEM domain-containing protein 3 (LEMD3)-Smad2/3 interaction is inversely correlated to substrate stiffness, leading to an antagonization of the SMAD2/3 signalling (Chambers et al., 2018). Additionally to a link between stiffness and SMAD3, the expression of SMAD3 seems to also be correlated with Ajuba expression since SMAD3 downregulation is lost in PDACA CRISPR 01 38 kPa versus 0.7 kPa (Figure 5-2, Table 5-1). To my knowledge, no correlation between Ajuba expression and the SMAD family was found in the literature.

Regarding the ETS family members listed in the 5.3 section C-ets-1, Ets2, ERF, ER81, and Elk-1 were downregulated, while others, C-ets-2, and Spi-B, were upregulated in PDACA CRISPR EV 38 kPa versus PDACA CRISPR EV 0.7 kPa conditions (Figure 5-1). The downregulation of Ajuba modifies the expression of 9 ETS members, including the loss of the 7 previously mentioned and the downregulation of PU-1 and Elf1 specifically in PDACA CRISPR 01 (Table 5-1). Similarly to previously cited families, to my knowledge, no information was available on the effect of stiffness on the ETS family nor any link between the expression of Ajuba and the ETS family. Interestingly, the ETS family and the expression pattern of its members is critical for the development, differentiation, proliferation, and tissue remodelling, in which mechanosensing plays a central role (Kar & Gutierrez-Hartmann, 2013). In the context of cancer, differentiation and development, the ETS family activity is particularly important (Kar & Gutierrez-Hartmann, 2013). It is to be noted that a link exists between the Ets1 gene and SMAD3/4. It has been

demonstrated that these 3 transcription factors cooperate, through synergy (Lindemann et al., 2001). Ajuba was also described by Ayyanathan et al., as a transcriptional repressor of SNAIL through the SNAG domain (Ayyanathan et al., 2007; Hou et al., 2008) and can also mediate transcriptional repression through cooperation with histone deacetylase (D. E. Montoya-Durango et al., 2008). Unfortunately, no sign of transcriptional repression of the SNAIL was observed in PDACA CRISPR 01 cell line. Taken together, it is important to remember that these transcription factor activities were based of RNA sequencing analysis using transcription factor regulatory motifs present within the gene list provided to emulate transcription factor activities. Additional experiments are required to validate these activities such as transcription factor activity assay via indirect ELISA method or via chromatin profiling techniques (Chawla et al., 2021; Straub & Newman, 2024). Indeed, transcription factor activities are also regulated through changes in the chromatin remodelling and its accessibility (Hadden et al., 2017; Wagh et al., 2021). After validation, it would be interesting to study the expression level of these transcription factors, in tumour tissue, versus physiological levels, for a better understanding of their expression during pathology.

This RNA sequencing dataset was also analysed using both G:Profiler and GSEA to highlight biological processes significantly modified by stiffness in PDAC. Cell cycle, DNA replication, chromosome organisation, and RNA processing were upregulated BP in PDACA CRISPR EV cells cultured on 38 kPa PAAM hydrogels compared to their 0.7 kPa counterparts. These biological processes are aligned with the higher proliferation rate observed on these stiffnesses (Figure 3-3).

Changes in metabolic processes were also highlighted between 0.7 kPa and 38 kPa stiffnesses. In cancer, a metabolic switch can be triggered by cells to optimise energy production, depending on cell environment, nutrient availability, nutrient uptake and cellular behaviour. This metabolic reprogramming became recently one of the hallmark of cancer (Hanahan & Robert, 2011). In Figure 5-2, PPARgamma, SREBP-1, PPARgamma-RXRalpha and LXRalpha-RXRalpha, members of the lipid metabolism pathways, are listed among the downregulated transcription factors in 38 kPa compared to 0.7 kPa. (Natalya & Craig, 2016). It led us to investigate a

potential metabolic shift toward lipid metabolism in 0.7 kPa condition. Lipid metabolism regulation depends on Sterol regulatory element binding protein (SREBP) and Liver X receptor (LXR) (Sunami et al., 2017) (Fu et al., 2021). SREBP-1 is a key element regulating lipid metabolism and uptake (Guo et al., 2014) while LXR-alpha regulates intracellular cholesterol by modulating gene expression affecting cholesterol transport. PPARs are ligand-activated transcription factors that regulate gene expression in fatty acid metabolism. A study combining hydrogel stiffnesses and metabolomics showed a clear relationship between ECM and lipid metabolism, in human epithelial breast cell lines (Bertolio et al., 2019). They showed that the actomyosin network contractility, which transduces ECM rigidity, directly acts on SREBP1 activities (lipid metabolism enzyme) through RhoA. Soft ECM reduces mechanical signalling pathways, induces SREBP1 activity and increases lipid droplet accumulation (Bertolio et al., 2019). Bertolio et al., showed that an increase in stiffness may inhibit SREBP1 functions and SREBP lipid biosynthesis (Bertolio et al., 2019). The correlation between our two studies might lead us to further investigate this lipid metabolic shift in PDAC cell line. Yuki Matsushita et al., nicely summarised in their paper an overview of available lipidomic techniques which could be used to investigate lipid pathways and quantify lipid molecules to investigate this lipid metabolic shift in PDAC cell line (Matsushita et al., 2021).

In addition to transcription factor activities and biological processes, the RNA sequencing results were also used to look at gene expression at the RNA level. In Table 5-2, Table 5-3 and Table 5-4, genes were separated according to stiffness-based and CRISPR-based effects. Some of these genes were selected for further validation by qPCR (Figure 5-10). Unfortunately, Fascin 1 and CGAS qPCR results do not recapitulate RNA sequencing results (Figure 5-10, Figure 5-11) I, therefore, removed these two candidates from further investigation. On the other hand, Aquaporin 1 and cadherin 16 RNA levels were validated by qPCR in 0.7 kPa conditions which recapitulate RNA sequencing results (Figure 5-10, Figure 5-12). The expression of Aquaporin 1 at the RNA level is deeply changed in response to stiffness (especially on 0.7 kPa), an effect which is lessened by the downregulation of Ajuba. Due to this fact, a link between the expression of Ajuba and Aquaporin

1 is a possibility, in soft substrate, though it does require further validation. Regarding the link between AQP1 and stiffness, similar results were corroborated in a paper published in 2019 by Harold D. Love and collaborators, where Aquaporin 1 was also found upregulated on softer substrates (0.5kPa) compared to stiffer (50kPa) in human renal tubule cell line (Love et al., 2019). Additionally, Aquaporins (AQP3 and 5) can modulate membrane rigidity, cellular morphology (volume, area, shape), cellular mobility and adhesion in pancreatic cancer, through control over membrane permeability. Water fluxes promote membrane protrusion and cell mobility through actin polymerisation (Silva et al., 2022). Aquaporin 1 could allow cells to respond to mechanical stress through modulation of cell shape, rigidity in PDAC cell line.

Following similar trends, Cadherin 16 expression at the RNA level was modulated by both stiffnesses and Ajuba downregulation (0.7 kPa condition) (Figure 5-10). Cadherin 16 expression in pancreatic cancer is low compared to other types of cancer, Cadherin 16 is a calcium-dependent cadherin involved in cell-cell adhesion, tissue cohesion and tissue architecture. Cadherins have been linked with mechanotransduction activities, briefly, E cadherin adhesion will use contraction to sense rigidity of the environment. N-Cadherin expression is also modulated by ECM stiffness, but its expression increases in stiffer substrates compared to softer (Keeley et al., 2015). Further analysis would need to be conducted to comprehend the role of cadherin 16 expression in both stiffness and pancreatic cancer. To my knowledge, no link was published between Ajuba and cadherin 16 but Ajuba enhances the transcription of N-cadherin in colorectal cancer (Z. Wu et al., 2021).

In conclusion, in this chapter, we have shown that ECM stiffness deeply impacts transcription factor activity, gene expression and multiple biological processes including metabolism. We also gathered multiple cues leading us to believe that lipid metabolism is upregulated on 0.7 kPa. Additionally, Ajuba downregulation has a specific effect on a small number of transcription factor activities as well as Cadherin 16 and Aquaporin 1 gene expression. All these leads could be investigated further for a better understanding of mechanotransduction in

pancreatic cancer and of Ajuba expression, aided by the generation of better Ajuba knockout cell lines.



## **Chapter 6. Future directions**

## 6.1 The environment stiffness deeply modifies PDAC gene expression and transcription factor activities

Since the seed and soil theory from Stephen Paget, years of research have demonstrated the complex and bidirectional relationship between a cell and its surrounding ECM. The ECM is a source of signals, which can be architectural, chemical and mechanical. Pancreatic ductal adenocarcinoma (PDAC) is one of the most aggressive and highly metastatic cancers, characterized by a severe desmoplastic reaction that increases ECM rigidity. Focussing on mechanical signals, I demonstrated that environment stiffness induces important modifications in cellular morphology, cellular proliferation, gene expression (mRNA) and transcription activities of PDACA cells *in vitro*. To do so, I used polyacrylamide hydrogels of 0.7kPa (healthy pancreas) and 38kPa (extreme stiffness) to mimic stiffnesses *in vitro*.

The use of G:Profiler and GSEA analysis have indicated several biological processes modified according to stiffness which are (A): Cell cycle and its regulation, (B): Chromosome organisation, DNA replication and RNA processing including Ribosome biogenesis and nucleic acid metabolic processes, and (C) Metabolic processes. Within the GO term “metabolism processes” was highlighted a potential metabolic shift toward an increase in lipid metabolism in 0.7kPa conditions compared to 38kPa conditions in PDACA cells. Efforts are ongoing to study PDAC matrix stiffness and its metabolic profiling both *in vitro* and *in vivo* (Mohan et al., 2024; Zhu et al., 2021). It has been shown that PDAC tumours frequently exhibit metabolic reprogramming to fuel their need for energy and to adapt better to their environment due to the extreme desmoplastic reaction (J.-T. Li et al., 2019). Lipids are fundamental material for cells as membrane components and are generated by glucose-derived glycerol and from mitochondrial-derived fatty acids (Chandel, 2021). Lipids are also signal transduction messengers, modifying protein activities and that can stimulate proliferation in pancreatic cancer (Sunami et al., 2017). It has been shown that mechanical cues from the ECM can regulate lipid metabolism, through cellular mechanosensing, YAP/TAZ signalling and actin cytoskeleton contractibility, regulating SREBP1/2 activity (J.-T. Li et al., 2019;

Romani et al., 2019). This potential shift toward lipid metabolism was identified in both G:Profiler and GSEA analysis and evolves around the downregulation of PPAR $\gamma$ , SREBP-1, PPAR  $\gamma$ -RXR-alpha and LXR alpha-RXR-alpha activities. All of these regulate the transcription of fatty acid oxidation genes and genes involved in cholesterol and lipid production. It would be interesting to see whether these changes are observed in other PDAC cell lines cultured in similar conditions and to further investigate these pathways in human patient data. An in-depth analysis of the lipidome is required to further investigate and validate this phenotype. Further analysis including mass spectrometry-based lipidomic or liquid chromatography-mass spectrometry would help us detect and characterize the lipidome in stiffness-mediated PDAC metabolism (Tumanov & Kamphorst, 2017).

The validation of such phenotype would open opportunities to identify new biomarkers. Biomarkers are molecules or combinations of molecules linked to tumour progression used for early diagnosis or disease and survival prognosis. The identification of stiffness-based prognostic gene signatures as biomarkers in PDAC would identify potential molecular treatment targets.

## **6.2 Ajuba: a new mechanotransducer protein?**

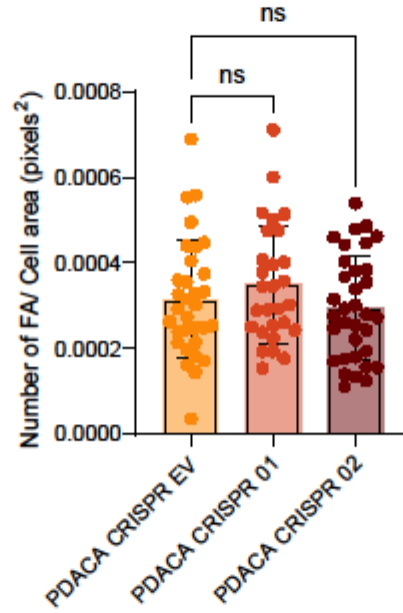
Through this thesis, I demonstrated that Ajuba is a mechanosensitive protein by the modification of its expression at both RNA and protein levels in a stiffness-dependent manner. I demonstrated that the downregulation of Ajuba in PDACA cells, using CRISPR technology induces a decrease in cell-matrix adhesion and an increase of cellular invasion. The role of Ajuba in cell-matrix adhesion and cell invasion requires further testing. To do so, it would be interesting to monitor adhesion strength, MMP activities, cytoskeletal turnover, cytoskeletal recycling and adhesion dynamic during invasion. Different hypotheses can be articulated. First, does Ajuba enhance MMP activities? A positive correlation was established between MMP activities and cell invasion (Najafi et al., 2019) and between Ajuba and MMP activities (Shi et al., 2016). Second, would Ajuba increase the recycling and cytoskeletal turnover of components during cell invasion? Indeed, the recycling of integrins, invadopodia components and MMPs are required during invasion to create invadopodia, adhesion sites and induce movement (Mukenhirn

et al., 2021; Rainero & Norman, 2013; Yamaguchi & Condeelis, 2007). Additionally, Ajuba has a role as a receptor responsible for the internalization of secreted factors from the ECM to the cell through endocytosis pathways in macrophages (La et al., 2018). On another note, to validate the invasive phenotype, it would also be interesting to investigate if the invasion phenotype is recapitulated *in vivo*. To do so, intraperitoneal or intrasplenic transplantation assay using nude mice would allow the monitoring of respectively the metastatic seeding and the invasion capabilities of the generated PDACA CRISPR cell lines (Juin et al., 2019; Papalazarou et al., 2020).

In addition, the downregulation of Ajuba induces the modification of gene expressions and the modifications of transcription factor activities in a stiffness-dependent manner. Taken together, these results would indicate that Ajuba is both a mechanosensitive protein and a mechanotransducer in PDACA cells. To deepen our knowledge about the role of Ajuba in PDAC, a tagged version of Ajuba becomes necessary to detect Ajuba and visualise its dynamic localisation and partners. Although previous attempts were unsuccessful, the use of a bicistronic vector allowing simultaneously the inducible depletion of Ajuba and the expression of tag version of Ajuba might increase cellular tolerance for Ajuba's constructs. If PDACA cells do not tolerate the complete loss of Ajuba's expression, the use of inducible shRNA would allow us to tune Ajuba gene expression and monitor the cell's reaction to Ajuba loss via time courses.

The different phenotypes triggered by the downregulation of Ajuba do not recapitulate previously published data from the literature (such as localisation, proliferation, migration, and invasion). In contrast, it offers the opportunity to consider the cancer-related role of Ajuba. To further our understanding, it would be interesting to use several PDAC cell lines and human cell lines, to test if the phenotypes observed are generalised within PDAC.

## Chapter 7. Annexes



**Figure 7-1: Ajuba depletion does not impact focal adhesion number**

Manual quantification of focal adhesion number reveals that Ajuba depletion does not impact focal adhesion number, in PDACA CRISPR 01 and PDACA CRISPR 02 cells compared to PDACA CRISPR EV.

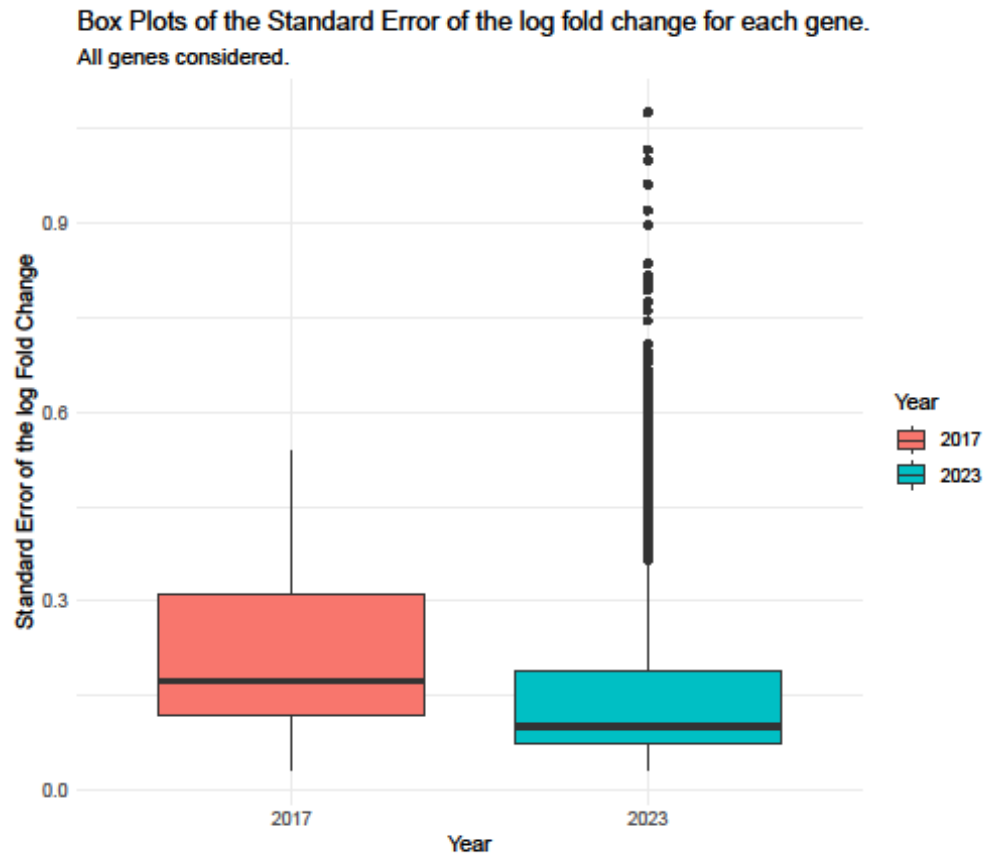
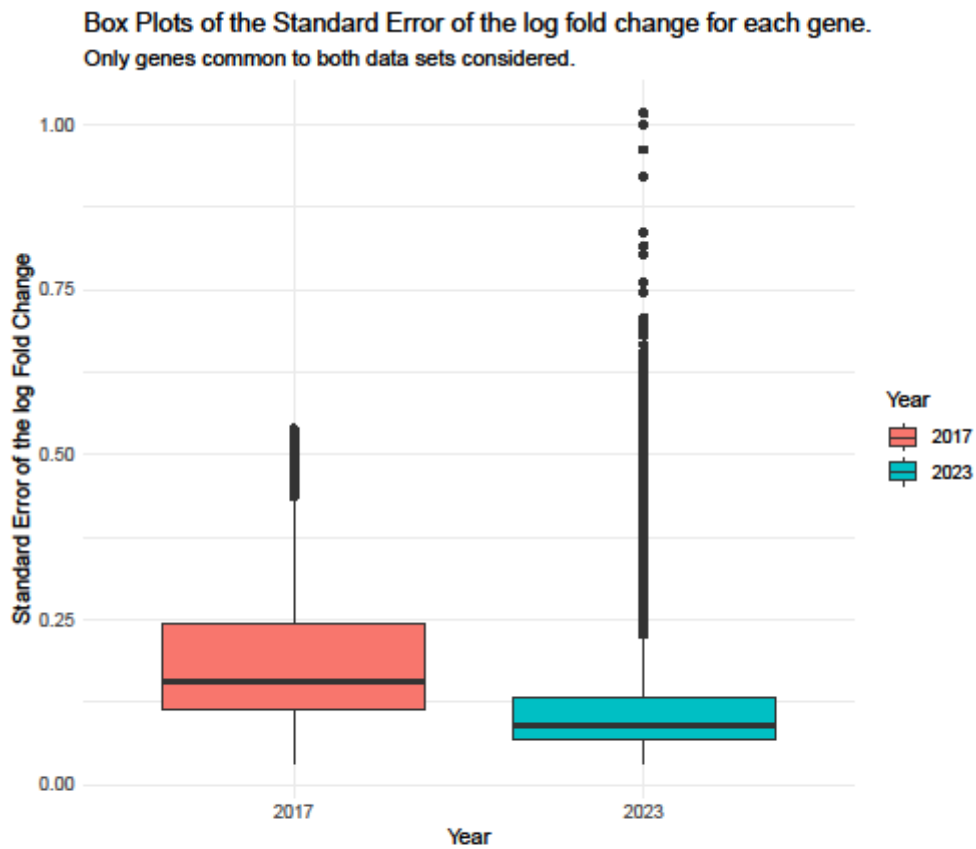


Figure 7-2: The standard error of the log fold change of the 2017 RNA sequencing dataset is superior to the 2023 dataset.

Visualisation of the standard error values attributed to the log fold change for every gene derived from both RNA sequencing datasets, comparing soft versus rigid conditions. 2017 represents the dataset generated by Vassilis Papalazarou, the basis for Chapter 3, while 2023 represents the RNA sequencing dataset that was generated and studied in Chapter 5.



**Figure 7-3:** The standard error related to common genes is superior in the 2017 RNA sequencing dataset compared to the 2023 dataset.

Visualisation of the standard error values attributed to the log fold change for commonly identified genes derived from both RNA sequencing datasets, comparing soft versus rigid conditions.

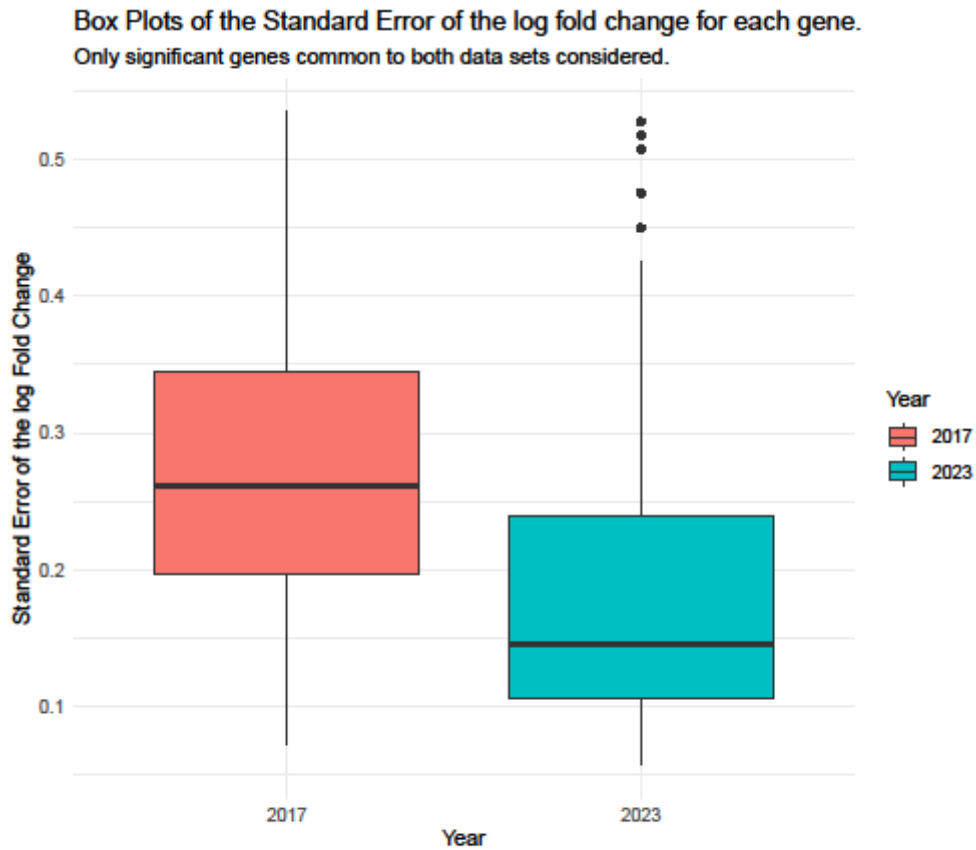


Figure 7-4: The standard error related to genes, both common and significantly modified, is superior in the 2017 RNA sequencing dataset compared to the 2023 dataset.

Visualisation of the standard error values attributed to the log fold change for significant genes, identified in both RNA sequencing datasets, comparing soft versus rigid conditions.



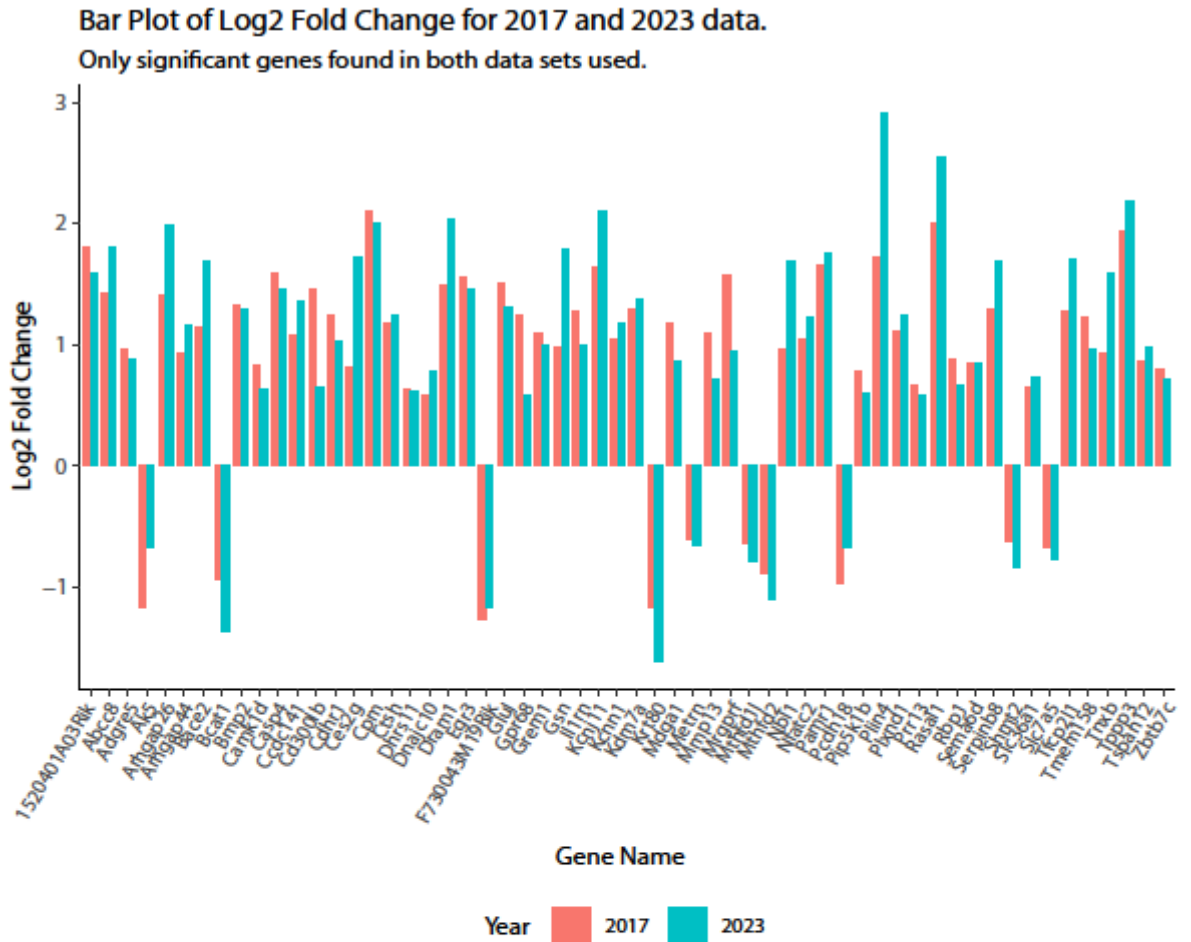
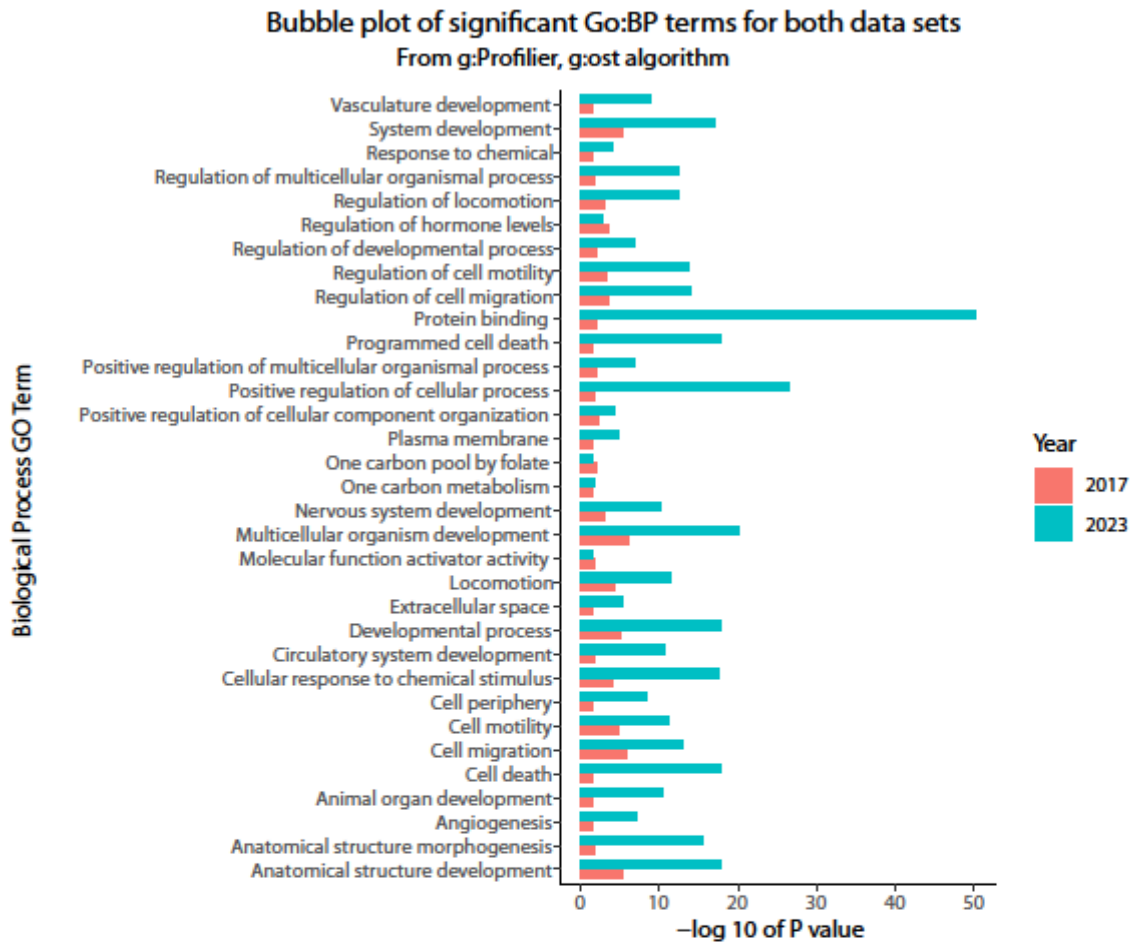


Figure 7-5: The fold change directionality of the significant genes is conserved in both datasets.

Visualisation of the Log 2-fold change values attributed to significant genes, identified in both RNA sequencing datasets, comparing soft versus rigid conditions.



**Figure 7-6:** The common biological processes have similar directionality with lower p-values observed in the 2017 dataset.

Visualisation of the significant biological processes highlighted by GO: BP and their directionality in both RNA sequencing datasets, comparing soft versus rigid conditions.

### Manhattan Plot of Functional Enrichment Analysis

Only significant genes from 2017 data set considered.

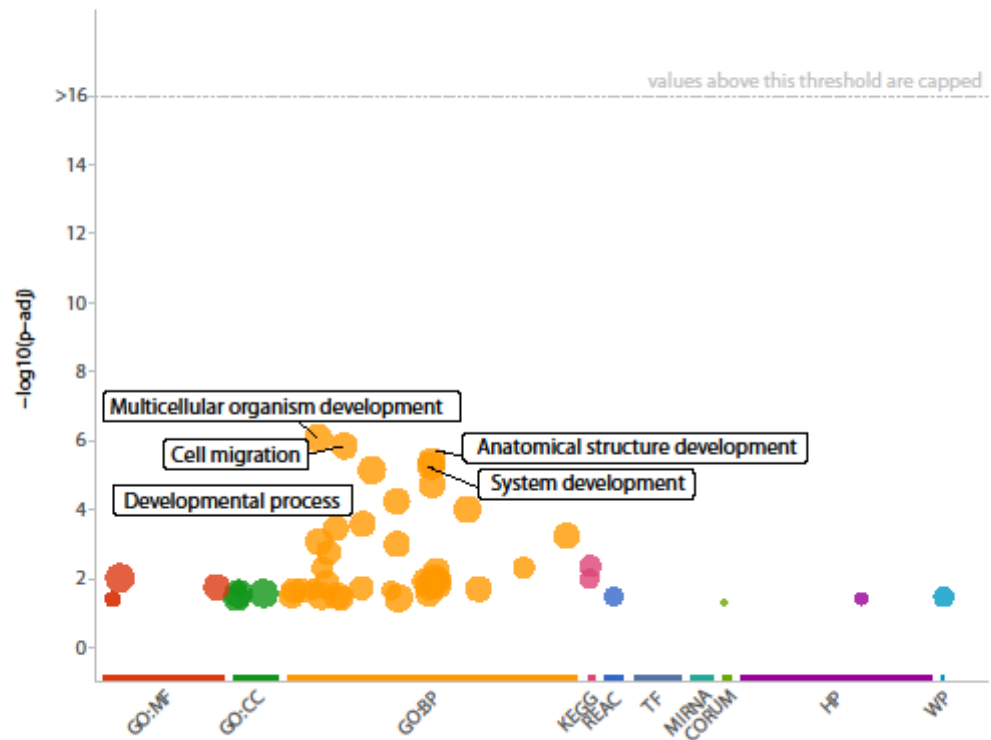
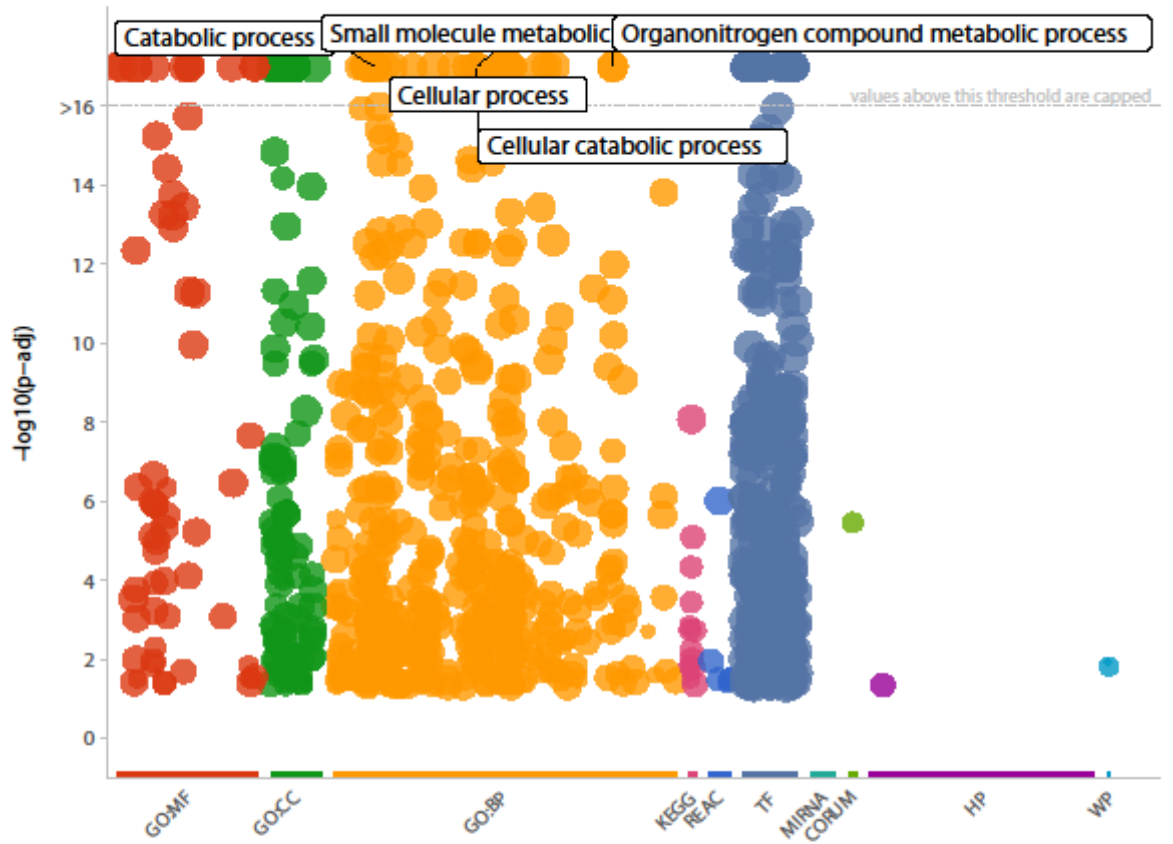


Figure 7-7: Functional enrichment analysis results representing the 2017 dataset

Visualisation of the number of significant pathways found in the 2017 dataset, reflecting significant genes, analysed with g:Profiler.

**Manhattan Plot of Functional Enrichment Analysis**  
 Only significant genes from 2023 data set considered.

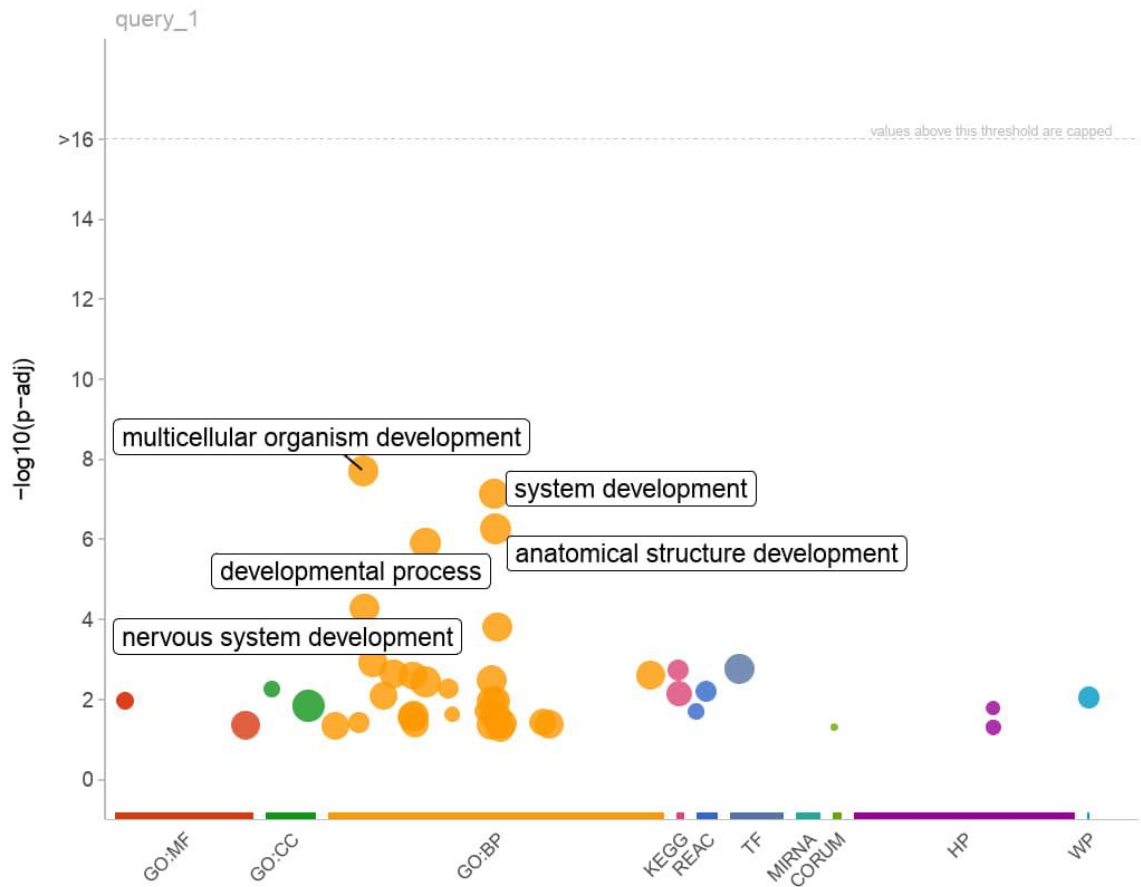


**Figure 7-8: Functional enrichment analysis results representing the 2023 dataset**

Visualisation of the number of significant pathways found in the 2023 dataset, reflecting significant genes, analysed with g:Profiler.

### Manhattan Plot of Functional Enrichment Analysis

Only significant genes common to both data sets considered.



**Figure 7-9: Functional enrichment analysis results representing the significant genes common to both datasets.**

Visualisation of the number of significant pathways found, reflecting significant genes, analysed with g:Profiler.

## Chapter 8. REFERENCES:

- Aguilar, R. C. (2018). Epsin. In (pp. 1617-1623). Springer International Publishing. [https://doi.org/10.1007/978-3-319-67199-4\\_101568](https://doi.org/10.1007/978-3-319-67199-4_101568)
- Ahluwalia, P., Ahluwalia, M., Mondal, A. K., Sahajpal, N., Kota, V., Rojiani, M. V., Rojiani, A. M., & Kolhe, R. (2021). Prognostic and therapeutic implications of extracellular matrix associated gene signature in renal clear cell carcinoma. *Sci Rep*, 11(1), 7561. <https://doi.org/10.1038/s41598-021-86888-7>
- Ahmed, S., Bradshaw, A.-D., Gera, S., Dewan, M., & Xu, R. (2017). The TGF- $\beta$ /Smad4 Signaling Pathway in Pancreatic Carcinogenesis and Its Clinical Significance. *Journal of Clinical Medicine*, 6(1), 5. <https://doi.org/10.3390/jcm6010005>
- Alégot, H., Markosian, C., Rauskolb, C., Yang, J., Kirichenko, E., Wang, Y.-C., & Irvine, K. D. (2019). Recruitment of Jub by  $\alpha$ -catenin promotes Yki activity and Drosophila wing growth. *Journal of Cell Science*, 132(5), jcs222018. <https://doi.org/10.1242/jcs.222018>
- Anderson, C. A., Kovar, D. R., Gardel, M. L., & Winkelman, J. D. (2021). LIM domain proteins in cell mechanobiology. *Cytoskeleton*, 78(6), 303-311. <https://doi.org/10.1002/cm.21677>
- Apte, S. S., & Naba, A. (2023). Beyond the matrisome: New frontiers in ECM research. *Matrix Biol*, 115, 133-138. <https://doi.org/10.1016/j.matbio.2022.12.003>
- Arsenijevic, T., Perret, J., Van Laethem, J. L., & Delporte, C. (2019). Aquaporins Involvement in Pancreas Physiology and in Pancreatic Diseases. *Int J Mol Sci*, 20(20). <https://doi.org/10.3390/ijms20205052>
- Ayyanathan, K., Peng, H., Hou, Z., Fredericks, W. J., Goyal, R. K., Langer, E. M., Longmore, G. D., & Rauscher, F. J., 3rd. (2007). The Ajuba LIM domain protein is a corepressor for SNAG domain mediated repression and participates in nucleocytoplasmic shuttling. *Cancer Res*, 67(19), 9097-9106. <https://doi.org/10.1158/0008-5472.CAN-07-2987>
- Azad, A. K., Raihan, T., Ahmed, J., Hakim, A., Emon, T. H., & Chowdhury, P. A. (2021). Human Aquaporins: Functional Diversity and Potential Roles in Infectious and Non-infectious Diseases. *Frontiers in Genetics*, 12. <https://doi.org/10.3389/fgene.2021.654865>
- Bach, I. (2000). The LIM domain: regulation by association. *Mechanism of development*, 91(1-2), 5-17. [https://doi.org/https://doi.org/10.1016/S0925-4773\(99\)00314-7](https://doi.org/https://doi.org/10.1016/S0925-4773(99)00314-7)

- Bailey, P., Chang, D. K., Nones, K., Johns, A. L., Patch, A.-M., Gingras, M.-C., Miller, D. K., Christ, A. N., Bruxner, T. J. C., Quinn, M. C., Nourse, C., Murtaugh, L. C., Harliwong, I., Idrisoglu, S., Manning, S., Nourbakhsh, E., Wani, S., Fink, L., Holmes, O., . . . Grimmond, S. M. (2016). Genomic analyses identify molecular subtypes of pancreatic cancer. *Nature*, 531(7592), 47-52. <https://doi.org/10.1038/nature16965>
- Bertolio, R., Napolitano, F., Mano, M., Maurer-Stroh, S., Fantuz, M., Zannini, A., Bicciato, S., Sorrentino, G., & Del Sal, G. (2019). Sterol regulatory element binding protein 1 couples mechanical cues and lipid metabolism. *Nature Communications*, 10(1). <https://doi.org/10.1038/s41467-019-09152-7>
- Bindschadler, M., Osborn, E. A., Dewey, C. F., & McGrath, J. L. (2004). A Mechanistic Model of the Actin Cycle. *Biophysical Journal*, 86(5), 2720-2739. [https://doi.org/10.1016/s0006-3495\(04\)74326-x](https://doi.org/10.1016/s0006-3495(04)74326-x)
- Birgersdotter, A., Sandberg, R., & Ernberg, I. (2005). Gene expression perturbation in vitro--a growing case for three-dimensional (3D) culture systems. *Semin Cancer Biol*, 15(5), 405-412. <https://doi.org/10.1016/j.semcancer.2005.06.009>
- Bonal, C., Thorel, F., Ait-Lounis, A., Reith, W., Trumpp, A., & Herrera, P. L. (2009). Pancreatic Inactivation of c-Myc Decreases Acinar Mass and Transdifferentiates Acinar Cells Into Adipocytes in Mice. *Gastroenterology*, 136(1), 309-319.e309. <https://doi.org/10.1053/j.gastro.2008.10.015>
- Bruun-Sorensen, A. S., Edamana, S., Login, F. H., Borgquist, S., & Nejsum, L. N. (2021). Aquaporins in pancreatic ductal adenocarcinoma. *APMIS*, 129(12), 700-705. <https://doi.org/10.1111/apm.13184>
- Butcher, D. T., Alliston, T., & Weaver, V. M. (2009). A tense situation: forcing tumour progression. *Nature Reviews Cancer*, 9(2), 108-122. <https://doi.org/10.1038/nrc2544>
- Buxboim, A., Ivanovska, I. L., & Discher, D. E. (2010). Matrix elasticity, cytoskeletal forces and physics of the nucleus: how deeply do cells 'feel' outside and in? *Journal of Cell Science*, 123(3), 297-308. <https://doi.org/10.1242/jcs.041186>
- Cai, X., Wang, K. C., & Meng, Z. (2021). Mechanoregulation of YAP and TAZ in Cellular Homeostasis and Disease Progression. *Front Cell Dev Biol*, 9, 673599. <https://doi.org/10.3389/fcell.2021.673599>
- Caliari, S. R., & Burdick, J. A. (2016). A practical guide to hydrogels for cell culture. *Nature Methods*, 13(5), 405-414. <https://doi.org/10.1038/nmeth.3839>
- Carroll, P. A., Freie, B. W., Mathsyaraja, H., & Eisenman, R. N. (2018). The MYC transcription factor network: balancing metabolism, proliferation and oncogenesis. *Frontiers of Medicine*, 12(4), 412-425. <https://doi.org/10.1007/s11684-018-0650-z>

- Carthew, R. W. (2021). Gene Regulation and Cellular Metabolism: An Essential Partnership. *Trends Genet*, 37(4), 389-400. <https://doi.org/10.1016/j.tig.2020.09.018>
- Cassani, M., Fernandes, S., Oliver-De La Cruz, J., Durikova, H., Vrbsky, J., Patocka, M., Hegrova, V., Klimovic, S., Pribyl, J., Debellis, D., Skladal, P., Cavalieri, F., Caruso, F., & Forte, G. (2023). YAP Signaling Regulates the Cellular Uptake and Therapeutic Effect of Nanoparticles. *Adv Sci (Weinh)*, e2302965. <https://doi.org/10.1002/advs.202302965>
- Chambers, D. M., Moretti, L., Zhang, J. J., Cooper, S. W., Chambers, D. M., Santangelo, P. J., & Barker, T. H. (2018). LEM domain-containing protein 3 antagonizes TGF $\beta$ -SMAD2/3 signaling in a stiffness-dependent manner in both the nucleus and cytosol. *Journal of Biological Chemistry*, 293(41), 15867-15886. <https://doi.org/10.1074/jbc.ra118.003658>
- Chandel, N. S. (2021). Lipid Metabolism. *Cold Spring Harbor Perspectives in Biology*, 13(9), a040576. <https://doi.org/10.1101/cshperspect.a040576>
- Chang, H. A., Ou Yang, R. Z., Su, J. M., Nguyen, T. M. H., Sung, J. M., Tang, M. J., & Chiu, W. T. (2023). YAP nuclear translocation induced by HIF-1 $\alpha$  prevents DNA damage under hypoxic conditions. *Cell Death Discov*, 9(1), 385. <https://doi.org/10.1038/s41420-023-01687-5>
- Chawla, A., Nagy, C., & Turecki, G. (2021). Chromatin Profiling Techniques: Exploring the Chromatin Environment and Its Contributions to Complex Traits. *International Journal of Molecular Sciences*, 22(14), 7612. <https://doi.org/10.3390/ijms22147612>
- Chen, X., Stauffer, S., Chen, Y., & Dong, J. (2016). Ajuba Phosphorylation by CDK1 Promotes Cell Proliferation and Tumorigenesis. *J Biol Chem*, 291(28), 14761-14772. <https://doi.org/10.1074/jbc.M116.722751>
- Cheng, B., Li, M., Wan, W., Guo, H., Genin, G. M., Lin, M., & Xu, F. (2023). Predicting YAP/TAZ nuclear translocation in response to ECM mechanosensing. *Biophys J*, 122(1), 43-53. <https://doi.org/10.1016/j.bpj.2022.11.2943>
- Cheng, C., Yan, X., Sun, F., & Li, L. M. (2007). Inferring activity changes of transcription factors by binding association with sorted expression profiles. *BMC Bioinformatics*, 8(1), 452. <https://doi.org/10.1186/1471-2105-8-452>
- Chi. (2012). MYC on the Path to Cancer. *Cell*, 149(1), 22-35. <https://doi.org/10.1016/j.cell.2012.03.003>
- Chiu, S.-C., Yang, X.-T., Wei, T.-Y. W., Liao, Y.-T. A., Chen, J.-M. M., Kuo, Y.-C., Liu, C.-C. J., Cheng, C.-Y., Huang, Y.-T. J., Huang, Y.-R. J., Wu, H.-L. J., Wan, C.-X., Tsai, J.-R., & Yu, C.-T. R. (2023). The crescent-like Golgi ribbon is shaped by the Ajuba/PRMT5/Aurora-A complex-modified HURP. *Cell Communication and Signaling*, 21(1). <https://doi.org/10.1186/s12964-023-01167-4>



- Chung, J. H., Zhang, Y., & Bunz, F. (2010). Checkpoint bypass and cell viability. *Cell Cycle*, 9(11), 2102-2107. <https://doi.org/10.4161/cc.9.11.11849>
- Conner, M. T., Conner, A. C., Brown, J. E., & Bill, R. M. (2010). Membrane trafficking of aquaporin 1 is mediated by protein kinase C via microtubules and regulated by tonicity. *Biochemistry*, 49(5), 821-823. <https://doi.org/10.1021/bi902068b>
- Coon, B. G., Drenzo, D. M., Konieczny, S. F., & Aguilar, R. C. (2011). Epsins' novel role in cancer cell invasion. *Commun Integr Biol*, 4(1), 95-97. <https://doi.org/10.4161/cib.4.1.14129>
- Cox, T. R. (2021). The matrix in cancer. *Nature Reviews Cancer*, 21(4), 217-238. <https://doi.org/10.1038/s41568-020-00329-7>
- D'Angelo, M., Benedetti, E., Tupone, M. G., Catanesi, M., Castelli, V., Antonosante, A., & Cimini, A. (2019). The Role of Stiffness in Cell Reprogramming: A Potential Role for Biomaterials in Inducing Tissue Regeneration. *Cells*, 8(9), 1036. <https://doi.org/10.3390/cells8091036>
- Das Thakur, M., Feng, Y., Jagannathan, R., Seppa, M. J., Skeath, J. B., & Longmore, G. D. (2010). Ajuba LIM proteins are negative regulators of the Hippo signaling pathway. *Curr Biol*, 20(7), 657-662. <https://doi.org/10.1016/j.cub.2010.02.035>
- David Sept, A. H. E. a. J. A. M. (1999). Computer Simulations of Actin Polymerization Can Explain the Barbed-Pointed End Asymmetry. *JMB*.
- David Taieb, j. R., Frederic Andre ,Stephane Garcia, Benedicte Masson, Anne Pierres, Juan-Lucio Iovanna, Philippe Soubeyran. (2008). ArgBP2-Dependent Signaling Regulates Pancreatic Cell Migration, Adhesion, and Tumorigenicity. *Cancer Res*.
- Del Pozo, M. A., Lolo, F.-N., & Echarri, A. (2021). Caveolae: Mechanosensing and mechanotransduction devices linking membrane trafficking to mechanoadaptation. *Current Opinion in Cell Biology*, 68, 113-123. <https://doi.org/https://doi.org/10.1016/j.ceb.2020.10.008>
- Dommann, N., Gavini, J., Sánchez-Taltavull, D., Baier, F. A., Birrer, F., Loforese, G., Candinas, D., & Stroka, D. (2022). LIM protein Ajuba promotes liver cell proliferation through its involvement in DNA replication and DNA damage control. *FEBS Letters*, 596(14), 1746-1764. <https://doi.org/10.1002/1873-3468.14371>
- Downing, T. L., Soto, J., Morez, C., Houssin, T., Fritz, A., Yuan, F., Chu, J., Patel, S., Schaffer, D. V., & Li, S. (2013). Biophysical regulation of epigenetic state and cell reprogramming. *Nature Materials*, 12(12), 1154-1162. <https://doi.org/10.1038/nmat3777>

- Dufort, C. C., Paszek, M. J., & Weaver, V. M. (2011). Balancing forces: architectural control of mechanotransduction. *Nature Reviews Molecular Cell Biology*, 12(5), 308-319. <https://doi.org/10.1038/nrm3112>
- Dupont, S., Morsut, L., Aragona, M., Enzo, E., Giulitti, S., Cordenonsi, M., Zanconato, F., Le Digabel, J., Forcato, M., Bicciato, S., Elvassore, N., & Piccolo, S. (2011). Role of YAP/TAZ in mechanotransduction. *Nature*, 474(7350), 179-183. <https://doi.org/10.1038/nature10137>
- Ebrahimighaei, R., Tarassova, N., Bond, S. C., McNeill, M. C., Hathway, T., Vohra, H., Newby, A. C., & Bond, M. (2024). Extracellular matrix stiffness controls cardiac fibroblast proliferation via the nuclear factor- $\kappa$ B (NF- $\kappa$ B) transcription factor. *Biochimica et Biophysica Acta (BBA) - Molecular Cell Research*, 1871(2), 119640. <https://doi.org/https://doi.org/10.1016/j.bbamcr.2023.119640>
- Echarri, A., & Del Pozo, M. A. (2015). Caveolae - mechanosensitive membrane invaginations linked to actin filaments. *Journal of Cell Science*, 128(15), 2747-2758. <https://doi.org/10.1242/jcs.153940>
- Elosegui-Artola, A., Andreu, I., Beedle, A. E. M., Lezamiz, A., Uroz, M., Kosmalka, A. J., Oria, R., Kechagia, J. Z., Rico-Lastres, P., Le Roux, A. L., Shanahan, C. M., Trepac, X., Navajas, D., Garcia-Manyes, S., & Roca-Cusachs, P. (2017). Force Triggers YAP Nuclear Entry by Regulating Transport across Nuclear Pores. *Cell*, 171(6), 1397-1410 e1314. <https://doi.org/10.1016/j.cell.2017.10.008>
- Elosegui-Artola, A., Bazellières, E., Allen, M. D., Andreu, I., Oria, R., Sunyer, R., Gomm, J. J., Marshall, J. F., Jones, J. L., Trepac, X., & Roca-Cusachs, P. (2014). Rigidity sensing and adaptation through regulation of integrin types. *Nature Materials*, 13(6), 631-637. <https://doi.org/10.1038/nmat3960>
- Emon, B., Joy, M. S. H., Lalonde, L., Ghayeb, A., Doha, U., Ladehoff, L., Brockstein, R., Saengow, C., Ewoldt, R. H., & Saif, M. T. A. (2023). Nuclear deformation regulates YAP dynamics in cancer associated fibroblasts. *Acta Biomater.* <https://doi.org/10.1016/j.actbio.2023.11.015>
- Eyckmans, J., Boudou, T., Yu, X., & Christopher. (2011). A Hitchhiker's Guide to Mechanobiology. *Developmental Cell*, 21(1), 35-47. <https://doi.org/10.1016/j.devcel.2011.06.015>
- Fan, H., Dong, W., Li, Q., Zou, X., Zhang, Y., Wang, J., Li, S., Liu, W., Dong, Y., Sun, H., & Hou, Z. (2015). Ajuba Preferentially Binds LXR $\alpha$ /RXR $\gamma$  Heterodimer to Enhance LXR Target Gene Expression in Liver Cells. *Molecular Endocrinology*, 29(11), 1608-1618. <https://doi.org/10.1210/me.2015-1046>
- Farrell, A. S., & Sears, R. C. (2014). MYC Degradation. *Cold Spring Harbor Perspectives in Medicine*, 4(3), a014365-a014365. <https://doi.org/10.1101/cshperspect.a014365>

- Feldmann, G., Beaty, R., Hruban, R. H., & Maitra, A. (2007). Molecular genetics of pancreatic intraepithelial neoplasia. *Journal of Hepato-Biliary-Pancreatic Surgery*, 14(3), 224-232. <https://doi.org/10.1007/s00534-006-1166-5>
- Feng, Y., & Longmore, G. D. (2005). The LIM Protein Ajuba Influences Interleukin-1-Induced NF- $\kappa$ B Activation by Affecting the Assembly and Activity of the Protein Kinase C $\zeta$ /p62/TRAF6 Signaling Complex. *Molecular and Cellular Biology*, 25(10), 4010-4022. <https://doi.org/10.1128/mcb.25.10.4010-4022.2005>
- Ferguson, J. P., Huber, S. D., Willy, N. M., Aygün, E., Goker, S., Atabey, T., & Kural, C. (2017). Mechanoregulation of clathrin-mediated endocytosis. *Journal of Cell Science*, 130(21), 3631-3636. <https://doi.org/10.1242/jcs.205930>
- Ferrand, A., Chevrier, V., Chauvin, J. P., & Birnbaum, D. (2009). Ajuba: a new microtubule-associated protein that interacts with BUBR1 and Aurora B at kinetochores in metaphase. *Biology of the Cell*, 101(4), 221-240. <https://doi.org/10.1042/bc20080060>
- Ferrara, B., Pignatelli, C., Cossutta, M., Citro, A., Courty, J., & Piemonti, L. (2021). The Extracellular Matrix in Pancreatic Cancer: Description of a Complex Network and Promising Therapeutic Options. *Cancers*, 13(17). <https://doi.org/10.3390/cancers13174442>
- Fisher, S., Barry, A., Abreu, J., Minie, B., Nolan, J., Delorey, T. M., Young, G., Fennell, T. J., Allen, A., Ambrogio, L., Berlin, A. M., Blumenstiel, B., Cibulskis, K., Friedrich, D., Johnson, R., Juhn, F., Reilly, B., Shamas, R., Stalker, J., . . . Nusbaum, C. (2011). A scalable, fully automated process for construction of sequence-ready human exome targeted capture libraries. *Genome Biology*, 12(1), R1. <https://doi.org/10.1186/gb-2011-12-1-r1>
- Ford, M. G. J., Mills, I. G., Peter, B. J., Vallis, Y., Praefcke, G. J. K., Evans, P. R., & McMahon, H. T. (2002). Curvature of clathrin-coated pits driven by epsin. *Nature*, 419(6905), 361-366. <https://doi.org/10.1038/nature01020>
- Fredriksson-Lidman, K., Van Itallie, C. M., Tietgens, A. J., & Anderson, J. M. (2017). Sorbin and SH3 domain-containing protein 2 (SORBS2) is a component of the acto-myosin ring at the apical junctional complex in epithelial cells. *PLoS One*, 12(9), e0185448. <https://doi.org/10.1371/journal.pone.0185448>
- Fu, Y., Zou, T., Shen, X., Nelson, P. J., Li, J., Wu, C., Yang, J., Zheng, Y., Bruns, C., Zhao, Y., Qin, L., & Dong, Q. (2021). Lipid metabolism in cancer progression and therapeutic strategies. *MedComm*, 2(1), 27-59. <https://doi.org/10.1002/mco2.27>

- Ge, H., Tian, M., Pei, Q., Tan, F., & Pei, H. (2021). Extracellular Matrix Stiffness: New Areas Affecting Cell Metabolism. *Front Oncol*, 11, 631991. <https://doi.org/10.3389/fonc.2021.631991>
- Ghosh, S., Ghosh, A., Maiti, G. P., Mukherjee, N., Dutta, S., Roy, A., Roychoudhury, S., & Panda, C. K. (2010). LIMD1 is more frequently altered than RB1 in head and neck squamous cell carcinoma: clinical and prognostic implications. *Molecular Cancer*, 9(1), 58. <https://doi.org/10.1186/1476-4598-9-58>
- Gudimchuk, N. B., & McIntosh, J. R. (2021). Regulation of microtubule dynamics, mechanics and function through the growing tip. *Nature Reviews Molecular Cell Biology*, 22(12), 777-795. <https://doi.org/10.1038/s41580-021-00399-x>
- Guilak, F., Cohen, D. M., Estes, B. T., Gimble, J. M., Liedtke, W., & Chen, C. S. (2009). Control of Stem Cell Fate by Physical Interactions with the Extracellular Matrix. *Cell Stem Cell*, 5(1), 17-26. <https://doi.org/10.1016/j.stem.2009.06.016>
- Guo, D., Bell, E., Mischel, P., & Chakravarti, A. (2014). Targeting SREBP-1-driven Lipid Metabolism to Treat Cancer. *Current Pharmaceutical Design*, 20(15), 2619-2626. <https://doi.org/10.2174/13816128113199990486>
- Hadden, M., Mittal, A., Samra, J., Zreiqat, H., Sahni, S., & Ramaswamy, Y. (2020). Mechanically stressed cancer microenvironment: Role in pancreatic cancer progression. *Biochim Biophys Acta Rev Cancer*, 1874(2), 188418. <https://doi.org/10.1016/j.bbcan.2020.188418>
- Hadden, W. J., Young, J. L., Holle, A. W., McFetridge, M. L., Kim, D. Y., Wijesinghe, P., Taylor-Weiner, H., Wen, J. H., Lee, A. R., Bieback, K., Vo, B.-N., Sampson, D. D., Kennedy, B. F., Spatz, J. P., Engler, A. J., & Choi, Y. S. (2017). Stem cell migration and mechanotransduction on linear stiffness gradient hydrogels. *Proceedings of the National Academy of Sciences*, 114(22), 5647-5652. <https://doi.org/10.1073/pnas.1618239114>
- Han, F., Zhu, C., Guo, Q., Yang, H., & Li, B. (2016). Cellular modulation by the elasticity of biomaterials. *Journal of Materials Chemistry B*, 4(1), 9-26. <https://doi.org/10.1039/c5tb02077h>
- Han, L., Huang, C., & Zhang, S. (2019). The RNA-binding protein SORBS2 suppresses hepatocellular carcinoma tumorigenesis and metastasis by stabilizing RORA mRNA. *Liver International*, 39(11), 2190-2203. <https://doi.org/10.1111/liv.14202>
- Hanahan, D. (2022). Hallmarks of Cancer: New Dimensions. *Cancer Discovery*, 12(1), 31-46. <https://doi.org/10.1158/2159-8290.cd-21-1059>
- Hanahan, D., & Robert. (2011). Hallmarks of Cancer: The Next Generation. *Cell*, 144(5), 646-674. <https://doi.org/10.1016/j.cell.2011.02.013>

- Hanahan, D., & Weinberg, R. A. (2000). The Hallmarks of Cancer. *Cell*, *100*(1), 57-70. [https://doi.org/10.1016/s0092-8674\(00\)81683-9](https://doi.org/10.1016/s0092-8674(00)81683-9)
- Henning Stumpf, B., Ambriović-Ristov, A., Radenovic, A., & Smith, A.-S. (2020). Recent Advances and Prospects in the Research of Nascent Adhesions. *Frontiers in Physiology*, *11*. <https://doi.org/10.3389/fphys.2020.574371>
- Herrmann, H., & Aebi, U. (2016). Intermediate Filaments: Structure and Assembly. *Cold Spring Harbor Perspectives in Biology*, *8*(11), a018242. <https://doi.org/10.1101/cshperspect.a018242>
- Hirota, T., Kunitoku, N., Sasayama, T., Marumoto, T., Zhang, D., Nitta, M., Hatakeyama, K., & Saya, H. (2003). Aurora-A and an Interacting Activator, the LIM Protein Ajuba, Are Required for Mitotic Commitment in Human Cells. *Cell*, *114*(5), 585-598. [https://doi.org/10.1016/s0092-8674\(03\)00642-1](https://doi.org/10.1016/s0092-8674(03)00642-1)
- Hong, M., Tao, S., Zhang, L., Diao, L.-T., Huang, X., Huang, S., Xie, S.-J., Xiao, Z.-D., & Zhang, H. (2020). RNA sequencing: new technologies and applications in cancer research. *Journal of Hematology & Oncology*, *13*(1). <https://doi.org/10.1186/s13045-020-01005-x>
- Horio, T., & Murata, T. (2014). The role of dynamic instability in microtubule organization. *Frontiers in Plant Science*, *5*. <https://doi.org/10.3389/fpls.2014.00511>
- Horton, E. R., Byron, A., Askari, J. A., Ng, D. H. J., Millon-Frémillon, A., Robertson, J., Koper, E. J., Paul, N. R., Warwood, S., Knight, D., Humphries, J. D., & Humphries, M. J. (2015). Definition of a consensus integrin adhesome and its dynamics during adhesion complex assembly and disassembly. *Nature Cell Biology*, *17*(12), 1577-1587. <https://doi.org/10.1038/ncb3257>
- Horton, E. R., Humphries, J. D., James, J., Jones, M. C., Askari, J. A., & Humphries, M. J. (2016). The integrin adhesome network at a glance. *Journal of Cell Science*, *129*(22), 4159-4163. <https://doi.org/10.1242/jcs.192054>
- Hou, Z., Peng, H., Ayyanathan, K., Yan, K. P., Langer, E. M., Longmore, G. D., & Rauscher, F. J., 3rd. (2008). The LIM protein AJUBA recruits protein arginine methyltransferase 5 to mediate SNAIL-dependent transcriptional repression. *Mol Cell Biol*, *28*(10), 3198-3207. <https://doi.org/10.1128/MCB.01435-07>
- Hou, Z., Peng, H., White, D. E., Negorev, D. G., Maul, G. G., Feng, Y., Longmore, G. D., Waxman, S., Zelent, A., & Rauscher, F. J., 3rd. (2010). LIM protein Ajuba functions as a nuclear receptor corepressor and negatively regulates retinoic acid signaling. *Proc Natl Acad Sci U S A*, *107*(7), 2938-2943. <https://doi.org/10.1073/pnas.0908656107>

- Huang, Y., Li, J., Du, W., Li, S., Li, Y., Qu, H., Xv, J., Yu, L., Zhu, R., & Wang, H. (2021). Nuclear translocation of the 4-pass transmembrane protein Tspan8. *Cell Research*, 31(11), 1218-1221. <https://doi.org/10.1038/s41422-021-00522-9>
- Huggins, C. J., & Andrulis, I. L. (2008). Cell cycle regulated phosphorylation of LIMD1 in cell lines and expression in human breast cancers. *Cancer Letters*, 267(1), 55-66. <https://doi.org/10.1016/j.canlet.2008.03.015>
- Humphries, J. D., Wang, P., Streuli, C., Geiger, B., Humphries, M. J., & Ballestrem, C. (2007). Vinculin controls focal adhesion formation by direct interactions with talin and actin. *The Journal of Cell Biology*, 179(5), 1043-1057. <https://doi.org/10.1083/jcb.200703036>
- Iacobuzio-Donahue, C. A., Velculescu, V. E., Wolfgang, C. L., & Hruban, R. H. (2012). Genetic Basis of Pancreas Cancer Development and Progression: Insights from Whole-Exome and Whole-Genome Sequencing. *Clinical Cancer Research*, 18(16), 4257-4265. <https://doi.org/10.1158/1078-0432.ccr-12-0315>
- Ibar, C., Kirichenko, E., Keepers, B., Enners, E., Fleisch, K., & Irvine, K. D. (2018). Tension-dependent regulation of mammalian Hippo signaling through LIMD1. *Journal of Cell Science*, 131(5), jcs214700. <https://doi.org/10.1242/jcs.214700>
- Ichikawa, T., Kita, M., Matsui, T. S., Nagasato, A. I., Araki, T., Chiang, S.-H., Sezaki, T., Kimura, Y., Ueda, K., Deguchi, S., Saltiel, A. R., & Kioka, N. (2017). Vinexin family (SORBS) proteins play different roles in stiffness-sensing and contractile force generation. *Journal of Cell Science*, 130(20), 3517-3531. <https://doi.org/10.1242/jcs.200691>
- Innocenti, M. (2018). New insights into the formation and the function of lamellipodia and ruffles in mesenchymal cell migration. *Cell Adh Migr*, 12(5), 401-416. <https://doi.org/10.1080/19336918.2018.1448352>
- Ishihara, S., Yasuda, M., Harada, I., Mizutani, T., Kawabata, K., & Haga, H. (2013). Substrate stiffness regulates temporary NF- $\kappa$ B activation via actomyosin contractions. *Experimental Cell Research*, 319(19), 2916-2927. <https://doi.org/10.1016/j.yexcr.2013.09.018>
- Jamali, T., Jamali, Y., Mehrbod, M., & Mofrad, M. R. K. (2011). Chapter six - Nuclear Pore Complex: Biochemistry and Biophysics of Nucleocytoplasmic Transport in Health and Disease. In K. W. Jeon (Ed.), *International Review of Cell and Molecular Biology* (Vol. 287, pp. 233-286). Academic Press. <https://doi.org/https://doi.org/10.1016/B978-0-12-386043-9.00006-2>
- Jansen, K. A., Atherton, P., & Ballestrem, C. (2017). Mechanotransduction at the cell-matrix interface. *Semin Cell Dev Biol*, 71, 75-83. <https://doi.org/10.1016/j.semcdb.2017.07.027>



- Jia, H., Peng, H., & Hou, Z. (2020). Ajuba: An emerging signal transducer in oncogenesis. *Pharmacol Res*, 151, 104546. <https://doi.org/10.1016/j.phrs.2019.104546>
- Jia, H., Song, L., Cong, Q., Wang, J., Xu, H., Chu, Y., Li, Q., Zhang, Y., Zou, X., Zhang, C., Chin, Y. E., Zhang, X., Li, Z., Zhu, K., Wang, B., Peng, H., & Hou, Z. (2017). The LIM protein AJUBA promotes colorectal cancer cell survival through suppression of JAK1/STAT1/IFIT2 network. *Oncogene*, 36(19), 2655-2666. <https://doi.org/10.1038/onc.2016.418>
- Joseph, J. G., & Liu, A. P. (2020). Mechanical Regulation of Endocytosis: New Insights and Recent Advances. *Advanced Biosystems*, 4(5), 1900278. <https://doi.org/10.1002/adbi.201900278>
- Joshi, V. B., Gutierrez Ruiz, O. L., & Razidlo, G. L. (2023). The Cell Biology of Metastatic Invasion in Pancreatic Cancer: Updates and Mechanistic Insights. *Cancers*, 15(7), 2169. <https://doi.org/10.3390/cancers15072169>
- Juin, A., Spence, H. J., Martin, K. J., McGhee, E., Neilson, M., Cutiongco, M. F. A., Gadegaard, N., Mackay, G., Fort, L., Lilla, S., Kalna, G., Thomason, P., Koh, Y. W. H., Norman, J. C., Insall, R. H., & Machesky, L. M. (2019). N-WASP Control of LPAR1 Trafficking Establishes Response to Self-Generated LPA Gradients to Promote Pancreatic Cancer Cell Metastasis. *Dev Cell*, 51(4), 431-445 e437. <https://doi.org/10.1016/j.devcel.2019.09.018>
- Kadmas, J. L., & Beckerle, M. C. (2004). The LIM domain: from the cytoskeleton to the nucleus. *Nature Reviews Molecular Cell Biology*, 5(11), 920-931. <https://doi.org/10.1038/nrm1499>
- Kai, F., Drain, A. P., & Weaver, V. M. (2019). The Extracellular Matrix Modulates the Metastatic Journey. *Developmental Cell*, 49(3), 332-346. <https://doi.org/10.1016/j.devcel.2019.03.026>
- Kaksonen, M., & Roux, A. (2018). Mechanisms of clathrin-mediated endocytosis. *Nature Reviews Molecular Cell Biology*, 19(5), 313-326. <https://doi.org/10.1038/nrm.2017.132>
- Kanetaka, K., Sakamoto, M., Yamamoto, Y., Yamasaki, S., Lanza, F., Kanematsu, T., & Hirohashi, S. (2001). Overexpression of tetraspanin CO-029 in hepatocellular carcinoma. *J Hepatol*, 35(5), 637-642. [https://doi.org/10.1016/s0168-8278\(01\)00183-0](https://doi.org/10.1016/s0168-8278(01)00183-0)
- Kar, A., & Gutierrez-Hartmann, A. (2013). Molecular mechanisms of ETS transcription factor-mediated tumorigenesis. *Critical Reviews in Biochemistry and Molecular Biology*, 48(6), 522-543. <https://doi.org/10.3109/10409238.2013.838202>
- Karamanos, N. K., Theocharis, A. D., Piperigkou, Z., Manou, D., Passi, A., Skandalis, S. S., Vynios, D. H., Orian-Rousseau, V., Ricard-Blum, S., Schmelzer, C. E. H., Duca, L., Durbeej, M., Afratis, N. A., Troeberg, L., Franchi, M., Masola, V., & Onisto, M. (2021). A guide to the composition

and functions of the extracellular matrix. *The FEBS Journal*, 288(24), 6850-6912. <https://doi.org/10.1111/febs.15776>

- Keeley, Yong, Gao, L., Liu, S.-L., Xu, T., Glenn, Christopher, & Richard. (2015). N-Cadherin Induction by ECM Stiffness and FAK Overrides the Spreading Requirement for Proliferation of Vascular Smooth Muscle Cells. *Cell Reports*, 10(9), 1477-1486. <https://doi.org/10.1016/j.celrep.2015.02.023>
- Kelsch, D. J., & Tootle, T. L. (2018). Nuclear Actin: From Discovery to Function. *Anat Rec (Hoboken)*, 301(12), 1999-2013.
- Kelsch, D. J., & Tootle, T. L. (2018). Nuclear Actin: From Discovery to Function. *The Anatomical Record*, 301(12), 1999-2013. <https://doi.org/10.1002/ar.23959>
- Khurana, T., Khurana, B., & Noegel, A. A. (2002). LIM proteins: association with the actin cytoskeleton. *Protoplasma*, 219(1-2), 0001-0012. <https://doi.org/10.1007/s007090200000>
- Kioka, N., Ueda, K., & Amachi, T. (2002). Vinexin, CAP/ponsin, ArgBP2: A Novel Adaptor Protein Family Regulating Cytoskeletal Organization and Signal Transduction. *Cell Structure and Function*, 27(1), 1-7. <https://doi.org/10.1247/csf.27.1>
- Kleeff, J., Korc, M., Apte, M., La Vecchia, C., Johnson, C. D., Biankin, A. V., Neale, R. E., Tempero, M., Tuveson, D. A., Hruban, R. H., & Neoptolemos, J. P. (2016). Pancreatic cancer. *Nat Rev Dis Primers*, 2, 16022. <https://doi.org/10.1038/nrdp.2016.22>
- La, X., Zhang, L., Li, H., Li, Z., Song, G., Yang, P., & Yang, Y. (2018). Ajuba receptor mediates the internalization of tumor-secreted GRP78 into macrophages through different endocytosis pathways. *Oncotarget*, 9(21), 15464-15479.
- Łabowska, M. B., Cierluk, K., Jankowska, A. M., Kulbacka, J., Detyna, J., & Michalak, I. (2021). A Review on the Adaption of Alginate-Gelatin Hydrogels for 3D Cultures and Bioprinting. *Materials*, 14(4), 858. <https://doi.org/10.3390/ma14040858>
- Langer, E. M., Feng, Y., Zhaoyuan, H., Rauscher, F. J., Kroll, K. L., & Longmore, G. D. (2008). Ajuba LIM Proteins Are Snail/Slug Corepressors Required for Neural Crest Development in Xenopus. *Developmental Cell*, 14(3), 424-436. <https://doi.org/10.1016/j.devcel.2008.01.005>
- Langley, R. R., & Fidler, I. J. (2011). The seed and soil hypothesis revisited--the role of tumor-stroma interactions in metastasis to different organs. *Int J Cancer*, 128(11), 2527-2535. <https://doi.org/10.1002/ijc.26031>
- Leask, A., & Abraham, D. J. (2004). TGF-beta signaling and the fibrotic response. *FASEB J*, 18(7), 816-827. <https://doi.org/10.1096/fj.03-1273rev>



- Li, A., Morton, J. P., Ma, Y., Karim, S. A., Zhou, Y., Faller, W. J., Woodham, E. F., Morris, H. T., Stevenson, R. P., Juin, A., Jamieson, N. B., Mackay, C. J., Carter, C. R., Leung, H. Y., Yamashiro, S., Blyth, K., Sansom, O. J., & Machesky, L. M. (2014). Fascin Is Regulated by Slug, Promotes Progression of Pancreatic Cancer in Mice, and Is Associated With Patient Outcomes. *Gastroenterology*, 146(5), 1386-1396.e1317. <https://doi.org/10.1053/j.gastro.2014.01.046>
- Li, H., Fu, L., Liu, B., Lin, X., Dong, Q., & Wang, E. (2019). Ajuba overexpression regulates mitochondrial potential and glucose uptake through YAP/Bcl-xL/GLUT1 in human gastric cancer. *Gene*, 693, 16-24. <https://doi.org/10.1016/j.gene.2019.01.018>
- Li, J.-T., Wang, Y.-P., Yin, M., & Lei, Q.-Y. (2019). Metabolism remodeling in pancreatic ductal adenocarcinoma. *Cell Stress*, 3(12), 361-368. <https://doi.org/10.15698/cst2019.12.205>
- Li, Q., Peng, H., Fan, H., Zou, X., Liu, Q., Zhang, Y., Xu, H., Chu, Y., Wang, C., Ayyanathan, K., Rauscher, F. J., Zhang, K., & Hou, Z. (2016). The LIM protein Ajuba promotes adipogenesis by enhancing PPAR $\gamma$  and p300/CBP interaction. *Cell Death & Differentiation*, 23(1), 158-168. <https://doi.org/10.1038/cdd.2015.83>
- Li, T., & Chen, Z. J. (2018). The cGAS-cGAMP-STING pathway connects DNA damage to inflammation, senescence, and cancer. *Journal of Experimental Medicine*, 215(5), 1287-1299. <https://doi.org/10.1084/jem.20180139>
- Li, X., Zhao, G., Mi, X., Xu, T., Li, X., & Liu, B. (2022). Ajuba Overexpression Promotes Breast Cancer Chemoresistance and Glucose Uptake through TAZ-GLUT3/Survivin Pathway. *BioMed Research International*, 2022, 1-13. <https://doi.org/10.1155/2022/3321409>
- Liang, X. H., Zhang, G. X., Zeng, Y. B., Yang, H. F., Li, W. H., Liu, Q. L., Tang, Y. L., He, W. G., Huang, Y. N., Zhang, L., Yu, L. N., & Zeng, X. C. (2014). LIM protein JUB promotes epithelial-mesenchymal transition in colorectal cancer. *Cancer Science*, 105(6), 660-666. <https://doi.org/10.1111/cas.12404>
- Liberti, M. V., & Locasale, J. W. (2016). The Warburg Effect: How Does it Benefit Cancer Cells? *Trends in Biochemical Sciences*, 41(3), 211-218. <https://doi.org/10.1016/j.tibs.2015.12.001>
- Lin, Y.-N., & Wellstein, A. (2022). Cell migration. In *Cell Movement in Health and Disease* (pp. 67-82). <https://doi.org/10.1016/b978-0-323-90195-6.00011-5>
- Lindemann, R. K., Ballschmieter, P., Nordheim, A., & Dittmer, J. (2001). Transforming growth factor beta regulates parathyroid hormone-related protein expression in MDA-MB-231 breast cancer cells through a novel Smad/Ets synergism. *J Biol Chem*, 276(49), 46661-46670. <https://doi.org/10.1074/jbc.M105816200>

- Linder, S., Cervero, P., Eddy, R., & Condeelis, J. (2023). Mechanisms and roles of podosomes and invadopodia. *Nature Reviews Molecular Cell Biology*, 24(2), 86-106. <https://doi.org/10.1038/s41580-022-00530-6>
- Liu, M., Jiang, K., Lin, G., Liu, P., Yan, Y., Ye, T., Yao, G., Barr, M. P., Liang, D., Wang, Y., Gong, P., Meng, S., & Piao, H. (2018). Ajuba inhibits hepatocellular carcinoma cell growth via targeting of  $\beta$ -catenin and YAP signaling and is regulated by E3 ligase Hakai through neddylation. *Journal of Experimental & Clinical Cancer Research*, 37(1). <https://doi.org/10.1186/s13046-018-0806-3>
- Loganathan, S. K., Schleicher, K., Malik, A., Quevedo, R., Langille, E., Teng, K., Oh, R. H., Rathod, B., Tsai, R., Samavarchi-Tehrani, P., Pugh, T. J., Gingras, A. C., & Schramek, D. (2020). Rare driver mutations in head and neck squamous cell carcinomas converge on NOTCH signaling. *Science*, 367(6483), 1264-1269. <https://doi.org/10.1126/science.aax0902>
- Love, H. D., Ao, M., Jorgensen, S., Swearingen, L., Ferrell, N., Evans, R., Gewin, L., Harris, R. C., Zent, R., Roy, S., & Fissell, W. H. (2019). Substrate Elasticity Governs Differentiation of Renal Tubule Cells in Prolonged Culture. *Tissue Engineering Part A*, 25(13-14), 1013-1022. <https://doi.org/10.1089/ten.tea.2018.0182>
- Luo, J. (2021). KRAS mutation in pancreatic cancer. *Semin Oncol*, 48(1), 10-18. <https://doi.org/10.1053/j.seminoncol.2021.02.003>
- Luo, J., Deng, L., Zou, H., Guo, Y., Tong, T., Huang, M., Ling, G., & Li, P. (2023). New insights into the ambivalent role of YAP/TAZ in human cancers. *Journal of Experimental & Clinical Cancer Research*, 42(1). <https://doi.org/10.1186/s13046-023-02704-2>
- Lv, Q., Dong, F., Zhou, Y., Cai, Z., & Wang, G. (2020). RNA-binding protein SORBS2 suppresses clear cell renal cell carcinoma metastasis by enhancing MTUS1 mRNA stability. *Cell Death & Disease*, 11(12). <https://doi.org/10.1038/s41419-020-03268-1>
- Maccurtain, B. M., Quirke, N. P., Thorpe, S. D., & Gallagher, T. K. (2021). Pancreatic Ductal Adenocarcinoma: Relating Biomechanics and Prognosis. *Journal of Clinical Medicine*, 10(12), 2711. <https://doi.org/10.3390/jcm10122711>
- Madhivanan, K., Cao, L., Staiger, C. J., & Aguilar, R. C. (2020). *Molecular determinants of the endocytic protein epsin controlling its localization and function in cancer cell migration and invasion*. Cold Spring Harbor Laboratory. <https://dx.doi.org/10.1101/2020.07.30.229195>
- Marie, H., Pratt, S. J., Betson, M., Epple, H., Kittler, J. T., Meek, L., Moss, S. J., Troyanovsky, S., Attwell, D., Longmore, G. D., & Braga, V. M. M. (2003). The LIM Protein Ajuba Is Recruited to Cadherin-dependent Cell Junctions through an Association with  $\alpha$ -Catenin. *Journal of Biological Chemistry*, 278(2), 1220-1228. <https://doi.org/10.1074/jbc.m205391200>

- Martinac, B., & Kloda, A. (2003). Evolutionary origins of mechanosensitive ion channels. *Prog Biophys Mol Biol*, 82(1-3), 11-24. [https://doi.org/10.1016/s0079-6107\(03\)00002-6](https://doi.org/10.1016/s0079-6107(03)00002-6)
- Martino, F., Perestrelo, A. R., Vinarsky, V., Pagliari, S., & Forte, G. (2018). Cellular Mechanotransduction: From Tension to Function. *Front Physiol*, 9, 824. <https://doi.org/10.3389/fphys.2018.00824>
- Martire, S., & Banaszynski, L. A. (2020). The roles of histone variants in fine-tuning chromatin organization and function. *Nature Reviews Molecular Cell Biology*, 21(9), 522-541. <https://doi.org/10.1038/s41580-020-0262-8>
- Matsuda, A., & Mofrad, M. R. K. (2022). On the nuclear pore complex and its emerging role in cellular mechanotransduction. *APL Bioengineering*, 6(1), 011504. <https://doi.org/10.1063/5.0080480>
- Matsushita, Y., Nakagawa, H., & Koike, K. (2021). Lipid Metabolism in Oncology: Why It Matters, How to Research, and How to Treat. *Cancers*, 13(3), 474. <https://doi.org/10.3390/cancers13030474>
- Maurer, M., & Lammerding, J. (2019). The Driving Force: Nuclear Mechanotransduction in Cellular Function, Fate, and Disease. *Annual Review of Biomedical Engineering*, 21(1), 443-468. <https://doi.org/10.1146/annurev-bioeng-060418-052139>
- Mierke, C. T. (2024). Extracellular Matrix Cues Regulate Mechanosensing and Mechanotransduction of Cancer Cells. *Cells*, 13(1), 96. <https://doi.org/10.3390/cells13010096>
- Miller, A. E., Hu, P., & Barker, T. H. (2020). Feeling Things Out: Bidirectional Signaling of the Cell-ECM Interface, Implications in the Mechanobiology of Cell Spreading, Migration, Proliferation, and Differentiation. *Adv Healthc Mater*, 9(8), e1901445. <https://doi.org/10.1002/adhm.201901445>
- Miroshnikova, Y. A., & Wickström, S. A. (2022). Mechanical Forces in Nuclear Organization. *Cold Spring Harbor Perspectives in Biology*, 14(1), a039685. <https://doi.org/10.1101/cshperspect.a039685>
- Mizrahi, J. D., Surana, R., Valle, J. W., & Shroff, R. T. (2020). Pancreatic cancer. *Lancet*, 395(10242), 2008-2020. [https://doi.org/10.1016/S0140-6736\(20\)30974-0](https://doi.org/10.1016/S0140-6736(20)30974-0)
- Mohan, M. D., Latifi, N., Flick, R., Simmons, C. A., & Young, E. W. K. (2024). Interrogating Matrix Stiffness and Metabolomics in Pancreatic Ductal Carcinoma Using an Openable Microfluidic Tumor-on-a-Chip. *ACS Appl Mater Interfaces*. <https://doi.org/10.1021/acsami.4c00556>
- Mokhtari, R. B., Ashayeri, N., Baghaie, L., Sambhi, M., Satari, K., Baluch, N., Bosykh, D. A., Szewczuk, M. R., & Chakraborty, S. (2023). The Hippo Pathway Effectors YAP/TAZ-TEAD Oncoproteins as Emerging Therapeutic

Targets in the Tumor Microenvironment. *Cancers (Basel)*, 15(13). <https://doi.org/10.3390/cancers15133468>

- Molinari, M. (2000). Cell cycle checkpoints and their inactivation in human cancer. *Cell Proliferation*, 33(5), 261-274. <https://doi.org/10.1046/j.1365-2184.2000.00191.x>
- Montoya-Durango, D. E., Velu, C. S., Kazanjian, A., Rojas, M. E., Jay, C. M., Longmore, G. D., & Grimes, H. L. (2008). Ajuba functions as a histone deacetylase-dependent co-repressor for autoregulation of the growth factor-independent-1 transcription factor. *J Biol Chem*, 283(46), 32056-32065. <https://doi.org/10.1074/jbc.M802320200>
- Montoya-Durango, D. E., Velu, C. S., Kazanjian, A., Rojas, M. E. B., Jay, C. M., Longmore, G. D., & Grimes, H. L. (2008). Ajuba Functions as a Histone Deacetylase-dependent Co-repressor for Autoregulation of the Growth Factor-independent-1 Transcription Factor. *Journal of Biological Chemistry*, 283(46), 32056-32065. <https://doi.org/10.1074/jbc.m802320200>
- Morton, J. P., Timpson, P., Karim, S. A., Ridgway, R. A., Athineos, D., Doyle, B., Jamieson, N. B., Oien, K. A., Lowy, A. M., Brunton, V. G., Frame, M. C., Evans, T. R. J., & Sansom, O. J. (2010). Mutant p53 drives metastasis and overcomes growth arrest/senescence in pancreatic cancer. *Proceedings of the National Academy of Sciences*, 107(1), 246-251. <https://doi.org/10.1073/pnas.0908428107>
- Mui, K. L., Chen, C. S., & Assoian, R. K. (2016). The mechanical regulation of integrin-cadherin crosstalk organizes cells, signaling and forces. *Journal of Cell Science*, 129(6), 1093-1100. <https://doi.org/10.1242/jcs.183699>
- Mukenhirn, M., Muraca, F., Bucher, D., Asberger, E., Cappio Barazzone, E., Cavalcanti-Adam, E. A., & Boulant, S. (2021). Role of Clathrin Light Chains in Regulating Invadopodia Formation. *Cells*, 10(2), 451. <https://doi.org/10.3390/cells10020451>
- Müller, M., Saunders, C., Senftleben, A., Heidbuechel, J. P. W., Halwachs, B., Bolik, J., Hedemann, N., Röder, C., Bauerschlag, D., Rose-John, S., & Schmidt-Arras, D. (2022). Tetraspanin 8 Subfamily Members Regulate Substrate-Specificity of a Disintegrin and Metalloprotease 17. *Cells*, 11(17), 2683. <https://doi.org/10.3390/cells11172683>
- Mustapha, F., Sengupta, K., & Puech, P. H. (2022). Protocol for measuring weak cellular traction forces using well-controlled ultra-soft polyacrylamide gels. *STAR Protoc*, 3(1), 101133. <https://doi.org/10.1016/j.xpro.2022.101133>
- Najafi, M., Farhood, B., & Mortezaee, K. (2019). Extracellular matrix (ECM) stiffness and degradation as cancer drivers. *J Cell Biochem*, 120(3), 2782-2790. <https://doi.org/10.1002/jcb.27681>

- Naqvi, S. M., & McNamara, L. M. (2020). Stem Cell Mechanobiology and the Role of Biomaterials in Governing Mechanotransduction and Matrix Production for Tissue Regeneration. *Frontiers in Bioengineering and Biotechnology*, 8. <https://doi.org/10.3389/fbioe.2020.597661>
- Narasimhan, B. N., Ting, M. S., Kollmetz, T., Horrocks, M. S., Chalard, A. E., & Malmström, J. (2020). Mechanical Characterization for Cellular Mechanobiology: Current Trends and Future Prospects. *Frontiers in Bioengineering and Biotechnology*, 8. <https://doi.org/10.3389/fbioe.2020.595978>
- Nasrollahi S, P. A. (2017). Matrix stiffness and confinement influence YAP localization in clustered epithelial cells. *Mechanical Engineering & Materials Science Independent Study*, 33.
- Natalya, & Craig. (2016). The Emerging Hallmarks of Cancer Metabolism. *Cell Metabolism*, 23(1), 27-47. <https://doi.org/10.1016/j.cmet.2015.12.006>
- Niethammer, P. (2021). Components and Mechanisms of Nuclear Mechanotransduction. *Annual Review of Cell and Developmental Biology*, 37(1), 233-256. <https://doi.org/10.1146/annurev-cellbio-120319-030049>
- Nola, S., Daigaku, R., Smolarczyk, K., Carstens, M., Martin-Martin, B., Longmore, G., Bailly, M., & Braga, V. M. (2011). Ajuba is required for Rac activation and maintenance of E-cadherin adhesion. *J Cell Biol*, 195(5), 855-871. <https://doi.org/10.1083/jcb.201107162>
- Northey, J. J., Przybyla, L., & Weaver, V. M. (2017). Tissue Force Programs Cell Fate and Tumor Aggression. *Cancer Discovery*, 7(11), 1224-1237. <https://doi.org/10.1158/2159-8290.cd-16-0733>
- Oakes, P. W., & Gardel, M. L. (2014). Stressing the limits of focal adhesion mechanosensitivity. *Current Opinion in Cell Biology*, 30, 68-73. <https://doi.org/10.1016/j.ceb.2014.06.003>
- Olaoba, O. T., Adelusi, T. I., Yang, M., Maidens, T., Kimchi, E. T., Staveley-O'Carroll, K. F., & Li, G. (2024). Driver Mutations in Pancreatic Cancer and Opportunities for Targeted Therapy. *Cancers (Basel)*, 16(10). <https://doi.org/10.3390/cancers16101808>
- Orth, M., Metzger, P., Gerum, S., Mayerle, J., Schneider, G., Belka, C., Schnurr, M., & Lauber, K. (2019). Pancreatic ductal adenocarcinoma: biological hallmarks, current status, and future perspectives of combined modality treatment approaches. *Radiat Oncol*, 14(1), 141. <https://doi.org/10.1186/s13014-019-1345-6>
- Paget, S. (1889). THE DISTRIBUTION OF SECONDARY GROWTHS IN CANCER OF THE BREAST. *The Lancet*, 133(3421), 571-573. [https://doi.org/https://doi.org/10.1016/S0140-6736\(00\)49915-0](https://doi.org/https://doi.org/10.1016/S0140-6736(00)49915-0)



- Pancierera, T., Azzolin, L., Cordenonsi, M., & Piccolo, S. (2017). Mechanobiology of YAP and TAZ in physiology and disease. *Nature Reviews Molecular Cell Biology*, 18(12), 758-770. <https://doi.org/10.1038/nrm.2017.87>
- Papalazarou, V., Zhang, T., Paul, N. R., Juin, A., Cantini, M., Maddocks, O. D. K., Salmeron-Sanchez, M., & Machesky, L. M. (2020). The creatine-phosphagen system is mechanoresponsive in pancreatic adenocarcinoma and fuels invasion and metastasis. *Nature Metabolism*, 2(1), 62-80. <https://doi.org/10.1038/s42255-019-0159-z>
- Parker, A. L., Bowman, E., Zingone, A., Ryan, B. M., Cooper, W. A., Kohonen-Corish, M., Harris, C. C., & Cox, T. R. (2022). Extracellular matrix profiles determine risk and prognosis of the squamous cell carcinoma subtype of non-small cell lung carcinoma. *Genome Medicine*, 14(1). <https://doi.org/10.1186/s13073-022-01127-6>
- Parreno, J., Raju, S., Wu, P.-h., & Kandel, R. A. (2017). MRTF-A signaling regulates the acquisition of the contractile phenotype in dedifferentiated chondrocytes. *Matrix Biology*, 62, 3-14. <https://doi.org/https://doi.org/10.1016/j.matbio.2016.10.004>
- Pascual-Garcia, P., & Capelson, M. (2021). The nuclear pore complex and the genome: organizing and regulatory principles. *Current Opinion in Genetics & Development*, 67, 142-150. <https://doi.org/https://doi.org/10.1016/j.gde.2021.01.005>
- Pellegrin, S. p., & Mellor, H. (2007). Actin stress fibres. *Journal of Cell Science*, 120(20), 3491-3499. <https://doi.org/10.1242/jcs.018473>
- Pratt, S. J., Epple, H., Ward, M., Feng, Y., Braga, V. M., & Longmore, G. D. (2005). The LIM protein Ajuba influences p130Cas localization and Rac1 activity during cell migration. *J Cell Biol*, 168(5), 813-824. <https://doi.org/10.1083/jcb.200406083>
- Raices, M., & D'Angelo, M. A. (2017). Nuclear pore complexes and regulation of gene expression. *Current Opinion in Cell Biology*, 46, 26-32. <https://doi.org/https://doi.org/10.1016/j.ceb.2016.12.006>
- Rainero, E., & Norman, J. C. (2013). Late endosomal and lysosomal trafficking during integrin-mediated cell migration and invasion: cell matrix receptors are trafficked through the late endosomal pathway in a way that dictates how cells migrate. *Bioessays*, 35(6), 523-532. <https://doi.org/10.1002/bies.201200160>
- Rauskolb, C., Han, A., Kirichenko, E., Ibar, C., & Irvine, K. D. (2022). Analysis of the Drosophila Ajuba LIM protein defines functions for distinct LIM domains. *PLoS One*, 17(8), e0269208. <https://doi.org/10.1371/journal.pone.0269208>

- Rauskolb, C., Sun, S., Sun, G., Pan, Y., & Irvine, K. D. (2014). Cytoskeletal tension inhibits Hippo signaling through an Ajuba-Warts complex. *Cell*, 158(1), 143-156. <https://doi.org/10.1016/j.cell.2014.05.035>
- Razzell, W., Bustillo, M. E., & Zallen, J. A. (2018). The force-sensitive protein Ajuba regulates cell adhesion during epithelial morphogenesis. *Journal of Cell Biology*, 217(10), 3715-3730. <https://doi.org/10.1083/jcb.201801171>
- Rice, A. J., Cortes, E., Lachowski, D., Cheung, B. C. H., Karim, S. A., Morton, J. P., & Del Río Hernández, A. (2017). Matrix stiffness induces epithelial-mesenchymal transition and promotes chemoresistance in pancreatic cancer cells. *Oncogenesis*, 6(7), e352-e352. <https://doi.org/10.1038/oncsis.2017.54>
- Ridley, A. J., Schwartz, M. A., Burridge, K., Firtel, R. A., Ginsberg, M. H., Borisy, G., Parsons, J. T., & Horwitz, A. R. (2003). Cell Migration: Integrating Signals from Front to Back. *Science*, 302(5651), 1704-1709. <https://doi.org/10.1126/science.1092053>
- Romanazzo, S., Forte, G., Ebara, M., Uto, K., Pagliari, S., Aoyagi, T., Traversa, E., & Taniguchi, A. (2012). Substrate stiffness affects skeletal myoblast differentiation *in vitro*. *Science and Technology of Advanced Materials*, 13(6), 064211. <https://doi.org/10.1088/1468-6996/13/6/064211>
- Romani, P., Brian, I., Santinon, G., Pocaterra, A., Audano, M., Pedretti, S., Mathieu, S., Forcato, M., Bicciato, S., Manneville, J.-B., Mitro, N., & Dupont, S. (2019). Extracellular matrix mechanical cues regulate lipid metabolism through Lipin-1 and SREBP. *Nature Cell Biology*, 21(3), 338-347. <https://doi.org/10.1038/s41556-018-0270-5>
- Rosso, G., Wehner, D., Schweitzer, C., Möllmert, S., Sock, E., Guck, J., & Shahin, V. (2022). Matrix stiffness mechanosensing modulates the expression and distribution of transcription factors in Schwann cells. *Bioengineering & Translational Medicine*, 7(1). <https://doi.org/10.1002/btm2.10257>
- Sahu, R. K., Singh, S., & Tomar, R. S. (2020). The mechanisms of action of chromatin remodelers and implications in development and disease. *Biochem Pharmacol*, 180, 114200. <https://doi.org/10.1016/j.bcp.2020.114200>
- Sandoval, K., & Weiss, W. A. (2022). Nuclear tetraspanin 8 promotes breast cancer progression. *Cell Research*, 32(6), 511-512. <https://doi.org/10.1038/s41422-022-00657-3>
- Sang, M., Ma, L., Sang, M., Zhou, X., Gao, W., & Geng, C. (2014). LIM-domain-only proteins: multifunctional nuclear transcription coregulators that interacts with diverse proteins. *Molecular Biology Reports*, 41(2), 1067-1073. <https://doi.org/10.1007/s11033-013-2952-1>

- Schimizzi, G. V., & Longmore, G. D. (2015). Ajuba proteins. *Curr Biol*, 25(11), R445-446. <https://doi.org/10.1016/j.cub.2015.02.034>
- Schleicher, K., & Schramek, D. (2021). AJUBA: A regulator of epidermal homeostasis and cancer. *Exp Dermatol*, 30(4), 546-559. <https://doi.org/10.1111/exd.14272>
- Schoumacher, M., El-Marjou, F., Lae, M., Kambou, N., Louvard, D., Robine, S., & Vignjevic, D. M. (2014). Conditional expression of fascin increases tumor progression in a mouse model of intestinal cancer. *Eur J Cell Biol*, 93(10-12), 388-395. <https://doi.org/10.1016/j.ejcb.2014.08.002>
- Schumacher, S., Vazquez Nunez, R., Biertümpfel, C., & Mizuno, N. (2022). Bottom-up reconstitution of focal adhesion complexes. *The FEBS Journal*, 289(12), 3360-3373. <https://doi.org/10.1111/febs.16023>
- Schwarz, N., & Leube, R. E. (2023). Plasticity of cytoplasmic intermediate filament architecture determines cellular functions. *Curr Opin Cell Biol*, 85, 102270. <https://doi.org/10.1016/j.ceb.2023.102270>
- Scott, R. W., & Olson, M. F. (2007). LIM kinases: function, regulation and association with human disease. *J Mol Med (Berl)*, 85(6), 555-568. <https://doi.org/10.1007/s00109-007-0165-6>
- Seo, M., Crochet, R. B., & Lee, Y.-H. (2014). Targeting Altered Metabolism—Emerging Cancer Therapeutic Strategies. In *Cancer Drug Design and Discovery* (pp. 427-448). <https://doi.org/10.1016/b978-0-12-396521-9.00014-0>
- Shemesh, T., Geiger, B., Bershadsky, A. D., & Kozlov, M. M. (2005). Focal adhesions as mechanosensors: A physical mechanism. *Proceedings of the National Academy of Sciences*, 102(35), 12383-12388. <https://doi.org/10.1073/pnas.0500254102>
- Shi, X., Chen, Z., Hu, X., Luo, M., Sun, Z., Li, J., Shi, S., Feng, X., Zhou, C., Li, Z., Yang, W., Li, Y., Wang, P., Zhou, F., Gao, Y., & He, J. (2016). AJUBA promotes the migration and invasion of esophageal squamous cell carcinoma cells through upregulation of MMP10 and MMP13 expression. *Oncotarget*, 7(24), 36407-36418. <https://doi.org/10.18632/oncotarget.9239>
- Sibony-Benyamini, H., & Gil-Henn, H. (2012). Invadopodia: the leading force. *Eur J Cell Biol*, 91(11-12), 896-901. <https://doi.org/10.1016/j.ejcb.2012.04.001>
- Sidorenko, E., & Vartiainen, M. A.-O. (2019). Nucleoskeletal regulation of transcription: Actin on MRTF. (1535-3699 (Electronic)).
- Silva, P. M., Da Silva, I. V., Sarmiento, M. J., Silva, Í. C., Carvalho, F. A., Soveral, G., & Santos, N. C. (2022). Aquaporin-3 and Aquaporin-5 Facilitate Migration and Cell-Cell Adhesion in Pancreatic Cancer by Modulating Cell



Biomechanical Properties. *Cells*, 11(8), 1308.  
<https://doi.org/10.3390/cells11081308>

- Sinha, B., Köster, D., Ruez, R., Gonnord, P., Bastiani, M., Abankwa, D., Stan, R. V., Butler-Browne, G., Védie, B., Johannes, L., Morone, N., Parton, R. G., Raposo, G., Sens, P., Lamaze, C., & Nassoy, P. (2011). Cells Respond to Mechanical Stress by Rapid Disassembly of Caveolae. *Cell*, 144(3), 402-413.  
<https://doi.org/10.1016/j.cell.2010.12.031>
- Siraj, A. K., Parvathareddy, S. K., Al-Rasheed, M., Annaiyappanaidu, P., Siraj, N., Lennartz, M., Al-Sobhi, S. S., Al-Dayel, F., Sauter, G., & Al-Kuraya, K. S. (2023). Loss of CDH16 expression is a strong independent predictor for lymph node metastasis in Middle Eastern papillary thyroid cancer. *Scientific Reports*, 13(1). <https://doi.org/10.1038/s41598-023-45882-x>
- Skinner, M. K., Rawls, A., Wilson-Rawls, J., & Roalson, E. H. (2010). Basic helix-loop-helix transcription factor gene family phylogenetics and nomenclature. *Differentiation*, 80(1), 1-8.  
<https://doi.org/10.1016/j.diff.2010.02.003>
- Smith, K. (2014). FASCINating insights into the metastatic nature of pancreatic cancer. *Nature Reviews Gastroenterology & Hepatology*, 11(3), 139-139. <https://doi.org/10.1038/nrgastro.2014.15>
- Song, N., Liu, J., Zhang, K., Yang, J., Cui, K., Miao, Z., Zhao, F., Meng, H., Chen, L., Chen, C., Li, Y., Shao, M., Su, W., & Wang, H. (2022). The LIM Protein AJUBA is a Potential Oncogenic Target and Prognostic Marker in Human Cancer via Pan-Cancer Analysis. *Frontiers in Cell and Developmental Biology*, 10. <https://doi.org/10.3389/fcell.2022.921897>
- Sotodosos-Alonso, L. A.-O., Pulgarín-Alfaro, M. A.-O., & Del Pozo, M. A.-O. X. (2023). Caveolae Mechanotransduction at the Interface between Cytoskeleton and Extracellular Matrix. *Cells*(2073-4409 (Electronic)).  
<https://doi.org/10.3390/cells12060942>
- Speight, P., Kofler, M., Szászi, K., & Kapus, A. (2016). Context-dependent switch in chemo/mechanotransduction via multilevel crosstalk among cytoskeleton-regulated MRTF and TAZ and TGF $\beta$ -regulated Smad3. *Nature Communications*, 7(1), 11642. <https://doi.org/10.1038/ncomms11642>
- Spitz, F., & Furlong, E. E. M. (2012). Transcription factors: from enhancer binding to developmental control. *Nature Reviews Genetics*, 13(9), 613-626.  
<https://doi.org/10.1038/nrg3207>
- Springer, T. A., & Dustin, M. L. (2012). Integrin inside-out signaling and the immunological synapse. *Current Opinion in Cell Biology*, 24(1), 107-115.  
<https://doi.org/10.1016/j.ceb.2011.10.004>
- Staley, B. K., & Irvine, K. D. (2012). Hippo signaling in *Drosophila*: recent advances and insights. *Dev Dyn*, 241(1), 3-15. <https://doi.org/10.1002/dvdy.22723>

- Straub, J. A., & Newman, J. J. (2024). Nuclear Transcription Factor Detection. In (pp. 367-390). Springer US. [https://doi.org/10.1007/978-1-0716-3762-3\\_26](https://doi.org/10.1007/978-1-0716-3762-3_26)
- Sun, X., Phua, D. Y. Z., Axiotakis, L., Smith, M. A., Blankman, E., Gong, R., Cail, R. C., Espinosa De Los Reyes, S., Beckerle, M. C., Waterman, C. M., & Alushin, G. M. (2020). Mechanosensing through Direct Binding of Tensed F-Actin by LIM Domains. *Developmental Cell*, 55(4), 468-482.e467. <https://doi.org/10.1016/j.devcel.2020.09.022>
- Sun, Z., Guo, S. S., & Fässler, R. (2016). Integrin-mediated mechanotransduction. *Journal of Cell Biology*, 215(4), 445-456. <https://doi.org/10.1083/jcb.201609037>
- Sunami, Y., Rebelo, A., & Kleeff, J. (2017). Lipid Metabolism and Lipid Droplets in Pancreatic Cancer and Stellate Cells. *Cancers*, 10(1), 3. <https://doi.org/10.3390/cancers10010003>
- Svitkina, T. (2018). The Actin Cytoskeleton and Actin-Based Motility. *Cold Spring Harbor Perspectives in Biology*, 10(1), a018267. <https://doi.org/10.1101/cshperspect.a018267>
- Swaney, K. F., & Li, R. (2016). Function and regulation of the Arp2/3 complex during cell migration in diverse environments. *Current Opinion in Cell Biology*, 42, 63-72. <https://doi.org/10.1016/j.ceb.2016.04.005>
- Swift, J., & Discher, D. E. (2014). The nuclear lamina is mechano-responsive to ECM elasticity in mature tissue. *Journal of Cell Science*, 127(14), 3005-3015. <https://doi.org/10.1242/jcs.149203>
- Tanaka, I., Osada, H., Fujii, M., Fukatsu, A., Hida, T., Horio, Y., Kondo, Y., Sato, A., Hasegawa, Y., Tsujimura, T., & Sekido, Y. (2015). LIM-domain protein AJUBA suppresses malignant mesothelioma cell proliferation via Hippo signaling cascade. *Oncogene*, 34(1), 73-83. <https://doi.org/10.1038/onc.2013.528>
- Tang, J., Zhu, L., Huang, Y., Shi, B., Zhang, S., Gu, L., Zhao, J., Deng, M., Zhu, J., Xun, H., Wang, Y., & Wang, C. (2019). Silencing of LIMD1 promotes proliferation and reverses cell adhesion-mediated drug resistance in non-Hodgkin's lymphoma. *Oncology Letters*, 17(3), 2993-3000. <https://doi.org/10.3892/ol.2019.9921>
- Termini, C. M., & Gillette, J. M. (2017). Tetraspanins Function as Regulators of Cellular Signaling. *Frontiers in Cell and Developmental Biology*, 5. <https://doi.org/10.3389/fcell.2017.00034>
- Tilghman, R. W., & Parsons, J. T. (2008). Focal adhesion kinase as a regulator of cell tension in the progression of cancer. *Seminars in Cancer Biology*, 18(1), 45-52. <https://doi.org/10.1016/j.semcancer.2007.08.002>
- Tomita, Y., Dorward, H., Yool, A., Smith, E., Townsend, A., Price, T., & Hardingham, J. (2017). Role of Aquaporin 1 Signalling in Cancer

Development and Progression. *International Journal of Molecular Sciences*, 18(2), 299. <https://doi.org/10.3390/ijms18020299>

- Torres, C., & Grippo, P. J. (2018). Pancreatic cancer subtypes: a roadmap for precision medicine. *Annals of Medicine*, 50(4), 277-287. <https://doi.org/10.1080/07853890.2018.1453168>
- Totaro, A., Panciera, T., & Piccolo, S. (2018). YAP/TAZ upstream signals and downstream responses. *Nature Cell Biology*, 20(8), 888-899. <https://doi.org/10.1038/s41556-018-0142-z>
- Totaro, A., Panciera, T., & Piccolo, S. (2018). YAP/TAZ upstream signals and downstream responses. *Nat Cell Biol*, 20(8), 888-899. <https://doi.org/10.1038/s41556-018-0142-z>
- Trujillo, S., Gonzalez-Garcia, C., Rico, P., Reid, A., Windmill, J., Dalby, M. J., & Salmeron-Sanchez, M. (2020). Engineered 3D hydrogels with full-length fibronectin that sequester and present growth factors. *Biomaterials*, 252, 120104. <https://doi.org/10.1016/j.biomaterials.2020.120104>
- Tse, J. R., & Engler, A. J. (2010). Preparation of hydrogel substrates with tunable mechanical properties. *Curr Protoc Cell Biol, Chapter 10*, Unit 10 16. <https://doi.org/10.1002/0471143030.cb1016s47>
- Tumanov, S., & Kamphorst, J. J. (2017). Recent advances in expanding the coverage of the lipidome. *Curr Opin Biotechnol*, 43, 127-133.
- Vanmunster, M., Rojo Garcia, A. V., Pacolet, A., Dalle, S., Koppo, K., Jonkers, I., Lories, R., & Suhr, F. (2022). Mechanosensors control skeletal muscle mass, molecular clocks, and metabolism. *Cellular and Molecular Life Sciences*, 79(6). <https://doi.org/10.1007/s00018-022-04346-7>
- Velyvis A, Q. J. (2013). LIM Domain and Its Binding to Target Proteins. *Madame Curie Bioscience Database [Internet]*. <https://www.ncbi.nlm.nih.gov/books/NBK6372/>
- Vining, K. H., & Mooney, D. J. (2017). Mechanical forces direct stem cell behaviour in development and regeneration. *Nature Reviews Molecular Cell Biology*, 18(12), 728-742. <https://doi.org/10.1038/nrm.2017.108>
- Wagh, K., Ishikawa, M., Garcia, D. A., Stavreva, D. A., Upadhyaya, A., & Hager, G. L. (2021). Mechanical Regulation of Transcription: Recent Advances. *Trends in Cell Biology*, 31(6), 457-472. <https://doi.org/10.1016/j.tcb.2021.02.008>
- Wang, J. H., & Li, B. (2010). Mechanics rules cell biology. *BMC Sports Science, Medicine and Rehabilitation*, 2(1), 16. <https://doi.org/10.1186/1758-2555-2-16>

- Wang, K., Seo, B. R., Fischbach, C., & Gourdon, D. (2016). Fibronectin Mechanobiology Regulates Tumorigenesis. *Cell Mol Bioeng*, 9, 1-11. <https://doi.org/10.1007/s12195-015-0417-4>
- Wang, Y., Zhang, C., Yang, W., Shao, S., Xu, X., Sun, Y., Li, P., Liang, L., & Wu, C. (2021). LIMD1 phase separation contributes to cellular mechanics and durotaxis by regulating focal adhesion dynamics in response to force. *Developmental Cell*, 56(9), 1313-1325.e1317. <https://doi.org/10.1016/j.devcel.2021.04.002>
- Wang, Z. (2022). Cell Cycle Progression and Synchronization: An Overview. In (pp. 3-23). Springer US. [https://doi.org/10.1007/978-1-0716-2736-5\\_1](https://doi.org/10.1007/978-1-0716-2736-5_1)
- Wei, L., Li, Y., & Suo, Z. (2015). TSPAN8 promotes gastric cancer growth and metastasis via ERK MAPK pathway. *Int J Clin Exp Med*, 8(6), 8599-8607.
- Whatcott, C. J., Posner, R. G., Von Hoff, D. D., & Han, H. (2012). Desmoplasia and chemoresistance in pancreatic cancer. In P. J. Grippo & H. G. Munshi (Eds.), *Pancreatic Cancer and Tumor Microenvironment*. © 2012, Transworld Research Network.
- Willcockson, M. A., Healton, S. E., Weiss, C. N., Bartholdy, B. A., Botbol, Y., Mishra, L. N., Sidhwani, D. S., Wilson, T. J., Pinto, H. B., Maron, M. I., Skalina, K. A., Toro, L. N., Zhao, J., Lee, C. H., Hou, H., Yusufova, N., Meydan, C., Osunsade, A., David, Y., . . . Skoultchi, A. I. (2021). H1 histones control the epigenetic landscape by local chromatin compaction. *Nature*, 589(7841), 293-298. <https://doi.org/10.1038/s41586-020-3032-z>
- Winkelman, J. D., Anderson, C. A., Suarez, C., Kovar, D. R., & Gardel, M. L. (2020). Evolutionarily diverse LIM domain-containing proteins bind stressed actin filaments through a conserved mechanism. *Proceedings of the National Academy of Sciences*, 117(41), 25532-25542. <https://doi.org/10.1073/pnas.2004656117>
- Wolfram, L., Gimpel, C., Schwämmle, M., Clark, S. J., Böhringer, D., & Schlunck, G. (2024). The impact of substrate stiffness on morphological, transcriptional and functional aspects in RPE. *Scientific Reports*, 14(1). <https://doi.org/10.1038/s41598-024-56661-7>
- Woodbury, S. M., Swanson, W. B., & Mishina, Y. (2023). Mechanobiology-informed biomaterial and tissue engineering strategies for influencing skeletal stem and progenitor cell fate. *Frontiers in Physiology*, 14. <https://doi.org/10.3389/fphys.2023.1220555>
- Wu, Y., Biswas, D., & Swanton, C. (2022). Impact of cancer evolution on immune surveillance and checkpoint inhibitor response. *Seminars in Cancer Biology*, 84, 89-102. <https://doi.org/10.1016/j.semcancer.2021.02.013>
- Wu, Y., Cao, Y., Xu, K., Zhu, Y., Qiao, Y., Wu, Y., Chen, J., Li, C., Zeng, R., & Ge, G. (2021). Dynamically remodeled hepatic extracellular matrix predicts

- prognosis of early-stage cirrhosis. *Cell Death Dis*, 12(2), 163. <https://doi.org/10.1038/s41419-021-03443-y>
- Wu, Y., & Zhou, B. P. (2010). Snail. *Cell Adhesion & Migration*, 4(2), 199-203. <https://doi.org/10.4161/cam.4.2.10943>
- Wu, Z., Zou, X., Xu, Y., Zhou, F., Kuai, R., Li, J., Yang, D., Chu, Y., & Peng, H. (2021). Ajuba transactivates N-cadherin expression in colorectal cancer cells through interaction with Twist. *Journal of Cellular and Molecular Medicine*, 25(16), 8006-8014. <https://doi.org/10.1111/jcmm.16731>
- Xie, W., Wei, X., Kang, H., Jiang, H., Chu, Z., Lin, Y., Hou, Y., & Wei, Q. (2023). Static and Dynamic: Evolving Biomaterial Mechanical Properties to Control Cellular Mechanotransduction. *Advanced Science*, 10(9), 2204594. <https://doi.org/10.1002/advs.202204594>
- Xu, B., Li, Q., Chen, N., Zhu, C., Meng, Q., Ayyanathan, K., Qian, W., Jia, H., Wang, J., Ni, P., & Hou, Z. (2019). The LIM protein Ajuba recruits DBC1 and CBP/p300 to acetylate ER $\alpha$  and enhances ER $\alpha$  target gene expression in breast cancer cells. *Nucleic Acids Research*, 47(5), 2322-2335. <https://doi.org/10.1093/nar/gky1306>
- Xue, F., Janzen, D. M., & Knecht, D. A. (2010). Contribution of Filopodia to Cell Migration: A Mechanical Link between Protrusion and Contraction. *International Journal of Cell Biology*, 2010, 1-13. <https://doi.org/10.1155/2010/507821>
- Yamaguchi, H., & Condeelis, J. (2007). Regulation of the actin cytoskeleton in cancer cell migration and invasion. *Biochimica et Biophysica Acta (BBA) - Molecular Cell Research*, 1773(5), 642-652. <https://doi.org/10.1016/j.bbamcr.2006.07.001>
- Yan, H., Li, Q., Li, M., Zou, X., Bai, N., Yu, Z., Zhang, J., Zhang, D., Zhang, Q., Wang, J., Jia, H., Wu, Y., & Hou, Z. (2022). Ajuba functions as a co-activator of C/EBP $\beta$  to induce expression of PPAR $\gamma$  and C/EBP $\alpha$  during adipogenesis. *Mol Cell Endocrinol*, 539, 111485. <https://doi.org/10.1016/j.mce.2021.111485>
- Yang, B., Wei, K., Loebel, C., Zhang, K., Feng, Q., Li, R., Wong, S. H. D., Xu, X., Lau, C., Chen, X., Zhao, P., Yin, C., Burdick, J. A., Wang, Y., & Bian, L. (2021). Enhanced mechanosensing of cells in synthetic 3D matrix with controlled biophysical dynamics. *Nature Communications*, 12(1). <https://doi.org/10.1038/s41467-021-23120-0>
- Yang, X., Li, Y., Liu, G., Zha, W., & Liu, Y. (2022). Cadherin-16 inhibits thyroid carcinoma cell proliferation and invasion. *Oncology Letters*, 23(5). <https://doi.org/10.3892/ol.2022.13265>
- Yao, M., Goult, B. T., Chen, H., Cong, P., Sheetz, M. P., & Yan, J. (2014). Mechanical activation of vinculin binding to talin locks talin in an unfolded conformation. *Scientific Reports*, 4(1). <https://doi.org/10.1038/srep04610>



- Yi, B., Xu, Q., & Liu, W. (2022). An overview of substrate stiffness guided cellular response and its applications in tissue regeneration. *Bioact Mater*, 15, 82-102. <https://doi.org/10.1016/j.bioactmat.2021.12.005>
- Yu, W., Yang, L., Li, T., & Zhang, Y. (2019). Cadherin Signaling in Cancer: Its Functions and Role as a Therapeutic Target. *Frontiers in Oncology*, 9. <https://doi.org/10.3389/fonc.2019.00989>
- Yu, X., Zech, T., McDonald, L., Gonzalez, E. G., Li, A., Macpherson, I., Schwarz, J. P., Spence, H., Futó, K., Timpson, P., Nixon, C., Ma, Y., Anton, I. M., Visegrády, B., Insall, R. H., Oien, K., Blyth, K., Norman, J. C., & Machesky, L. M. (2012). N-WASP coordinates the delivery and F-actin-mediated capture of MT1-MMP at invasive pseudopods. *Journal of Cell Biology*, 199(3), 527-544. <https://doi.org/10.1083/jcb.201203025>
- Yue, B. (2014). Biology of the extracellular matrix: an overview. *J Glaucoma*, 23(8 Suppl 1), S20-23. <https://doi.org/10.1097/IJG.000000000000108>
- Yue, S., Mu, W., & Zöller, M. (2013). Tspan8 and CD151 promote metastasis by distinct mechanisms. *Eur J Cancer*, 49(13), 2934-2948. <https://doi.org/10.1016/j.ejca.2013.03.032>
- Zammit, P. S. (2017). Function of the myogenic regulatory factors Myf5, MyoD, Myogenin and MRF4 in skeletal muscle, satellite cells and regenerative myogenesis. *Seminars in Cell & Developmental Biology*, 72, 19-32. <https://doi.org/https://doi.org/10.1016/j.semcdb.2017.11.011>
- Zhang, B., Song, L., Cai, J., Li, L., Xu, H., Li, M., Wang, J., Shi, M., Chen, H., Jia, H., & Hou, Z. (2019). The LIM protein Ajuba/SP1 complex forms a feed forward loop to induce SP1 target genes and promote pancreatic cancer cell proliferation. *Journal of Experimental & Clinical Cancer Research*, 38(1). <https://doi.org/10.1186/s13046-019-1203-2>
- Zhang, C., Wei, S., Sun, W. P., Teng, K., Dai, M. M., Wang, F. W., Chen, J. W., Ling, H., Ma, X. D., Feng, Z. H., Duan, J. L., Cai, M. Y., & Xie, D. (2020). Super-enhancer-driven AJUBA is activated by TCF4 and involved in epithelial-mesenchymal transition in the progression of Hepatocellular Carcinoma. *Theranostics*, 10(20), 9066-9082. <https://doi.org/10.7150/thno.45349>
- Zhang, Z., Zhang, H., Liao, X., & Tsai, H.-I. (2023). KRAS mutation: The booster of pancreatic ductal adenocarcinoma transformation and progression. *Frontiers in Cell and Developmental Biology*, 11. <https://doi.org/10.3389/fcell.2023.1147676>
- Zhao, B., Wei, X., Li, W., Udan, R. S., Yang, Q., Kim, J., Xie, J., Ikenoue, T., Yu, J., Li, L., Zheng, P., Ye, K., Chinnaiyan, A., Halder, G., Lai, Z.-C., & Guan, K.-L. (2007). Inactivation of YAP oncoprotein by the Hippo pathway is involved in cell contact inhibition and tissue growth control. *Genes & Development*, 21(21), 2747-2761. <https://doi.org/10.1101/gad.1602907>

- Zhao, Y., Sheldon, M., Sun, Y., & Ma, L. (2023). New Insights into YAP/TAZ-TEAD-Mediated Gene Regulation and Biological Processes in Cancer. *Cancers (Basel)*, 15(23). <https://doi.org/10.3390/cancers15235497>
- Zhao, Z., & Liu, W. (2020). Pancreatic Cancer: A Review of Risk Factors, Diagnosis, and Treatment. *Technology in Cancer Research & Treatment*, 19, 153303382096211. <https://doi.org/10.1177/1533033820962117>
- Zheng, Q., & Zhao, Y. (2007). The diverse biofunctions of LIM domain proteins: determined by subcellular localization and protein–protein interaction. *Biology of the Cell*, 99(9), 489-502. <https://doi.org/10.1042/bc20060126>
- Zhou, J., Zhang, L., Zhou, W., Chen, Y., Cheng, Y., & Dong, J. (2019). LIMD phosphorylation in mitosis is required for mitotic progression and its tumor-suppressing activity. *The FEBS Journal*, 286(5), 963-974. <https://doi.org/10.1111/febs.14743>
- Zhu, F., & Rui, L. (2019). PRMT5 in gene regulation and hematologic malignancies. *Genes Dis*, 6(3), 247-257. <https://doi.org/10.1016/j.gendis.2019.06.002>
- Zhu, X. G., Chudnovskiy, A., Baudrier, L., Prizer, B., Liu, Y., Ostendorf, B. N., Yamaguchi, N., Arab, A., Tavora, B., Timson, R., Heissel, S., De Stanchina, E., Molina, H., Victora, G. D., Goodarzi, H., & Birsoy, K. (2021). Functional Genomics In Vivo Reveal Metabolic Dependencies of Pancreatic Cancer Cells. *Cell Metabolism*, 33(1), 211-221.e216. <https://doi.org/10.1016/j.cmet.2020.10.017>
- Zigmond, S. H. (1998). Actin cytoskeleton: The Arp2/3 complex gets to the point. *Current Biology*, 8(18), R654-R657. [https://doi.org/10.1016/s0960-9822\(07\)00415-0](https://doi.org/10.1016/s0960-9822(07)00415-0)
- Zöller, M. (2009). Tetraspanins: push and pull in suppressing and promoting metastasis. *Nature Reviews Cancer*, 9(1), 40-55. <https://doi.org/10.1038/nrc2543>
- Zollinger, A. J., & Smith, M. L. (2017). Fibronectin, the extracellular glue. *Matrix Biol*, 60-61, 27-37. <https://doi.org/10.1016/j.matbio.2016.07.011>